TECHNISCHE UNIVERSITÄT DRESDEN

FAKULTÄT Forst- Geo- und Hydrowissenschaften

Institut für Photogrammetrie und Fernerkundung

Title of the Dissertation

Estimating Carbon Pool and Carbon Release due to Tropical Deforestation Using High-resolution Satellite Data

Submitted by:
Md. Mahmudur Rahman
Date of birth: 01.02.1972
Place of birth: Mymensingh, Bangladesh

A thesis submitted for the partial fulfilment of
Doctor of Natural Science (Dr. rer.nat.)

Faculty of Forest, Geo and Hydro Sciences,
Dresden University of Technology, Germany

Date of submission: July 2004

Supervisors:

Prof. Dr. Elmar Csaplovics, Institute of Photogrammetry and Remote Sensing, TU Dresden

Prof Dr. Barbara Koch, Department of Remote Sensing and Land Information System, Albert-Ludwigs University, Freiburg

Prof. Dr. Michael Köhl, Department of World Forestry, University of Hamburg

Lending admitted / not admitted   Chairman of Examination Commission

Dresden, July 2004

Declaration

ii

I hereby declare that this submission is my own work and that, to the best of my knowledge and belief, it contains no material previously published or written by another person nor material which to a substantial extent has been accepted for the award of any other degree or diploma of the university or other institute of higher learning, except where due acknowledgment has been made in the text.

Necessary contacts to the officials and private individuals and use of image processing facilities have been done as mentioned in this dissertation and with the agreement of the supervisors.

(Md. Mahmudur Rahman)

Dresden, Germany

July, 2004

Dedicated to my mother

Mrs. Sufia Khatun

Table of Contents

List of Tables

training set pixels

Illustrations

Forward

This dissertation is prepared for the partial fulfilment of the degree, Doctor of Natural Science at the Institute of Photogrammetry and Remote Sensing, Faculty of Forest, Geo and Hydro Sciences. Field sampling was done during October 2002 – February 2003 for result formulation and November 2003 – February 2004 for validation. During that field data collection some remote sensing data were analysed in the Image Processing Laboratory, Bangladesh Space Research and Remote Sensing Organization (SPARRSO). Field sampling was done at the study area of southern Chittagong, Bangladesh with a close collaboration of Bangladesh Forest Department.

The content of the work is presented in seven Chapters. A short introduction about the climate change scenario, its causes, necessity and objective of the current study is described in chapter one. Chapter two describes the background and literature review of the study. The study area and stand information are presented in chapter three. Methodology is described in chapter four. Chapter five and six describe the results and discussions respectively. The study has been concluded in chapter seven.

Abstract

Forest-cover in the tropics is changing rapidly due to indiscriminate removal of timber from many localities, which might be one of the major sources of carbon emission and global climate change in recent decades. The main focus of the current study is to develop an operational tool for monitoring above-ground biomass and carbon of tropical forest ecosystem. It will also able to detect any changes in the pool due to deforestation or growth. Finally the method was applied to a test site. The test site is located at the south-eastern Bangladesh where a considerable amount of deforestation has been noticed in the recent years. The research used Landsat ETM+, Landsat TM and IRS pan images on the 2001, 1992 and 1999 respectively. Geometrically corrected Landsat ETM+ imagery was obtained from USGS and later was adjusted in the field using GPS. Historical images were corrected using image-to-image registration. Atmospheric correction was done by modified dark object subtraction method. Selected study area was separated from the whole image. Stratified sampling design based on remote sensing data was applied for assessing the above-ground biomass and carbon content in the selected study area. Recent image was classified using supervised method to establish strata for field inventory. Eight different vegetation types were recognized. Field sampling was done during 2002-2003. A total of seventy field samples were collected from different strata. The plot size was variable in different vegetation types. *Dbh* and height of all the trees inside plots were measured. Field measurement was finally converted to carbon content using allometric relations. Three different methods: stratification, regression and *k*-nearest neighbors were tested for combining remote sensing image information and terrestrial carbon pool from field sample plots. Additional field sampling was conducted during 2003-2004 for testing the accuracy of different methods. Thirty field sample plots were collected for this validation purpose. Finally regression method was selected to predict the terrestrial carbon pool of the study area from Landsat images of 2001 and 1992 as the other two methods have some constraints. The amount of carbon released and sequestrated from the ecosystem due to deforestation or growth was estimated. The dissertation has also discussed the limitations of the above-described estimation procedure. The method can also be applied for estimating carbon pool of the temperate forest, which is rather straight-forward. The application of the above technique would be quite useful for understating the terrestrial carbon dynamics and global climate change.

Symbols, Names and Units

Symbol	Physical Name	Unit
σ^2	Variance	
D	Earth-sun distance	AU (astronomical unit)
$Edown$	Downwelling spectral irradiance at the surface due to the scattered solar flux in the atmosphere	$Wm^{-2}\mu m^{-1}$
Eo	Solar spectral irradiance on a surface perpendicular to the sun's rays outside the atmosphere	$Wm-2\mu m-1$
$ESUN\lambda$	Solar Exoatmospheric Spectral Irradiances	Milliwatts/(cm squared*μm) or Watts/(meter squared*μm)
$Lhaze$	Upwelling atmospheric spectral radiance scattered in the direction of and at the sensor entrance pupil and within the sensor's field of view	$Wm^{-2}sr^{-1}\mu m^{-1}$
$LMAX^\gamma$	Spectral radiance at maximum DC (255) for band γ	$mW*cm^{-2}*ster^{-1}*\mu m^{-1}$ /$W*m^{-2}*ster^{-1}*\mu m^{-1}$
$LMIN^\gamma$	Spectral radiance at minimum DC (0) for band γ	$mW*cm^{-2}*ster^{-1}*\mu m^{-1}$ /$W*m^{-2}*ster^{-1}*\mu m^{-1}$
$L_{sat}\gamma$	At satellite spectral radiance for band γ	
R^2	Coefficient of determination	
$TAUv$	Atmospheric transmittance along the path from the ground surface to the sensor.	Decimal point or percentage
$TAUz$	Atmospheric transmittance along the path from the sun to the ground surface	Decimal point or percentage
TZ	Angle of incidence of the direct solar flux onto the Earth's surface (solar zenith angle).	Thetaz
$\overline{V}$	Average variance of the difference between all pairs of strata	

Abbreviations

C	Carbon
CIR	Colour Infra-Red
dbh	Diameter at Breast Height
DC	Digital Count
DEM	Digital Elevation Model
DN	Digital Number
DVI	Difference Vegetation Index
ETM+	Enhanced Thematic Mapper Plus
IHS	Intensity Hue Saturation
IPCC	Intergovernmental Panel on Climate Change
IRS-1C	Indian Remote Sensing Satellite 1C
LAI	Leaf Area Index
MSS	Multi Spectral Scanner
NDVI	Normalized Difference Vegetation Index
NIR	Near Infrared Region
NOAA	National Oceanic and Atmospheric Administration
PCA	Principal Component Analysis
PVI	Perpendicular Vegetation Index
RGB	Red Green Blue
RMS	Residual Mean Square
RMSE	Root Mean Squared Error
RVI	Ratio Vegetation Index
SAVI	Soil Adjusted vegetation Index
SPARRSO	Bangladesh Space Research and Remote Sensing Organization
SWIR	Short-wave Infrared Region

TM	Thematic Mapper
TREES	Tropical Ecosystem Environment Observation by Satellite
TVI	Transformed Vegetation Index
US EPA	United States Environmental Protection Agency
USGS	United States Geological Survey

Chapter I

1 Climate Change and Carbon-di-oxide Emission

1.1 Global Climate System and Recent Climate Change

Global climate change is a change in the long-term weather patterns of the world. The greenhouse effect is a one example of the recent climate change, which is a warming process that balances Earth's cooling processes. During this process, sunlight passes through Earth's atmosphere as short-wave radiation. Some of the radiation is absorbed by the planet's surface. As Earth's surface is heated, it emits long wave radiation toward the atmosphere. In the atmosphere, certain gases called greenhouse gases absorb some of the long wave radiation. Greenhouse gases include carbon dioxide (CO_2), chlorofluorocarbons (CFC's), methane (CH_4), nitrous oxide (N_2O), tropospheric ozone (O_3), and water vapours. Each molecule of greenhouse gas becomes energized by the long wave radiation. The energized molecules of gas then emit heat energy in all directions. By emitting heat energy toward Earth, greenhouse gases increase Earth's temperature.

The greenhouse effect is a natural occurrence that maintains Earth's average temperature at approximately 60 degrees Fahrenheit. The greenhouse effect is a necessary phenomenon that keeps all Earth's heat from escaping to the outer atmosphere. Without the greenhouse effect, temperatures on Earth would be much lower than they are now, and the existence of life on this planet would not be possible. However, too many greenhouse gases in Earth's atmosphere could increase the greenhouse effect. This could result in an increase in mean global temperatures as well as changes in precipitation patterns. When weather patterns for an area change in one direction over long periods of time, they can result in a net climate change for that area. The key concept in climate change is time. Natural changes in climate usually occur over; that is to say they occur over such long periods of time that they are often not noticed within several human lifetimes. This gradual nature of the changes in climate enables the plants, animals, and microorganisms on earth to evolve and adapt to the new temperatures, precipitation patterns, etc.

The real threat of climate change lies in how rapidly the change occurs. For example, over the past 130 years, the mean global temperature appears to have risen 0.6 to 1.2 degrees Fahrenheit (0.3 to 0.7 degrees Celsius). The increasing steepness of the curve suggests that changes in mean global temperature have occurred at greater rates over time. Further evidence suggests that future increases in mean global temperature may occur at a rate of 0.4 degrees Fahrenheit (0.2 degrees Celsius) each decade. Figure 1.1 describes the changes in global temperature (degrees Fahrenheit) from 1861 to 1996 (Graph adapted from image courtesy of the US EPA).

The geological record and the physical evidence of the results of processes that have occurred on Earth since it was formed, provides evidence of climate changes similar in magnitude to those in the above graph. This means during the history of the earth, there have been changes in global temperatures similar in size to these changes. However, the past changes occurred at much slower rates, and thus they were spread out over long periods of time. The slow rate of change allowed most species enough time to adapt to the new climate. The current and predicted rates of temperature change, on the other hand, may be harmful to ecosystems. This is because these rates of temperature change are much faster than those of Earth's past. Many species of plants, animals, and micro-organisms may not have enough time to adapt to the new climate. These organisms may become extinct.
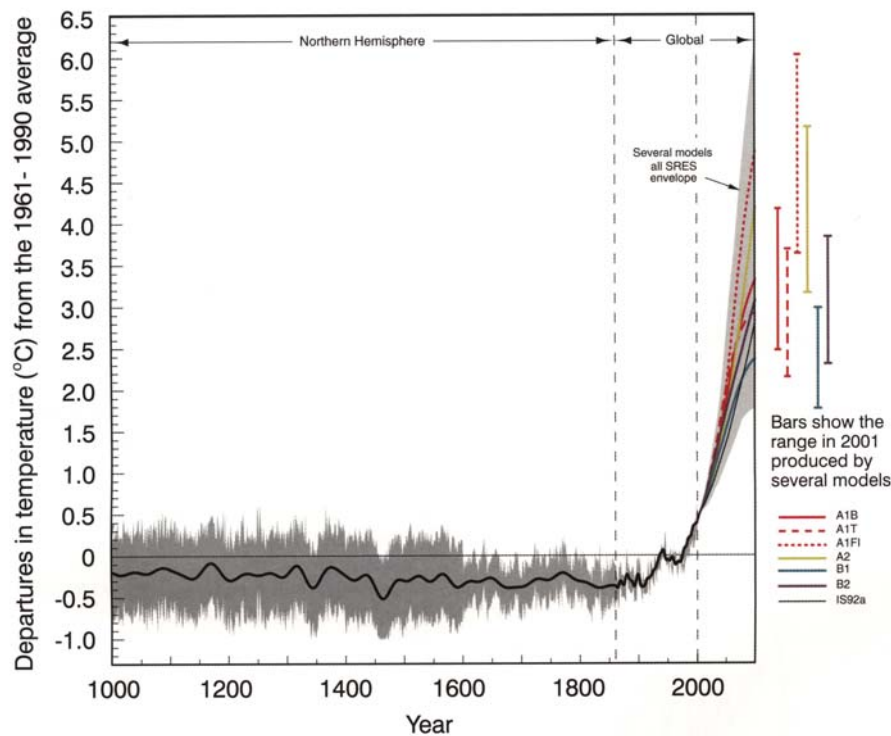
Figure 1.1 Variations of Earth's surface temperature (1000 to 2100 AD). Data from IPCC Third Assessment Report (Prentice *et al.* 2001). Sources of data from 1000-1861 AD-northern hemisphere, proxy data (tree rings, sediment cores etc.); 1861-2000 AD- global instrumental data; 2000-2100 AD- Special Report on Emission Scenarios projections.

Analyses of air bubbles in ice cores from Greenland and Antarctica have given a reasonably clear idea about variations in atmospheric CO_2 concentration since the end of the last glacial maximum. The global atmospheric CO_2 concentration is now nearly 100 ppmv higher than the interglacial

maximum; this recent rise is equal to the entire range of CO_2 concentrations between glacial minima and interglacial maxima. Atmospheric concentrations of carbon dioxide have risen to current levels at least ten- possibly a hundred- times faster than at any other time in the last 429,000 years, and continue to rise sharply. The recent dramatic increase in atmospheric CO_2 is unquestionably the result of human activities. It is highly likely the observed changes toward a warmer climate over the last century are a consequence of this increase (Figure 1.1 and Prentice *et al.* 2001).

Carbon dioxide has received a lot of attention with respect to global warming; 50% to 60% of the anthropogenic greenhouse effect is attributed to this gas. 160,000 years prior to the industrial revolution the atmospheric concentration of carbon dioxide varied from approximately 200 to 300 ppm (Post *et. al.* 1990). The major anthropogenic greenhouse gases are listed in table 1.1. The table also lists the recent growth rate in percent to the anthropogenic greenhouse effect.

Table 1.1 Relative contributions of trace gases to the anthropogenic effect

Trace Gases	Relative Contribution (%)	Growth Rate (% yr)
CFC	15[a]-25[b]	5
CH_4	12[a]-20[b]	1[c]
O_3 (troposphere)	8d	0.5
N_2O	5d	0.2
Total	40-50	
Contribution of CO_2	50-60	0.3[e]-0.5[d,f]

[a] W. A. Nierenberg. 1989.

[b] Hanson *et al.* 1989.

[c] Growth stopped in 1991-1992 possibly due to control of leaks in Russian natural gas production systems (Botkin and Keller. 1998).

[d] Rodhe 1990.

[e] Kellogg 1989

[f] Abelson 1990.

About 130 years ago, at the beginning of the industrial revolution, the atmospheric concentration of carbon dioxide was approximately 280 ppm, a level apparently constant for the last 700 years (Moss and Lins 1989). Beginning in about 1860, the concentration of carbon dioxide in the atmosphere has grown exponentially. Currently, the rate of increase of carbon dioxide in the

atmosphere is about 0.5% per year; if it continues to grow at this rate, it will be doubled approximately in 140 years (Botkin and Keller 1998).

Today the concentration of carbon dioxide in the atmosphere is approaching 400 ppm, and it is predicted that the level may rise to approximately 450 ppm by the year 2050, more than 1.5 times the pre-industrial level (Titus *et al.* 1985). Figure 1.2 compares the global emission of carbon dioxide to the average concentration of the gas to the atmosphere. These data suggest a direct correlation between the emission of carbon dioxide and its concentration in the atmosphere. It is interesting to note, however, that the rate of increase of carbon emission from burning of fossil fuels, deforestation and other anthropogenic processes has been approximately 4.3% per year since the industrial revolution began, more than 8 times the 0.5% per year rate of increase in concentration of carbon dioxide in the atmosphere (Botkin and Keller 1998).
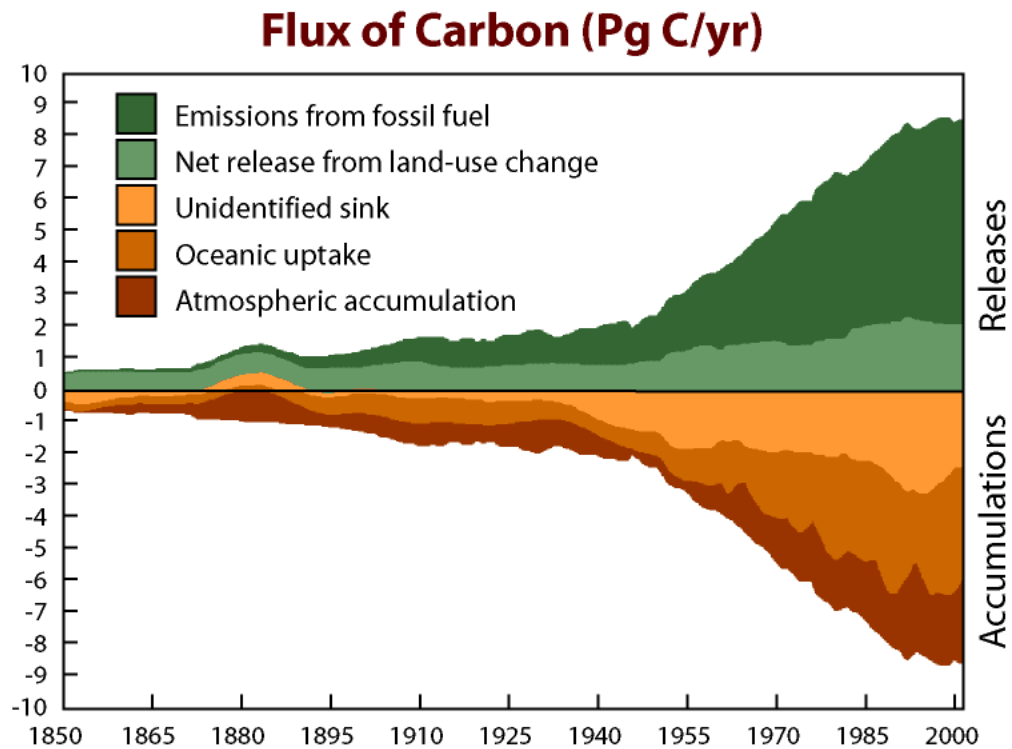
Figure 1.2 Flux of global carbon in 1850-2000 (source: Woods Hole Research Center)

1.2   Carbon Cycle

All life is based on the element carbon. Carbon is the major chemical constituent of most organic matter, from fossil fuels to the complex molecules (DNA and RNA) that control genetic reproduction in organisms. The movement of carbon, in its many forms, between the biosphere, atmosphere, oceans and geo-sphere is described by the carbon cycle. Carbon is stored on our planet in the

following major sinks (1) as organic molecules in living and dead organisms found in the biosphere, (2) as the carbon dioxide in the atmosphere (3) as organic matters in soils (4) in the lithosphere as fossil fuels and sedimentary rock deposits such as limestone, dolomite and chalk and (5) in the oceans as dissolved atmospheric carbon dioxide and as calcium carbonate shells in marine organisms.

Table 1.2 Estimated major stores of carbon on the earth (Pidwirny 2004)

Sink	Amount in Billions of Metric Tons
Atmosphere	578 (as of 1700 A.D.) to 766 (as 1999 A.D.)
Soil organic matter	1500 to 1600
Ocean	38,000 to 40,000
Marine sediments and sedimentary rocks	66,000,000 to 100,000,000
Terrestrial plants	540 to 640
Fossil fuel deposits	4000

Ecosystems gain most of their carbon dioxide from the atmosphere. A number of autotrophic organisms have specialized mechanisms that allow for absorption of gas into their cells. With the addition of water and energy from solar radiation, these organisms use photosynthesis to chemically convert the carbon dioxide to carbon based sugar molecules. These molecules can then be chemically modified by these organisms through the metabolic addition of other elements to produce more complex compounds like proteins, cellulose and amino acids. Some of the organic matter produced in plants is passed down to heterotrophic animals through consumption.

Carbon dioxide enters the waters of the ocean by simple diffusion. Once dissolved in seawater, the carbon dioxide can remain as is or can be converted into carbonate CO_3^-) or bicarbonate (HCO_3^-). Certain forms of sea life biologically fix bicarbonate with calcium (Ca^{++}) to produce calcium carbonate ($CaCO_3$). This substance is used to produce shells and other body parts by organisms such as coral, calms, oysters, some protozoa and some algae. When these organisms die, their shells and body parts sink to the ocean floor where they accumulate as carbonate-rich deposits. After long period of time, these deposits are physically and chemically altered into sedimentary rocks. Ocean deposits are by far the biggest sinks of carbon on the planet.

Carbon is released from ecosystems as carbon dioxide gas by the process of respiration. Respiration takes place in both plants and animals and involved the breakdown of carbon-based

organic molecules into carbon dioxide gas and some other compound by-products. Food chain contains a number of organisms whose primary ecological role is the decomposition of organic matter into its abiotic component also plays role in carbon release. The carbon cycle can be presented by figure 1.3.
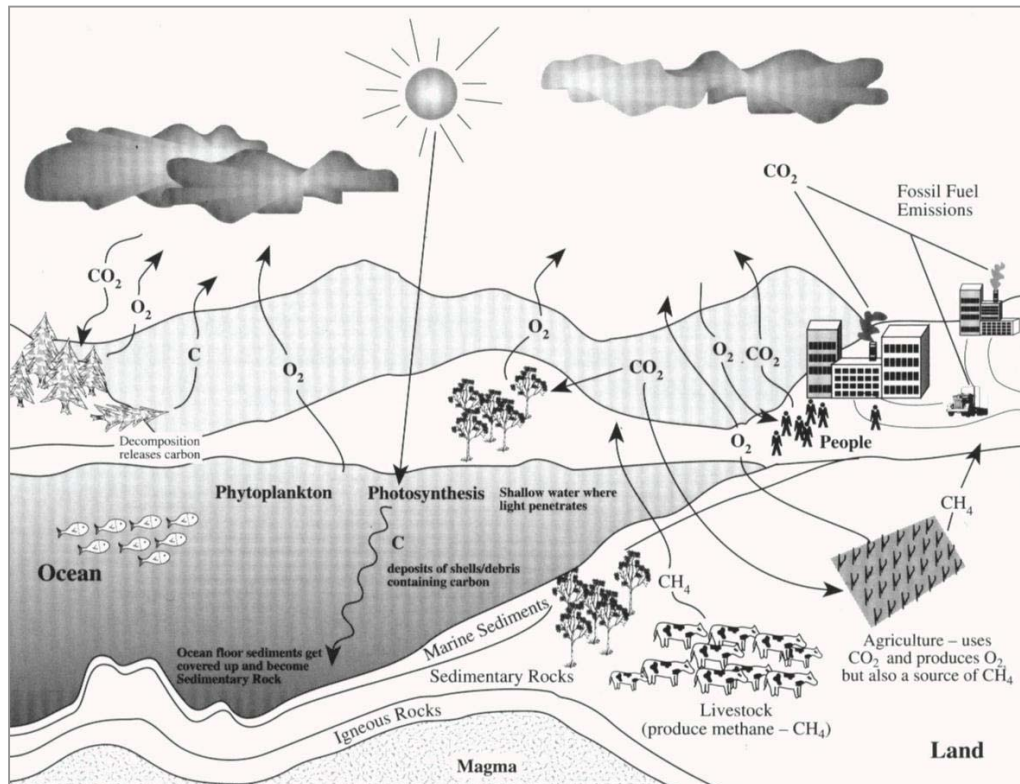
Figure 1.3 Schematic representation of carbon cycle

The other major problem in estimating carbon transfer to the atmosphere on the route is that there may be less obvious movements of carbon to the atmosphere, such as oxidation of organic matter from soils that accompanies forest destruction. This is obviously difficult to quantify and varies considerably from one ecosystem to another. Fortunately for the balance of carbon on earth, there are also parts by which carbon is removed from the atmosphere. One of these is absorbed by solution in the oceans. Seawater is slightly alkaline and this assists the solution of CO_2 where it may form hydrogen carbonate ions. These can be used by the phytoplankton as a source of carbon synthesis and some of the carbons fixed in this way will sediment into deeper waters as the dead bodies of the phytoplankton sink downwards. Hydrogen carbonate ions may also combine with calcium to generate calcium carbonate (lime), especially forming the lime-impregnated outer coats on some of the planktonic organisms (Moore *et al.* 1996).

6

Over millions of years buried organic matter is compressed between layers of sediment, where it forms carbon-containing fossil fuels such as coal and oil. This carbon is not released to the atmosphere as CO_2 for recycling until these fuels are extracted and burned or until long-term geological processes expose these deposits to air. In the short time period of a few hundred years, we have been extracting and burning fossil fuels that took million of years to form from dead plant matter, which is why fossil fuels are non-renewable resources on a human time scale.

1.3   Forests and Carbon Fluxes

1.3.1   Storage of carbon in forest ecosystem

The high-latitude zone is suggested to contain the highest forest carbon reserves per surface area, principally due to belowground carbon stocks. Biomass-carbon stocks are highest in tropical forests but show average soil-carbon contents of the same order as those of the temperate zone (Houghton 1996). Dixon and Wisniewski (1995) estimate 31% of the total global forest carbon reserve to be locked in vegetation and 69% in soils and peat. The aboveground portion of the total forest-biomass carbon is thought to be approximately 75-90%. The remaining 10-25% is located in the soil, particularly as root biomass. Ratios of aboveground biomass to belowground biomass may though vary in a range of between 1.32 and 0.1 in different ecosystem types (Olson *et al.* 1983, Körner 1989, Nilsson and Schopfhauser 1995). Within any latitude belt, soil-carbon contents tend to diminish (according to increasing disturbance) from primary forest to secondary forest and agricultural land use.

Each of the vegetation types is described in relation to categories used in the Olson *et al.* (1985) ecosystems map (figure 1.4) although many modifications to this framework is necessary. The detailed tabular statement of the map is enumerated in table 1.3.
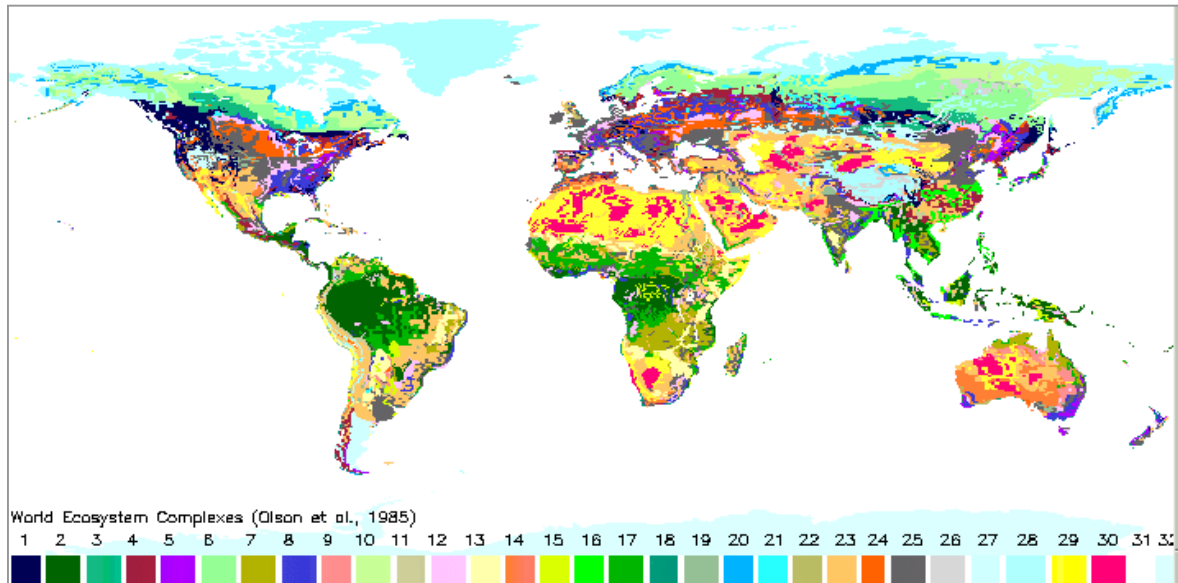
Figure 1.4 World Ecosystem Complexes in terms of carbon storage (Olson *et al.* 1985)

Global estimates in short- and long-lived wood products amount to approximately 15 Pg carbon, of which approximately 25% or 2-8 Pg carbon would correspond to long-lived (>1 year) products. Thus, carbon storage in wood products would amount to approximately 3-4% of that in the forest biomass and approximately 1.3-1.4% of the whole forest ecosystem (Matthews *et al.* 1996). According to Vitousek (1991), worldwide, approximately 4 Pg carbon (~0.7-1.1% of the carbon storage of forest vegetation) is presently contained in buildings and 0.5 Pg carbon is in paper and other wood products. The annual global logging yield is 0.6 Pg carbon, of which approximately half is used as fuel wood and only 0.1 Pg is used as construction material. In contrast to the buildup of the carbon pool in wood products, decay or destruction rates of the different wood products vary widely and are difficult to calculate (Puhe and Ulrich 2001).

Table 1.3 World Ecosystem Complexes in terms of carbon storage

Color-Id	Ecosystem complexes	Grid cell count (0.5°)	Medium carbon density (Kg C/m2)	Revised medium carbon density (Kg C/m2)	Minimum carbon density (Kg C/m2)	Maximum carbon density (Kg C/m2)	Ecosystem codes
1	Conifers	1719	16.00	13.00	12.0	20.0	22,27
2	Tropical/Subtropical Broad-leaved Humid Forest	3430	15.00	12.00	4.0	25.0	29,33,73
3	Southern Taiga	903	11.00	8.00	6.0	14.0	60,61
4	Mid-Latitude Mixed Woods (Deciduous/Evergreen/Conifer)	1589	10.00	7.00	6.0	14.0	23,24
5	Mid-Latitude Temperate Broad-leaved Forest	676	10.00	9.00	8.0	14.0	25,26
6	Main Boreal Taiga	3579	8.00	6.00	4.0	11.0	20,21
7	Tropical/Subtropical Dry Forest and Woodland	1584	7.00	6.00	5.0	9.0	32
8	Second Growth Forest/Fields (Tropical/Subtropical Humid, Temperate/Boreal Forests)	2232	5.00	4.00	4.0	8.0	56,57
9	Semi-arid Woodland or Low Forest	324	5.00	4.00	2.0	10.0	48
10	Northern or Maritime Taiga, Sub alpine	3175	5.00	5.00	2.0	8.0	62
11	Tropical Montane Complexes	394	5.00	5.00	1.0	15.0	28
12	Second Growth Field/Woods (Tropical/Temperate Woods, Fields/Grass/Scrub) 1680		4.00	3.00	2.0	5.0	55,58
13	Succulent and Thorn Woods and Scrub	1350	4.00	3.00	2.0	6.0	59
14	Mediterranean Types & Dry, Highland Woods	1374	4.00	3.00	2.0	8.0	46,47
15	Warm or Hot Wetlands	546	3.00	2.00	1.0	6.0	45,72
16	Paddy land	697	3.00	3.00	2.0	4.0	36
17	Tropical Savanna and Woodland (Interrupted Woods)	2229	3.00	3.00	2.0	5.0	43
18	Shore and Hinterland Complexes	403	3.00	3.00	0.0	10.0	65,66,67,68
19	Other Irrigated Dryland	627	2.00	2.00	1.0	3.0	37,38,39
20	Wooded Tundra	1236	2.00	2.00	1.0	5.0	63
21	Bog/Mire of Cool or Cold Climates	576	2.00	2.00	1.0	6.0	44
22	Heath and Moorland	72	1.50	1.00	1.0	2.0	64
23	Warm or Hot Shrub and Grassland (Marginal Lands)	6400	1.30	0.90	0.5	3.0	41
24	Cool or Cold Farms, Towns	1477	1.00	0.70	0.4	2.0	30
25	Warm/Hot Farms, Towns, Cool Grass/Scrub	5553	1.00	0.80	0.6	2.0	31,40
26	Tibetan Meadows, Siberian Highlands	425	1.00	1.00	0.5	4.0	42
27	Cool Semidesert Scrub	930	0.60	0.60	0.3	1.0	52
28	Tundra, Arctic Desert and Ice	10561	0.50	0.50	0.0	1.2	53,54,69,70
29	Non-Polar Desert and Semidesert, Sparse Vegetation	4070	0.40	0.30	0.2	1.0	51,71,49
30	Non-Polar Sand Desert	1930	0.05	0.05	0.0	0.2	50
31	Water Bodies	172495	0.00	0.00	0.0	0.0	0
32	Antarctica	24964	0.00	0.00	0.0	0.0	17

In the above table, minimum, medium, and maximum carbon densities were taken from Table 5 in Olson *et al.* (1983). The revised medium carbon densities were taken from Table 1 in Olson *et al.* (1985) and were specified by J. S. Olson at the time of publication of Olson *et al.* (1985). "Colour-Id" refers to the World Ecosystem Complexes shown in the figure 1.4.

1.3.2   Carbon fluxes from forests

All forest biomes have undergone major changes in distribution since the last ice age (18000 years ago), when the climate was both cooler and more arid than it is today. Boreal and northern temperate forests were squeezed between advancing ice sheets and steppe tundra from the north and expanding semi-desert and steppe tundra from the south, while tropical rain forests retreated into small pockets as savannah expanded. The amount of carbon stored in terrestrial biomes was 25 to 50 percent lower than at present. Terrestrial carbon storage peaked in the warm, moist early Holocene period about 10 000 years ago and subsequently declined about 200 Gt to reach today's level (2 200 Gt of carbon), probably because of a gradual cooling and aridification of the climate (FAO 2001).

Prior to the nineteenth century humans exerted only a modest influence on terrestrial carbon storage through fire, fuel use and deforestation, but since the outset of the industrial revolution, human activities have had a major effect on the global carbon cycle. Between 1850 and 1980, more than 100 Gt of carbon were released into the atmosphere as a result of land use changes, representing about one-third of the total anthropogenic carbon emission over this period (Houghton 1996) (figure 1.5 - 1.6) though the estimate from different scientists varied slightly (figure 1.7).
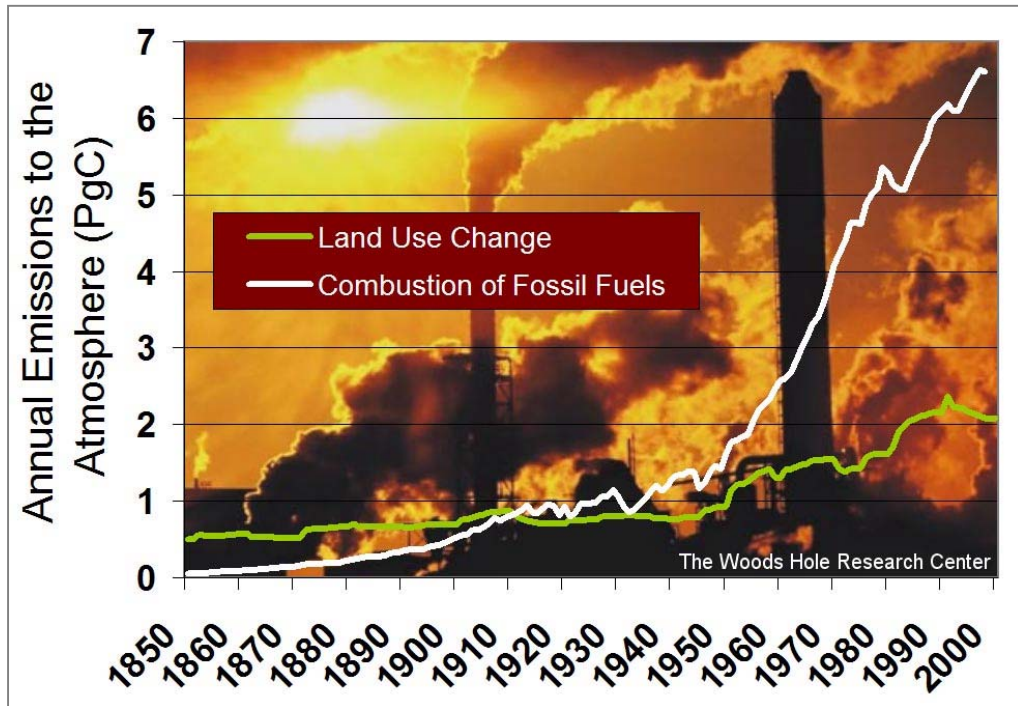
Figure 1.5 Estimated annual global carbon emission from fossil fuel burning and land use change (source: Woods Hole Research Center)
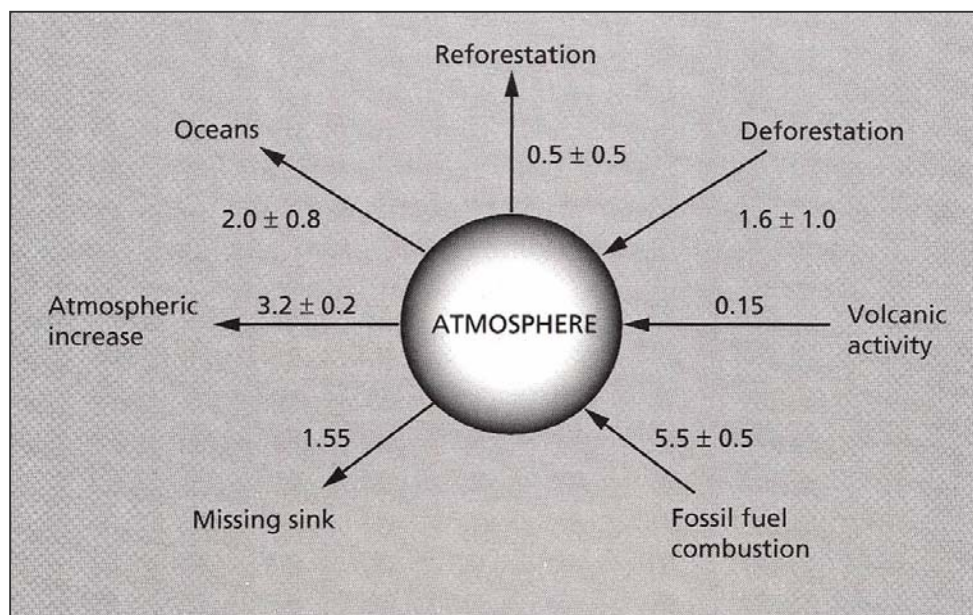
Figure 1.6 Atmospheric budget for carbon showing sources and sinks with estimated fluxes (Gt yr^{-1})[1] (source: Moore *et al.* 1996)

---

[1] The missing sink could be in large part be accounted for by vegetation biomass growth as a result of CO_2 fertilization (estimated at 1.0+0.5) [after Schimel 1995].
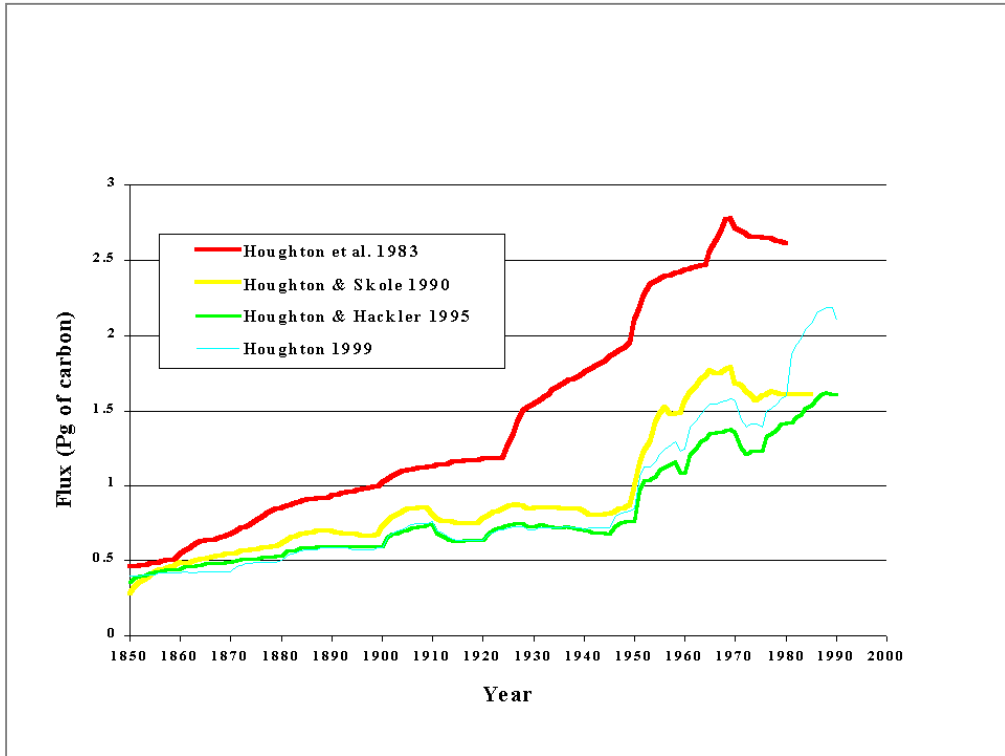
Figure 1.7 Comparison of estimates of net flux of carbon to the atmosphere from land-use changes during 1850 to 1990 (Houghton and Haker 2001).
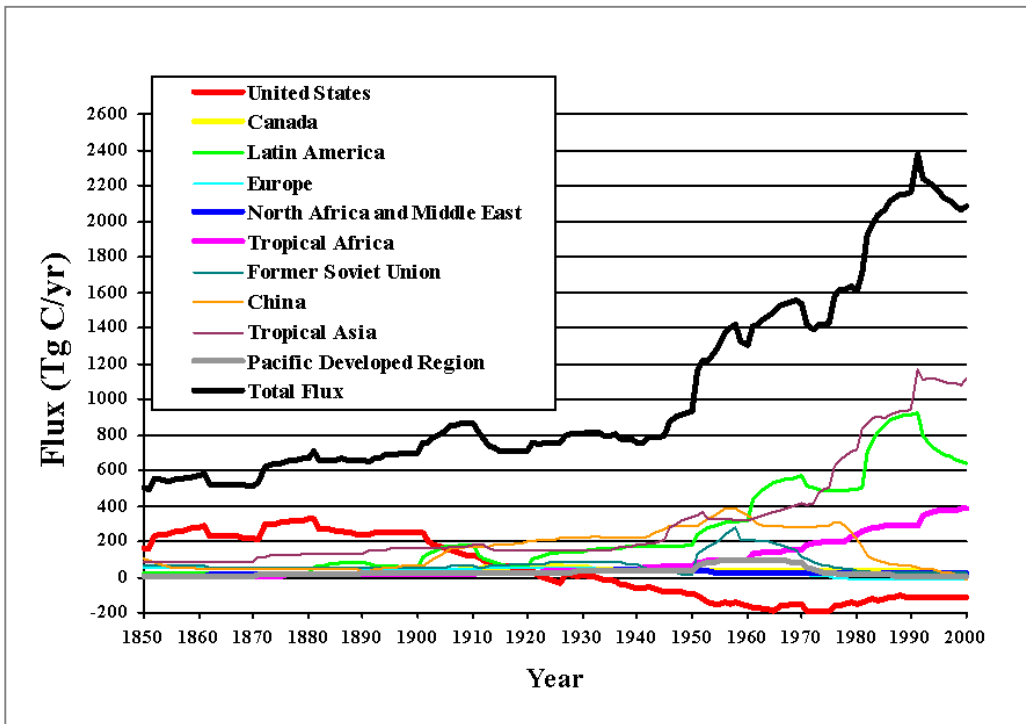
Figure 1.8 Net flux of carbon to the atmosphere from land-use changes, by region, 1850 to 1990 (Houghton and Haker 2002).

12

Until the late nineteenth century most forest clearing and degradation took place in temperate regions. In the twentieth century, the area of temperate forest largely stabilized and tropical forest became the primary source of carbon emissions from terrestrial ecosystems (Houghton 1996) (figure 1.8). Today, forest cover in developed countries is still increasing slightly between 1980 and 1995 there was an average increase of 1.3 million ha per year (FAO 1999). In recent decades, many temperate forest regions (such as Europe and eastern North America) have become moderate carbon sinks through the establishment of plantations, the re-growth of forests on abandoned agricultural lands, and increased growing stock in forests. In contrast tropical forests have become a major source of carbon emissions; the rate of tropical deforestation is estimated to have been 15.5 million per year in the period 1980-1995 (FAO 1999).

The main sources of atmospheric carbon are the burning of fossil fuel (75%) as well as clearing of land (25%) (Miller 1999). The main sinks are the absorption by ocean and terrestrial biosphere (IPCC 1992). One source that is reasonably well documented and therefore can be calculated with some accuracy is the combustion of fossil fuels. For the years 1989-1990 this has been estimated at between 5.5 and 6.0 Gt (IPCC 1992), most of which derived from industrial activity in the northern hemisphere. Obviously, this total varies from year to year.

The net flux of C to the atmosphere from land use change (primarily, though not exclusively due to deforestation in the tropics) depends on the area covered, carbon density per ha, the fate of the altered land and the ecosystem processes that control flux of carbon. The IPCC (1990) estimate the flux in 1980 was 0.6-2.5 GtC, somewhat higher than the 1980 estimate of 0.6-2.5 GtC. The IPCC (1990) estimate of net average annual emissions for the decade 1980-1989 was 1.6 ± 1.0 GtC, which is consistent with Houghton's estimate within the limits of uncertainty (IPCC 1992).

The area of global forests has been declining for centuries and the process has accelerated to an alarming rate within the last half of the 20th century (FAO 1997). Between 1850 and 1980, 15% of the world's forests and woodlands were cleared (Rowe *et al.,* 1992), while 5% were decreased during 1980 - 1995. There was a net increase of 20 million hectares in developed nations while net loss of 200 million hectares in developing countries between 1980 and 1995. The estimate of forest cover change in natural forests of developing countries was an annual loss of 13.7 million hectares (where most deforestation is taking place) between 1990 and 1995, compared with 15.5 million hectares per year over the decade 1980-1990 (FAO 1999). Table 1.4 enumerated the estimate of change of major terrestrial ecosystem and carbon pool since the industrial revolution began.

Table 1.4 Areas and carbon contents of major terrestrial ecosystems in 1850 and 1980 and changes over the 130-year period (Houghton 1996).

Biotic system	Area (10^6 ha)			Carbon content					
	1850	1980	Change	Vegetation (Pg carbon)			Soil (pg carbon)		
				1850	1980	Change	1850	1980	Change
Tropical evergreen forest	608	540	-68	116	100	-15	67	59	-8
Tropical seasonal forest	1,647	1,345	-302	208	173	-36	149	124	-25
Tropical open forest/woodland	420	282	-138	23	5	-8	28	19	-9
Subtotal tropical forests	2,675	2,167	-508	347	288	-59	245	203	-42
Temperate evergreen forest	558	564	6	83	71	-12	73	67	-6
Temperate deciduous forest	461	398	-63	55	41	-14	61	51	-9
Temperate woodland	564	530	-34	15	14	-1	39	37	-2
Subtotal temperate forests	1,583	1,492	-91	153	127	-26	173	155	-17
Boreal forest	1,172	1,167	-4	102	96	-6	240	237	-3
Subtotal all forests and woodlands	5,430	4,827	-603	601	510	-91	657	595	-62
Desert scrub	1,120	849	-271	3	2	-1	65	49	-15
Tropical fallows (shifting cultivation)	199	229	30	8	8	1	17	19	2
Tropical grassland and pasture	459	545	86	8	9	1	20	28	8
Temperate grassland and pasture	2,150	2,010	-140	34	26	-8	310	270	-41
Cultivated, temperate zone	261	762	501	2	5	2	49	105	56
Cultivated, tropical zone	28	417	389	0	4	4	2	24	22
Other[a]	4,080	4,088	8	18	18	0	351	351	0
Total	13,727	13,727	0	673	583	-90	1,471	1,440	-31

[a]Includes tundra, alpine meadow, marsh, rock, ice and sand (Whittaker and Likens 1973, Schlesinger 1984).

The area of the world's forests, including natural forests and forest plantations, was estimated to be 3,454 million hectares that represents about one fourth of the land area of earth in 1995. About 55% of these forests are located in developing countries (mainly tropical and sub-tropical and some temperate countries), with the remaining 45% in developed countries (FAO, 1999). South-Asia contains only 6.07% of the tropical forest area but supports 22% of the earth's population (FAO 1993). Bangladesh is a part of South-Asia that represents 0.05% forest of it (FAO 2000). It is a densely populated country and consequently, its forests are subjected to heavy demanded

pressure in terms of both wood production and competing landuse. Bangladesh has a relatively low proportion of forest cover which is 7% of its total land area (FAO 1997, FAO 1999).

1.4   Methods of Estimating C Flux

The amount of carbon held in the vegetation and soils of terrestrial ecosystems varies spatially and temporally as a result of natural processes and human activities. There are a number of methods exist for measuring the amount of carbon in all components of terrestrial ecosystems, as well as for measuring changes in this amount. The methods vary in complexity, precision, accuracy, and cost. Different methods are appropriate for different pools and components of terrestrial carbon and for different temporal and spatial scales (table 1.5). Methods used to measure carbon, or a change in carbon, are different from those used to attribute cause to an observed change in carbon (e.g., direct human activity versus natural causes). This distinction is important because the protocol is concerned with human-induced, rather than total, changes in carbon. Even the most direct measurements on small plots do not distinguish mechanisms or yield attribution. Attribution must be inferred from controlled experiments or from ecosystem process models that are based on the mechanism responsible for the change (e.g., land-use change versus CO_2 fertilization) (IPCC 2000).

Table 1.5 Characteristics of methods for determining changes in carbon storage (IPCC 2000)

Methods	Scale of Applicability	Time Span	Parameter Assessed	Suitable to Monitor Soils and Additional Activities[1]	Suitable for Full Carbon Accounting	Sampling Density	Costs[2]	Accuracy[3]	Verifiability
Vegetation Inventory	$0.01–10^9$ ha	1–100 yr	Aboveground stemwood volume and increment, harvesting and mortality; derived from whole-tree biomass	Mainly for specific additional measures that impact forest C stock, such as thinning, fertilization, etc.	No—usually excludes soils	Project basis: 400 plots on 5,000 ha; in national-scale inventories: 1 plot represents 1,000 ha	US$ 0.05–0.6 ha^{-1} in national scale inventories; US$11–18 at project levels (10,000 ha)	Area: s.e. = 0.4% Growing Stock: s.e. = 0.7% Increment: s.e. = 1.1% (Tomppo, 1996)	Relatively easy
Soil Inventory	$0.1–10^3$ ha	10–1,000 yr	Soil C stock and changes over time	Yes	Assesses one compartment only	Depending on soil heterogeneity ~300 sample points per 10,000 ha; one sample for every 10-cm depth	US$ 3–20 per sample	2–3% error for analytical precision; total error much higher due to spatial heterogeneity and sampling error	Relatively easy
Eddy Flux	~20 ha	Day – 10 yr	Net Ecosystem Production	For verification only	No—excludes harvesting and decay of wood products	Required sampling density to obtain a large area representative flux must still be determined	US$ 100,000 per site initial costs; US$20,000 yr^{-1} running costs	10–20%	Relatively easy through forest inventory and soil analyses
Flask Measurements	~10^9 ha	Decades	Atmospheric CO_2 concentration	No	No—excludes wood products	Required sampling density to obtain a large area representative flux must still be determined	Unknown	Sample analysis is very accurate	Verification of analysis is relatively easy

Satellite Remote Sensing	0.05–10^9 ha	Day – decades	Area (sometimes derived estimates of biomass and NPP)	Suitable for monitoring, e.g., fire management; in general, all area-related parameters of non-ARD	No, mainly to assess areas	~80 sites in Northern Hemisphere Integral coverage through pixel size	US$ 0.0002 ha$^-$ ^{1} for the picture and same amount for labor to process it; aircraft-derived pictures more expensive	Precise for area measurements (15%); for biomass, less precise	Relatively easy with ground truth data
Ecosystem Modeling	0.1–1 ha	Day – 100s of years	NPP, NEP per compartment	Yes, when management activities can be modeled	Yes, if all components of C cycle are included in model	Usually integral coverage	Cheap once model is developed	Uncertain; subject to many assumptions	Difficult in long term
Biome Models	Grid – 10^9 ha	Day – 100s of years	NPP, NEP per grid	Often soils are included in these	Yes, if all components of C cycle are included in model	Usually integral coverage	Cheap once model is developed	Uncertain; subject to many assumptions	Difficult

1.5   Objective and Research Hypothesis

In the continental and global scale the estimates of C flux, uncertainties exist for all forests but are largest in tropical forests. Many of the temperate or boreal forests are covered by permanent national forest inventories, on relatively homogenous landscapes and currently subject to less modification by humans than the tropical systems (Apps and Kurz 1991, Harmon *et al* 1990, Birdsey *et al* 1993, Birdsey, 1992, Turner *et al.* 1995, Kurz and Apps, 1993, Kurz *et al.* 1992). In the tropics, uncertainties in estimated rates of forest area change (deforestation and reforestation) are high and may vary by 10-30%. Moreover, spatial variation in vegetation C density estimates may be up to 90% of mean values (Brown *et al.* 1991, Brown *et al.* 1989). National forest inventories and continuous forest monitoring systems are not uniformly available, particularly in the tropical nations. Thus, there is no consistent method to measure and detect changes (degradation or accumulation) in the C stored in the forests. Uncertainties in balancing the C flux from forest landscapes will remain until a coordinated global network of permanent forest inventory plots and the application of remote sensing technology to measure changes in area and condition of forests, including 'mature' forest, is undertaken (Dixon *et al.* 1994).

Therefore, the goal of the current study is to develop an operational tool of estimation of carbon pool and any changes in that pool by accumulation or degradation using a low-cost method in the tropical forest ecosystems. The specific objectives of the research are:

(1) Search an optimal method of estimating above-ground carbon pool in a tropical forest ecosystem using remote sensing and *in-situ* measurements.

(2) Estimate the carbon pool and carbon release due to tropical deforestation in a particular test site using the recommended method.

To fulfil the above objectives a number of additional aims have been set. Those include:

(3) Atmospheric correction and radiometric normalization of the remote sensing data sets used in the quantification.

(4) Generation of visual-interpretation key and spectral library for identifying different types of tropical vegetation in the test site.

The approach has coupled remote sensing, geographic information systems (GIS) and *in-situ* measurements by the mathematical and statistical analysis. Following questions need to be investigated to fulfil the above objectives: given that estimates of deforestation and carbon emission rates and how may we improve the accuracy of remote sensing estimates of deforestation and land-use change at the local and regional scales such that the data are more useful both for modelling carbon fluxes and for land-use management?

To get the answer of the above question a general statistical procedures can be followed which will usually examine a hypothesis. The first stage in formulating hypothesis entails stating the initial question as a research or geographical hypothesis. Even when the question arises from empirical observation, such as the apparent tendency of forest to grow and accumulate carbon at early stage of succession or decay and release carbon if there is no human or catastrophic intervention. The second stage of hypothesis formulation involves deriving two statistical hypotheses, which are expressed in terms of operational definitions. These statistical hypotheses are mirror images of each other. One is known as the null hypotheses (H_0) and the other as the alternative hypothesis (H_1). Most investigations require the researcher to the broad geographical question. For example, different stages in the analysis may build on each other, which separate null and alternative hypotheses needed at each point (Walford 1995).

The current study will formulate two sets of null and research hypotheses. The first pair will examine the applicability of remote sensing technology for monitoring the timber stocking and carbon pool in a tropical forest ecosystem. It basically deals with the measurement system and its effectiveness. However, the second pair of hypotheses will be process oriented for particular ecosystem. It is directly related to change in carbon pool over time in a particular study area.

Hypothesis 1:

H_0 : Remote sensing technique supplemented by *in situ* observation can effectively monitor the carbon storage and carbon release from a forest ecosystem. Any significant (can be arbitrarily fixed, for this study 5-10%) change of carbon storage in a forest ecosystem is detectable in a remote sensing image.

This could be expressed in symbol as

H_0: $\overline{x}_{ri}$ equal to $\overline{x}_{ai}$

Where, $\bar{x}_{ri}$ and $\bar{x}_{ai}$ represent the mean carbon content observed by remote sensing supplemented by ground survey and the actual carbon storage at various ecosystems (i = 1 to n) during the recent study year respectively. The alternative hypothesis could be expressed as follows:

H_1 : The difference between the estimated carbon (remote sensing information supplemented by *in-situ* measurements) and the actual carbon content is significantly greater than that would have been expected through the chance of sampling variations alone.

In symbols, this could be stated as

H_1: $\bar{x}_{ri}$ not equal to $\bar{x}_{ai}$

Hypothesis 2:

H_0 : The amount of carbon content (variable X) of different ecosystems over a given time period is the same, irrespective to their density class. Any observed difference in mean carbon pool between the historical and recent time has merely arisen through the chance and is not significant, in spite of change might occur due to forest growth and decay.

This could be expressed in symbol as:

H_0: $\bar{x}_{ci}$ equal to $\bar{x}_{hi}$

Where, $\bar{x}_{ci}$ and $\bar{x}_{hi}$ represent the mean carbon content of different ecosystems (the value of i = 1 to n) at the current and historical study year respectively. The alternative hypothesis could be expressed as follows:

H_1 : The difference between the mean carbon content over a specified period of time is greater than that would have been expected through the chance of sampling variations alone.

In symbols, this could be stated as

H_1: $\bar{x}_{ci}$ not equal to $\bar{x}_{hi}$

The form of H_0 depends on the particular research question under investigation; nevertheless reference can normally be made to some statistical quantity (such as the mean, variance or

standard deviation), to the difference between the observed and expected frequencies, or to an association between two or more attributes or variables (Walford 1995).

The study period deals with the last decade, starting from 1992 to 2001. Landsat ETM+, TM and IRS pan data have been used for this study. Ground survey was conducted by measuring tree *dbh* (diameter at breast height) and height, and then converted to biomass and carbon stocks by allometric relation and using form factor.

Chapter II

2   Quantifying Forest Attribute and Carbon Flux

2.1   Estimating Carbon Stocks using Remote Sensing

2.1.1   Measuring carbon stocks in forest ecosystem

Direct measurement of carbon stocks in forest ecosystem is not a practical approach because it needs destructive sampling, which is rather expensive and time consuming. However, an indirect approach is rather easy to apply. For small-scale ecosystem carbon analysis researchers take samples of the ecosystem components, measure their biomass and carbon content and calculate in per unit area basis.

Even estimating the volume of each component can be resource intensive for sites of significant size, so researchers have developed models that correlate easily observed or measured characteristics of forests to the variables of interest. For example, for a given forest type and age, it is possible to relate a sample measurement of tree diameters on the site in question to the total biomass on the site. One of the simplest forms of forestry models, the allometric model, relates diameter at breast height (DBH) and canopy height to forest biomass.

Carbon models can be developed that express carbon stocks as a function of any number of forest characteristics. A typical carbon model of the carbon content of a forest stand might include some combination of the following independent variables that are listed (NBS 1998, Brown 1996, Brown 1999, MacDicken 1997):

$C = f$ (D, A, L, R, H, O, S, F, P, Cr, B, W)

Where,
C = total carbon in the stand,
D = average tree diameter at breast-height
A = stand age
L = leaf area index
H = canopy height
O = canopy cover
R = total area of the stand
S = stems per unit area
F = forest type
P = species
Cr = crown height

B = bole height

W = crown width

Cl = leaf cluster index

Another challenge in the application of allometric models to carbon stock estimates is that the models can be sensitive to the species composition of the forest, the age and history of the forest, the soil type, climate, and solar exposure. Incorporating these additional factors would require developing more sophisticated carbon models, but the range and combination of independent variables is great (Richards and Anderson 2004).

2.1.2   Remote sensing as a tool of carbon stock estimation in forest ecosystem

Remote sensing instruments can play a significant role in improving the accuracy of national forest inventories, especially if employed early in the monitoring process. Starting the national inventory process by analysing satellite images is both costs saving and accuracy-enhancing. As the technology improves, so will the viability of using a combination of complimentary remote sensing instruments in the estimate of woody biomass stocks and changes. Experimental research on how to combine different technologies and measurement methods can provide useful lessons for other countries that are discussing how to do national inventories of their forest carbon.

Scientists have employed a variety of remote sensing methods that provide data about the type of forest (F), its spatial extent (R), canopy cover (O), canopy height (H), stems per stand (S), Leaf area index (L) and with some instruments even the degree of succession and approximate stand age (A) without the need to dispatch field research teams to measure those parameters. This section examines the tools that are currently available for gathering the data on those forest parameters.

Four major sources of remote sensing data are used to estimate forest structure parameters today: lidar, radar, photogrammetric, and image sensors, respectively. For the purposes of estimating forest structure with adequate accuracy and precision, it is critical to select the proper type of remote sensing data and image processing methods (Adapted from Anon 2002).

2.1.2.1   Very high spatial resolution data

Air photo is an important data source for characterizing forest structural parameters manually and digitally. Multiple-bands digital air-photos of high spatial resolution (< 2m) are capable of estimating stem density and delineating crown, as well as identifying tree species (Sheng *et al.* 2001, Pouliot *et al.* 2002, Huang *et al.* 2001). The tree height information can be gained by processing the stereopair of aerial photos (Gong *et al.* 2002, Sheng *et al.* 2001).

Very high spatial resolution images come from either airborne systems such as CASI (0.25 - 1m multiple bands), AVI (0.3 m), AVIRIS (hyper-spectral sensor, xm multiple bands) and ADAR (xm multiple bands) or space-borne systems like IKONOS (0.82 m pan, 4 m multiple bands) and Quickbird (0.61 - 1 m pan, 2.44 - 4 m multiple bands). High spatial resolution imagery, particularly airborne high spatial resolution imagery, has been extensively used in identifying tree species, reconstructing crown surface, estimating stem density and crown bulk density within last couple of years (Burnett *et al.* 1998, McGraw *et al.* 1998, Heyman, 2000).

Airborne profiling radar and space-boarded synthetic aperture radar (SAR) interferometry data Airborne radar (HUTSCAT) and interferometric SAR (ERS-1/ERS-2) can provide forest structural information in centimeters- to meters-scales. HUTSCAT data have been used to derive tree height profile, while radar interferometric data (C-band and L band) were used in reconstructing crown structure and estimating stem volumes (Hyyppa *et al.* 1996, Hyyppa *et al.* 2000, Santoro *et al.* 2002).

2.1.2.2   High and intermediate spatial resolution data

RADARSAT, SIR-C/X-SAR, JERS, ERS-1/ERS-2 Satellite radars normally provide intermediate spatial resolution data (10 m - 100 m). Radar data have been applied to many forest regions for the purposes of estimating forest structural parameters (Castel *et al.* 2001, Hyyppa *et al.* 2000, Liao *et al.* 1999). SAR imagery has a variety of wavelengths and polarization combinations. Selecting proper combinations of wavelength and polarization is critical to process such datasets successfully. To date, L-band appears to be the best data to derive structural info such as biomass, size of stems and branches, basal area, leaf area index (LAI), tree height, crown closure and crown base height (Castel *et al.* 2001, Fransson and Isrelsson 1999).

Landsat and SPOT images are the most common remote sensing data source for mapping forest structure at regional and landscape scales. With a 10m - 120m spatial resolution range, Landsat and SPOT images normally need ground truthing or high spatial resolution data as training datasets to yield models. Recently, there is a significant trend in remote sensing of forest structure analysis in which Landsat or SPOT data are used in conjunction with Lidar or air-photo high spatial resolution imagery to map regional- and landscape-scales forest structures (Sabol *et al.* 2002, Hudak *et al.* 2002).

Remote sensing instruments, extractable information, their advantages and disadvantages are summarized in table 2.1.

Table 2.1 Summary of Remote Sensing Instruments: Advantages, disadvantages and extractable information (Richards and Anderson 2004).

Remote sensing instruments	Advantages	Disadvantages	Extractable information
Optical: Aircraft	Detailed images Flexibility in geographic targets	Small area Expensive Sensitive to daylight and cloud cover	Canopy height (H) Canopy cover (O) Total area of stand (R)
Optical: Satellite (high resolution)	Detect small (15 m) changes in land use and deforestation with ETM+ panchromatic Frequent global coverage (weekly to semi-monthly) Long historical record of global images (early 1970s) Multi-angle sampling can characterize forest structure	Sensitive to daylight and cloud cover Insensitive to differences in dense biomasses	Canopy cover (O) Leaf area index (up to level of 3 or 4) (L) Total area of stand (R) Leaf cluster index (Cl)
Optical: Satellite (coarse resolution)	Detect trends at the continental and global scale Very frequent global coverage (daily to weekly) Long historical record of global images (early 1970s)	Sensitive to daylight and cloud cover	Total area of stand (R)
Synthetic Aperture Radar	Not dependent upon daylight or cloud cover Use of multiple polarization can increase measurable density to 400 tonnes per hectare	Saturation at relatively low levels of biomass density Only used on relatively flat topography	Canopy height (H) Total area of stand (R) Forest type (F) Leaf area index (L) Branch surface to volume ratios
Synthetic Aperture radar (VHF)	Not dependent upon daylight or cloud cover Measures biomass density up to 1000 tonnes per hectare	Airplane deployment only Only used on relatively flat topography	Canopy height (H) Total area of stand (R) Forest type (F) Leaf area index (L) Branch surface to volume ratios
LIDAR	Characterizes 3-D structural characteristics of forests Useful in steeply sloped areas	Airplane deployment only Narrow coverage with each pass	Leaf area index (L) Canopy height (H) Canopy cover (O) Stems per unit area (S) Bole height (B) Crown width (W)

2.1.3   Spectral reflectance properties of vegetation and forest canopies

Reflectance properties of vegetation depend upon the wavelength region. Plants pigments, primarily chlorophyll a, chlorophyll b, xanthophylls and carotenes, are the main pigments, which influence reflectance and absorption of radiation in the visible region (400-700 nm) of spectrum. The main chlorophyll absorption bands are cantered at approximately 480 and 680 nm. Several

other chloroplasts (carotenes, xanthophylls and anthocyanins), which contain no chlorophyll, exhibit a green reflectance peak at about 550 nm. That absorption in the blue and red regions of the visible spectrum is comparatively greater than in the green region causes leaves appear to green (Murtha 1997). Many published spectral reflectance curves of stressed vegetation show a reflectance increase (red rise) at about 633 nm. The red edge is the sharp change in leaf reflectance, which occurs in the 680-to 750 nm range of the spectrum (Horler *et al*. 1983).

High reflectance in the NIR plateau (700 – 1100 nm) is primarily due to multiple refractions occurring at the interface of hydrated cell walls with intercellular spaces, as a result of different refraction indices (Gaters 1970, Wooley 1971, Kumar and Silva 1973, Gausman 1974). Chlorophyll does not reflect and is transparent to NIR radiation (Coblentz and Stair 1929). NIR wavelengths are relatively long and thus are not scattered by the chlorophyll. Gausman (1977) reported that leaf components including stomata, nuclei, cell walls, crystals and cytoplasm, directly contribute a small percentage of reflectance within the 700 to 1100 nm range.

Spectral characteristic of vegetation in the short wave infrared region, SWIR (1100 to 2100 nm) are dominated by absorption of energy by liquid water within leaves (Gates 1970, Knipling 1970, Myers *et al.* 1970). Strong water absorption bands occur at 1450 and 1900 nm (Gaters *et al.* 1965, Gausman *et al.* 1969, Knipling 1970, Wooley 1971) and according to Tucker (1980), the 1650 to 2200 nm region can provide an indication of leaf water content.

Spectral reflectance of vegetation canopies is modified from those of individual leaves due to natural variations in leaf orientation, solar and viewing geometries, and background element characteristics. Colwell (1974), Jarvis *et al.* (1976), Curran and Milton (1983) and Goel (1988) have discussed these effects. Reflectance from a plant canopy with many leaves and branches, often in several layers, as its own particular characteristics, which include volume reflectance and included or contained shadows. However, the spectral reflectance of a forest curve of a forest canopy has more variability as compared to other types of vegetation communities, such as agricultural croplands and rangelands, because of the in homogeneity and complexity in the structure of forests (Lee 1990).

Krinov (1947) used an aerial photographic method to determine the spectral reflectance of forest canopies. He reported reflectance from continuous broad-leaved canopies near 5 to 35 percent in the visible and NIR, respectively. This is less than the reflectance of individual leaves, which have corresponding values nearer 10 and 45 percent. These lower reflectance values result from shadows contained within the canopy. Reflectance from a plant canopy depends upon the total leaf area, canopy geometry, and absorption and scattering coefficients (optical properties) of leaves.

Natural variations in spectral reflectance patterns for a given plant species are associated with the species phenotype and genotype, leaf morphology, leaf development, structural differences, foliage age (changes through the growing season), leaf senescence, and plant maturity. External environmental factors including soil, site, latitude, altitude, atmospheric attenuation of incident energy, and stress- both biotic (insects and disease) and abiotic (fire, moisture, atmospheric depositions, acid rain, air pollution, etc.)-also affect the reflectance. These natural factors may cause the spectral reflectance to increase or decrease, the red rise to fluctuate, and the red edge to shift (Murtha 1997).

2.2   Remote Sensing Image Pre-processing

2.2.1   The effect of the atmosphere on radiation

The presence of the atmosphere as a transmission medium through which radiation must travel from its source to the sensors as well as instrumentation effects can result in two broad types of radiometric distortion. First, the relative distribution of brightness over an image in a given band can be different to that in the ground scene. Secondly, the relative brightness of a single pixel from band to band can be distorted compared with the spectral reflectance character of the corresponding region on the ground.

The sun, as a source of energy emits a given rate of Joule per second, or Watts. At a given distance, the sun's emission can be measured as Watts per square meter. This power density is so called irradiance and can be used to describe the strength of an emitter of electromagnetic energy. We can measure a level of solar irradiance at the earth's surface. If the surface is perfectly uniform then this amount is scattered diffuse into the upper hemisphere. The amount of power density scattered in a particular direction is defined by its density per solid angle, since equal amounts are scattered into equal cones of solid angle. This amount is called radiance and has units of Watts per square meter per steradian [$W\ m^{-2}\ sr^{-1}$]. Spectral irradiance is used to describe how much power density is available incrementally across a wavelength range. Due to absorption and scattering only a fraction of the incoming solar radiation reaches the ground, the direct irradiance**.**

We can measure a level of solar irradiance at the earth's surface. If the surface is perfectly diffuse then this amount is scattered uniformly into the upper hemisphere. The amount of power density scattered uniformly into the upper hemisphere. The amount of power density scattered in a particular direction is defined by its density per solid angle. This quantity is called radiance and has units of Watts per square meter per steradian ($Wm^{-2}sr^{-1}$)

Absorption by atmospheric molecules is a selective process that converts incoming energy into heat. In particular, molecules of oxygen, carbon dioxide, ozone and water attenuate the radiation very strongly in certain wavebands. Sensor commonly used in solid earth and ocean remote sensing is usually designed to operate away from these regions so that the effects are small. Scattering by atmospheric particles is then the dominant mechanism that leads to radiometric distortion in image data (apart from sensor effects) (Richards and Jia 1999).

There are two broadly identified scattering mechanisms. The first is scattering by the air molecules themselves. This is called Rayleigh scattering and is an inverse fourth power function of the wavelengths used. The other is called aerosol or Mie scattering and is a result of scattering of the radiation from larger particles such as those associated with smoke, haze and fumes. These particulates are of the order of one-tenth to ten wavelengths. Mie scattering is also wavelength dependents, although not as strongly as Rayleigh scattering. When the atmospheric particulates become much larger than a wavelength, such as those common in fogs, clouds and dust the wavelength dependence disappears (Richards and Jia 1999).
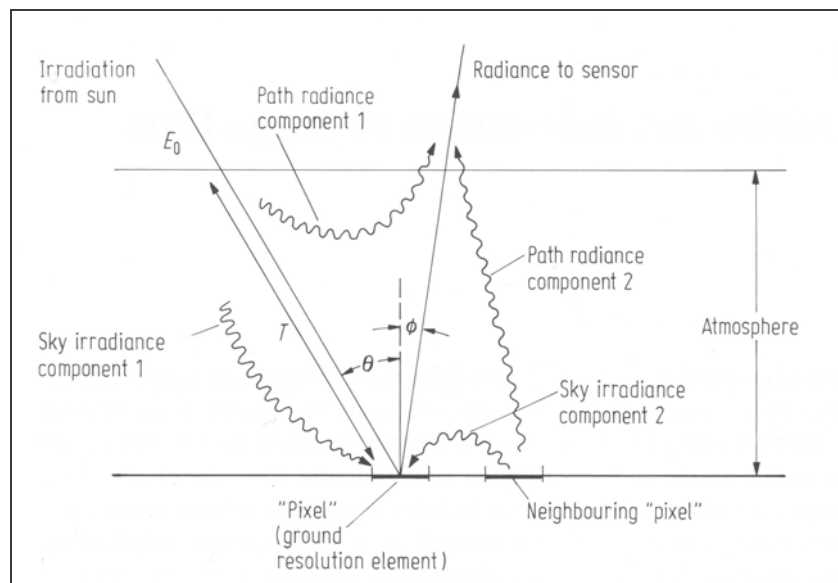
Figure 2.1 Effect of atmosphere in determining various paths for energy to illuminate a (equivalent ground) pixel and to reach the sensor

Figure 2.1 presents the atmospheric effects and the radiance that ultimately reach to the sensor. Some of the scattered photons contribute to the illumination of the target by means of scattered paths and compensate for attenuation of the direct solar path. This is called sky irradiance. Path radiance is a part of incoming solar radiation, which is backscattered towards the sensor without

reaching the ground. It does not carry information about the target and blurs the satellite signal. Some of the photons reaching the sensor are reflected from objects adjacent to the target under consideration due to the scattering effect on the path target-sensor; as long as the surface is homogeneous, it is a useful component but if the surface has a patchy structure, this term will introduce a perturbation. It is called trapping effect when photons which interact multiple times with atmosphere and ground contribute to the image. After one or two interactions, the phenomenon can be neglected.

Atmospheric radiance is defined as the photons scattered by the atmosphere alone. It could be computed over a black uniform surface. Background radiance is defined as the photons reflected by the background surface of a given pixel of small size and then scattered by the atmosphere towards the sensor. Thus, it depends upon surface and atmospheric properties.

Only a fraction of the photons coming from the target reaches the satellite sensor so that the target seems less reflective. Transmittance describes the amount of ground reaching irradiance relative to that for no atmosphere. Transmittance depends on the zenith angle of the source. The bigger the zenith angles the longer the path length through the atmosphere. Upward transmittance is the way between the point of reflection and sensor called.

2.2.2   Computation of haze

Several different atmospheric scattering or haze removal techniques have been developed for use with digital remotely sensed data. Many of these techniques can be grouped into a simple dark-object subtraction method (Vincent 1973, Rowan *et al.* 1974, Chavez 1975). Many haze correction techniques involve subtracting a constant DN value from the entire digital image, assuming a constant haze throughout the image. Subtracting a single value from the entire image gives a first order correction, which is better than no correction, because it removes the major effect of the additive scattering component. A different constant must be used for each spectral band, with a different set of constants used from image to image. However, using a uniform correction for the entire image will leave local errors due to non-homogeneity in the atmosphere.

The atmosphere affects remote sensing images by scattering, absorbing and refracting light. Often, the most dominant of these effects is scattering (Siegel *et al.* 1980, Slater *et al.* 1983). A method developed by Chavez (1988) to correct for the additive component of atmospheric scattering uses a relative power law model to predict the haze values for the multispectral bands based on a starting band haze value selected by the user. In this stand-alone method the user selects a starting band

dark-object subtraction haze value, typically using the histogram of band 1 or 2. The method then utilizes a relative power law scattering model that represents the atmospheric conditions at the time of data collection. The amplitude of the starting haze value is used as a guide to identify the type of atmospheric conditions that existed during the time the data were collected. Using the information supplied by Curcio (1961) and Slater *et al.* (1983), and extrapolating to very clear and very hazy atmospheres, one possible set of relative scattering models are enumerated in table 2.2.

Table 2.2 Relative atmospheric models for variable atmospheric condition

Atmospheric conditions	Relative Scattering Model
Very clear	$\lambda^{-4.0}$
Clear	$\lambda^{-2.0}$
Moderate	$\lambda^{-1.0}$
Hazy	$\lambda^{-0.7}$
Very Hazy	$\lambda^{-0.5}$

In this study, the starting haze value was selected from the image DN values using the histogram/dark-object method. If a valid dark object does not exist in the image, an iteration process can often be used to generate more acceptable values. This is done by iteratively using a lower starting haze value until no over corrections occurs. That is, if a starting haze value results as the predicted values for other bands that are higher than some of the actual image DNs, a lower starting haze value must be used. Also, a completely black or zero reflectance surfaces usually does not exist and a minimum reflectance value of 1 or 2 percent is more realistic (Chavez 1989).

2.2.3 Dark Subtraction

It is assumed that each band of data for a given scene should have contained some pixels at or close to zero brightness value. It is also supposed that atmospheric effects, and especially path radiance, have added a constant value to each pixel in a band. Histograms taken of each band outlines that the lowest significant occupied brightness value will be non-zero as shown in figure 2.2. Correction amounts first to identifying the amount by which each histogram is "shifted" in brightness away from the origin and then subtracting the amount from each pixel brightness in that band. The method causes a lightning of the image. Every band is shifted with a different value, so one wants to correct the bands relative to each other. The dynamic range of image intensity is improved. In literature this procedure is also called haze removal, because the subtracted values displayed look like whitish-bluish haze.
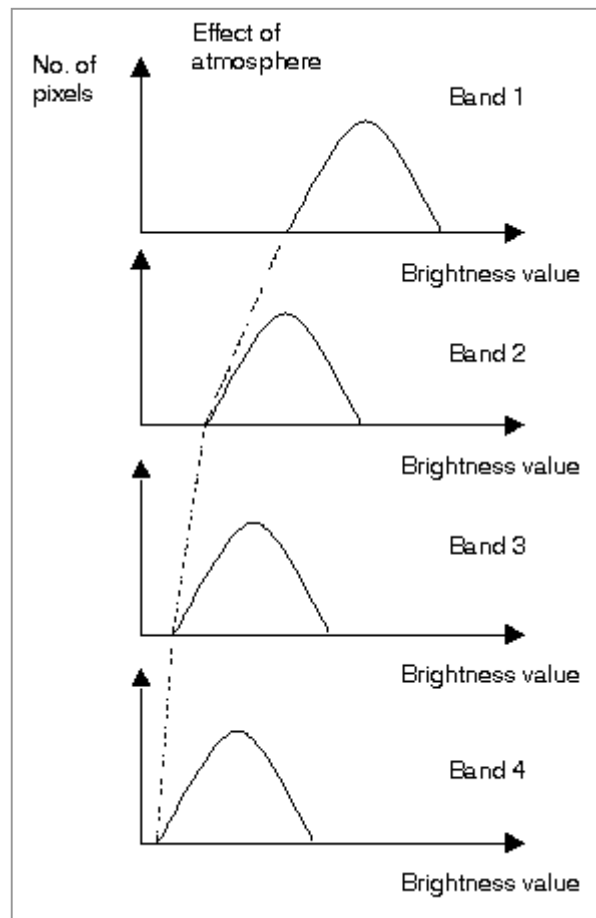
Figure 2.2 Illustration of the effect of path radiance, resulting from atmospheric scattering on the four histograms of Landsat MSS image data (Richards and Jia 1999).

The electromagnetic radiation signals collected by satellites in the solar spectrum are modified by scattering and absorption by gases and aerosols while travelling through the atmosphere from the earth surface to the sensor. Each image has to go through a pre-processing step in which correction for atmospheric effects is often a primary task before classification and change detection analysis can be applied. Landsat TM/ETM+ sensors have spectral bands placed in portions of the spectrum relatively unaffected by gases absorption in the atmosphere, and the gases scattering, or Rayleigh scattering, can be well characterized. However, scattering and absorption by aerosols are difficult to characterize due to their variation in time and space (Kaufman 1993), thus constituting the most sever limitation to the radiometric normalization of satellite data (Coppin and Bauer 1994, Laing *et al.* 1997).

The interaction of solar radiation with atmosphere has been well characterized by Chandrasekhar (1960). A number of radiative transfer codes (RTCs) based on radiative transfer theory have been

developed to correct for atmospheric effects in satellite images (for example, Kneizys *et al.* 1988, Haan *et al.* 1991, Vermote *et al.* 1997). Studies have shown that these radiative transfer codes can accurately convert the satellite measurements to surface reflectance (Holm *et al.* 1989, Moran *et al.* 1992). However these corrections require accurate measurements of atmospheric optical properties at the time of image acquisition. These measurements are frequently unavailable or of questionable quality, which makes routine atmospheric correction of images difficult with RTCs. Many applications of remote sensing have to rely on algorithms that utilize information derived from the image itself to correct the atmospheric effects (Song *et al* 2001).

Depending on the application, atmospheric correction can either be absolute, where a digital number is converted to surface reflectance, or relative, where the same digital number (DN) values in corrected image represents the same reflectance, irrespective of what the actual reflectance value may be on the ground (Chavez and Mackinnon 1994)

For many applications involving image classification and change detection, atmospheric correction is unnecessary. A typical example of a remote sensing application for which atmospheric correction is not necessary is image classification with a maximum likelihood classifier using a single date image. As long as the training data and image to be classified are on the same relative scale (corrected or uncorrected), atmospheric correction has little effect on classification accuracy (Potter 1974, Fraser *et al.* 1977, Kawata *et al.* 1990) For Landsat TM/ETM+ data the dominant atmospheric effect is scattering which is additive to the remotely sensed signals, while multiplicative effect from absorption is often neglected because the TM/ETM+ bands were selected to avoid effects due to absorption. Thus atmospheric correction for a single date image is often equivalent to subtracting a constant from all pixels in a spectral band. Such correction is essentially nothing but translating the origins in multidimensional space as illustrated in figure 2.3. Although the means of the classes change, the variance-covariance matrix remains the same regardless of correction. The unnecessary nature of atmospheric correction on classification with single date image can be extended to post classification change detection (Singh 1989) where multiple images are classified individually and the resulting maps are compared to identify changes (Foody *et al.* 1996). Similarly, atmospheric correction is also unnecessary for change detection based on classification of multidate composite imagery in which multiple dates of remotely sensed image are rectified and placed in single dataset, and then classified as if it were a single date image. In essence, as long as the training data are derived from the image being classified, atmospheric correction is unnecessary (Song *et al.* 2001).
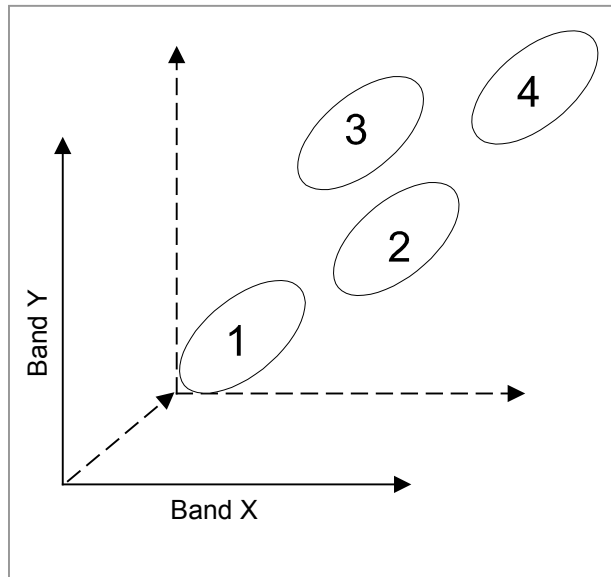
Figure 2.3 Subtracting a constant from a band is equivalent to translate the origin of the data set. It has no effect on the variance-covariance matrix for the classes of interest. Thus dark object subtraction for single date image has no effect on classification results.

2.2.4 Data normalization

Variations in solar illumination conditions, atmospheric scattering, atmospheric absorption and detector performance results in differences in radiance values unrelated to the reflectance of the land surface. Given sufficient time and resources, it would be possible to model or calibrate each of these effects and generate corrected multi-spectral data sets for use in the analysis of land cover change. Radiometric data normalization represents a first order data transformation approach used to reduce the variability between multi-temporal datasets acquired over the same geographic area. The process substantially reduces or normalizes the inter-scene variability resulting from different atmospheric conditions, radiation incidence angle, and detector disparity. Relative radiometric normalization uses one image as a reference (Hall *et al.* 1991). Among the most commonly used radiometric normalization techniques are (a) pseudovariat features (Schott *et al.* 1988), (b) dark-pixel subtraction (Gonima 1993) and (c) relative radiometric normalization (Elvidge *et al.*, 1995).

When performing multi-temporal image analyses, radiometric corrections are required because of the following atmospheric effects (Lunetta 1999):

1. Modifications of the spectral and spatial distribution of the radiation incident on the earth surface.

33

2. Attenuation of the radiation reflected by the surface

3. Addition of path radiance

Accordingly, multi-temporal analysis approach necessitates corrections for the variations in atmospheric conditions, which affect the transmittance of surface reflected radiance. For example, in two TM images collected 16 days apart, a resultant 6° change in solar elevation was sufficient to prevent accurate radiometric comparisons of steeply sloping areas (Thomson 1992). As a first approximation, radiometric normalization can be applied to minimize the above atmospheric effects (Maracci and Aifadopoulou 1990).

Additionally, variations across identical sensors also contribute to radiometric discontinuity. For example, although the Landsat 1-4 MSS and Landsat 4-5 TM sensors are essentially identical among platforms, their spectral characteristics vary slightly. In a study conducted by Markham and Baker (1983), the spectral variation between the Landsat MSS sensor's spectral responses ranged from 3.0 to 10.0 percent in the red band (0.6-0.7 μm) and 3.0 to 11.0 percent in the near-IR band (0.7-0.8 μm). Because the Landsat MSS and TM sensors have no onboard calibration systems, there are uncorrected differences between data collected by different sensors (e.g., Landsats 1-5). Drift in radiometric performance also occurs over time (Elvidge *et al.* 1995). The spectral variations between identical sensors can be minimized by using a first approximation radiometric normalization correction.

The current study followed the modified dark-object subtraction technique of Chavez (1988, 1989). The method is quite useful, especially when the absolute atmospheric parameters are not available. To account for slope and aspect related illumination differences, topographic corrections can be applied to the atmospherically corrected radiance values of each band based on methods reported by Smith *et al.* (1980). However, the current study has excluded the topographic normalization due to lack of appropriate digital elevation model available for the study area.

2.3   Remote Sensing Image Interpretation

2.3.1   *Elements of visual interpretation*

The six primary elements of visual interpretation are tone or colour, size, shape, texture, shadow and pattern (Estes and Simonett 1975). In addition of those height, size and association may be added (Howard 1970). Tone refers to the relative brightness or colour of objects on imagery. Size, shape and position (site), are combined under the term contextual information. Size of the object

often help to identify it, which includes the recognition of old over-mature trees, maturing trees, saplings, seedlings and shrubs on an image. Shape relates to the configuration or the general outline of objects as recorded on imagery. Man-made feature sometimes follow a regular boundary, but the natural features usually follow natural boundary. Site refers to topographic or geographic location and is a particular important aid in the identification of vegetation types. Texture is the frequency of tonal change on the photographic image. It determines the overall visual 'smoothness' or 'coarseness' of image features. On a satellite image, presence of shadow within a particular pixel reduces the reflectance and might cause problems for accurate interpretation. Pattern relates to the spatial arrangement of objects. Association refers to the occurrence of certain features in relation to others. The shape, tone, pattern, texture, area, height and/or site are associated with a class of object not recorded or not clearly recorded on the imagery. Studying one or more of these image characteristics, which have been observed to be associated with the object not clearly seen on the imagery, enables the latter to be evaluated (Lillesand and Kiefer 2000, Howard 1991).

2.3.2   Visual-interpretation keys

On a SPOT false colour composite natural forest, bamboos, scattered trees, brush, plantation, reed forest could be identified in northeastern Bangladesh (Arquero 1997). The principal Dipterocarp (Garjan) could be easily distinguish on 1:20,000 scale photographs because of its characteristic crown in southeastern Bangladesh (Zahir-ud-Din 1954). In Thailand, one dipterocarp (Yang) could be distinguished because of its large crown and bright shining leaves. On 1:50,000 scale aerial photographs covering moist tropical forest of Kerala and Tamilnadu, India, the following forest cover and land use types were delineated: tropical evergreen, tropical semi-evergreen, moist deciduous, dry deciduous, teak plantation, eucalyptus plantation, reeds, bamboos, rubber plantations and tea estates (Tomar 1968). In tropical moist deciduous and tropical dry deciduous forests of Bastar region (India) the following forest cover types could be interpreted on 1:15,000 scale aerial photographs: sal, teak, young plantation and regeneration areas, scattered bamboos, medium and dense bamboos, regrowth on abandoned shifting cultivation areas, scrub lands and degraded forest, shifting cultivation and grass lands (Tomar 1970).

An image-interpretation key is a set of guidelines used to assist interpreters in rapidly identifying features on a remote sensing image. Depending on the method of presenting diagnostic features, image-interpretation keys may be grouped into two classes: selective keys and elimination keys. Selective keys are usually made up of typical illustration and descriptions of objects in a given category. In contrast, elimination keys require the user to follow a step-by-step procedure, working form the general to the specific. One of the more common forms of elimination keys is the dichotomous type. Here, the interpreter must continually select one of two contrasting alternatives until he or she progressively eliminates all but one item of the category, which is correctly describing the feature under investigations (Avery and Berlin 1992).

Following the above principles several interpretation keys have been developed both for tropical and temperate forests based on aerial photographs, satellite and radar imagery. For example, selective interpretation keys were developed for tropical woodland of Tanzania (Howard, 1959), and for coniferous and hardwoods of Middle-European trees (Grundman 1984, Anthony 1986 modified by Hildebrandt 1996).

2.4 Remote Sensing Image Processing

An important part of image analysis is identifying groups of pixels that have similar spectral characteristics and to determine the various features or land cover classes represented by these groups. This form of analysis is known as classification. Visual classification relies on the analyst's ability to use visual elements (tone, contrast, shape, etc) to classify an image. Digital image classification is based on the spectral information used to create the image and classifies each individual pixel based on its spectral characteristics. The result of a classification is that all pixels in an image are assigned to particular classes or themes (e.g. water, coniferous forest, deciduous forest, corn, wheat, etc.), resulting in a classified image that is essentially a thematic map of the original image. The theme of the classification is selectable, thus a classification can be performed to observe land use patterns, geology, vegetation types, or rainfall.

The analyst classifying an image must distinguish between spectral classes and information classes. Spectral classes are groups of pixels that have nearly uniform spectral characteristics. Information classes are the various themes or groups the analyst is attempting to identify in an image. Information classes may include such classes as deciduous and coniferous forests, various agricultural crop types, or inland bodies of water. The objective of image classification is to match the spectral classes in the data to the information classes of interest.

Though any image can be classified, multispectral imagery tends to be used most often. One band classification is usually very difficult to classify since more than one surface type will exhibit the same digital number. Thus, any spectral classes in a single band classification will likely contain several information classes, and distinguishing between them would be difficult. Normally two or more bands are used for classification, and their combined digital numbers are used to identify the spectral signatures of the spectral classes present in the image. The more bands used to create a classification, the more likely the analyst will get a set of unique land cover classes.

2.4.1 Supervised classification

A classification process in which an image is separated into a number of information classes based on the statistical characteristics of training areas outlined by the operator. The process of assigning each pixel in an image to one of a number of classes (ground cover types etc.), by comparing the properties of the pixels (training data) known to belong to the various classes. The properties (features) of a pixel can be specified by a vector x in N-dimensional feature space. The components of this vector will often be the digital numbers or reflectance in each of N spectral bands, but could also be, for example, radar backscatter coefficients in different polarization states, texture parameters, or single-band digital numbers in a multi-date composite image. For forest stratification the procedure might play an important role as the operator can assign different types of forest specially when track is sufficiently large and homogeneous.

2.4.2 Vegetation indices

The use of a vegetation index has two primary advantages over the use of raw data: 1) providing a continuous measure of green biomass over a large geographic area and 2) the relative calibration effect of eliminating different solar angle effect effects between scenes. However, in general, the use of vegetation indices has been limited to areas of grasslands and agricultural lands (Lee 1990).

Although numerous researchers have reported on the use of a vegetation index for assessment of green biomass over large geographical areas of grasslands and agricultural areas where foliage is the primary component of biomass, there have been relatively few studies using the vegetation index in forested areas. In coniferous forests, the ratio of red and near infrared bands exhibits positive correlations with leaf are index (Peterson *et al.* 1987). Sader *et al.* (1989) studied the feasibility of detecting tropical forest successional age class and total forest biomass by using the normalized difference vegetation index derived from Landsat TM data. They concluded that the vegetation index did not work well for estimating forest biomass. Considering that the major portions of forest biomass are occupied by woody components, such as branches and stems, it is not surprising that the vegetation index derived from the optical data is not as good a predictor for forests as it is with areas of grasslands and croplands (Lee 1990).

Vegetation indices are mathematical transformations design to assess the spectral contribution of vegetation to multispectral observations. The most widely used green vegetation indices are formed with data from discrete red and infrared (NIR) bands. These vegetation indices operate by contrasting intense chlorophyll pigment absorptions in the red against the high reflectivity of plant materials in the NIR (Tucker 1979). The value of these vegetation indices lies in their potential use

to estimate vegetation variables such as percent green cover, Leaf Area Index (LAI) or absorbed Photosynthetically Active Radiation (APAR), which in turn can be used to analyse such as Net Primary Productivity and evapotranspiration.

The vegetation indices developed in the 1970s are based on discrete red NIR bands, and can be generally divided into two basic categories: ratios and orthogonal indices. The ratio-based indices include the Ratio Vegetation Index (RVI) and the Normalized Difference Vegetation Index (NDVI). More recently a hybrid set of vegetation indices have emerged, such as the Soil Adjusted Vegetation Index (SAVI). Selected vegetation indices were calculated from Landsat image bands using the equations enlisted in table 2.3 (Chen *et al.* 1999 and Murtha 1997).

Table 2.3 Vegetation indices formulas

Abbreviation	Name	Vegetation index	Reference
NDVI	Normalized difference vegetation index	(NIR – RED) / (NIR + RED)	Rouse *et al.* (1973)
RVI	Ratio vegetation index	NIR / RED	Jordan (1969)
SAVI	Soil adjusted vegetation index	(NIR – RED) (I + L*) / (NIR + RED + L)	Heute (1988)
DVI	Difference vegetation index	NIR – RED	Tucker (1979)
TVI	Transformed Vegetation Index	SQRT[{Blue/(Blue+Green+Red)}+0.5]	Rouse *et al.* (1973)
PVI	Perpendicular Vegetation Index	[-0.8736(Red)+0.4866(NIR)]	Richardson *et al.* 1983

* The L term (soil adjustment factor) ranges form 0 to 1 and is typically set to 0.5.

2.4.3   Tasseled cap based

Tasseled cap transformation (Crist and Kauth 1986) developed by Kauth and Thomas (1976) is a means for highlighting the most important (spectrally observable) phenomena of crop development in a way that allows discrimination of specific crops from other vegetation cover, in Landsat multitemporal, multispectral imagery. Its basis lies in an observation of crop trajectories in an observation of crop trajectories in band 6 versus band 5, and band 5 versus band 4 subspaces (Figure 2.4 - 2.5).
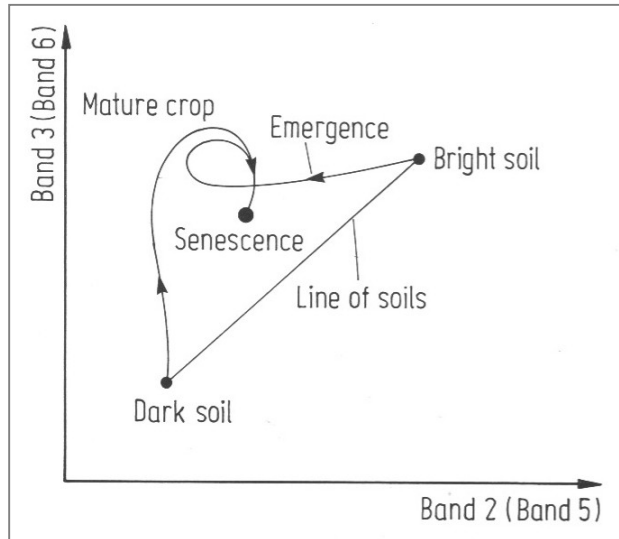
Figure 2.4 Band 6 versus band 5 Landsat multispectral scanner subspace showing trajectories of crop development (Richards and Jia 1999)
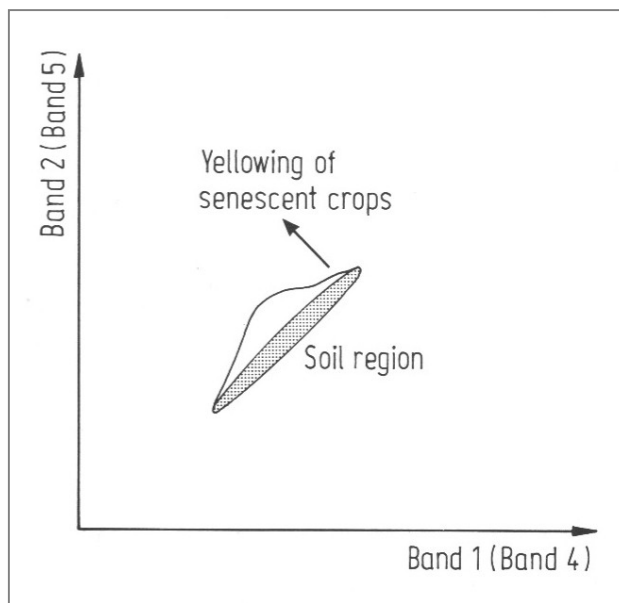
Figure 2.5 Band 5 versus band 4 subspace also depicting crop development (Richards and Jia 1999)

A first observation that can be made is that the variety of soil types on which specific crops might be planted appear as points along a diagonal in the band 6, band 5 spaces as shown. This is well known and can be assessed from an observation of the spectral reflectance characteristics for soils. Darker soils lie nearer the origin and the lighter soils at higher values in both bands. The actual slope of this line of soils will depend upon global external variables such as atmospheric haze and soil moisture effects. If the transformation to be derived is to be used quantitatively these effects need to be modelled and the data calibrated or corrected beforehand.

Consider now the trajectories followed in the band 6 versus band 5 subspace for crop pixels corresponding to growth on different soils- in this case take the extreme light and dark soils as depicted in figure. For both regions at planting the multispectral response is dominated by soil types. As the crops emerge the shadows cast over the soil dominate any green matter response. As a result there is considerable darkening of the response of the lighter soil crop field and only a slight darkening of that on dark soil. When both crops reach maturity their trajectories come together implying closure of the crop canopy over the soil. The response is then dominated by green biomass, being in a high band 6 and low band 5 region, as is well known. When the crops senesce and turn yellow their trajectories remain together and move away from the green biomass point in the manner depicted in the diagram. However whereas the development to maturity takes place almost totally in the same plane, the yellowing development in fact moves out of this plane, as can be assessed by how the trajectories develop in the band 5 versus band 4 subspace during senescence as illustrated in figure 2.5.

Figure 2.4 and 2.5 can be combined into a single three dimensional version in which stages of crop transectories can be described according to the parts of a cap, with tassels, from which the name of the subsequent transformation is derived (Figure 2.6). The behaviour observable in that figure led Kauth and Thomas to consider the development of a linear transformation that would be useful in crop discrimination.
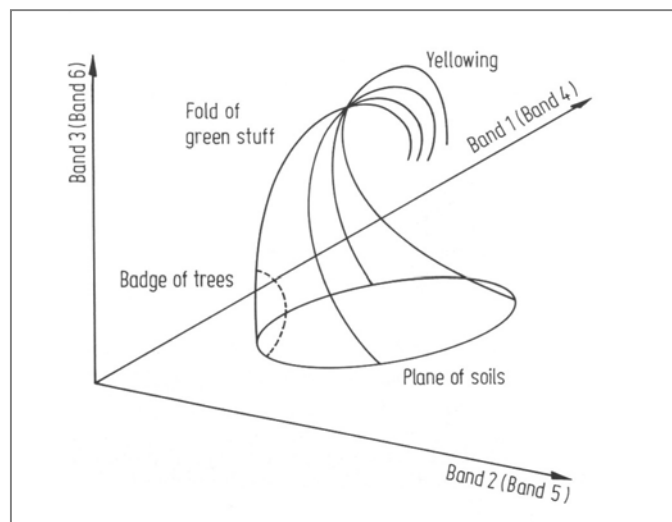
Figure 2.6 Crop trajectories in Landsat multispectral scanner band 4, 5, 6 spaces, having the appearance of a tasselled cap (Richards and Jia 1999)

Three major orthogonal directions of significance in agriculture can be identified. The first is the principal diagonal along which solid are distributed. This was chosen by kauth and Thomas as the first axis in the tasselled cap transformation. The development of green biomass as crops move towards maturity appears to occur orthogonal to the soil major axis. This direction was then chosen as the second axis, with the intension of providing a greenness indicator. Crop yellowing takes place in a different manner of maturity. Consequently choosing a third axis orthogonal to the soil line and greenness axis will give a yellowness measure (Richards and Jia 1999).

Tasseled cap transformation was developed by Kauth and Thomas (1976). They defined a transform space that was designed to improve the analysis of agricultural scenes using Landsat MSS data. The tasselled-cap transform (named after the shape of the population distribution) is designed to project the data along a set of axis where the first three axes correspond roughly with the brightness of soils (brightness axis), the vegetation biomass (greenness axis), and the senescence of vegetation (yellowness axis) (Schott 1997).

The 'tasselled cap' transformation rotates the MSS data such that the majority of information is contained in two components or features that are directly related to physical scene characteristics. Brightness, the first feature, is a weighted sum of all bands and is defined by the direction of the principal variation in soil reflectance. The second feature, greenness, is approximately orthogonal to brightness and is a contrast between the near-infrared and visible bands. Greenness is strongly related to the amount of green vegetation present in the scene.

Crist and Cicone (1984) extended the tasselled cap concept to Landsat TM data and found that the six bands of reflected data effectively occupy three dimensions, defining planes of soils, vegetation, and a transition zone between them. The third feature, called wetness, relates to canopy and soil moisture. Crist's transformation defines three properties: brightness, greenness and wetness.

These transformations use predefined co-efficient, derived from agricultural areas in the U.S.A. Their suitability for other types of vegetation cannot be guaranteed (Anon 1999). However, for forest stratification it may contain some better information for classifying forest. Because when apply the concept to Landsat TM data it transform 6 bands information into three bands and magnify the information in those components.

The tasselled cap transformation is sensor specific and is designed to transform the input data to a feature space where the features are more directly correlated with an application parameter and more inter-comparable over time. While not an optimised transform, it has the advantage from the

user's standpoint of using a constant pre-computed transform matrix. It must, however, be recognized that the transform was designed for particular types of scenes and is sensor-specific (Schott 1997). For example, tasseled cap coefficients enumerated in table 2.4 and 2.5 (Crist *et al.* 1986, Anon 1997) need to be multiplied to the Landsat TM image to separate the layers consist information on brightness, greenness and wetness.

Table 2.4 Tasseled cap multiplicative matrix (Landsat TM)

Tasseled Cap Index	Band 1	Band 2	Band 3	Band 4	Band 5	Band 6	Band 7
Brightness	0.2909	0.2493	0.4806	0.5568	0.4438	0.0000	0.1706
Greenness	-0.2728	-0.2174	-0.5508	0.7221	0.0733	0.0000	-0.1648
Wetness	0.1446	0.1761	0.3322	0.3396	-0.6210	0.0000	-0.4186
Haze	0.8461	-0.0731	-0.4640	-0.0032	-0492	0.0000	0.0119
Other 1	0.0549	-0.0232	0.0339	-0.1937	0.4162	0.0000	-0.7823
Other 2	0.1186	-0.8069	0.4094	0.0571	-0.0228	0.0000	-0.0220

Table 2.5 Tasseled cap additive matrix (Landsat TM)

	Brightness	Greenness	Wetness	Haze	Other 1	Other 2
Scale	10.3695	0.7310	-3.3828	0.7879	-2.4750	-0.0336

Brightness is a particular sum of all bands. Greenness describes the contrast between near infrared and the visible bands, with the mid-infrared bands especially cancelling one another. Wetness component contrasts middle-infrared reflectance with visible and near-infrared reflectance, would show a degree of moisture sensitivity. Fourth component may present some information of interest, particularly with respect to soils. The fifth and sixth components, unrotated from those produced in the original principal components analysis, show little variation and are likely to carry much, if any, important information with respect to agricultural crops or soils (Crist and Cicone 1984).

2.4.4 *Principal Component Analysis*

The transformation of the raw remote sensor data using Principal Component Analysis (PCA) may be more interpretable than the original data (Singh and Harrison 1985). PCA may also be used to

compress the information content of a number of bands of imagery (for example six TM bands) just two or three transformed principal component images. The ability to reduce the dimensionality from n to two or three bands is an important economic consideration, if the potential information recoverable from the transformed data as good as the original remote sensor data. The goal is to use principal component analysis to translate and/or rotate the original axes so that the original brightness values on axes X_1 and X_2 are redistributed (reprojected) onto a new set of data set of axes or dimensions X_1' and X_2' (Wang 1993). The X' coordinate system might then be rotated about its new origin in the new coordinate system some degrees so that the first axis X1' is associated with the maximum amount of variance in the scatter of points. The new axis is called the first principal component. The second principal component is perpendicular (orthogonal) to PC1 (Figure 2.8). The first band, or feature, in the multiple principal component image will account for most of the variance in the data, with decreasing amounts in the remaining bands. The latter bands in a many-band image tend to contain mostly random noise.
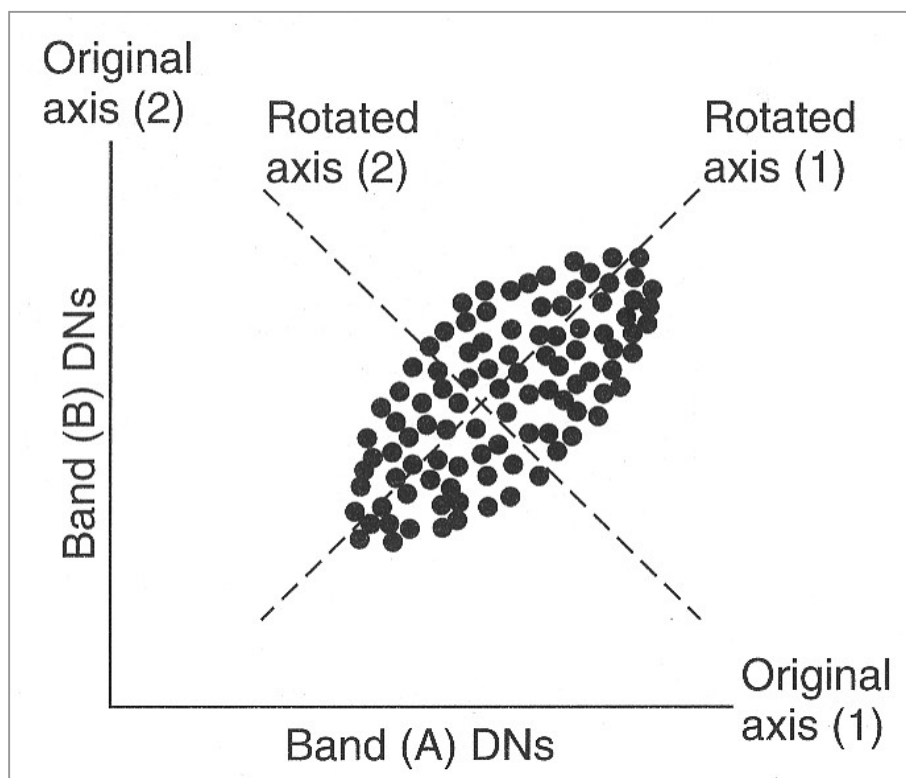
Figure 2.7 Rotation of axes in two-dimensional space for a hypothetical two-band data set by principal components analysis (Avery and Berlin 1992)

The Principal Component Transformation is computed from the original spectral statistics as follows (Short 1982):

1. The *nXn* covariance matrix of the *n*-dimensional remote sensing data is to be computed. Use of the covariance matrix results in an unstandardized PCA, whereas use of the correlation matrix results in a standardized PCA (Eastman and Fulk 1993).

2. The eigenvalues, $E = [\lambda_{1,1}, \lambda_{2,2}, \lambda_{3,3}, \ldots\ldots, \lambda_{n,n}]$, and eigenvectors EV [$a_{kp}$….. for k = 1 to *n* bands, and p = 1 to *n* components] of the covariance matrix should be computed such that

$$
\begin{array}{c} EV \quad Cov \quad EV^T \\ [n \times n][n \times n][n \times n] \end{array} = \overset{E}{\begin{bmatrix} \lambda_{1,1} & 0 & 0 & 0 & 0 & 0 & 0 \\ 0 & \lambda_{2,2} & 0 & 0 & 0 & 0 & 0 \\ 0 & 0 & \lambda_{3,3} & 0 & 0 & 0 & 0 \\ 0 & 0 & 0 & \lambda_{4,4} & 0 & 0 & 0 \\ 0 & 0 & 0 & 0 & \lambda_{5,5} & 0 & 0 \\ 0 & 0 & 0 & 0 & 0 & \lambda_{6,6} & 0 \\ 0 & 0 & 0 & 0 & 0 & 0 & \lambda_{n,n} \end{bmatrix}}
$$

Where, EV^T is the transpose of the eigenvector matrix, *EV* and *E* is the diagonal covariance matrix whose element λ_{ii}, called *eigenvalues*, are the variances of the *p*th *principal components*, where *p* = 1 to *n* components. The non-diagonal eigenvalues, λ_{ij} , are equal to zero and therefore can be ignored. The number of nonzero eigenvalues is an *nXn* covariance matrix always equals *n*, the numbers of bands examined. The eigenvalues are often called components (i.e. eigenvalue 1 may be referred to as principal component 1) (Jensen 1996).

2.4.5 Structure or image texture analysis

Texture matrices are a class of neighbourhood operations designed to characterize the variability (texture) in the neighbourhood around a pixel. In general they utilize a window of some size that moves over the image in the same fashion as a kernel operation. The output pixels are formed from some measure of the texture in the window when it is cantered over the pixel location. One of simplest structure matrices is the range. For example, using a 3X3 window centred on f(i,j), the output g(i,j) would be the range (Dc_{max}-Dc_{min}) computed over the set of pixels comprised of f(i,f) and its eight nearest neighbours. The output image would be bright in regions with structure and dark in regions with little structure. Another similar local texture metric is local standard deviation. Again, the output image pixel value g(i,j) is simply the standard deviation of the pixels under a window cantered on f (i,j) in the input image (Schott 1997).

There are a large variety of texture matrices. Some are very direction-specific, some require fairly large windows and are aimed at characterizing low-frequency texture, others require fairly large windows and are designed to differentiate high-frequency texture patterns. One of these texture matrices is the co-occurrence metrics described by Haralick *et al.* (1973). In most cases it is necessary to consider many texture matrices to aid in separating different material classes or to merge texture matrices with multispectral digital count values to provide greater differences between classes (Scott 1997).

Co-occurrence (spatial dependence) matrices are widely accepted for the classification of texture (Haralick 1979, Gonzalez and Woods 1992). Given the 5X5 digital image, a co-occurrence matrix is developed as follows (E-W direction only). First the number of different pixel values is determined. Second, these pixel values are ranked, smallest to largest. Third, the digital image is scanned in the direction noted (E-W in this case) to determine the frequency with which one of these pixel values follows another (Carr and Miranda 1998).

1	1	2	2	5
3	2	3	1	1
0	1	1	0	1
3	2	4	0	1
2	1	1	2	2

With respect to the digital image presented earlier, six different pixel values are observed: 0-5. Hence, the co-occurrence matrix is 6X6 matrix (in this case co-occurrence matrix is larger than the input image. If the matrix is called [A]

$$[A] = $$

	0	1	2	3	4	5
0	0	3	0	0	0	0
1	1	4	2	0	0	0
2	0	1	2	1	1	1
3	0	1	2	0	0	0
4	1	0	0	0	0	0
5	0	0	0	0	0	0

Once the matrix is determined, seven statistical parameters are chosen for this study (described follow, Gonzalez and Woods 1992, more parameters may be computed for higher orders of element of difference and inverse element difference:

1) Each entry in matrix [A] is divided by n, the number of pixels that satisfy the algorithm (in this case, one pixel to the right; in this example, n is 20; let this resultant matrix be called [C].

2) Once step 1 is finished, the first statistical parameter is extracted, and it is the maximum value for any entry in [C]; in this example the maximum value is 4/20 or 0.2.

3) First-order element difference moment is computed:

$$\sum_i \sum_j (i-j) c_{ij} \quad \text{..(2.1)}$$

4) Second-order element difference moment is computed:

$$\sum_i \sum_j (i-j)^2 c_{ij} \quad \text{.......................................(2.2)}$$

5) First-order inverse element difference moment is computed:

$$\sum_i \sum_j \frac{c_{ij}}{(i-j)} \quad \text{.......................................(2.3)}$$

6) Second-order inverse element difference moment is computed:

$$\sum_i \sum_j \frac{c_{ij}}{(i-j)^2} \quad \text{.....................................(2.4)}$$

7) Entropy is computed:

$$\sum_i \sum_j c_{ij} \log c_{ij} \quad \text{.....................................(2.5)}$$

8) Uniformity is computed:

$$\sum_i \sum_j c_{ij}^2 \qquad \text{...(2.6)}$$

Once these statistical parameters are computed for an MXM training class, a similar sized window is used, centred over pixels to be classified. Similar statistical measures are computed, from which a minimum distance metric is computed to determine to which class, or threshold, pixels are assigned.

2.4.6   Integration of the higher and lower resolution images

A number of methods have been developed in recent years in order to combine the information from two co-registered data sets of different spatial resolution, including pixel-by-pixel arithmetic like adding, subtracting, or rationing of image channels (Chavez 1986), intensity-hue-saturation transformation and principal component analysis (Haydn *et al.* 1982). However, due to the fact that the spectral windows used by two sensors usually are not the same, merging may modify the colour balance of the land cover types known from the original images. Therefore, image fusion should be well tuned and the new image product requires careful interpretation.

The following two techniques of image fusion were applied for this study:
      (i) pixel addition using the Brovey transformation, and
      (ii) the RGB-IHS-RGB transformation.

The Brovey transformation, presented by Musa *et al.* (2000) is a pixel addition method, which would preserve the higher resolution of the single-band IRS-Pan image as well as the multi-spectral information of the lower resolution TM bands. It allows adding the IRS-Pan image equally to each of the TM bands without distorting the spectral balance of signatures within the latter image.

The IHS colour transform on the other hand, has been found useful for integrating and displaying the remotely sensed data in many applications (Andreadis *et al.* 1995, Carper *et al.* 1990, Chavez and Bowell 1988, Chavez *et al.* 1991, Koutsias *et al.* 2000). The IHS transformation is defined by three separate, orthogonal and easily perceived colour attributes, those of intensity, hue and saturation. While geometrically, the RGB system can be represented as a cube with the red, green and the blue axes defining x, y and z vectors respectively, the IHS coordinate system can be

represented as a cylinder or a sphere. Intensity, which represents the total energy or brightness of the image, defines the vertical axis of the cylinder, or the radius of the sphere. Hue represents the average wavelength of colour and defines the circumferential angle of the cylinder or sphere, and ranges from blue (0 degrees) through green, yellow, red and purple (360 degrees). Saturation can be thought of as purity of the colour (i.e. percentage of white light in the image) and defines the colatitudes of the sphere, or the radius of the cylinder.

For creation of a multi-sensor data set the Landsat TM bands 5 4 3, displayed as RGB (red, green and blue) composition, were re-sampled to pixels of a spatial resolution of 5m by 5m in order to be compatible with the IRS-Pan image. This combination of TM bands was judged to be optimal for separation of different forest and land cover classes.

For the Bovey transformation the three re-sampled Landsat TM bands were normalized and multiplied with the IRS pan image by the following equations:

Red band = {TM band 5 / (TM bands 5 + 4 + 3)}*IRS pan……………….(2.7)

Green band = {TM band 4 / (TM bands 5 + 4 + 3}*IRS pan……………..(2.8)

Blue band = {TM band 3 / (TM bands 5 + 4 + 3}*IRS pan……………….(2.9)

For the IHS transformation the three TM bands (5, 4, 3) were transformed to the intensity-hue-saturation (IHS) domain. Intensity of TM band was then replaced by the panchromatic band of the IRS image. Finally, the new IHS combination was transformed back to the RGB domain.

2.4.7   Accuracy assessment of classification

One of the most common means of expressing classification accuracy is the preparation of a classification error matrix (sometimes called a confusion matrix or a contingency table). Error matrices compare, on a category-by-category basis, the relationship between known reference data (ground truth) and corresponding results of an automated classification. Such matrices are square, with the number of rows and columns equal to the number of categories whose classification accuracy is being assessed (Lillesand and Kiefer 2000).

Several descriptive measures can be obtained from the error matrix. For example, the overall accuracy is computed by dividing the total number of correctly classified pixels by the total number of reference pixels. Likewise, the accuracies of individual categories can be calculated by dividing the number of accurately classified pixel in each category by either the total number of reference pixels. Likewise, the accuracies of individual categories can be calculated by dividing the number of

correctly classified pixel in each category by the number of training set pixels in the corresponding row or column. What are often termed producer's accuracies result from dividing the number of correctly classified pixels in each category by the number of training set pixels used for that category. This figure indicates how well the training set pixels of the given cover type are classified. User's accuracies are computed by dividing the number of correctly classified pixels in each category by the total number of pixels that were classified in that category.

The error matrix based on training data only indicates how well the statistics extracted from these areas can be used to categorize the same area. If the results are good, it means nothing more than that the training areas are homogenous, the training classes are spectrally separable, and the classification strategy being employed works well in the training areas. This aids in the training set refinement process, but it indicates little about how the classification performs elsewhere in a scene. Random sampling of classified pixels circumvents the above problems, but it is plagued its own set of limitations. First collection of reference data for a large sample of randomly distributed points is often very difficult and costly. For example, travel distance and access to random sites might be prohibitive. Second, the validity of random sampling depends on the ability to precisely register the reference data to the image data. This is often difficult to do so. One-way is to overcome this problem is to sample only pixels whose identity is not only influenced by potential registration errors (for example, points at least several pixels away from field boundaries (Lillesand and Kiefer 2000).

2.5   Sampling Strategy

2.5.1   *Double and two-stage sampling*

Many variables that are of interest to foresters are difficult and /or expensive to measure but are related to other variables that are less difficult or expensive to estimate. If the relationship between such variables can be established, it becomes possible to use the data from the latter to make estimates of the former. This process is known as double sampling (Johnson 2000). Usually the term double sampling is reserved for situation where estimates are made of population means or totals. However, whenever regressions are developed to obtain estimate of difficult-to-measure quantities as, for example, the volume of standing trees using spectral response, the procedure could be considered a form of double sampling.

When the universe of interest is divided into subsets that are to be used as sampling units, those subsets are primary samples. Each of these primary samples can be considered as mini-universe, which can be made up either of individual elements or group of individual elements. Those are the secondary samples. When sampling process is limited to drawing primary samples, it is referred to

as simple one-stage or single stage sampling. If sub-samples are drawn from randomly drawn primary samples, either individual elements or secondary samples two-stage sampling or sampling with sub-sampling is being used (Johnson 2000).

Double sampling has been applied to combine remote sensing image and field-based forest inventory. Double sampling is a two-phase sampling strategy, where one phase consists of the auxiliary variable, which is relatively easy to measure, and the other phase the variable of interest, which is difficult or expensive, and those two phases are somehow related. In our study the auxiliary variable is the remote sensing spectral information. Our variable of interest is the carbon content which is a function of forest biomass or volume.

Double sampling can be applied in several ways: double sampling for stratification, double sampling with regression estimator or knn estimate. Double sampling for stratification will stratify our forest to conduct an efficient ground sampling. Double sampling with regression estimator will correlate the remote sensing spectral response and field measured forest volume or biomass to generate a geographic carbon database. Double sampling with knn estimate will relate field-based information with satellite spectral response in terms of Euclidian distance.

2.5.2   First phase sampling

The first sampling phase will only deal with the selection of the image pixel from the remote sensing image. Those Image pixels are auxiliary variable. The next question is that what should be the size of a sample unit. Usually there are four categories of sample units on a remote sensing image: a single pixel, a cluster of pixels (often a 3x3 pixel square), a polygon or a cluster of polygons. A cluster of pixels, typically a 3x3 box, is the most common choice for the sample unit. A cluster minimizes registration problems, because it is larger than 1 pixel and therefore easier to locate in the reference data. However, clusters of pixels, especially a 3x3 window, may still be an arbitrary delineation of the landscape, if the sample unit covers more than one class. To avoid this problem, some researchers suggest that only homogenous clusters of pixels should be sampled. However, such restrictions may result in a biased sample that avoids heterogeneous areas, which could be a function of mixed pixels (e.g., a mixed hardwood conifer stand of trees). It is important to remember that the sample unit dictates the level of accuracy. If the assessment is performed on a 3x3 cluster of pixels, nothing can be criticized about the selection of individual pixel nor about polygons (management areas, forest stands, agricultural fields, etc.) (Congalton and Green 1999).

Therefore, in our case the pixel group should not be smaller (for example one pixel) because reaching of that level of accuracy on the field-sample plot in the second phase will not be possible

without a differential GPS. The other reason of not having a smaller plot is that often a single pixel spectral reflectance is affected by the surrounding pixel due to the illumination effect. The size of the pixel group was not larger because that might increase variability within the sample unit and reduce the correlation coefficient with the field measurement.

2.5.3 Second-phase sampling (application of two-stage sampling in this phase)

The second phase sampling deals with the field sampling of forest biomass. Though our variable of interest is carbon but it is very difficult to measure directly, however this variable is strongly associated with forest biomass. Therefore this study measures forest biomass and it is our variable of interest. The next problem is that what should be the appropriate size of sample unit. According to the first phase sampling the size should be 90mX90m (corresponds to the 3X3 pixel window). However, measuring all the trees inside that plot involves a high cost and time. Therefore two-stage sampling is decided to apply in this phase.

Two-stage sampling is a hierarchical structured sampling where within a bigger-sized sample a smaller sub-sample will be selected and measured. For example, each unit of a population can be divided into a number of smaller units, or subunits. A sample of n units has been selected. If subunits within a selected unit give similar results, it seems uneconomical to measure them all. A common practice is to select and measure a sample of the subunits in any chosen unit. This technique is called sub-sampling, since the unit is not measured completely but is itself sampled. Another name of the process is two-stage sampling, because the sample is taken in two steps. The first is to select a sample of second-stage units, often called the primary units, and the second is to select a sample of second stage units or subunits from each chosen primary unit (Cochran 1977).

In the second phase of double sampling of our project the variable of interest (i.e. forest volume/carbon content) can be estimated by two-stage sampling. In the first stage a bigger size of sampling (known as primary sampling unit) is selected and in the second stage a smaller sample size would be selected (secondary sampling unit) and measured. The estimate of parameters of first stage can be obtained from the measurement of second stage sampling. Direct measurement of carbon content is cost-effective approach, however, there is a direct relationship between forest volume/biomass and carbon content. Hence, our variable of interest is forest volume and this will be converted to carbon by the ratio of an established relationship.

Theoretically primary sampling unit selected on a satellite image will be homogeneous in group. However, in practice there might be variability in terms of volume and biomass on the ground. As

the area is still large (approximately 90mx90m) to measure the details of forest parameters, second stage sampling would be applied. The area may be arbitrarily selected as those followed by local inventory or determined by the optimisation process described by Zeide (1980). The number and distribution of secondary sample plots would be determined by the optimising.

There are two reasons for stratification. It ensures that the sample will be well distributed across the primary sampling units, thus increasing the probability of obtaining a representative sample. The second reason for stratification is that it will reduce the magnitude of the standard error of the mean. Since some of the sample must come from each of the strata, the likelihood of a sample containing all high or low values is greatly reduced and consequently repeated samples will have more nearly alike means than would be the case if the sampling was unrestricted. Thus, the variance and standard error of the mean would be less in the case of the stratified sample than it would be if the sampling is unrestricted (Johnson 2000).

2.5.4 Determination the sample size

The sample size n for this study is calculated by

Sample size n = $\dfrac{t^2 c^2}{AE^2}$ ………………………………………(2.10)

Where *AE* is the maximum allowable error specified for this study as a percent of the mean and t is the weighting factor from student *t* distribution and accounts for the probability of achieving the specified level of accuracy with a given sample size. *C* is the coefficient of variation, which is a measure of variability within a population.

2.6 Field Estimation of Forest Volume/Biomass/Carbon Pool

2.6.1 Estimation by direct measurement

Volume estimation is based on measurement of diameter and length. These measurements may be made most accurately when the logs are separate and accessible to the measurer. Logs are neither cylindrical nor often a regular geometrical shape. Usually the model of a frustum of a quadratic paraboloid (Figure 2.8) is adopted and the formulae enumerated in table 2.6 are used to calculate volume.
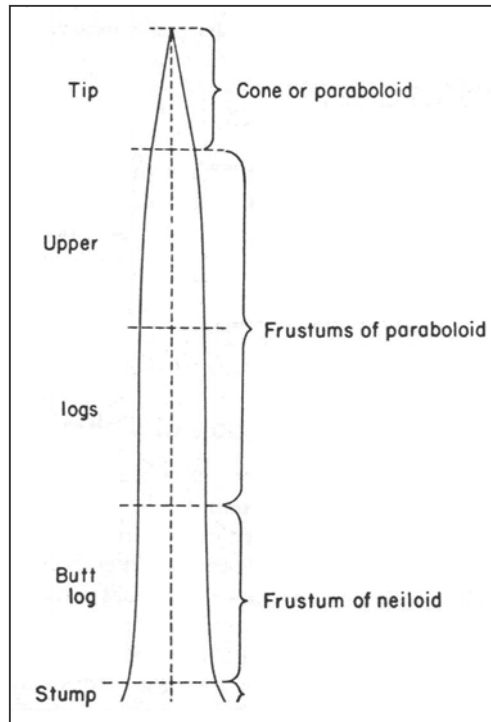
Figure 2.8 Geometric forms assumed by portions of a tree stem

Table 2.6 Equations for computation of cubic volume of important solids

Geometrical solid	Equation for volume	Name
Cylinder	$V = A_b h$	
Paraboloid	$V = \frac{1}{2}(A_b h)$	
Cone	$V = \frac{1}{3}(A_b h)$	
Neiliod	$V = \frac{1}{4}(A_b h)$	
Paraboloid frustum	$V = \frac{h}{2}(A_b + A_u)$	Smalian's formula
	$V = (A_m)$	Huber's formula
Cone frustum	$V = \frac{h}{3}(A_b + \sqrt{A_b A_u} + A_u)$	
Neiloid frustum	$V = \frac{h}{4}(A_b + \sqrt[3]{A_b^2 A_u} + \sqrt[3]{A_u^2 A_b} + A_u)$	
Neiloid, cone, or paraboloid frustum	$V = \frac{h}{6}(A_b + 4A_m + A_u)$	Newton's formula

h = height or length of the log

A_b = cross-sectional area at base

A_m = cross-sectional area at middle

A_u = cross-sectional area at top

However, direct measurements are laborious and time consuming and hence the other methods, for example, using form factor and volume or biomass tables are widely used for practical purpose.

2.6.2   Estimation by tree form factor

Form of a tree actually is its shape. The shape of a tree is usually irregular. The tree form may be measured by the form factor that is the ratio of the volume of the tree or log to that of cylinder of equal basal cross-sectional area and height. For trees, the equivalent basal area is usually taken at 1,3 m above ground level, that is at breast height; in some circumstances the cross-sectional area at (0,9) (total height) from the growing point may be used so the form factors of trees of different total heights may be compared on a rational basis. Form factor can be calculated by (for field practice):

Form factor = $V_t/(g_{bh}*h_t)$………………………………..(2.11)

Where, V_t = total volume overbark, g_{bh} = cross-sectional area at breast height, i.e. 1,3 m above ground level and h_t = total height.

Apart from the variables used in this calculation, form factor has the following sources of variation:

- Species and genotype
- Age
- Stocking
- Crown size
- Site factors – especially wind exposure (Philip 1998).

2.6.3   Estimation using functions and tables

A volume table is a tabulation that provides the average contents for standing trees of various sizes and species. The principal objective of volume tables is to estimate volume of standing trees that would correspond with the volume obtained if the same trees were felled, bucked and scaled as logs. Thus such tables are used in timber estimating as a means of ascertaining the volume and value of standing trees in a forested tract. In modern practice, equations are usually used to predict tree volumes rather than obtaining the values from tables. Tree weight tables are analogous to volume tables except that weights (green or dry) of standing trees are predicted rather than

volumes. The principal variables ordinarily associated with standing tree volume or weight is diameter at breast height (*dbh*), tree height, and perhaps, tree from (Avery and Burkhart 1994).

Volume or weight tables are usually single entry or multiple entries. Those tables, whether of single or multiple entry can be classified as species tables or composite tables. In the first instance, separate tables are constructed for each important timber species or groups of species that are similar in terms of tree form. On the other hand, composite tables are intended for application to diverse species. To compensate for inherent differences in stem taper and volume between various species groups, provision is usually made for additionally measuring tree form, or correction factors developed for various species. Otherwise, composite tables will overestimate volumes of some trees while underestimating the volumes of others (Avery and Burkhart 1994).

The main disadvantage of species tables is the large number of species encountered in most regions. When it is not feasible to construct separate tables for each species, those of similar taper and shaped may be grouped together. To avoid such difficulties, composite tables utilizing some measurement of tree form in lieu of species differentiation have been adopted in several regions (Avery and Burkhart 1994).

2.7   Combine Remote Sensing and Terrestrial Information

2.7.1   *Incorporation of field measurement on the pixel level*

Field estimation of sub-sample can be accurately matched by a differential correction of GPS signal. Post-processing differential correction will provide the accuracy better than 5 meter. As Landsat images have the spatial resolution of 30 m the measured value can be easily incorporated on the pixel level. Alternatively, it can also be incorporated by a statistical method. First a mean value of 3X3 pixels and field measurements will be correlated. Using the best-fitted correlation coefficient the field measured carbon content will be simulated to the spectral response. Then it will be matched by a statistical approach to find the accurate location of the pixel. In this approach the field measurements will be fit into a moving window matrix. In that matrix, digital count of the nine pixels and the simulated spectral reflectance from the secondary sample plot will be plotted in two directions. The moving window will calculate the variance between field simulations with the reflectance count of each pixel from satellite data and select where the variance is minimum. The pixel with minimum variance or bias in that calculation should be used for establishing a correlation between two phases of the double sampling (figure 2.9). There are other approaches of location uncertainty has been discussed by Jaquez and Waller (2000).
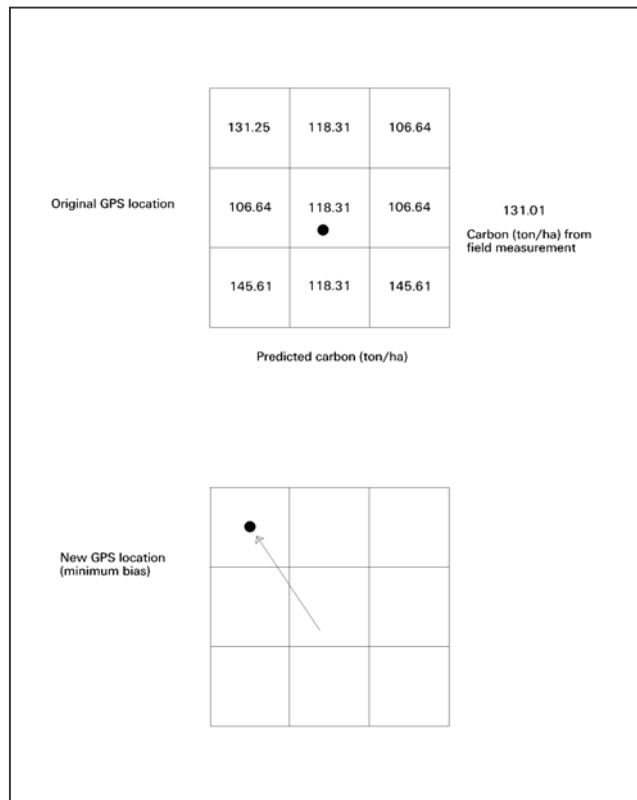
Figure 2.9 Reducing location uncertainties by a geo-statistical approach

2.7.2   Double sampling for stratification

2.7.2.1   Background information

In forest survey applications it has often been shown that cost-effectiveness can be improved by combining information assessed in aerial photographs/satellite images and field-assessments. The proposed study will stratify the forest based on the supervised classification of remote sensing image inside the test site. As supervised classification separates the image pixels into a number of spectral classes depending on their spectral distribution related to particular class, it could be used as a base of stratification. A number of studies used double sampling for stratification to estimate forest volume or biomass using remote sensing data and field inventory (Chojnacky 1998, Franklin 1986, Glass *et al.* 2001, Köhl 1994, Köhl and Kushawaha 1994, Leyk *et al.* 2002, Nelson *et al.* 2000).

Although double sampling for stratification offers the potential for estimating forest biomass more efficiently than simple field plot sample, there is no guarantee of success. The success depends on how well the method might work to guide primarily by the experience of others to make the stratification. In particular, it is necessary to know whether double sampling will result in lower

sampling errors than might be obtained by simple field surveys of equal cost, and if so, how much of a reduction in sampling error the analyst can expect. If he decides to adopt the method, he will need to decide how many strata to identify and what boundaries to give them. In addition, he will need to decide how to allocate the field samples among these strata.

Also double sampling for stratification, both the auxiliary variable at the first level (satellite image) and the variable of interest at the second level (field survey) are computed. In contrast to double sampling with regression estimators no measurable parameter on the satellite image is taken as an auxiliary variable. The auxiliary variable serves in allocating a sampling unit to a particular stratum. The sampling procedure is very similar to stratified sampling; the difference is that employs estimated strata sizes instead of known ones.

Various stratification variables such as forest type, degree of mixture, canopy density, stand structure, stage of development etc with ground sampling can be investigated on satellite image. Stage of development proved the most suitable parameter for stratification. It was divided into several classes; young growth, pole-wood, young and medium mature timber, mature timber and mixed growth.

2.7.2.2   Strata as a domains of study:

This section deals with surveys in which the primary purpose is to make comparisons between different strata, assumed to be identifiable in advance. The rules for allocating sample sizes to the strata are different from those that apply when the objective is to make over-all population estimates. If there are only two strata, we might choose n_1, n_2 to minimize the variance of the difference ($\bar{y}_1 - \bar{y}_2$) between the estimated strata means. Omitting the fpc's, we have

$$V(\bar{y}_1 - \bar{y}_2) = \frac{S_1^2}{n_1} + \frac{S_2^2}{n_2}$$ ……………………………………(2.12)

With L strata, $L>2$, the optimum allocation depends on the amounts of precision desired for different comparisons. For instance, the cost might be minimized subject to the set of $L(L-1)/2$ conditions that $V(\bar{y}_h - \bar{y}_i \leq V_{hi}$, where the values of V_{hi} are chosen according to the precision considered necessary for a satisfactory comparison of strata h and i.

Frequently a simpler method of allocation is adequate, especially if the S_h and c_h do not differ greatly. One approach is to minimize the average variance of the difference between all $L(L\text{-}1)/2$ pairs of strata, that is, to minimize (Cochran 1977).

$$\bar{V} = \frac{2}{L}\left(\frac{S_1^2}{n_1} + \frac{S_2^2}{n_2} + \text{.................} + \frac{S_L^2}{n_L}\right) \quad \text{...............................(2.13)}$$

2.7.3   Double sampling with regression estimator

2.7.3.1   Background information

Double sampling with regression estimator will measure x variable on each sampling unit and predict y by using a regression parameter. In this strategy x are measured on each sampling unit and the regression parameters for predicting y from x are estimated from measurements of x and y taken on a sub-sample. This enables the surveyor to predict Y as a function of the estimated X from the main sample. The application of this technique implies that the residual variance of the regression is very much smaller than the variance of the x values in the population (Philip 1998).

The general linear regression model can be written as:

$$Y_j = b_1 + b_1 X_{1j} + b_2 X_{2j} + b_3 X_{3j} + \text{.............................} + b_m X_{mj} + \varepsilon_j \text{.........................(2.14)}$$

$b_1, b_2, b_3 \text{.............} b_m$ = parameters of the model
$X_{1j}, X_{2j}, \text{.....................................} X_{mj}$ = values of the predictor (independent) variables for the jth population element

The quantity εj represents the value of a random variable that expresses the difference between Y_j and the average of all *Y* values associated with the specific combination of predictor variables values $X_{1j}, X_{2j} \text{.....................} ,X_{mj}$. The random variable ε is assumed to be additive to the model and randomly distributed with mean 0 and constant variance σ^2. From an analysis standpoint, $b_0, b_1, \text{.................} b_m$ and σ^2 are unknown parameters to be estimated from the data, while the values of the predictor variables are treated as known constants. The random variable *Y* is therefore distributed with a mean of $b_0 + b_1 X_1 + \text{.................} + b_m X_m$ and a variance of σ^2.

The first step in any regression analysis is data collection. A sample of n element is selected from the population, and the values for the dependent and independent variables are determined for each of the sample elements. Sample relationships are expressed by writing equation as:

$$Y_i = b_0 + b_1X_{1i} + b_2X_{2i} + \ldots\ldots\ldots\ldots b_mX_{mi} + \varepsilon_i \ldots\ldots\ldots\ldots\ldots\ldots\ldots\ldots\ldots(2.15)$$

Where,

$X_{1i}, X_{2i}, \ldots\ldots\ldots X_{mi}$ = values of the predictor variables for the ith sample element

Y_i = value of the dependent variable for the ith sample element

ε_I = value of the random variable ε that is associated with the ith sample element (I = 1,……….,n)

When predicted values of $b_0 + b_1, \ldots\ldots\ldots\ldots b_m$ are available (these predicted values are denoted as $b_0, b_1, \ldots b_m$), predicted values of the response variable can be obtained as

$$Y = b_0 + b_1X_{1i} + b_2X_{2i} + b_mX_{mi} \ldots\ldots\ldots\ldots\ldots\ldots\ldots\ldots\ldots\ldots\ldots(2.16)$$

And predicted values of ε values can be calculated as:

$$\varepsilon_I = Y_i - \hat{Y}_i \ldots\ldots\ldots\ldots\ldots\ldots\ldots\ldots\ldots\ldots\ldots\ldots(2.17)$$

In our case, the easily measured variable is the digital count of remote sensing image *(x)* and the variable difficult to measure is the carbon content *(y)*. Constant and coefficient of the regression was calculated by using SPSS software.

Figure 2.10 listed some different patterns of scattergram and a possible fit of regression lines.
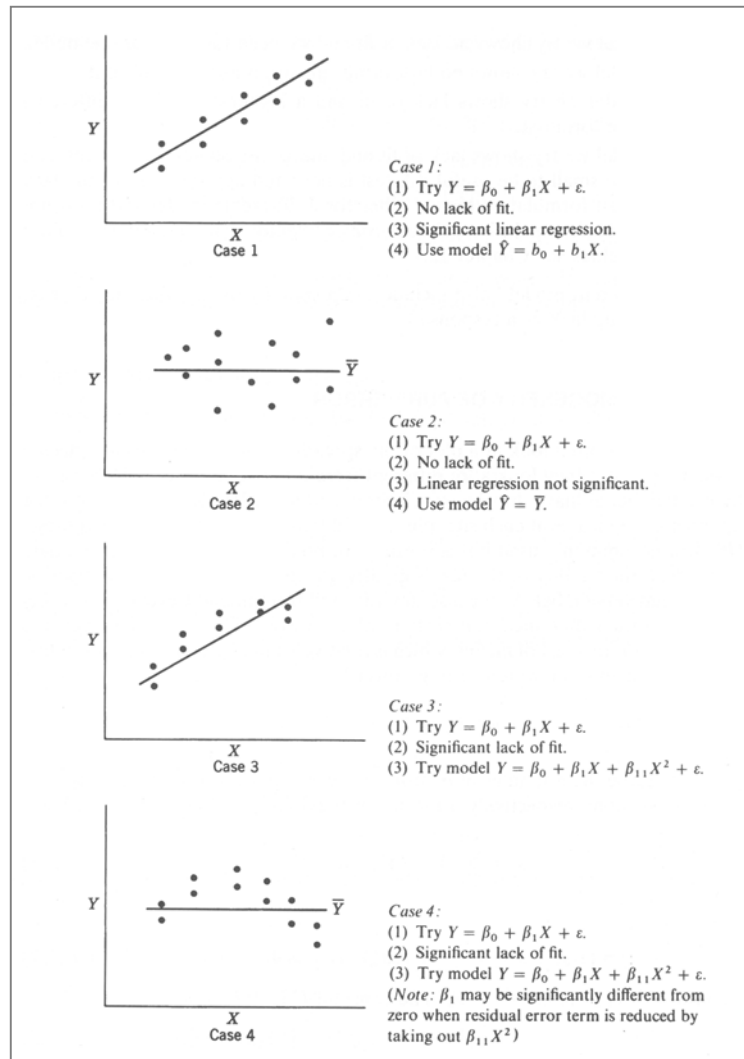
Figure 2.10 Typical straight-line regression situations (Draper and Smith 1998)

A number of studies used regression technique for estimating and predicting forest attributes based on remote sensing data (Ardö 1992, Foody *et al.* 2003, Gjertsen 1996, Häme *et al.* 1996, Roy and Ravan 1996, Trotter *et al.* 1997, Lu *et al.* 2002, Thenkbail *et al.* 2004).

2.7.3.2   Residual analysis

The residuals are often used to detect and assess the degree of discrepancy between the model assumed (includes assumptions made) and the data observed. A simple plotting of ordinary residuals against the fitted values $\hat{Y}_i$ is often beneficial in highlighting either model under specification or a deviation from the homogenous variance assumption. The classical appearance of such a residual plot for an ideal situation is depicted in figure 2.11. The picture indicates a random pattern around zero with no detectable trend.
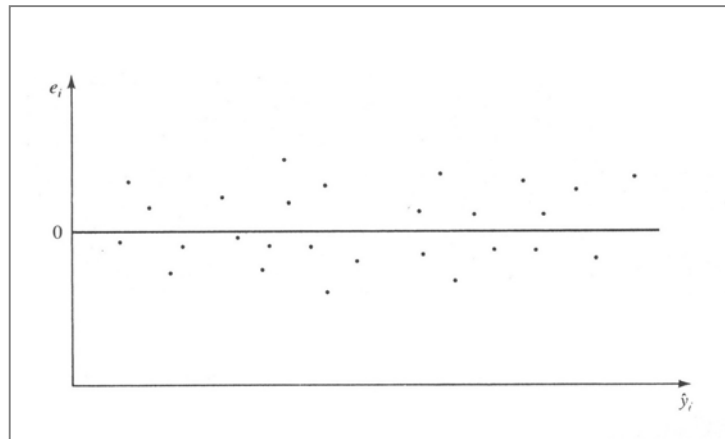
Figure 2.11 Ideal residual plot

Figure 2.12 reveals residual patterns that give evidence of model under specification and heterogeneous variance. The figure 2.12 (b) shows the funnel effect, which indicates that as the response variable gets larger, the deviations from the residuals from zero become greater. Hence one detects a condition whereby the error variance is not constant but increases as the measured response increases. In figure a, the systematic trend in the residuals usually indicates a model term is missing, perhaps a quadratic term in one of the repressor variables (Myers 1990).

(a)

(b)
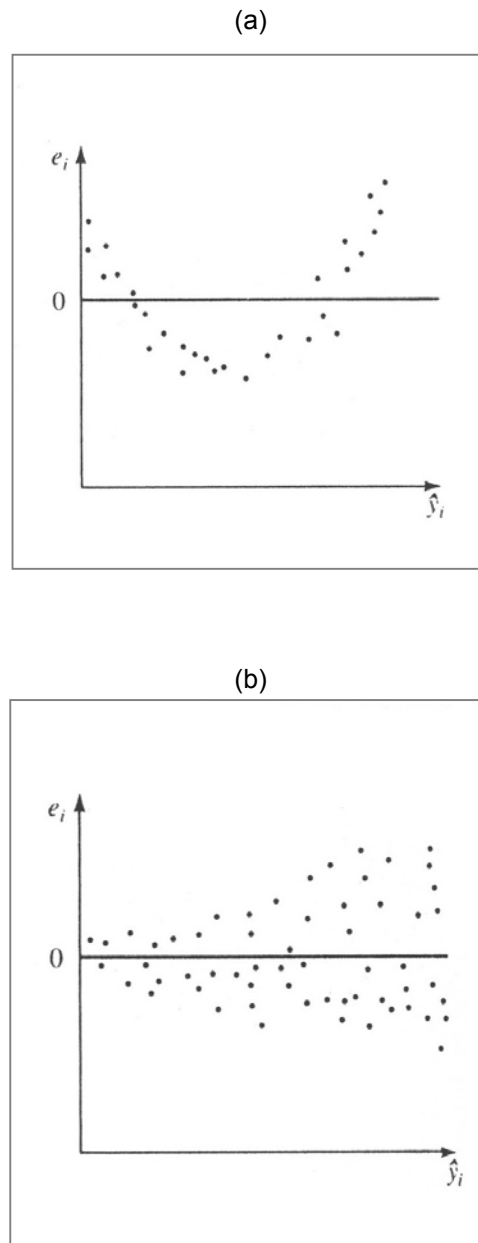
Figure 2.12 Residuals plots indicating violation of assumptions (a) model should involve curvature

(b) heterogeneous variance

2.7.3.3   'Dummy' Variables to Separate Blocks of Data

The variables considered in regression equations usually can take values over some continuous range. Occasionally we must introduce a factor, which has two or more distinct levels. For example, data may arise from three machines, or two factories, or six operators. In such a case we cannot set up a continuous scale for the variable 'machine' or 'factory' or 'operator'. We must assign to these variables some levels in order to take account of the fact that the various machines

or factories or operators may have separate deterministic effects on the response. Variables of this sort are usually called dummy variables. They are usually (but not always) unrelated to any physical levels that might exist in the factors themselves (Draper and Smith 1998).

Suppose we wish to introduce into a model the idea that there are two types of machines (types A and B) that produce different levels of response, in addition to the variation, which occurs due to other variables. One-way is doing this is to add to the model a dummy variable Z and a regression coefficient α so that an additional term αZ appears in the model. The coefficient α must be estimated at the same time the β's are estimated. Values can be assigned to Z as follows:

Z = 0 if the observation is from machine A,
Z = 1 if the observation is from machine B.

Any two distinct values of Z would actually be suitable, though the above is usually best. However, other assignments are sometimes convenient; for example, suppose of a total of n observations, n_1 comes from type A machines and $n_2 = n-n_1$ from type B machines. If we choose levels

$$Z = \frac{-n2}{\sqrt{n1n2(n1+n2)}} \quad \text{for machine A} \dots\dots\dots\dots\dots\dots\dots\dots\dots\dots(2.18)$$

$$Z = \frac{n1}{\sqrt{n1n2(n1+n2)}} \quad \text{for machine B} \dots\dots\dots\dots\dots\dots\dots\dots\dots(2.19)$$

It will be found that the corresponding column of the X matrix is orthogonal to the 'β_0 column' and has sum of squares unity, which may be convenient.

If it were desired to take account of three distinct machines, two dummy variables Z_1 and Z_2 would be required. Then we should set

(Z_1, Z_2) = (1,0) for machine A
(0, 1) for machine B
(0,0) for machine C

and the, model would include extra terms $\alpha_1 Z_1 + \alpha_2 Z_2$, with coefficients α_1, α_2 to be estimated. Again, many different allocations of levels are possible. If desired, columns which are orthogonal to the β_0 column which have sum of squares unity can be achieved by setting

$$(Z_1, Z_2) = \left(0, \quad \frac{-n3}{\sqrt{n1n3(n1+n3)}} \quad 0 \right) \qquad \text{for machine A}$$

$$\left(0, \quad \frac{-n3}{\sqrt{n2n3(n2+n3)}} \quad \right) \qquad \text{for machine B}$$

$$\left(\frac{-n1}{\sqrt{n1n3(n1+n3)}} \quad , \quad \frac{n2}{\sqrt{n2n3(n2+n3)}} \quad \right) \text{for machine C}$$

where, n_1, n_2 and n_3 are, respectively, the numbers of observations from machines A, B and C.

In general, by an extension of this procedure we can deal with r levels by the introduction of $(r - 1)$ dummy variables. The basic allocation pattern is obtained by writing down an $(r-1) \times (r-1)$ I matrix and adding a row of $(r-1)$ zero (Draper and Smith 1998).

In order to get an easy understating of different possibilities of regression lines using different forms of dummy variables are presented in figure 2.13.
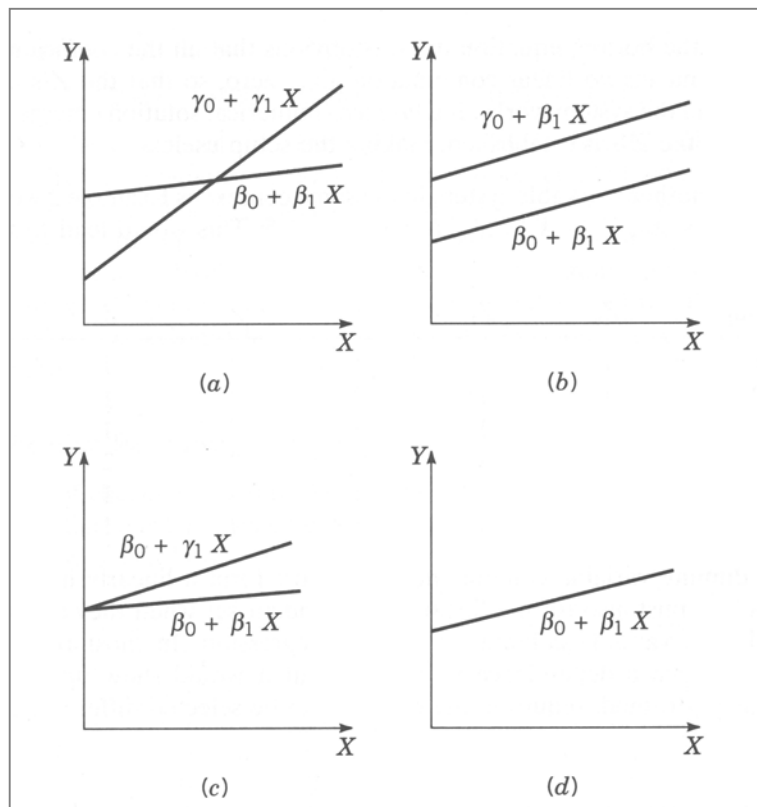
Figure 2.13 Different possibilities of two straight lines using dummy variables

(Draper and Smith 1998)

2.7.3.4   Criteria for comparing candidate models

In the ideal regression analysis, the analyst specifies an initial model that, when fitted to the sample data, produces a regression equation composed entirely of statistically significant variables. In addition, plotting of the residuals from this model over predicted Y, and the independent variables show a random, constant variance pattern around a residual value of zero. In such a situation, the analyst will have fitted only one model and will generally adopt the calculated equation as the final regression. Since the sample data played no role in dictating the form of the model, the analyst can expect such sample statistics as r^2 (proportion of variation explained) and the residual mean square to be good indicators of the predictive performance of the final regression when it is applied in the population.

The only practical difficulty with the ideal regression analysis situation is its infrequency of occurrence with real-world data sets. All too commonly, the analyst will, for various reasons, be forced to fit a number of candidate models to the data set involved. Residual analysis will often rule

out some of the candidate models for such reasons as heterogeneous variance or non-random relationship between the residuals and one or more independent variables. Usually, however, selected candidate models will remain after dismissal of the equations with unacceptable residual patterns. These remaining candidate models may or may not have the same number of independent variables. One or more independent variables might be included in all the candidate models. On the other hand, each model could include only variables that occur in no other model. Therefore, the following criteria can effectively help to choose the model, especially when the candidate models have the same dependent variables.

(i) Residual Mean Square:

The Residual Mean Square (RMS_p) statistic has been used fairly extensively as a selection criterion. Some analysts simply select as the final model the candidate regression with smallest value of RMS_p. However, it has been pointed out (Hocking 1976) that this practice is most appropriate when the objective of analysis is parameter estimation or development of a model with good explanation properties. If the objective of the analysis is the development of a model that will provide good predictions, the RMS_p statistic should probably be employed as follows:

(a) Plot the RMS_P values over p. For the larger values of p, the RMS_P values will generally fluctuate around a horizontal line. The RMS value associated with the line is denoted as $\hat{\sigma}^2$ since this values is usually be a satisfactory estimate of σ^2 (This assumes that the largest model contains all variables present in any of the smaller models.

(b) Selection of the final model is accomplished by selecting the candidate model that represents the best compromise between (i) minimizing the size of the model, and (ii) having an RMSP value that is reasonably close to the $\hat{\sigma}^2$ value.

(ii) Squared Multiple Correlation Coefficient:

Since a decrease in R^2 never occurs whenever a model is expanded by the addition of another variable, it is seldom appropriate to use maximization of R^2 as a selection rule. Instead, the model selected as best should (a) contain as few variables as possible, and (b) have an R^2 value that is not substantially less than $R_{\max}^2$, where $R_{\max}^2$ is the maximum of R_p^2 values. If the largest model contain all variables present in other models, it is often useful to plot the R_p^2 values over p. Typically, such a plotting shows the R_p^2 values for larger p lying closer to an upper asymptote of $R_{\max}^2$. As p decreases, however, there will be a point where R_p^2 values begin to decrease sharply.

The model associated with the *p* value at which this decrease begins is often a good choice as the final model.

(iii) Adjusted Squared Multiple Correlation Coefficient

The statistic is essential equivalent to RMS_p, which is far easier to interpret. It is therefore recommended that RMS_P be used in preference to R^2_{ap} as a selection criterion. The R^2_{ap} statistic has been defined because some computer programs (for example, SPSS) use maximization of R^2_{ap} as the selection criterion. Such a procedure is equivalent to selecting those subset regressions that have minimum RMS_p values.

2.7.4   Double sampling with knn estimate

2.7.4.1   Background information

The *knn* algorithm searches the feature space for the *k* nearest pixels, whose field data vectors are known, applying a distance measure, *d*, defined in the feature space. Field data from the *k* nearest pixels is transferred to the unknown pixel. The method has been widely in pattern recognition (Cover & Hart 1967, Keller *et al.* 1985) and statistics (Linton & Härdle 1998). Altman (1992) showed that the *knn* estimator might give biased estimates as the value of *k* increases, but that the bias can be weighted by weighted average of the *k* neighbours. The error rate asymptotically approaches the optimal rate of the Bayes decision rule for discrete variables when both the *k* and *n* (number of observations) tend to infinity in such a way that *k/n*→ 0 (Keller *et al.* 1985).

2.7.4.2   *Knn* estimate procedure

Fix and Hodges (1951) developed the k-nearest neighbour rule in an attempt to non-parametrically model multivariate density functions. In this rule, a neighbourhood is defined as a fixed number of pixels (k) centred on the unlabeled pixel's coordinate (x) in feature space. The class labels of these neighbouring training pixels are examined, and the class label represented most frequently is given to the query pixel. In performing classification of pixels to be utilized as a neighbourhood, and the manner in which ties in the voting will be resolved. In figure 2.14, the neighbourhood for the query pixel is predefined as its seven nearest neighbours. The unlabeled pixel is assigned to class 2, because it constitutes a majority of the seven pixels (Hardin 1994).
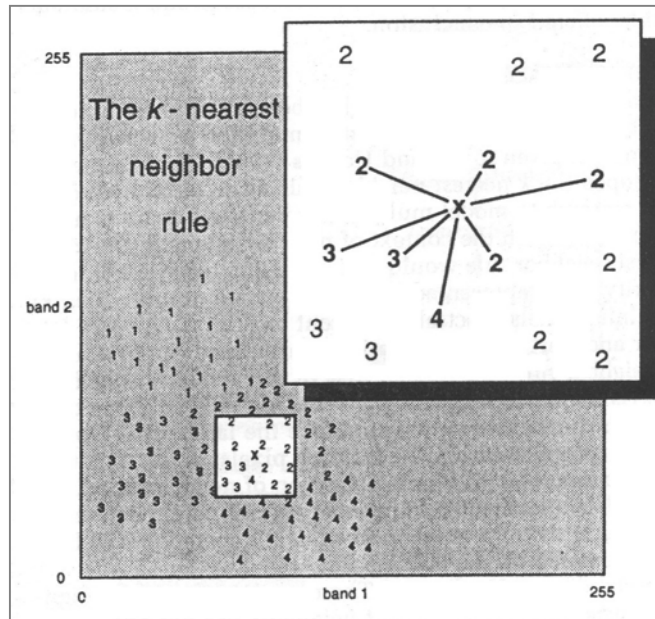
Figure. 2.14 The multiple (k) nearest neighbour rule (Hardin 1994)

The *knn* method is used here to generalize information from field plots to pixels for map production and local area estimation. The method assumes that similar forest exists within a large reference area covered by a satellite image and that the spectral radiometric responses of the pixels are only dependent on the state of the forest. Several examples can be found in literature, including: Fazakas and Nilsson (1996), Muinonen and Tokola (1990), Nilsson (1997) and Tomppo (1991, 1993, 1997a, 1997b), Franco-Lopez (2001), McRoberts *et al.* (2002.) etc.

A general description of *knn* method is as follows: the spectral distance, d_p, p is computed in the feature space from the pixel p to be classified to each pixel p_i for which the ground measurement or class is known. For each pixel p, take *k*-nearest field plot pixels (in the feature space) and denote the distances from the pixel p to the nearest field plot pixels by d_{pi}, p,,.....,d_{pk},p (d_{pi},$p \leq$....$\leq d_{pk}$,p). The estimate of the variable value for the pixel p is then expressed as a function of the closest units, each such unit value weighted according to a distance function in a particular feature space. A commonly used function for weighting distances is:

$$W_{(pi)p} = \frac{1}{d^t_{(pi)p}} \Big/ \sum_{j=1}^{k} \frac{1}{d^t_{(pi)p}} \quad \text{...(2.20)}$$

With $t = 2$. The estimate of the variable m for pixel p is then:

$$m_p = \sum_{i=1}^{k} w_{(pi)p} \, m_{(pi)} \text{,...(2.21)}$$

68

Where $m_{(pi)}$, i = 1,……………………,k is the value of the variable m in sample plot i corresponding to the pixel $p_{(i)}$, which is ith closest pixel (of 'known' pixels) in the spectral space to the pixel p (Tomppo 1997a).

This estimation procedure is used on an operational basis in the Finnish national forest inventory. Even though the procedures involved have been documented, the analysis of the behaviour and quality of the estimation has not been explored in depth. Tomppo (1997b) reported that a method for error evaluation for this technique was under development.

2.8 Literature Review: Extraction of Forest Attributes from Remote Sensing Data

Numbers of studies have already been carried out to conduct a forest inventory or predict forest attributes using remote sensing imagery. Most of the studies used the regression method. However, *knn,* stratification and neural networks were used in some cases. All of those studies were done in different forest regions including boreal, temperate and tropical forests.

2.8.1 *Boreal forest*

Gjertsen (1996) applied two different approaches for forest inventory in the boreal forest of Norway: using traditional methods based on field measurements and using two-phase sampling based on SPOT and Landsat TM data. The study used regression to predict the forest attributes from satellite data. Ardö (1992) investigated the relationship between the spectral radiance recorded by Landsat Thematic Mapper and the volume of forest compartments in a coniferous forest area of southern Sweden. The study established a relationship using regression. Häme *et al.* (1996) developed a model to predict biomass of conifer-dominated boreal forests of southern Finnland from ground measurements and Landsat TM data using regression method. The spectral models were applied to a calibrated AVHRR image mosaic covering the northern Europe reaching from the west coast of Norway to the Ural Mountains. The result was quantitatively tested in Finland.

Tomppo *et al.* (2002) estimated tree stem volume and above-ground biomass of boreal forests of Sweden and checked with the forests of Finnland using data of National Forest Inventories (NFI) and Landsat TM and IRS 1C WiFS satellite. A nonparametric K-nearest neighbour estimation method was applied using Landsat TM and field sample plot data of the Swedish National Forest Inventory (SNFI). Non-linear regression models were developed for predicting volume and biomass from WiFS data. Finally the results were evaluated from the independent estimates of Finnish Multi-source Forest Inventory.

Katila and Tomppo (2001) examined the selection of parameters for the nonparametric *knn* estimation method, which was used in the Finnish Multi-source National Forest Inventory (MS-NFI). The MS-NFI utilised NFI field plot data, satellite images and digital maps to produce forest

attributes from the single pixel to the national level. Hyyppä *et al.* (2000) conducted a research from a variety of remote sensing data on the retrieval of stem volume, basal area and mean height on typical boreal forest in southern Finland. The data includes Landsat TM, Spot PAN and XS, ERS-1/2, airborne data from imaging spectrometer AISA, radar-derived forest canopy profiles and aerial photographs. Leyk *et al.* (2003) examined two different sampling approaches in test sites of boreal forest in Eastern Finland: stratified sampling and sampling with regression estimators. Two alternative stratification rules were tested: stratification with terrestrial a-priori information (i.e. supervised classification on the image) and without (i.e. unsupervised classification) using that information. The study used airborne *E-SAR* (Experimental Synthetic Aperture Radar) and terrestrial survey data. Systematically distributed field sample plots provided a detailed reference data source for studying the relation of the backscatter signal as auxiliary variable and the terrestrial information as variable of interest. Segmentation was performed to estimate radar cross section as a basis to apply regression or stratification.

2.8.2   *Temperate and subtropical forests*

Jakubauskas and Price (1997) related various environmental and forest variables of Yellowstone Lodgepole pine forest with Landsat TM data. Franklin (1986) correlated basal area and leaf biomass for a selected study area of California. The area was dominated by Red Fir and mixed conifer stands. McRoberts (2000) estimated forest area in Minnesota using stratification. A classified Landsat Thematic Mapper satellite imagery was used as the basis for stratification. Franco-Lopez (2001) applied the *knn* method for estimation of forest cover type, basal area and volume for Aspen-Birch and Spruce-Fir forests of north-eastern Minnesota. The study tested several variations within the method including distance metric, weighting function, feature-weighting parameters, and number of neighbours. Using the nearest neighbours (k = 1), Euclidean distance, a three date 18-band composite image and feature weighting parameters, maps were constructed for basal area, volume and cover type. The study by Lee (1990) used SIR-B and Landsat TM data to obtain a better characterization of forest stand parameters of sub-tropical forests of northern Florida. Glass *et al.* (2001) examined the sampling gain due to stratification using Landsat TM satellite data of four Mississippi counties, USA. Three categories of forest composition were mapped, based on a continuous spectral metric applied to leaf-off data: 1) mostly deciduous; 2) mostly evergreen; and 3) mixed. A priori variability information about the forest within each county was used to estimate the initial number of plots, which were then allocated proportionally by the area associated with each cover-type. Incorporating the stratifications derived from the Landsat data resulted in gains in sampling efficiency by identifying and spatially locating homogeneous populations within a fragmented landscape. The study conducted by Atmawidjaja (1972) applied double sampling technique using aerial photographs for volume estimation of Heiberg Memorial

Forest, New York. The study used double sampling with regression estimator. The study discussed about the optimum sample size and compared the efficiency of double sampling with simple random sampling of similar standard error.

Salvador and Pons (1998) conducted a study for estimating forest variables in north-east Spain using Landsat TM. They analysed the relationship between tree canopy coverage and leaf area index with six non-thermal TM bands and NDVI. A two phase or double sampling for stratification has been introduced in the second Swiss national forest inventory (Köhl 1994), where in a first phase strata weights are assessed on a large sample of aerial photographic plots and variable of interests are assessed on a smaller sample of field plots. The study by Dees *et al.* (2000) presents two elements of a study on forest inventory and mapping for the test site in Germany. The area is dominated by oak and beech among broad-leaved stands and spruce among the coniferous. The study examined the gain of stratified random sampling based on aerial photographs using tree volume. The study also used *knn* method using terrestrial sample data with Landsat TM and IRS LISS data for mapping the dominant tree species.

Trotter *et al.* (1997) compared the three different methods: regression analysis, non-parametric line fitting, and an N-dimensional *k*-nearest neighbour classification scheme to predict wood volume of coniferous plantations in New Zeland from Landsat TM data. Chiao (1996) compared the three types of satellite sensors data airborne multispectral, Landsat TM and SPOT HRV for estimating forest crown closure and volume in central Taiwan. The study used stepwise regression technique for predicting tree volume and crown closure from digital count of individual band and vegetation indices.

2.8.3 Tropical forests

Lu *et al.* (2002) estimated above-ground biomass of succesional and mature forest in the Amzon basin using TM images and field-inventory. Atmospherically corrected TM data and field-measured forest variables were used in the analysis. The study examined the utility of different vegetation indices and texture measures to predict forest biomass. The study by Nelson *et al.* (2000) estimated biomass and carbon of selected sites of tropical forests in the Amazon basin using double sampling for stratification from Landsat TM image. Twenty one different classes were identified on a Landsat scene. The image was later classified. Biomass and carbon of each class was estimated from the previous studies. Steininger (2000) tested the ability of estimating above-ground biomass of tropical secondary forest from canopy spectral reflectance using satellite optical data. Data were collected from 34 re-growth stands of the selected test sites of Brazil and Bolivia.

Sader *et al.* (1989) evaluated the feasibility of detecting tropical forest succesional age class and total biomass differences using Landsat Thematic Mapper (TM) in the mountain forest of Puerto Rico.

Thenkabail *et al.* (2004) compared narrowband hyperspectral Hyperion data with broadband hyperspatial IKONOS data, multispectral Advanced Land Imager (ALI) and Landsat-7 Enhanced Thematic Mapper Plus (ETM+) data through modelling and classifying complex rainforest vegetation of southern Cameroon. Foody *et al.* (1996) used NOAA AVHRR data for estimation of tropical forest biophysical properties in south-west Ghana.

Roy and Ravan (1996) conducted regional biomass mapping in Madhav National Park, India. A stratified random sampling in the homogenous vegetation strata was done. The sample point biomass data were extrapolated for the whole study area using satellite remote sensing. The study has also generated empirical models with spectral responses. A study by Köhl and Kushwaha (1994) applied a four-phase sampling strategy based on Landsat TM data, Colour Infra-Red, Black and White panchromatic aerial photographs as well as field assessments. The study estimated the standing volume using stratification in the tropical forests of Karnataka, India. The study stratified seven classes based on Landsat TM in the first phase, density classes based on Black and White aerial photographs in the second phase and heights, number of stems and crown diameter using CIR aerial photos in phase three. Field inventory was carried out in the phase four. Foody *et al.* (2003) studied the estimation of tropical forest biomass from Landsat TM data between sites in Brazil, Malaysia and Thailand using regression and neural networks. The study also discussed the transferability of the estimates among the region.

Chapter III

3   Study Area and Stand Information

3.1   Location

The study area is located at the southern Chittagong, which is the southeastern part of Bangladesh. The area corresponds to the selected part of 136/045 scene of Landsat TM /ETM+. The size of the study area is about 300 sq. km (20km x 15km). It covers 21°29´to 21°37´ N Latitude and 92°05´ to 92°13´ E longitude (Figure 3.1).
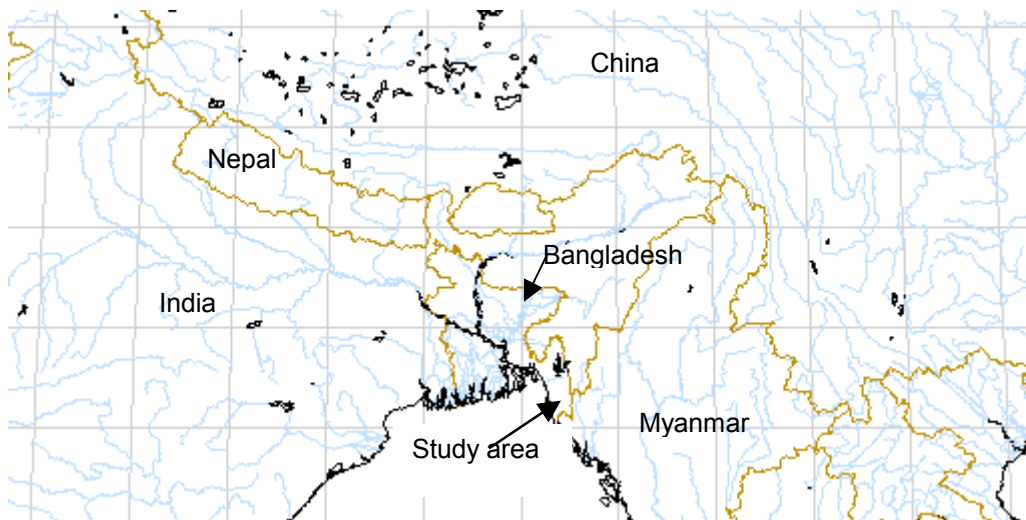
Figure 3.1 Location of the study area

3.2   Climate

The area enjoys a sub-tropical monsoon climate. Though there are six seasons in a year, three namely winter, summer and monsoon are prominent. Winter is quite pleasant, begins in November and ends in February. Usually there is no fluctuation in temperature, which ranges minimum of 18° C to maximum of 29° C. The maximum temperature recorded in summer is 32° C to minimum 26° C. Monsoon starts in July and stays up to October. The period accounts for 80% of the total rainfall. The average monthly annual rainfall varies from 400-500 mm in monsoon period (June to October) to 100 mm in dry period.

3.3   Topography

The eastern part of the study area consists of plain-lands and in some places small hills, whereas the western part consists of medium-high to high hills. The elevation starts just above mean sea level. The hills consist of alternate broad valleys. The hills usually rise from the flat valley; gradually

reach to peaks of maximum 457 meters (Das 1990). The characteristic morphological features of the region are low elongated hills running almost north south with intervening parallel valleys.

3.4   Geology and Soil

Geologically the area belongs to the tertiary period (Pliocene and Miocene epoch), whose origin dates back to 25 million years (Chaudhury 1969). In the study region different types of soils and land formations are observed. Coastal and estuarine plain-lands represent the recent alluvial soil formations of the Quaternary geological age. Low hills with rolling to steep slopes belong to the Dupi Tila Series and medium-high to high hills belong to the upper-middle Tipam Series of the Pliocene epoch. In some areas, sandy sales and fine-grained sandstone with some soils of Tertiary Miocene epoch are also found (Khan 1979).

The plain-land and valley soils of the study area are formed with recent and sub-recent alluvial sediments of tidal and river flood plains. Most of these soils are seasonally flooded, medium to moderately fine textured and have low contents of organic matter. They are moderately alkaline to wildly acid in reaction and are slightly saline. Extremely acid soils, however, locally occur in the coastal mangrove tidal flood plains. Soils developed in the hills from un-consolidated rocks with moderately well to excessive drainage are probably the oldest soils in this region. They are yellowish brown to yellowish red, sandy loam to clay loam, moderate to strong blocky and strongly to very strongly acidic. They have few to many iron-manganese concretions. Soils develop on the hills with consolidated rocks are mainly sandy loam to clay loam. They are excessively drained, pale brown to yellowish brown in color. The sub-soils are mainly sandy loam to silty clay loam, weak to strong blocky and medium to strongly acidic (Khan 1979).

3.5   Description of Forest Types

The forests of the study area can be classified as tropical wet evergreen forests and tropical semi-evergreen forest (Champion *et al.* 1965) (Figure 3.2). In the regional context the Chittagong flora differs from the Eastern Himalayan flora by the absence of Sal (*Shorea robusta*) and that from Myanmar by the absence of Teak (*Tectona grandis*). The outstanding feature of the forest vegetation is the frequent occurrence of the general Dipterocarpus, Quercus and Eugenia (*Syzygium* spp) (Baten 1969).

Figure 3.2 Tropical evergreen and semi-evergreen forests of the study area (photographs acquired during winter 2002-2003)

As all the accessible areas were transformed to shifting cultivation, virgin forests can be seldom noticed in the area. Present crop mostly consists of secondary re-growth, which is still in the process of succession to the climax evergreen type. This process of succession is often influenced by the repeated disturbance and thus leads to a drier scrubby forest or to a savanna in many areas (Khan 1979).

3.5.1 Tropical wet evergreen forests

This forest type is characterized by the presence of a considerable amount of evergreen trees in the upper canopy. The top canopy reaches a height of 40-60 meters. A few semi-evergreen or deciduous species may occur, but usually they do not change the evergreen character of the forest. The forest is rich in epiphytes, orchids, woody climbers, ferns, mosses and palms particularly in shady moist places (Das 1990).

The *Dipterocarpus* are characteristic for the evergreen stratum. A certain amount of deciduous species like *Anacardaeous*, *Swintonia* is predominating. *Sterculiaceae*, *Artocarpus* and *Sygigium* that generally form an important part of the upper canopy are often present. *Mesua ferrea* and *Hopea* are generally also found, but not at an abundant amount. Sometimes bamboo appears in certain places where upper canopy is disturbed. Bamboo is typically absent in the virgin forests where canes and palms are the main woody monocotyledons. Tree ferns sometimes occur but epiphytes and ground-ferns are frequent. In the shrubby undergrowth Rubiaceae and Acanthaceae

are common. In certain areas, gregarious occurrence of the several *Dipterocarpus* species is observed in the top canopy with a rare occurrence of any other species (Khan 1979).

3.5.2 Tropical semi-evergreen forests

The main characteristic of this forest is the presence of appreciable proportion of deciduous species in the main canopy. The canopy is correspondingly lighter during the period of minimum rainfall (November to March) due to shed of leaves. The predominance of epiphyte and climbers, as well as bamboo, which later in some extent is replaced by the canes, and palms of the climax evergreen formation.

In the upper canopy *Dipterocarpus* spp are common but not always present with evergreen species like *Mangifera*, *Lophopetalum*, *Amoora*, *Cinnamomum* and *Sygigium.* However, there is a fair proportion of deciduous species such as *Tetramcies*, *Artocarpus*, *Salmalia*, *Duabanga*, *Garuga*, *Albizzia*, *Cederala* and *Chickrassia* are usually present in the canopy. The lower canopy is mostly evergreen with various Meliaoca, Louracea, Myrtaodae and Cupuliferace. Several species of Bamboo with a few dwarf palms such as *Phryniun*, *Alpina* and *Clinogyne* are locally abundant especially in wet places. Rubiaeoae and Acanthaeae are also common in the shrub layer (Khan 1979).

3.5.3 Semi-evergreen shrub forest and savannas

This type of vegetation formation usually occurs nearby the habitation and at the accessible part of forest areas. The forests were disturbed repeatedly and formed to the scrubby vegetation. Repeated clear felling or temporary cultivation favors growth of grass, which usually burns regularly. This treatment tends to eliminate almost all the evergreen species and results in a very open savanna type forest with the presence of scattered deciduous trees of poor growth condition over dense grass. The common tree species are *Albizia* spp. *Lannea coromandelica*, *Caruga pinnata*, *Salmalia*, *Sterculia* spp. *Ficus* spp. The undergrowth of weed *Eupatorium* may be noticeable and weedy climbers are often strongly developed in many places of this forest (Khan 1979). Some areas in the study region are invaded by Sungrass (*Imperata arundinaceas*) and Khagra (*Saceftram spontaneum*) (Baten 1969).

3.5.4 Moist bamboo brakes

Mostly bamboo occurs as undergrowth and associates with other trees, but in some places pure bamboo forest is also observed. The bamboo brakes occupy extensive areas in the Chittagong Hill Tracts, which is the eastern part of study area. The important species of bamboo are Muli (*Melocanna baccifera*), Mitenga (*Bambusa tulda*), Dalu (*Neohouzeaua dullooa*), Orah

(*Dendrocalamus longispathus*) and Kalichari (*Oxytenanthera nigrociliata*). In some places extensive bamboo is found without overstorey, which is the result of former clearing. A more or less complete cover of bamboo (mainly *Melocanna*) is common in other areas. But scattered singletree over the bamboo is also found especially in depression. The different species of bamboo tend to be concentrated in separate groups though appreciable proportion of overlapping is also observed. *Melocanna* appears to flower and die gregariously at 45-50 years interval after producing seeds. The dense growth precludes the natural regeneration of most tree species and makes the areas of pure bamboo formations (Khan 1979).

3.6 Forest Jurisdiction

The study area consists of two Forest Divisions under the administrative control of Forest Department. Forest Divisions have been usually sub-divided into several Forest Ranges. Each Forest Range consists of a number of Forest Beats, which are the local administrative unit of forest management. The names of the administrative units covered by the study area are enlisted in table 3.1.

Table 3.1 Distribution of study area controlled by the Bangladesh Forest Department

Division	Range	Beat
Cox's Bazar North Forest Division	Fulchari	Khutakhali
		Fulchari
		Napithkhali
		Rajkhat
	Bhomoriaghona	Bhomorighona Sadar
		Dumchakata
		Purnagram
	Idgarh	Idgarh
		Tulatuli
		Baishari
	Meherghona	Meherghona
		Machukhali
		Kalirchara
		Dhalirchara
	Joarianala	Joarianala
		Bengdhepa
		Jumchari
		Rubber Bagans
	Bagkhali	Gilatali
		Barabil
Lama Forest Division	Sangu Range	-

4 Methodology

The aim of the current study is to extract spectral information from satellite data and relate those with field-based carbon estimation and finally simulate the carbon pool for the whole study region. The remotely sensed imagery contains spectral information on vegetation from the reflection of the electromagnetic wavelengths by the chlorophyll pigments and the physiological structure of mesophyll tissue of leaf. Field sampling provides the quantity of forest biomass and carbon stocks o the selected sample plots. Statistical and mathematical techniques combine and analyse all those information.

The schematic workflow is represented in figure 4.1. However, overlaying the classified historical and recent images generates forest cover change map and matrix; those activities are not presented in the flow chart because it makes clumsier to understand.
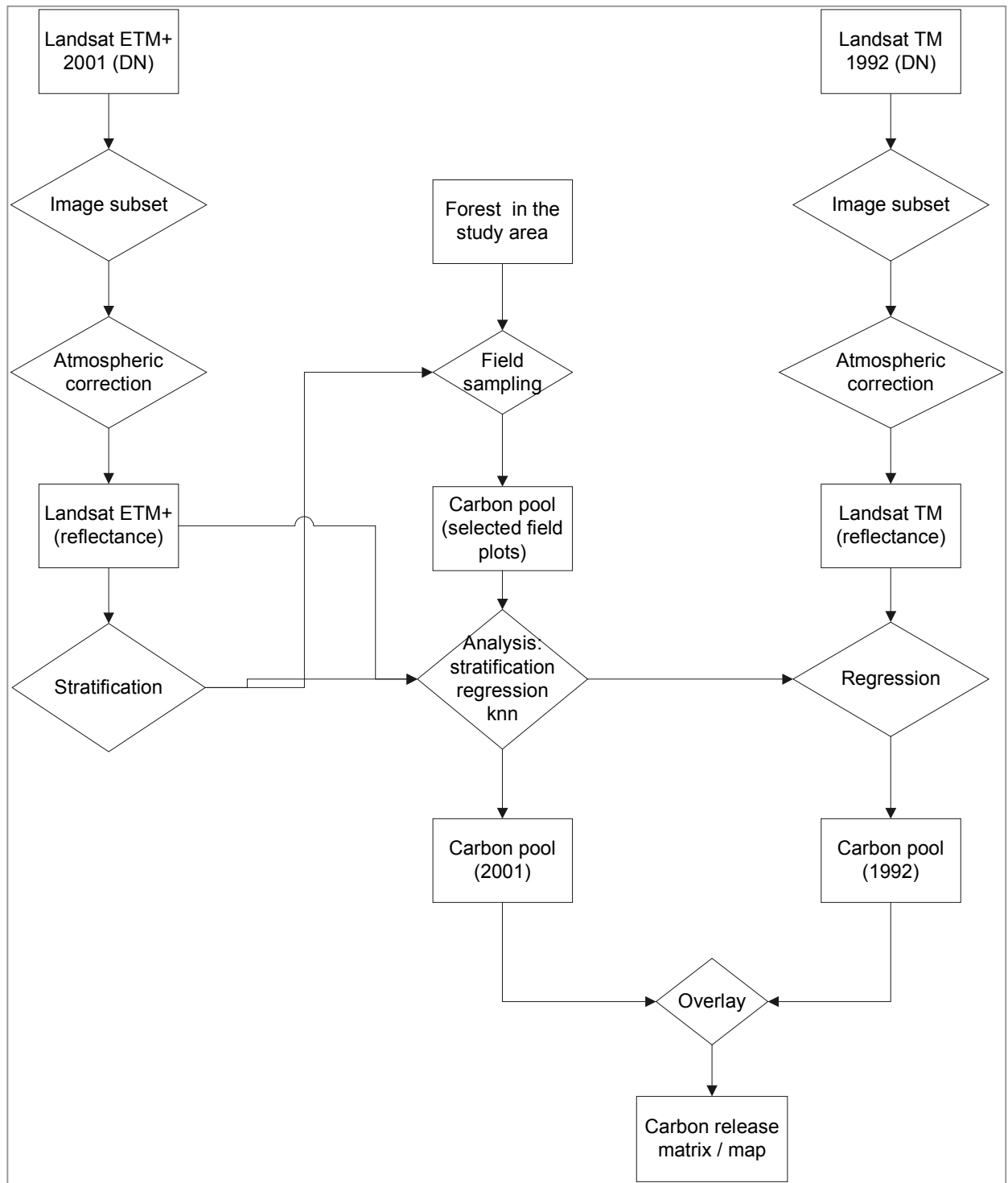
Figure 4.1 Representation of the research methodology

4.1   Remote Sensing Image Information

Landsat ETM+ & TM data are used for the study because those are relatively cheap and having satisfactory radiometric bands and also available for the designed study period. The time interval for the investigation is fixed as 1992 to 2001. Additional data set of IRS pan is used to get high spatial resolution (5mm) information. All the images are chosen at the mid of dry season when most of the perennial shrubs and grasses are dead and having minimal spectral influence over the forest vegetation. However, there is a chance of loosing information from the deciduous forest canopy due to shading of their leaves during the period. The data set corresponds to the 136/045 Landsat TM and 112/057 of IRS pan scene. ERDAS imagine and ENVI were used for image processing.

During the image purchase (mid of 2002), an effort was made to select the image as close as possible to the recent time, however it was impossible to choose any other than the selected one due to the presence of cloud coverage on the scene (Table 4.1)

Table 4.1 Remote sensing data-set of the study area and corresponding cloud coverage.

Date	Cloud coverage
18 Oct 2000	72
03 Nov 2000	5
21 Dec 2000	0
07 Feb 2001	0
27 Mar 2001	17
28 Apr 2001	52
14 May 2001	11
02 Aug 2001	99
18 Aug 2001	40
03 Sep 2001	39
19 Sep 2001	96
21 Oct 2001	3
09 Jan 2002	18
10 Feb 2002	0[*]
15 Apr 2002	58

[*]the required area was covered by fog

The cloud-free image of 7th February 2001 was selected for procurement. One scene available at the SPARRSO archive on 7th February 1992 was selected as the historical image. The IRS-scene of 10th March 1999 was purchased by TREES Project. The spectral characteristics of Landsat ETM+/TM and IRS pan channels and their utility on vegetation science are enlisted in table 4.2.

Table 4.2 Landsat Thematic Mapper /ETM+ and IRS pan spectral bands for vegetation studies
(adapted from Jensen 1996, Sabins 1997 and Irish 2004)

Satellite	Band	Wave Length (µm)	Nominal spectral location	Principal applications
Landsat 5 / 7	1	0.45-0.52 (TM) 0.45 - 0.52 (ETM+)	Blue-green	Useful for distinguishing soil from vegetation and deciduous from coniferous plants.
	2	0.52-0.60 (TM) 0.53 - 0.61 (ETM+)	Green	This band spans the region between the blue and red chlorophyll absorption bands and therefore corresponds to the green reflectance of healthy vegetation.
	3	0.63-0.69 (TM) 0.63 - 0.69 (ETM+)	Red	This is the red chlorophyll absorption band of healthy green vegetation and represents one of the most important bands for vegetation discrimination. The 0.69-µm cutoff is significant because it represents the limit of a spectral region from 0.68 to 0.75 µm where the crossover of vegetation reflectance takes place.
	4	0.76-0.90 (TM) 0.78 - 0.90 (ETM+)	Reflected infrared	For the above reasons, the lower cutoff for this band was placed over 0.75 µm. This band is especially responsive to the amount of vegetation biomass present in a scene. It is useful for crop identification and soil-crop separation.
	5	1.55-1.75 (TM) 1.55 - 1.75 (ETM+)	Mid-infrared	This band is sensitive to the turgidity or amount of water in plants. Such information is useful for plant stress and plant vigour investigations.
	7	2.08-2.35 (TM) 2.09 - 2.35 (ETM+)	Mid-infrared	This band is sensitive to the turgidity or amount of water in plants. Such information is useful for plant stress and plant vigour investigations.
	8	0.52 – 0.90 (ETM+)	Green, red and reflective infrared	As bands 2, 3 and 4 above.
IRS	Pan	0.50 - 0.75µm	Visible green-red	As Landsat bands 2 and 3 above.

4.2   Remote Sensing Image Pre-processing

4.2.1   Radiometric correction

Atmospheric correction is essential for the current study because of two reasons. First, the study uses a relationship between field-based carbon content and Landsat spectral information of different time. Although those images are on the same date but different years, atmospheric condition might be similar but not the same. Therefore, the relationship established for one time frame might mislead the result if it used for the other time unless the digital counts (DC) being converted to a common unit. Second reason is that the two images are from different sensors, where information is recorded in a very similar but not the same spectral range (table 4.2).

Generally, the objective of a radiometric atmospheric correction procedure is to convert satellite-generated digital counts (DCs) to ground reflectance (i.e. absolute surface reflectance). How the different models parameters are derived depends on the available information (i.e. ground and/or atmospheric in-situ measurements). DCs must first be converted to at-satellite radiances by removing the offset effects introduced by the imaging system. If the data have been processed to remove striping noise by using a statistical technique, these additional gains and offsets must also be included in the correction. The equation to convert satellite DCs to at-satellite radiances is

$$L_{sat\gamma} = (DC - Offset)/Gain \dots\dots\dots\dots\dots\dots\dots\dots\dots(4.1)$$

Alternatively this can also be calculated by the following equation

$$L_{sat\gamma} = LMIN\gamma + \frac{(LMAX\lambda - LMIN\lambda)}{DCMAX} \times DC\gamma \dots\dots\dots\dots\dots\dots(4.2)$$

Where,

$DC\gamma$ = Calibrated and quantized scaled radiance in units of DN, digital number for band γ

$L_{sat\gamma}$ = At satellite spectral radiance for band γ

$LMIN\gamma$ = Spectral radiance at minimum DC (0) for band γ

$LMAX\gamma$ = Spectral radiance at maximum DC (255) for band γ

$DCMAX$ = Range of rescaled radiance in DN = 255

Basically, both the equation is the same only the coefficient factors are different. $LMIN\gamma$ and $LMAX\gamma$ values for Landsat ETM+ and TM are enumerated in table 4.3 (Markham and Barker 1986, Irish 2004).

Table 4.3 Spectral radiance at minimum and maximum DC for Landsat TM and ETM+ images

Band (γ)	Landsat 5 (TM)		Landsat 7 (ETM+)			
			Low gain		High gain	
	LMINγ	LMAXγ	LMINγ	LMAXγ	LMINγ	LMAXγ
1	-0,15	15,21	-6,2	293,7	-6,2	191,6
2	-0,28	29,66	-6,4	300,9	-6,4	196,5
3	-0,12	20,43	-5,0	234,4	-5,0	152,9
4	-0,15	20,62	-5,1	241,1	-5,1	157,4
5	-0,037	2,719	-1,0	47,57	-1,0	31,06
7	-0,015	1,438	-,35	16,54	-0,35	10,80
8	-	-	-4,7	243,1	-4,7	158,3

It should be noted that the units are different for two Landsat sensors. The units are in milliwatts per square centimetre per steradian per micrometer ($mW*cm^{-2}*ster^{-1}*\mu m^{-1}$) and watts per square meter per steradian per micrometer ($W*m^{-2}*ster^{-1}*\mu m^{-1}$) for TM and ETM+ respectively. The values are applicable after 15 January 1984 (TIPS-era processing) for TM and 1 July 2000 for ETM+ (high gain, obtained from image header).

Next, at-satellite radiance must be converted to surface reflectance by correcting for both solar and atmospheric effects. The general model/equation used to do this and presented by Moran *et al*. (1992) is

$$REF = \frac{\{PI*(Lsat\lambda - Lhaze\lambda)}{TAUv*\{Eo*Cos(TZ)*TAUz + Edown)\}} \qquad \ldots\ldots\ldots\ldots\ldots(4.3)$$

REF = Spectral reflectance of the surface

Lhaze = Upwelling atmospheric spectral radiance scattered in the direction of and at the sensor entrance pupil and within the sensor's field of view ($Wm^{-2}sr^{-1}\mu m^{-1}$), i.e., the path radiance.

TAUv = Atmospheric transmittance along the path from the ground surface to the sensor.

Eo = Solar spectral irradiance on a surface perpendicular to the sun's rays outside the atmosphere ($Wm-2\mu m-1$). *Eo* contains the Earth-sun distance term (d*d) imbedded and is in astronomical units. Therefore, mathematically *Eo* = ESUNλ / d^2, where, *ESUNλ* for TM/ETM+ scene is presented in table 4.4 (Markham and Barker 1986 and Irish 2004). The Earth-sun distance in astronomical unit

is a function of time of year and range from about 0,983 to 1,017 and can be calculated by the formula

$$d = \frac{1}{1 - 0,01674\cos\{0,9856(JD - 4)\}} \quad\ldots\ldots\ldots\ldots\ldots\ldots\ldots\ldots\ldots\ldots(4.4)$$

d can also be obtained from an Ephemeris for the date of image acquisition (for example http://ssd.jpl.nasa.gov/cgi-bin/eph where observer range and rate option in the output format should be activated).

TZ = Angle of incidence of the direct solar flux onto the Earth's surface (solar zenith angle, Thetaz).

TAUz = Atmospheric transmittance along the path from the sun to the ground surface.

Edown = Downwelling spectral irradiance at the surface due to the scattered solar flux in the atmosphere ($Wm^{-2}\mu m^{-1}$)

Table 4.4 Landsat TM/ETM+ Solar Exoatmospheric Spectral Irradiances

Band (γ)	Landsat 5 (TM) Milliwatts/(cm squared*μm)	Landsat /(ETM+) Watts/(meter squared*μm)
1	195,700	1969,000
2	182,900	1840,000
3	155,700	1551,000
4	104,700	1044,000
5	21,930	225,700
7	7,452	82,070
8	-	1368,000

All the radiometric correction procedures start with this general model (equation 4.3). But make different by simplifying assumptions that eliminate certain parameters. The information available about the data and atmospheric conditions determines what assumptions must be made and

therefore, the specific model that is to be used. Often, the method used to derive the required parameters can also determine assumptions that must be made (Chavez 1996).

4.2.1.1   DOS model

Dark object subtraction (DOS) is perhaps the simplest yet most widely used image-based absolute atmospheric correction approach for classification and change detection applications (Spanner *et al.* 1990, Ekstrand 1994, Jakubauskas 1996, Huguenin *et al.* 1997). The basic assumption is that within the image some pixels are in complete shadow and their radiances received at the satellite are due to the atmospheric scattering (path radiance). This assumption is combined with the fact that very few targets on the Earth's surface are absolutely black, so an assumed one percent minimum reflectance is better than zero percent. The article by Chavez (1989) discusses an improved method of selecting the dark-object haze values for the separate spectral bands. The objective of the improved dark-object method is to select spectral-band haze values that are correlated to each other, rather than by using the histograms of each spectral band independently, which can cause haze-selection problems when topographic/shadow conditions are minimal. Both methods generate haze values that are very similar when sufficient topography exists, as in the images used for this study (Chavez 1996).

Besides correcting for the same parameters that the apparent reflectance model does, the image-based DOS radiometric correction model also corrects for the atmospheric additive scattering component attributed to the path radiance. Therefore, in the general radiance-to-reflectance model shown in Equation 4.3, the following applies for the DOS model:

TAUz = 1.0 (ignores atmospheric transmittance),
TAUv = 1.0 (ignores atmospheric transmittance),
Edown = 0.0 (ignores downwelling), and
Lhaze = value derived from the digital image using the dark-object criteria.

The main advantages of the DOS model are that it is strictly an image-based procedure and does not require *in-situ* field measurements and that is simple and relatively straightforward to apply. The main disadvantages are that for reflectance values greater than about 15 percent the accuracy is often not acceptable and that the selection of the haze values must be done with care (Chavez 1996).

4.2.1.2   Improved image-based model (COST model)

The improvement in this model is to add a correction for multiplicative transmittance effect. The equation 4.3 shows that is the error for not including a multiplicative transmittance factor is approximately 1/(TAUz * TAUv). The study by Chavez (1996) shows that it incurs an approximate overall error of 30 percent. Therefore, a correction for multiplicative transmittance component can substantially improve the DOS model results. In that study two different methods were used to derive the required TAU values in equation 4.3. Both methods that correct for multiplicative transmittance effects are independent of *in-situ* atmospheric and ground measurements. Field-independent derived TAU values were used, along with the DOS Lhazeλ additive-scattering component due to path radiance, in the general radiance-to-reflectance model (equation 4.3) to compute surface reflectance.

The first method used to derive TAU values independent of *in-situ* field measurements. The multiplicative transmittance component for scattering and weak absorption is approximated by the following equations (Moran *et al.* 1992):

TAUz = EXP {-del * sec (TZ)}…………………………………….(4.5)
TAUv = EXP {-del * sec (TV)}…………………………………….(4.6)

 Where, del = optical thickness at given wavelengths

   TZ = solar zenith angle (θz)

   TV = viewing angle, zero degrees for Landsat scenes (θv)

The above equations show that transmittance is a function of the solar zenith angle (TZ) and the optical depth (del). For most of the required images, TZ is in the range of 30 to 55 degrees and del has a range of 0,08 to 0,30. Therefore, in the EXP {-del * sec(TZ)} function, the variation of sec(TZ) is about 2,7 times larger than that for del, which implies that TZ (the solar zenith angle) is the more dominant variable. So, a relation that is strictly dependent on TZ to approximate the exponential function, to a first order, may be acceptable (i.e. set it equal to the cosine of TZ).

To examine the empirically observed relation between the cosine of solar zenith angle (TZ) and EXP(-del * sec (TZ)}, the power series expansion was used. The first four terms of the power series are

Cos(TZ) = 1 $-TZ^2/2!$ + $TZ^4/4!$ $- TZ^6/6!$…………………………….(4.7)

EXP{-del * sec(TZ)} = 1 −   del * sec(TZ) + (del^2) * {sec(TZ)^2}/2! − (del^3) * {sec(TZ)^3}/3!
………………(4.8)

Where, the solar zenith angle TZ is in radians and ! represents factorial.

The average TZ and del values for all the dates used in that study are 0.64 and 0.17 respectively. Using these two average values in the power series expansions generates values of 0.8021 for the cosine and 0.8087 for the exponential when carried out four terms; if only the first two terms are used, the cosine value is 0.7952 and the exponential value is 0.7882 (both are within one percent of each other). Therefore, using the cosine of the solar zenith angle for TAUz substantially improves the DOS result. In fact, the results are as good as those generated by HBC model. The correction using the cosine of the solar zenith angle, cos(TZ) is termed as COST model.

COST model uses the following criteria in the general radiance-to reflectance model in Equation 4.3:

TAUz = Cos(thetaz)
TAUv = Cos(thetav) = 1 because thetav is zero degrees for nadir view,
Edown = 0.0 (ignores downwelling) and
Lhaze = Values derived from the digital image using the dark-object criteria (identical to the DOS model)

The current study assumed the reflectance of a dark object is 1 percent (Chavez 1996, Moran *et al.* 1992).

There are several ways to choose an appropriate dark object DN. The following methods were used for the current study
(http://www.gis.usu.edu/docs/projects/swgap/ImageStandardizationFAQ.htm):

   a)   Landsat images were loaded using ERDAS Imagine software.

   b)   Image statistics were recalculated with an X and Y skip factor of 1 (ignore value 0 icon was activated as well) from ImageInfo Edit menu.

c) The histograms were displayed and examined. The DN choice for the Dark Object would be the lowest value at the base of the slope of the histogram. If the slope is gradual (i.e. contains very few (< 100 pixels of low DN values) these should be ignored, and the DN value chosen where slope of the histogram begins to increase more dramatically. In the figure, an appropriate DN value for the Dark Object would be 31 (figure 4.2).

As in the DOS model, the main advantage of these models are that they are strictly image-based procedures and therefore, do not require *in-situ* field measurements and they are simple and very straightforward to apply. Compared to that DOS model, the accuracy generated by the COST models substantially improved, and use of RTC software is not required. However, as for the DOS model, a disadvantage is that the dark object DN value for Lhazeλ must be selected carefully (Chavez 1996).
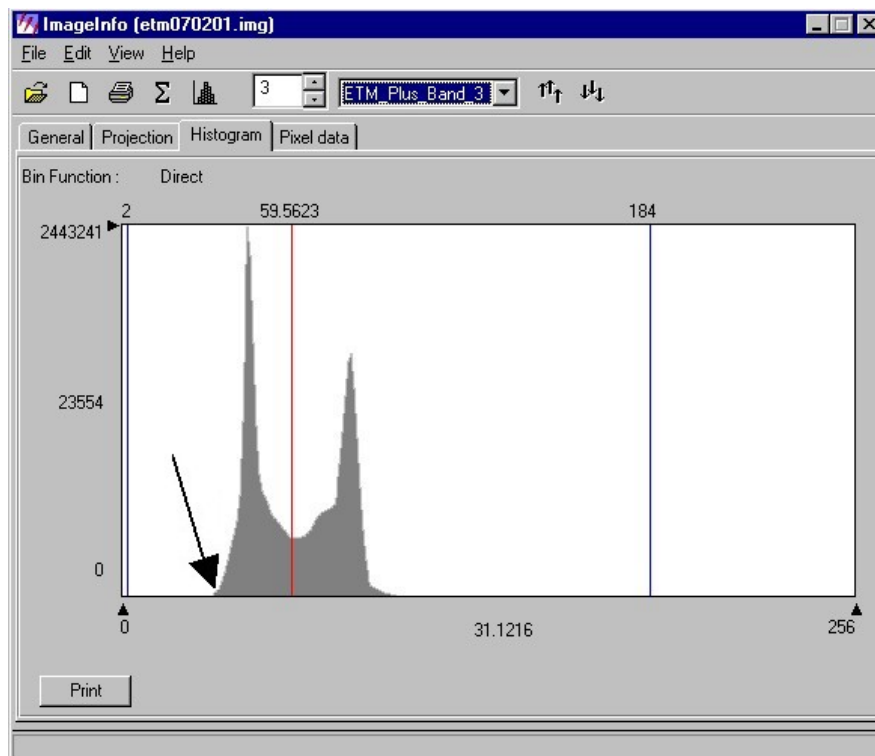
Figure 4.2 Selection of appropriate dark object from a Landsat image. In this figure 31 was selected as an appropriate DN value for the dark object (Landsat ETM+ 2001, Band 3).

This approach assumes the existence of dark objects (zero or small surface reflectance) throughout a Landsat scene and a horizontally homogenous atmosphere. The minimum DN value in the histogram from the entire scene is thus attributed to the effect of the atmosphere and is subtracted from all the pixels (Chavez 1989) More sophisticated algorithms derive atmospheric

optical properties from dark objects in the image, and correct the images with the derived information.

4.2.2   Geometric corrections

Accurate geometric fidelity is particularly important for change detection analysis study and also for which incorporates field information. Overlay analysis of post-classification thematic coverage, or the simultaneous analysis of multi-spectral data necessitates accurate spatial orientation of the input datasets. Because analysis is performed on a pixel-by-pixel basis, any mis-registration greater than one pixel will provide an anomalous result for that pixel. To overcome this problem, the RMS error between any two dates should not exceed 0.5 pixels. This is typically accomplished by performing an image-to-image registration. Usually, one date is selected for absolute registration to ground coordinates, followed by the image-to-image registration to the geo-coded image. In locations with a high degree o topographic relief, the employment of a digital elevation model (DEM) data may be required to achieve the necessary degree of geometric agreement (Lunetta 1999). For the second case field plots usually use GPS to identify its location. If the geometric location of the image pixel is not accurate it will create mis-match of the field plot and it will create bias result during the incorporation of field information on remote sensing image.

The accurate geometric registration is very important for the current study. The geometrically corrected recent image (Landsat ETM+) was acquired form USGS. However, a linear shipment was discovered during the field mission and therefore the image was shifted accordingly. Lambert Conformal Conic (LCC) (detailed parameters on Appendix II) is used as projection. Image to image registration was done using standard method to geo-code all the remaining images. Nearest neighbour method was used for re-sampling using ERDAS Imagine software to the images to keep the original spectral value as close as possible to the raw image.

The study area consists of small hills. But topographic normalization was not possible to apply due to the unavailability of digital elevation model. The accuracy of geo-coding was checked using a portable GPS from the known location of the geodetic points of Survey General of Bangladesh. The result is presented in Appendix III.

4.3   Development of Visual Interpretation Key

A computer-aided unsupervised classification scheme was applied to the Landsat ETM+ image. Simultaneously a variety of image channels were displayed on computer-screen and tried to find an optimal combination where a variety of vegetation classes were distinguishable. Additionally a

correlation matrix of different spectral bands for the sample pixels was calculated to ease the band selection process. Interpretation could delineate eight different vegetation classes. All variety of vegetation classes was reached during 2002-2003 for field investigation. The location was identified by a portable GPS. A detailed description of vegetation was recorded and a panoramic camera photo was taken for each of the field-plots. A total number of seventy sample plots were collected. The surface reflectance value of the Landsat ETM+ image corresponding to the field samples was separated. The values were further categorized for different vegetation types and presented in the results. The interpretation key was generated from the experience of image characteristics of each vegetation class and corresponding vegetation types in the field.

4.4 Pre-stratification of Landsat ETM+ Image by Supervised Classification

A number of training areas were selected for classification using image signature editor menu of Erdas Imagine. Care was taken to select only the homogeneous class as the training sets. Training areas were distributed throughout the class to ensure the adequate representation of all those classes. Approximately 1000 pixels were chosen form each forest class. Region growing properties tool of signature editor was used expand the training pixels in some cases. Feature space image having two-dimensional scattergram of various band combinations of Landsat channels was sometimes useful to separate some classes.

4.5 Field Sampling:

4.5.1 Location of sample plot

All the field sample plots were located by using a portable GPS. The plot was distributed among various strata. Care was taken to locate the plots (i) in relatively homogenous area so that the error originated from the location uncertainty can be minimized and (ii) in the area which did not change during the last decade so that error generates from the estimation of carbon of historical image would be minimum. Local forestry officials helped to collect the field samples. A number of 90mX90m plots (known as primary sampling unit) corresponding to the 3X3 sample pixel window of remote sensing image was located on the field. A handheld GPS (Garmin GPS 12, further information:http://www.garmin.com/products/gps12/spec.html) provides 15 m real-time accuracy in the field; therefore it provides a satisfactory precision. The study area consists of a mixed forest with a variable density. In few cases GPS signal was hindered by the dense canopy and adjacent hills. Then GPS signal was recorded at the adjacent area and the location of the plot was estimated by geodetic techniques. As 90mX90m plot in the ground is large and in a relatively homogenous

ground a sub-sampling (known as two-stage sampling) would be economic. Figure 4.3 and table 4.5 represent the distribution of the field sample plots.
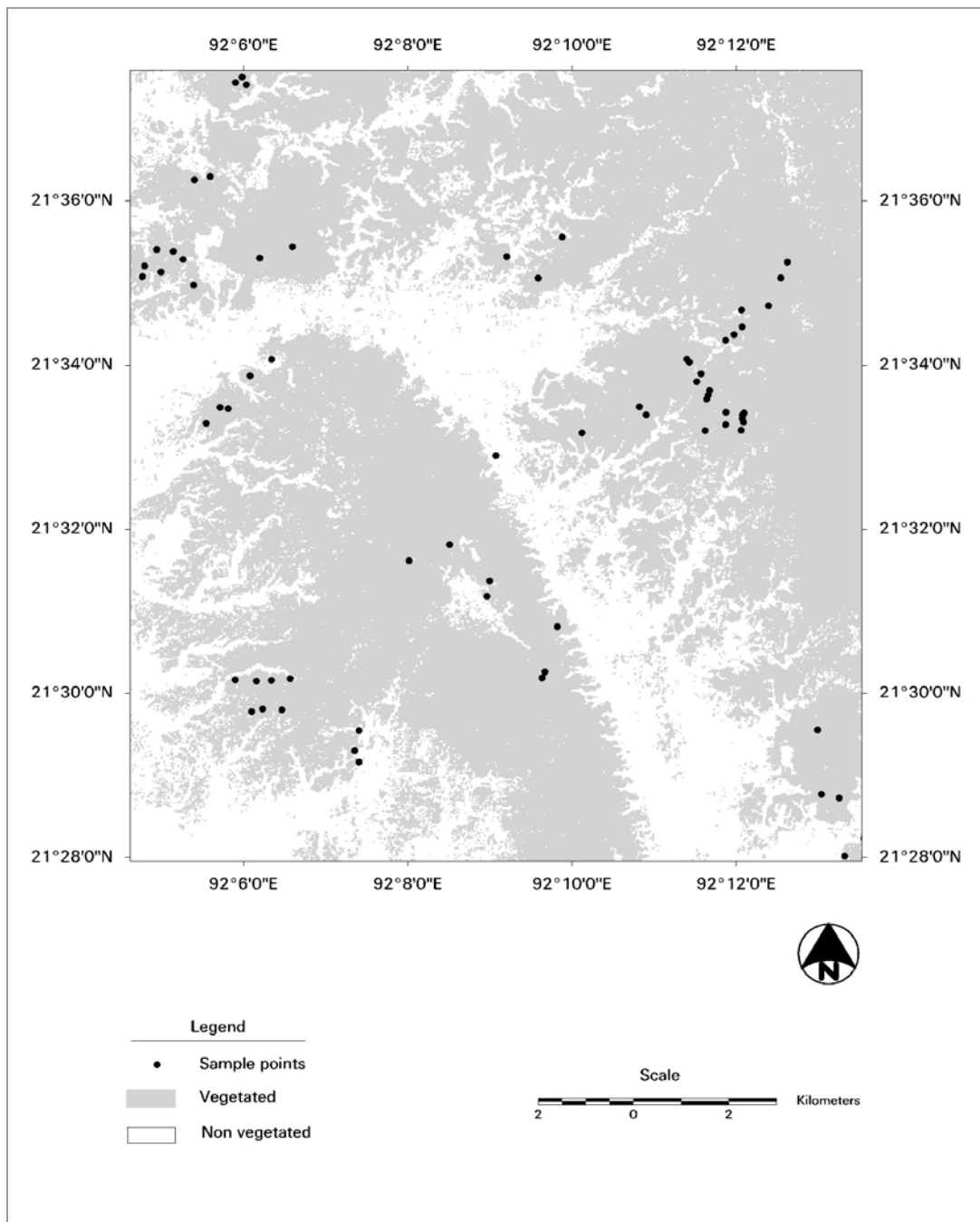
Figure 4.3 Location of field sample plots among different strata in the study area.

Table 4.5 Distribution of field samples among various vegetation classes

	Phase I		Phase II			
Nr.	Landsat image class	Total area in image (ha)	Field sampling			Sampling intensity (%)
			Plot size (ha)	Number of plots	Area sampled	
1	Primary forest	3 950	0,09	12	1,08	0,0273
2	Secondary forest	1 032	0,01	7	0,07	0,0068
3	Bamboo	2 565	0,0025	7	0,0175	0,0007
4	Shrub	3 023	0,0025	7	0,0175	0,0006
5	Plantation of indigenous species	2 555	0,01 0,0225	9 5	0,2025	0,0079
6	Teak plantation	3 745	0,01 0,0225	6 3	0,1275	0,0034
7	Acacia	342	0,01	6	0,06	0,0175
8	Rubber plantation	3 006	0,01	8	0,08	0,0027
9	Non-forest	11 035	-	0	-	-
	Total	31 255		70		

4.5.2 Sample size calculation

The finite population sample size (approximate 95% confidence level) (Shiver & Borders 1996):

$$n = \frac{\sum_{h=1}^{L} \dfrac{N_h^2 S_{yh}^2}{W_h}}{\dfrac{N^2 B_M^2}{4} + \sum_{h=1}^{L} N_h S_{yh}^2} \quad \ldots\ldots\ldots\ldots\ldots\ldots\ldots\ldots\ldots\ldots\ldots 4.8$$

where,

n = estimated sample size

N = number of sampling units in population = $\sum_{h=1}^{L} N_h$

N_h = number of sampling units in stratum h

L = number of strata into which population is divided

S_{yh}^2 = sample variance among sampling units within stratum h

B_M = desired bound on the overall population mean per sampling unit (for this study 5%)

W_h = proportion of sample size allocation to stratum h ($0 < W_h < 1$)

Table 4.6 represents the statistics of the collected sample plots.

Table 4.6 Mean and variance of different strata

Serial no.	Forest type	Mean carbon content (ton/ha)	Variance
1	Primary forest	134,37	2722,24
2	Secondary forest	86,84	261,90
3	Bamboo	62,70	231,32
4	Shrub	0,87	0,20
5	Plantation of indigenous species	83,73	2927,24
6	Teak	60,81	680,86
7	Acacia	30,62	49,58
8	Rubber	30,95	524,16

The numerator of the equation 1 = 8649191.35

The denominator of the equation 1 = 102216.73

The required sample size= 85

If we would like to make proportional allocation each stratum requires 85 X 0.125=10.6 or 11 sample plots.

The number of sub-sample plots within each primary sampling unit was arbitrarily selected; one secondary plot within one primary sampling unit. The number of primary sample plots within each stratum can be determined by the following formula (Harding and Scott 1978):

Sample size $n = \dfrac{t^2 (cv)^2}{AE^2}$ …………………………………………(4.9)

Where AE is the maximum allowable error specified for this study as a percent of the mean and t is the weighting factor from student t distribution and accounts for the probability of achieving the specified level of accuracy with a given sample size. CV is the coefficient of variation, which is a

93

measure of variability within a population. First a number of plots should be measured within each stratum to calculate *CV*. Then required number of sample plots can be calculated by using the above formula.

4.5.3 *Sub-sampling plot size*

Usually, plot sizes for forest sampling (in this study those plots are termed as secondary sample unit) are often chosen on the basis of experience (Avery and Burkhart 1994) for particular forest type or region. The plot size represented in table 4.7 is common for sampling in Chittagong forest, Bangladesh. The two-sage sampling is presented in figure 4.4.

Table 4.7 Plot size for two-stage sampling in the second phase of sampling strategy

Stage I	Stage II
Plot size: 90mX90m (corresponds to 3X3 pixel window of Landsat image)	Primary forest: 30mX30m Old plantation: 15mX15m Young plantation or Secondary forest: 10mX10m Bamboo: 5mX5m Shrubs: 5mX5m
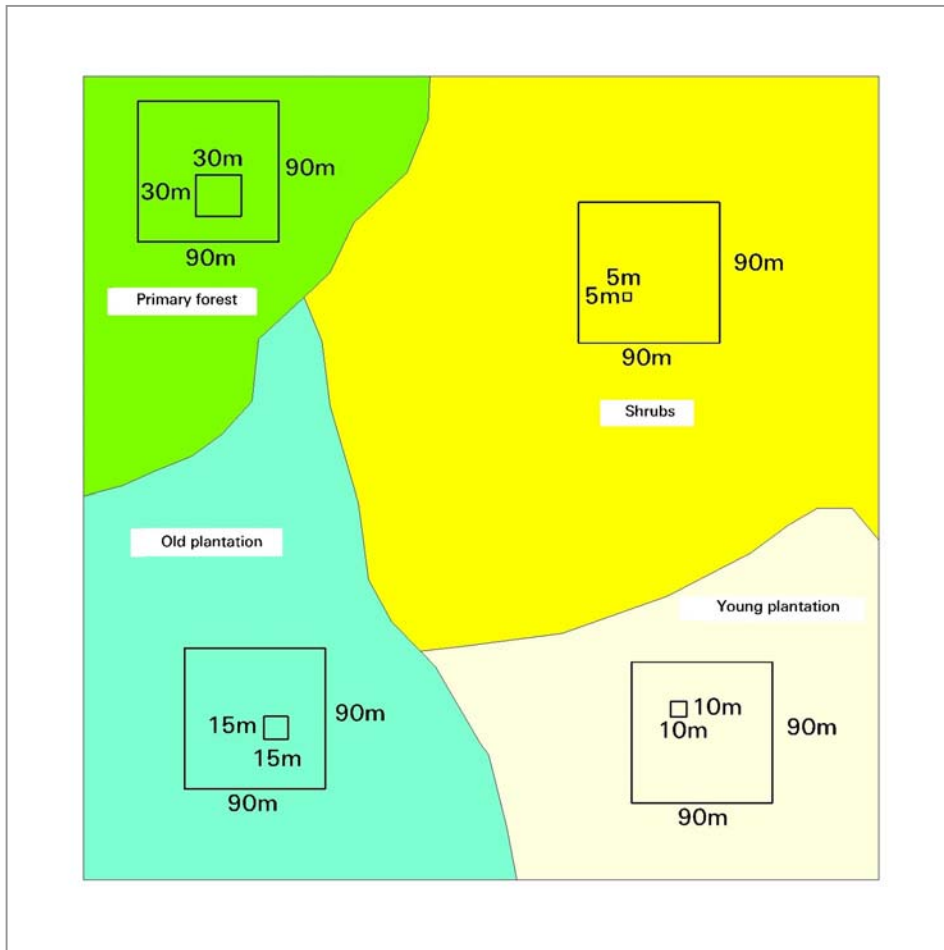
Figure 4.4 Representation of two-stages sampling for various vegetation types

Therefore, the current study aims to use the above sized sample plots. The efficient plot size can also be calculated by optimisation process. Where the coefficient of variation has been determined for plots of a given size, the coefficient of variation for different-sized plots may be approximately calculated by the following formula (Freese 1962):

$$(cv_2)^2 = (cv_1)^2 \sqrt{\frac{P1}{P2}} \quad \dots\dots\dots\dots\dots\dots\dots\dots\dots\dots\dots(4.10)$$

Where, cv_2 = estimated coefficient of variation for new plot size

cv_1 = known coefficient of variation for plots of previous size

P_1 = previous plot size

P_2 = new plot size

The optimisation process to determine a plot size is described by Zeide (1980). However, this will increase the research cost. It should be noted that if we increase the plot size, the required number of sample to meet a desired precision level would decrease.

4.5.4   Field measurement of sub-sample plots

All trees with a diameter at breast height *(dbh)* exceeding 5 cm inside the plot were measured. Under-storey vegetation consisting of small trees with less than 5 cm *dbh*, shrubs, herbs and grasses was sampled from one 2mx2m sub-sample plot located at the centre of the sample plot to determine the under-storey biomass. Available allometric relation was used to convert *dbh* and height to volume for those species where available. In case of the unavailability of the relationship for a particular species one equation for mixed species was applied. For shrubs, bole volume was calculated using a formula for cone and then a particular ratio was added to include the branches and biomass volume.

4.5.5   Estimation of plot biomass

4.5.5.1   Measurement of tree diameter and height

Diameter is commonly measured in forestry. Again, because tree boles are not circular, different measurements of diameter are possible. Diameter at breast height (dbh) is probably the most common measurement made on a standing tree as this exhibits better correlation with volume and biomass as well as provides efficiency in measurement. Direct measurement of diameter is commonly done by measuring two different axes: the diameter of the maximum and minimum axis of the bole on trees that are clearly elliptical or the diameter of the maximum axis and the axis at 90 degrees or the diameter of any two axes at 90 degrees to each other. The two diameter measurements are averaged using an arithmetic mean (most common) or a geometric mean (for highly elliptical boles). The measurement of diameter on one axis is often acceptable when the data is only being used to group trees into a stand table (Anon 2002). However, such problem of measurement can be minimized by using a diameter tape and hence this was used for the current study.

4.5.5.2   Conversion of *dbh* and height to biomass by allometric relationship

Plot biomass was calculated from measured *dbh* and height by using the allometric relationships developed by Bangladesh Forest Research Institute (BFRI) (detail in Appendix V). Volume will be converted to biomass by using appropriate conversion factors (Appendix VI). When the factor for a

particular species is not available a mean value was calculated from the other species and applied. Bole biomass was converted to the total tree biomass by adding 0.65 of stem as followed by FAO (1997) when those are not available. It would be assumed that the carbon fraction for the aboveground biomass is 0.5. Multiplication of carbon fraction with stand biomass generates the aboveground carbon stocks of each plot. The list of the species found during field sampling is enlisted in Appendix VII. Data collected by field sampling is presented in Appendix VIII.

4.6   Estimation of Carbon Pool

4.6.1   Stratification

Supervised classification was used to stratify the forest. Eight classes were separable on a remote sensing image (table 4.6). Details of all the classes have already been described. A number of variables have been selected for post-stratification. At first all the individual bands were selected for stratification. Image enhancement and transformation based on Vegetation Indices, Tasselled Cap and Principal Component Analysis were also used as a basis of stratification. In all the cases the plots were categorized into five groups according to the above-mentioned criteria. Variances $\bar{V}$ were calculated in each cases and the best method were selected based on the minimum variance.

4.6.2   Regression estimator

Regression was calculated by SPSS software. A backward selection method was applied to select the best method. Backward elimination begins with all regressors and eliminates one at a time. The first removal is the regressor, which results in the smallest decrease in R^2 (thus the smallest partial F-statistic). The procedure is continued until the candidate regressor for removal experiences a partial F values which exceeds the pre-selected F_{out}.

The forms of linear and non-linear equations examined in the current study are enumerated in table 4.8.

Table 4.8 Various forms of regression equations

Keyword	Equation	Linear equation
Linear	$Y = b_0 + b_1X$	
Logarithmic	$Y = b_0 + b_1\ln(X)$	
Inverse	$Y = b_0 + b_1/X$	
Quadric	$Y = b_0 + b_1X + b_2X_2\ b_3X_3$	
Cubic	$Y = b_0 + b_1X + b_2X_2 + b_3X_3$	
Compound	$Y = b_0b_1X$	$\ln(Y) = \ln(b_0) + X\ln(b_1)$
Power	$Y = b_0(Xb_1)$	$\ln(Y) + \ln(b_0) + b_1\ln(X)$
S	$Y = e^{b_0+b_1/X}$	$\ln(Y) = b_0 + b_1/X$
Growth	$Y = e^{b_0+b_1X}$	$\ln(Y) = b_0 + b_1X$
Exponential	$Y = b_0(e^{b_1X})$	$\ln(Y) = \ln(b_0) + b_1X$
Logistic	$Y = (1/u + b_0b_1^X)-1$	$\ln(1/Y - 1/u) = \ln(b_0) + X\ln(b_1)$

Where,

Y = Carbon (ton/ha)

b_0 = a constant

b_n = regression coefficient

X = independent variable (spectral reflectance at specific band)

ln = the natural log base

e = base e logs

u = upper bound value for logistic

The current study applied the concept of dummy variables to estimate the carbon from remote sensing image. The variables considered in the study come from the result of stratification. The coefficients of dummy variables for different strata are presented in table 4.9.

Table 4.9 Use of dummy variables (dummy variables generated from the result of stratification)

Group	Z1	Z2	Z3	Z4	Z5	Z6	Z7
Acacia	1	1	1	1	1	1	1
Bamboo	0	1	1	1	1	1	1
Plantation of indigenous species	0	0	1	1	1	1	1
Primary forest	0	0	0	1	1	1	1
Rubber	0	0	0	0	1	1	1
Shrubs	0	0	0	0	0	1	1
Teak	0	0	0	0	0	0	1
Secondary forest	0	0	0	0	0	0	0

4.6.3   *Knn method*

4.6.3.1   Distance metric

Distances between neighbours were computed using the Euclidean distance metric. The general expression for the distance between pixel *p* (to be classified) and pixel p_i, for which the ground data is known, is as follows:

$$d_{p(pi)} = \sqrt{\sum_{j=1}^{nf} (x_{p,j} - x_{(pi),j})^2} \quad \dots\dots\dots\dots\dots\dots\dots\dots\dots\dots\dots\dots\dots\dots\dots(4.11)$$

Where $x_{p,j}$ = digital number for the feature *j*, *nf* = number of feature in the spectral space

4.6.3.2   Neighbour's weighting function

In order to investigate the relative importance of the neighbours in constructing estimators, the weight of the pixel p_i in estimating a variable on pixel p was computed using three different weighting functions: (a) equal, (b) inversely proportional to the distance and (c) inversely proportional to the square of the distance. These weights are obtained from Equation (1) by choosing t = 0, 1 or 2 respectively.

For carbon estimation, once the distances among neighbours and their weights in the estimation were calculated, the *knn* method estimator was applied to each pixel. The estimator of the variable *m* for the pixel *p* is then obtained from Equation 2.20.

4.6.3.3   Feature weighting parameters

Not all the features in the feature space share the same influence in the prediction of a forest variable for a given pixel. Assuming that there exists a linear combination of features that can provide the best result, additional weights were computed and applied to the original features. This weighting parameter was developed by Nelder and Mead (1965), adapting the amoeba 'recipe' from Press, Teukolsky, Vetterling, and Flannery (1994) to cross-validation problem. The resulting expanded form of Eq 4.11 is:

$$Dp(pi) = \sqrt{\sum_{j=1}^{nf} a_j^2 (x_{p,j} - x_{(pi),j})^2} \quad \dots\dots\dots\dots\dots\dots\dots\dots\dots\dots\dots\dots\dots\dots(4.12)$$

Where a_j = weighting parameter for feature *j*.

4.6.3.4   Estimation procedure

The *knn* software developed by Department of Forest Resources, University of Minnesota (Haapanen and Ek 2001) was used in this study. The programs are coded in a DOS-environment so that they can be compiled Unix, Linux or Windows. They are written for the most part in C, but utilize some features of C++.

The following parameters were used to compute carbon content of 2001 using Landsat ETM+ and filed sampling plots:

Used in calculation: only satellite image
Number of satellite image: 1

Use coefficients: no coefficient

Number of bands: 6

Number of plots: 70

Number of neighbours used in the estimation: 1

Weight function used: equal weight

Most variable band: band 4

Search radius for uplands and lowlands in meters: no limit.

4.6.4 *Selection of the best method*

4.6.4.1 Prediction error estimation

After obtained an independent estimate based on the above all methods for each one of the pixels in the training set, the results were evaluated using prediction error, which measures how well a model predicts the response value of a future observation.

For every trial, the accuracy of our estimates of carbon was examined using the root mean squared error (*RMSE*) (omitting the sampling error term, variance)

$$RMSE = \sqrt{\sum_{i=1}^{n} (y_j - \hat{y}_i)^2 / n}$$ ....(4.13)

Where y_i is the variable of the interest on the *i*th observation and y_i is the predicted value from applying the entire above prediction rule. However, estimating the true prediction error of a model using the same data used to fit it tends to be too 'optimistic,' since the model is fine-tuned to that data. In other words, the test sample is the same as the training sample and the estimator tends to be downwardly biased. Estimates of prediction error obtained in this were aptly called apparent error estimates (Efron and Tibshirani 1993).

4.6.4.2 Bias calculation

Bias is the absolute difference of the observed and predicted value. Mean and standard error of bias can be calculated by the following formulas:

$$\bar{e} = \sum_{i=1}^{n}(y_j - \hat{y}_i) \, / \, n \quad \ldots\ldots\ldots\ldots\ldots\ldots\ldots\ldots\ldots\ldots\ldots\ldots\ldots\ldots\ldots(4.14)$$

$$s(\bar{e}) = \frac{s(e)}{\sqrt{n}} \quad \ldots\ldots\ldots\ldots\ldots\ldots\ldots\ldots\ldots\ldots\ldots\ldots\ldots\ldots(4.15)$$

Where, *s(e)* is the standard deviation of errors $\hat{y}_i - y_i$ and also the variance component of RMSE, which does not include the possible bias.

The quantity $s(\bar{e})$ can be used for testing whether the bias deviates significantly from zero. Deviations greater than $2\,s(\bar{e})$ from the field plot based estimate of mean are here considered to be statistically significant.

4.7 Estimation of Carbon Release

An overlay analysis of the geographic carbon databases (recent and historical) provides a spatio-temporal estimate of the amount of carbon release from the ecosystem during the synoptic time interval. The total amount of carbon release due to changes in forest cover classes is calculated by using the co-occurrence of the carbon classes. A number of carbon release classes representing a certain quantity of carbon loss from the historical to recent time, can be defined on the superimposed databases. The sum of the individual carbon release classes multiplied by the extension (area) allows for the estimation of total carbon release during the synoptic study period. The study used the following equations:

i) Initial carbon stock

$$C_I = C_{ii} * \sum_{i=1}^{n} A_i \quad \ldots\ldots\ldots\ldots\ldots\ldots\ldots\ldots\ldots\ldots\ldots\ldots(4.16)$$

ii) Final carbon stock

$$C_F = C_{ff} * \sum_{i=1}^{n} A_i \quad \cdots\cdots\cdots\cdots\cdots\cdots\cdots\cdots\cdots\cdots (4.17)$$

iii) Net carbon release

$$C_R = (C_{ff} - C_{ii}) * \sum_{i=1}^{n} Ai \quad \cdots\cdots\cdots\cdots\cdots\cdots (4.18)$$

When ($C_{ff} > C_{ii}$)

iv) Net carbon sequestration

$$C_S = (C_{ii} - C_{ff}) * \sum_{i=1}^{n} Ai \quad \cdots\cdots\cdots\cdots\cdots\cdots (4.19)$$

When ($C_{ii} > C_{ff}$)

Where, A is area in ha, C_I and C_F are the total initial and final carbon stock in ton respectively, C_{ii} and C_{fi} are the initial and final carbon stocks of individual polygons representing a unique carbon class i (i = 1,2,3….n) in ton/ha respectively; C_R is the net carbon release and C_S is the net carbon sequestration between the synoptic study year.

Chapter V

5   Results

5.1   Atmospheric Correction

The digital numbers (DNs) of satellite image has been converted to surface reflectance by the calculation process (section 4.2.1). The details of calculation of calibration and radiometric correction of Landsat images are presented in Appendix I. An example of one correction of Landsat ETM+ image scene (selected subset) is shown in figure 5.1.
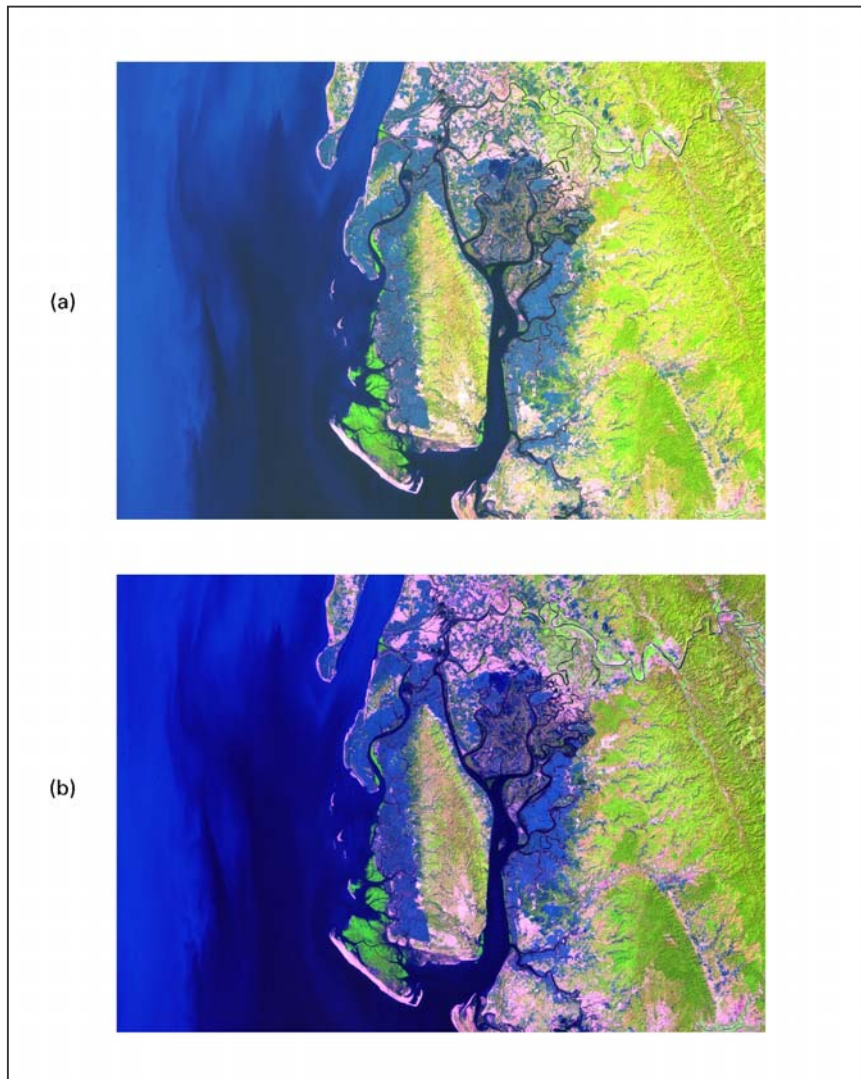
Figure 5.1 Results of radiometric correction of Landsat ETM+ 2001 image using COST method: (a) not corrected (b) corrected image

Figure 5.1 shows that the atmospheric haze in the image before correction is reduced by the radiometric correction process. This is visually detectable in all different features of the image especially concerning sediments in water, vegetation and bare ground. The essential part of the correction (i.e. the conversion of digital number to surface reflectance) cannot be visualized.

5.2   Interpretation of Vegetation

5.2.1   Selection of optimal band combination

The correlation matrix of the spectral bands contains useful information about the redundancy of information and selection of optimal band combination for interpretation purpose. If the bands show strong correlation (value near to 1.000) this indicates that the bands usually contain similar information to each other. When those bands are visualized, the minimum separibilty among different feature would be noticed. The correlation matrix of spectral values of six bands of the selected seventy plots can be represented as:.

Bands	1	2	3	4	5	7
1	1.000					
2	0.861	1.000				
3	0.856	0.942	1.000			
4	0.070	0.175	0.012	1.000		
5	0.609	0.809	0.847	0.210	1.000	
7	0.660	0.832	0.898	0.096	0.978	1.000

From the above table it can be noticed that the correlation is very high within the visible (band 1-3) and mid-infrared bands (band 5-7). It means that there is a high redundancy of information within those bands in the vegetated areas. So it makes more sense to select the bands, which contain

minimum redundancy. Therefore, only one band from each of the above categories i.e. visible, near infrared and mid-infrared, can be selected for getting the best separibilty of different kinds of vegetation using Landsat ETM+ image. As it is common to use band 3 from the visible bands and 5 from the mid-infrared bands the current study has also decided to do so. Therefore, bands 3, 4 and 5 were finally selected for the interpretation purpose.

5.2.2   Interpretation of tropical vegetation

Band 1, 2 and 3 of Landsat ETM+ represent the visible light of blue-green, green and red reflectance respectively. The reflectance of vegetation in the visible spectrum dominates due to the presence of leaf pigments. Shrubs usually contain a lower amount of biomass, which has higher reflectance in the three visible channels. In contrast, bamboo, which is a monocotyledon, appears with a high spectral absorption in this region. Vegetation, which contains a huge amount of green leaves and biomass (i.e. bamboo, natural forest, Acacia plantation etc.) usually shows greater absorption in the visible green and red spectral region. On the other hand, vegetation that has fewer amounts of those components (i.e. shrub, rubber) exhibits relatively higher reflectance in that spectral region. It should be noted that vegetation containing a little amount of green biomass might have included some of the reflectance from underneath soil. It is interesting to note that the reflectance in visible-red is higher than the green region for vegetation containing little amount of biomass, however, the relationship is opposite for those vegetation layers containing huge amounts of biomass, because red light is largely absorbed by chloroplasts and used in photosynthesis. Therefore, it can be concluded that the first derivative of visible-red to green reflectance might contain some useful information on the green biomass content of tropical broad-leave vegetation. As band 3 provides the highest variability among the visible channels and hence it makes sense to use this channel for interpretation of vegetation (Figure 5.2).
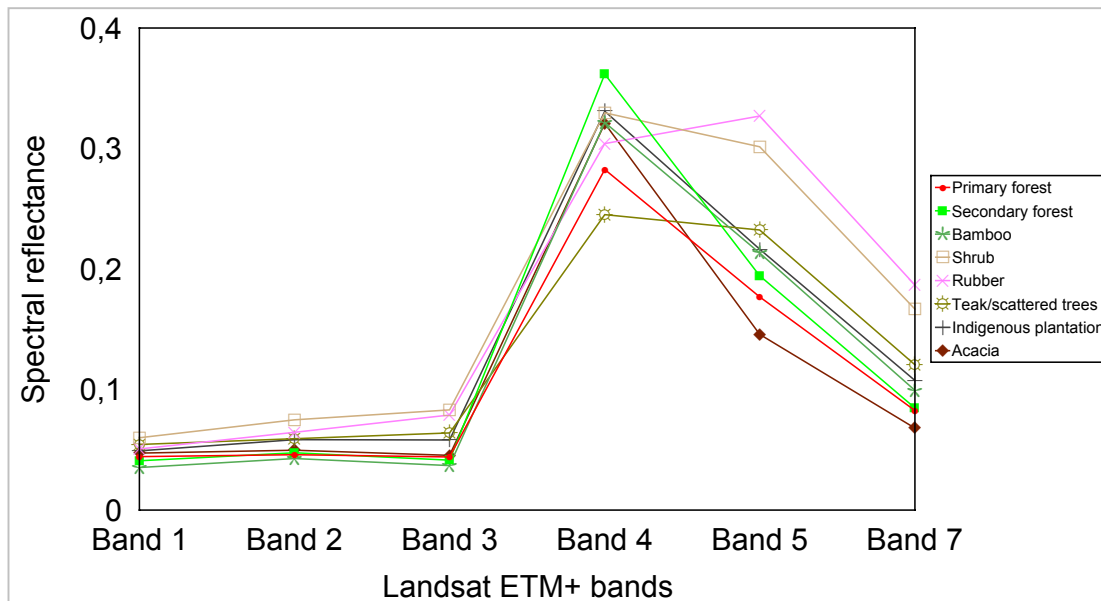
Figure 5.2 Comparison of spectral reflectance for different vegetation types

Band 4 corresponds to the reflectance of near infrared region, which is very high for vegetation and therefore it is widely used to separate vegetation from other types of landuse. Usually reflectance in this band is transparent to chloroplasts, but highly reflected by spongy mesophyl. Young secondary forest shows the highest reflectance in this region and teak/scattered trees have the lowest. Mature natural forest shows relative lower reflectance than the young secondary forest. Though mature forests have the similar species composition as the young secondary forests, the difference might be the result of the difference of the structure of mesophyl tissue. The mesophyl tissue in the leaves of young vegetation creates stronger reflectance than the mature vegetation. In addition, presence of more shadows on mature forest canopy might have some influence on it. As band 4 shows a high variability among different vegetation classes it would be useful to use this band for vegetation interpretation.

Band 5 corresponds to the shortwave-infrared region, which is quite sensitive to the amount of water present in plant leaves. Rubber plantation and shrub vegetation class shows a high reflectance in this spectral region. This is because of either presence of little amount of water on plant leaves in these classes or the reflectance was dominated by the soil-background. Acacia plantation exhibits the lowest reflectance. This vegetation does not contain any true-leaf. Leaves usually shed at the seedling stage and the phyllod become swollen and act the function of leaf. Probably those modified phyllods contain a large amount of water than the leaves of other vegetations of the study area. This spectral region shows a high variability of reflectance within various classes of vegetation. It means that the band could be quite suitable for separation of different types of vegetation on a satellite image. All the spectral lines in figure 5.2 have crossed

each other in between the region of near-infrared and mid-infrared. Consequently, the first derivative of bands 5 to 4 might contain valuable information for vegetation class separation in the tropics.

Band 7 also contains the information of shortwave-infrared channel, which is also an indicator of the presence of water in plant leaves. However, all the lines in figure 5.2 from the band 5 to 7 remain almost parallel among each other. So, band 7 contains only the redundant information of band 5 for interpretation of vegetation. Hence, if band 5 is already used in rgb visualization further use of 7 will not improve the interpretation capability.

From the above discussion it can be concluded that the use of bands 3, 4 and 5 could be optimal for interpretation of vegetation as we can only use maximum three channels as the basic colour combinations. The next question arise which band should be used in which combination. If 5 4 3 bands are assigned to red, green and blue the vegetated area will appear as green. If 4 5 3 combination is used the vegetation will be red. As human eye can distinct red better than green the latter combination could separate vegetation classes in a better way. However, working continuously with red on computer screen is a stressful for eye, the other combination is recommended for certain time.

5.2.3   Separation of individual class

As figure 5.2 shows only the mean value of reflectance, further graphs were developed to show the variability of reflectance in each class (Figure 5.3). In this figure, high-low graph represents the mean value at the centre with a plus and minus of 95% confidence limit, which means that a chance at this probability level the mean value of reflectance lies within this threshold.
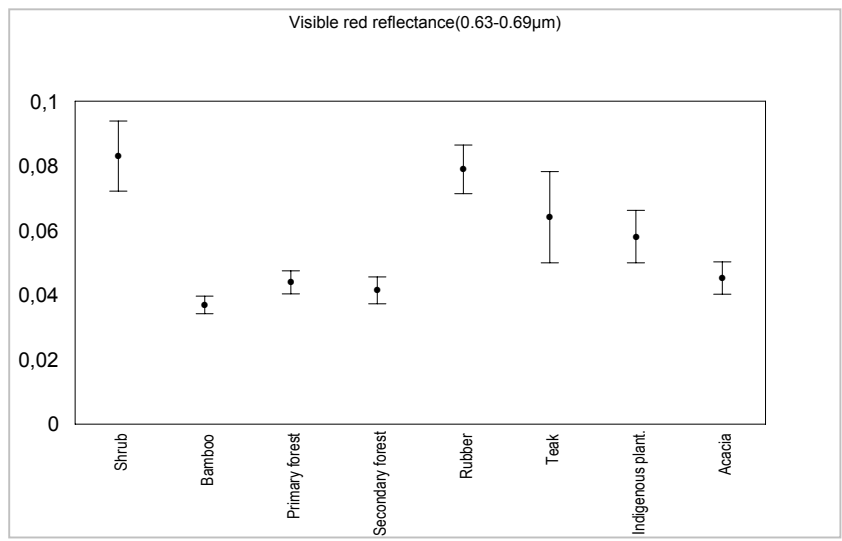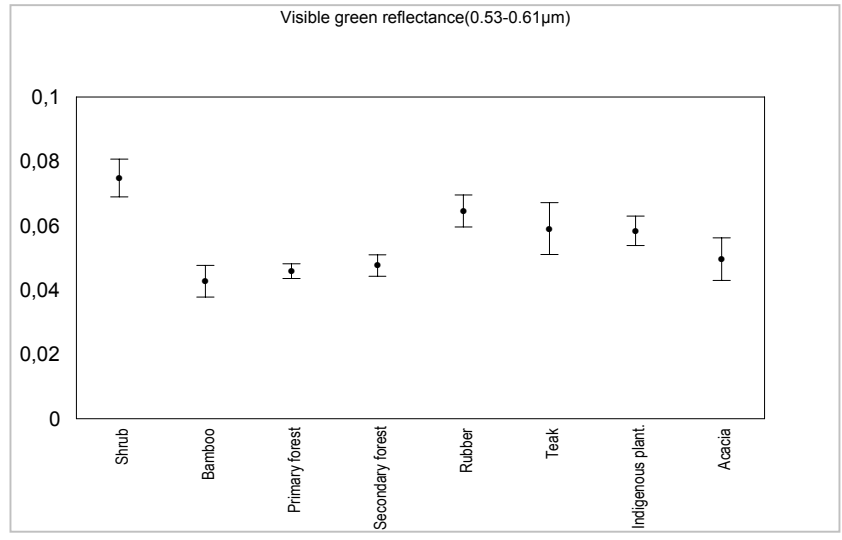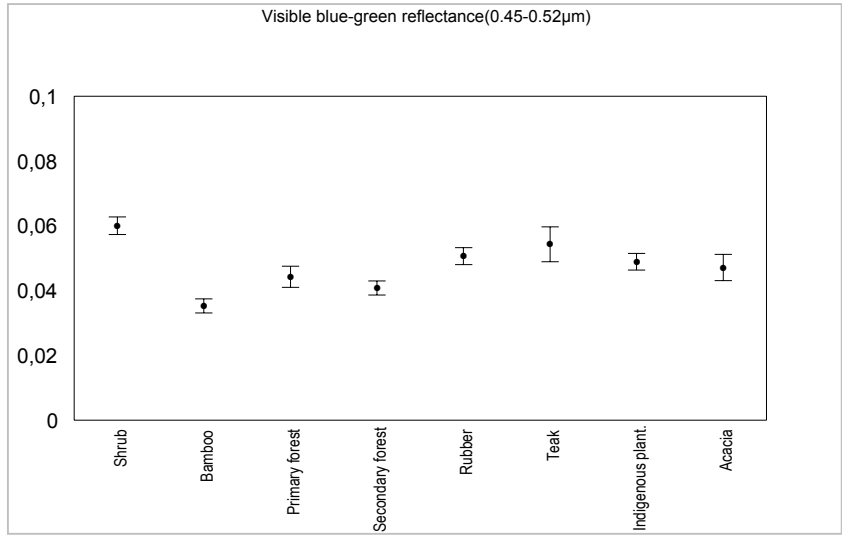
Figure 5.3 Spectral reflectance for different vegetation types. Vertical lines show mean values with 95% confidence limit (contd.)
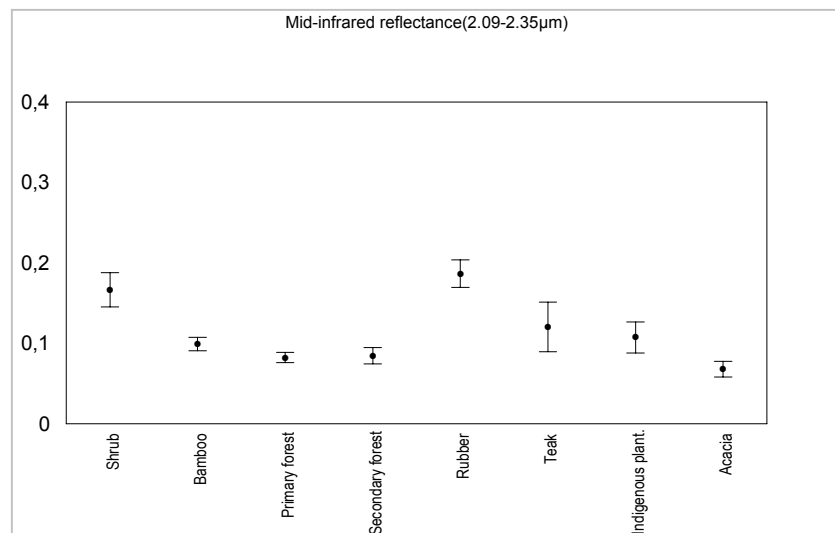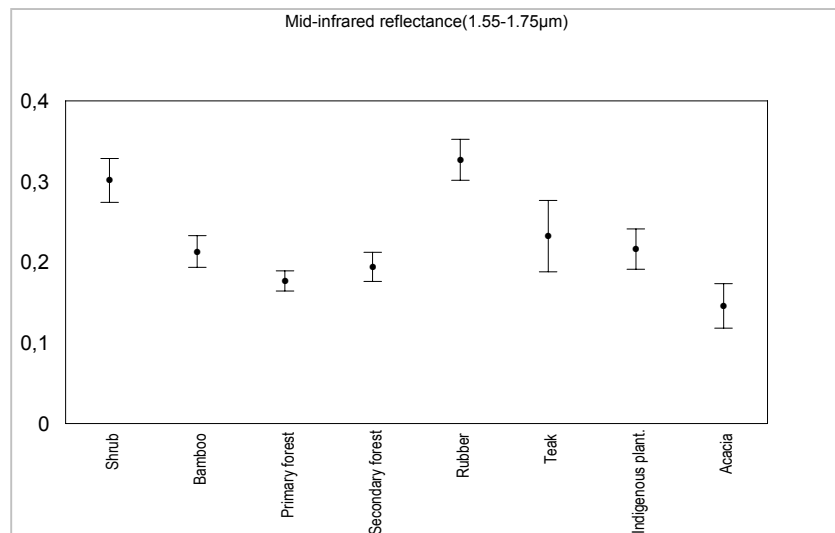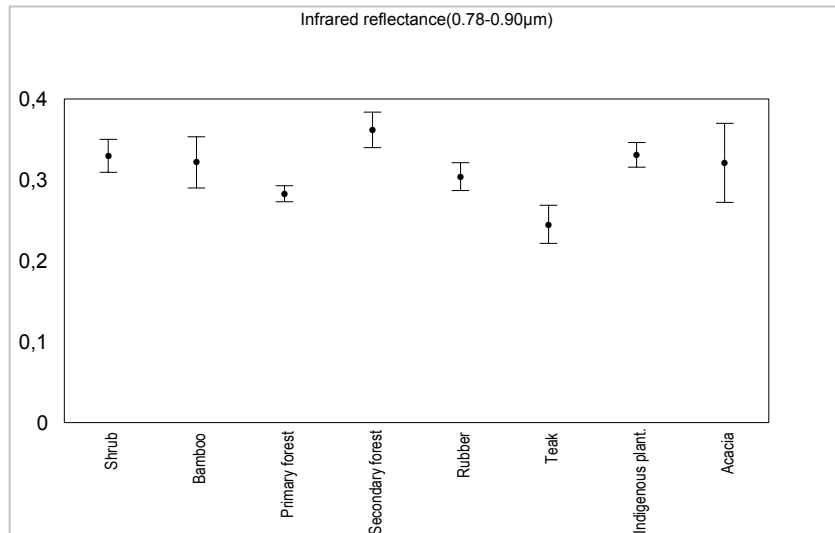
Figure 5.3 Spectral reflectance values for different vegetation types. Vertical lines show mean values with 95% confidence limit

The reflection in the visible region occurs due to the presence of plant pigments (i.e. chlorophyll). The reflections in this region for different vegetation types show a distinct pattern (Figure 5.3). From the figure, it can be concluded that the visible red reflectance (band 3) has a relative better separability than other spectral bands.

In the visible red-reflectance shrub, rubber and teak are identically different than primary and secondary forest, bamboo and acacia. Differentiation between primary and secondary forests using only the reflectance in the visible bands is not possible. However, image texture might help to separate primary from secondary forests. Secondary forests usually have a smooth texture than the primary one. The class shrub and rubber has quite similar and high reflectance. The reflectance of teak just follows them partly. Shrub is usually having a relatively thin layer of canopy than the other vegetation types and sometimes mixed with background soil reflectance. Though the canopy of rubber is quite different than the shrub, during the time of image acquisition rubber canopy was quite leafless, and therefore the understorey shrub layers dominated the reflection. Consequently the reflection is not identically different from the scrubby vegetation. Furthermore, teak has bigger leaves, which usually are not dense enough to hide the understorey. This plantation strongly discourages the growth of understorey vegetation and therefore, the reflection perhaps was a mixture of upper canopy leaves which are intermixed with background soil reflectance. This assumption is likely being true for the scattered trees, which are also not differentiable form teak plantation using Landsat ETM+ image.

The reflectance of primary and secondary forests, bamboo and acacia are identically lower than the above vegetation types in the visible red reflectance. All these vegetations are having a thick layer of canopy and are often multi-storeyed. Plantations with indigenous species are having reflectance in between these two categories. Those plantations are often not having thick multi-storeyed canopy due to the previous weeding and thinning operation.

However, the applicability of the visible blue-green and green (band 1 and 2) cannot be ignored for particular cases. For example, the reflectance from shrub and rubber is not identically different in the visible red reflectance but they are in the visible blue-green and green reflectance.

The reflection in the near infrared region is dominated by the interface of hydrated cell walls and intercellular spaces are different for various vegetation types. The reflection of primary forests and teak is identically lower than shrubs, secondary forests and indigenous plantation in this spectral region. The reflection of the rest category lies in between these two types of vegetation. It is interesting to note that the reflectance from the primary and young secondary forest is different

111

though they are having the similar species composition in their top-canopy. This difference might be associated with the difference of age. So it can be concluded that the spectral reflectance due to the internal leaf structure varies with age, and young vegetation has a higher reflectance than the mature one in this spectral region though shadow might have an additional influence on it.

The reflectance in the mid-infrared region is dominated by the absorption of energy by liquid water on plant leaves. The reflectance pattern from different categories of vegetation is similar for two of the bands at mid-infrared region (Figure 5.3). Acacia plantation shows a high absorption in this region. This is followed by the class of primary and secondary forests, bamboo, indigenous and teak plantation. It is observed that the reflection from shrub and rubber is significantly higher than the other classes. This phenomenon has also been noticed in the visible red spectral region.

5.2.4 Selective interpretation key

The above result can be summarized and presented in table 5.1 for interpretation purpose. To ease the interpretation, the Landsat image and its corresponding field photos have also been included (Figure 5.4 and Figure 5.5).

Table 5.1 Description of vegetation type and their appearance on a Landsat image (4→red, 5 → green and 3 → blue)

Vegetation type	Vegetation characteristic	Interpretation remark
Primary (tropical wet evergreen and semi-evergreen) forests	• Multi-storeyed forests with a number of matured trees in the upper canopy; shrubs and sometimes bamboo in lower canopy • In some areas a gregarious occurrence of *Dipterocarpus* species is noticed	• Dark brown with sometimes reddish brown spots • Rough texture • Irregular boundary
Secondary (young) forests	• Mixture of a number of species at pole-stage • Cleared several years ago and left undisturbed	• Red to reddish brown • Smoother texture than the mature forests
Mixed vegetation dominated by bamboo	• Dominated by bamboo (Muli: *Melocanna baccifera*, Mitinga: *Bambusa tulda*) with sometimes scattered trees in the upper canopy • Assoication varies with local topography, top and mid slope covered by small-sized bamboo (Muli) whereas foothill and valleys by larger bamboos (Mitinga) • Some bamboo plots are subject to extreme human interference	• Yellow and yellowish brown • Texture varies with region • Difficult to distinguish from natural forests when bamboo is intermixed
Shrubs	• Shrubs intermixed with seedling and sapling of natural vegetation, bamboo and grasses • Formerly covered by natural forests, repeated disturbance resulted scrubby or bush type vegetation	• Light yellow with green, smooth texture • If canopy is closed appears light yellow but in case of exposed soil it appears green • Located nearby the habitation
Acacia plantation	• Plantation with *Acacia auriculformis* and *A. mangium* • Excellent growth was noticed	• Dark red with smooth texture, dark tone is sometimes identical • Identification between two species is not possible without ground information • Usually follows a regular boundary
Mixed plantation of indigenous species	• A variety of indigenous species: *Dipterocarpus turbinatus, Sysygium grande, Artorcarpus Chaplasha, Gmelina arborea, Chikrassia tabularis* etc.	• Reddish brown, smooth texture, regular boundary
Scattered trees, teak plantation, teak coppice	• This class has a large variability, all the mentioned class appears as the same spectral response on a Landsat image • Teak coppice appears if teak plantations were removed • Scattered trees appear due to the extreme human interference on natural forests	• Green with dark brown spots. Those spots might appear due to scattered remaining of natural vegetation inside this class • Teak trees have large leaves with no undergrowth, scattered trees with scrubby surrounding appears as same. • No difference can be made with teak plantation or coppice
Rubber plantation	• Introduced before one-two decades for the production of rubber • The spacing is variable • Rubber tree sheds leaves during winter. Beginning of January the leaves turn to pale; by the end of the month trees are complete leafless	• Green on Landsat image. This tone appears from bare soil because trees were leafless during the time of image acquisition
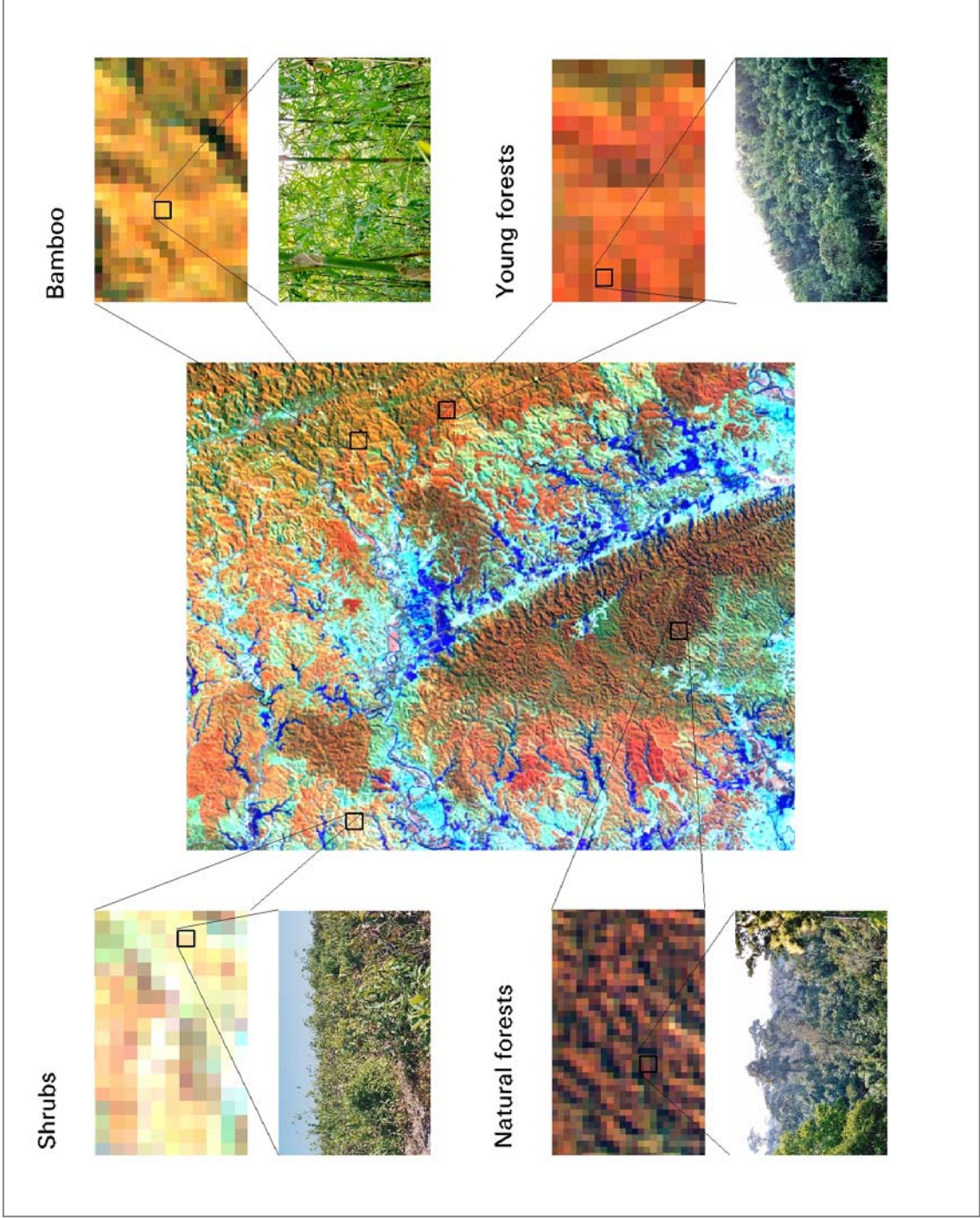
Figure 5.4 Interpretation of natural tropical vegetation on Landsat ETM+ imagery
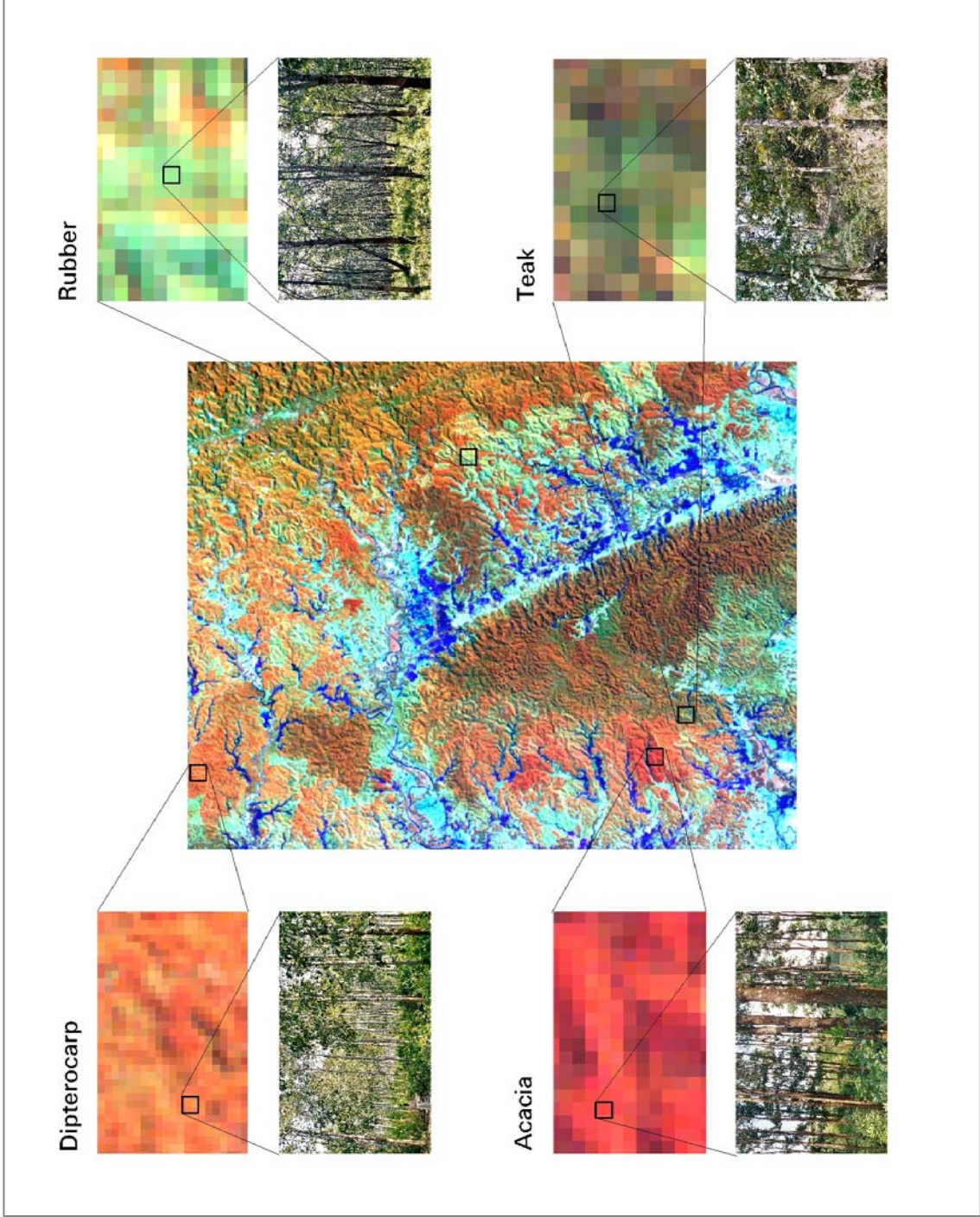
Figure 5.5 Interpretation of tropical plantation on Landsat ETM+ imagery

One additional IRS-pan dataset of 1999 was used to get a better interpretation. IRS-pan data was integrated with the Landsat ETM+ image by using rgb-his-rgb and Brovey transformation. Result of such a transformation is presented in Figure 5.6.
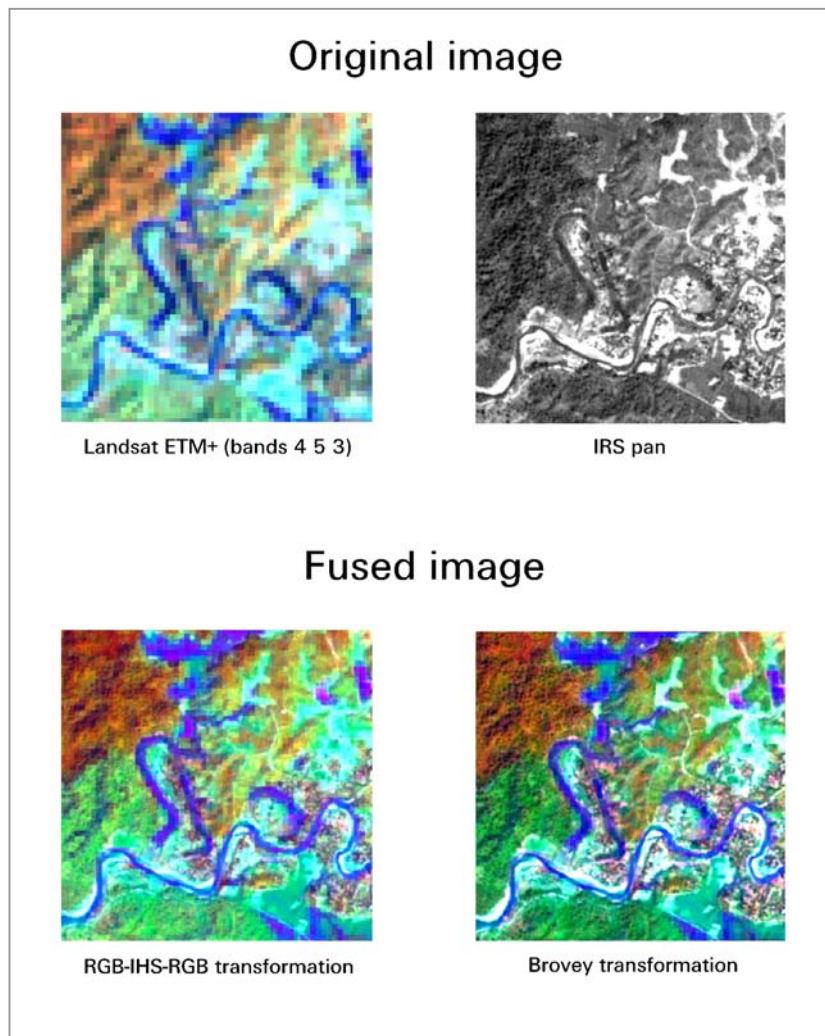
Figure 5.6 Improving interpretations using multi-sensor image fusion

The above figure shows that the transformations have significantly improved the interpretation capability of certain land cover and landuse classes. Settlements can be easily separated. The difference of the density of forest biomass can be easily detected on the fused image, which is not possible on Landsat ETM+ multispectral image.

The above result can be used for better interpretation of vegetation classes, which would be later used for making an optimal stratification. The success of stratified sampling also depends on how well the stratification is done.

5.3   Estimation of Recent Carbon Pool

5.3.1   Using forest stratification

The objective of any stratification is to reduce variance within a stratum, whereas increase variance between or among strata. The more variance among the strata can be reduced the more gain from stratification can be achieved. The current study used double sampling for stratification technique to examine the optimal information or technique from the phase I (satellite image), which could reduce the variance among strata in phase II (field samples). Phase one used six Landsat ETM+ optical bands with a number of transformations that are widely applied in remote sensing and phase two used seventy sample plots.

5.3.1.1   Pre-stratification using terrestrial information

The study identified eight different vegetation types on Landsat ETM+ image. Preliminary field visit prior to field sampling confirmed the individual classes. It was noticed that most of the classes are identical. However some classes on satellite imagery are a mixture of two or three types of vegetation. Further separation from Landsat ETM+ image was not possible. For example, teak plantation, teak coppice re-growth and scattered trees are having similar spectral reflectance. Field sampling was carried out in teak and teak coppice. Scattered trees were omitted and this could add some sampling error in the analysis. A similar situation also occurred for indigenous plantations. Those plantations were raised using a variety of species. Further separation of individual species was not possible using ETM+ imagery. Plantations at the very early stage could be separated. But after canopy closure (age depends on species, site quality, intermediate operation, for example weeding or thinning etc.) it could not be further separated. This might incur a large standard deviation in this class. Similar observation was also noticed for the mature natural vegetation. These forests are multistoried and often consist of valuable trees at the upper storey with a high amount of biomass. But during the retrogression process due to human interference those trees are often removed from the top layer leaving the mid or lower canopy open. This vegetation could not be separated from the mature well-stocked forest based on Landsat ETM+ image. This often led to a high standard deviation in this class. Table 5.2 presents the variance within each stratum and the average variance from the stratification based on forest types.

Table 5.2. Pre-stratification using vegetation types as domains of comparison

Strata no	Forest type	Variance (S^2)	$\overline{V}$
1	Mature primary forest	2722,24	
2	Young secondary forest	261,90	
3	Bamboo	231,32	
4	Shrub	0,20	163,97
5	Plantation with indigenous species	2927,24	
6	Teak	680,86	
7	Acacia	49,58	
8	Rubber	524,16	

The overall variance using one phase sampling was 2763. In contrast, two-phase strategy (from the above table) could certainly minimize variance in most of the classes than the one phase sampling strategy. Two classes, mature primary forest and plantation with indigenous species have a large variance, which is close to the one-phase sample variance. The class, shrub has an extreme low variance. This is not because of the class is extremely homogenous but because of the numeric value of the sample statistics. Shrubs contain a very little amount of biomass and consequently the value is very low in comparison with the other classes.

5.3.1.2 Post-stratification without terrestrial information

A number of stratification rules were tested to find out the best result after collecting the field samples. These post-stratification did not use any terrestrial field-based information, rather it was solely dependent on the phase I remote sensing image. The current study not only used the individual optical band information for strata construction but also a number of other transformations, for example normalized difference vegetation indices, tasselled cap transformation, principal component analysis etc., all widely used in remote sensing. The number of strata should be in between 5 and 10 (Cochran 1977). Because of the low number of terrestrial field sample plots the current study used 5 strata. Equal allocation was used to allocate field sample plots in each stratum. In this case the number of plot was 14 per stratum.

Individual band information is the most basic form of obtainable information from satellite imagery. Some of the bands contain redundant information and some have more useful information related to forest biomass than the others. Table 5.3 examines the utility of all different bands for obtaining forest biomass (carbon) information.

Table 5.3 Post-stratification using Landsat band information as domains of comparison

Variable	Variance (S^2)					$\overline{V}$
	Strata 1	Strata 2	Strata 3	Strata 4	Strata 5	
Band 1	2122,71	1962,07	1402,37	3853,72	494,06	281,00
Band 2	1890,30	3012,73	2119,93	2423,50	320,48	279,06
Band 3	2042,87	2160,50	2275,36	3276,25	585,32	295,44
Band 4	1895,03	3344,24	5079,16	1880,81	1619,09	394,81
Band 5	2612,14	2024,04	3617,73	923,64	496,35	276,40
Band 7	2777,96	1971,47	3838,35	859,62	496,79	284,12

From the above table it is observed that the average variance was minimum when band 5 was used and maximum in case of band 4. Band 5 represents 1.55 to 1.75 µm, which corresponds to mid-infrared and band 4 represents 0.78 to 0.90 µm, which is reflected infrared. The rest of the band lies in between. Reflection at the mid-infrared part is dominated by the presence of water in plant leaves, whereas near-infrared reflectance is dominated by the internal structure of plant leaves. Therefore, it can be concluded that the mid-infrared region of reflectance contains the most valuable information for stratification.

Vegetation indices are widely used in many of the studies that deal with the remote sensing image and vegetation canopy closure, LAI or even biomass study. The current study has also examined the utility of the selected vegetation indices for stratification and the result is presented in table 5.4.

Table 5.4 Post-stratification using Vegetation Indices as domains of comparison

Variable	Variance (S^2)					$\overline{\overline{V}}$
	Strata 1	Strata 2	Strata 3	Strata 4	Strata 5	
NDVI	749,22	4459,66	3993,16	1785,62	1269,80	350,21
RVI	749,22	4459,66	3993,16	1785,62	1269,80	350,21
SAVI	806,26	3611,71	4952,64	2266,80	1210,40	367,08
DVI	2100,93	3233,78	5476,21	2426,55	1197,77	412,44
TVI	489,93	2413,41	2493,11	2675,89	2631,64	305,83
PVI	806,26	3611,71	4952,64	2266,81	1210,40	367,08

From the above table transformed vegetation index (TVI) shows the best result for stratification. TVI uses only the band information of the visible channels. NDVI, which is widely used, did not provide the best result. The performance of the difference vegetation index, which is the numeric difference of near infrared and red, is the lowest for stratification.

Tasselled cap transformation concept is well suited for agriculture or even vegetation having thin-layer of biomass. For forestry purposes its usefulness needs to be investigated. The current study has explored the utility of various components of tasselled cap for obtaining information of biomass or carbon estimation. The result of stratification based on tasselled cap transformation is presented in table 5.5.

Table 5.5 Post-stratification using Tasseled Cap information as domains of comparison

Variable	Variance (S^2)					$\overline{\overline{V}}$
	Strata 1	Strata 2	Strata 3	Strata 4	Strata 5	
Brightness	2373,27	2202,64	3465,18	1805,94	848,11	305,58
Greenness	970,39	4121,81	4752,36	2072,51	1210,40	375,07
Wetness	496,79	2300,96	3114,54	1935,80	2758,93	303,06
Tasseled Cap 4	2222,03	2838,83	4139,02	2913,44	1089,85	377,23
Tasseled Cap 5	2375,76	3428,59	3993,18	1892,68	2425,87	403,32
Tasseled Cap 6	1676,74	2991,77	3388,80	1018,16	3559,65	361,00

Tasselled cap wetness provides the best result among all the other components, which is closely followed by brightness. Wetness component is an indicator for presence of moisture in soil or vegetation and brightness component usually indicates the brightness of soil it has certainly some utility on vegetated area. It was expected that the greenness component, which is a measure of the amount of green vegetation present in an area would provide the best result, but it did not.

Principal component transformation is a rotational transformation, which reduces the dimension of image and generates an image without correlation. Principal component 1 includes the largest percentage of total scene variance and succeeding components (PC2, PC3….PCn) contain a decreasing trend of the value. Image bands usually contain redundant information if they are highly correlated. The stratification based on the principal component transformation is presented in table 5.6.

Table 5.6 Post-stratification using Principal Components as domains of comparison

Variable	Variance (S^2)					$\overline{\overline{V}}$
	Strata 1	Strata 2	Strata 3	Strata 4	Strata 5	
Principal Component 1	3070,34	1617,06	2446,14	2434,78	526,71	294,14
Principal Component 2	2494,13	2616,52	5267,86	1986,56	1289,14	390,12
Principal Component 3	1582,36	1810,07	5011,73	3940,96	382,20	363,64

From the above table the first principal component provides the best result for stratification as it was expected. Principal component 3 performed better than the principal component 2. From the above result it is noticed that a variety of transformation does not contain better information for stratification among the post-stratification rules tested. All the individual bands except band 4 (near-infrared band) contain good information for stratification. Among the various transformations tested, principal component 1 provides the best result. Neither vegetation indices nor tasselled cap improve the result of stratification in compare with the individual band information.

5.3.1.3   Estimates of carbon

The study estimates the carbon pool using an optimal stratification rule. Pre-stratification using terrestrial information provides the best result among all different stratification rules examined. Therefore, the aboveground carbon was estimated using forest types information (table 5.7).

Table 5.7 Carbon pool of the test site in 2001 using stratification

Serial no.	Forest type	Area (ha)	Mean carbon content (ton/ha)	Standard deviation	Total carbon content (ton)	95% confidence level	
						Upper limit	Lower Limit
1	Mature primary forest	3 950	134,37	52,18	530 768	637 613	423 923
2	Young secondary forest	1 032	86,84	16,18	89 697	101 975	77 420
3	Bamboo	2 565	62,70	15,21	160 842	189 499	132 186
4	Shrub	3 023	0,87	0,45	2 645	3 637	1 654
5	Plantation of indigenous species	2 555	83,73	54,10	213 929	279 353	148 505
6	Teak	3 745	60,81	26,09	227 716	288 285	167 147
7	Acacia	342	30,62	7,04	10 468	12 449	8 488
8	Rubber	3 006	30,95	22,89	93 016	139 112	46 920
9	Non-forest	11 035	0		0		
	Total	31 255			1 329 082		

From the above table it is observed that the mature primary forest contains the highest amount of carbon per unit area, which is more than 130 ton/ha and shrub contains the lowest, which is less than 1 ton/ha. Some class, for example, young forest or plantation with indigenous species contains a considerable amount of carbon, which is more than 80 ton/ha. Teak plantation also has more than 60 ton/ha. Among the plantations acacia or rubber contains the lowest amount, which is slightly higher than 30 ton/ha.

Mature primary forest, teak, rubber and shrub contain the highest area, which is more than about 3 000 ha in each category. This figure is followed by bamboo and plantation with indigenous species, which are more than 2 500 ha. Young secondary forest and acacia have more than 1 000 ha and

300 ha respectively. The amount and distribution of carbon in 2001 at the study area using stratification is presented in figure 5.7.
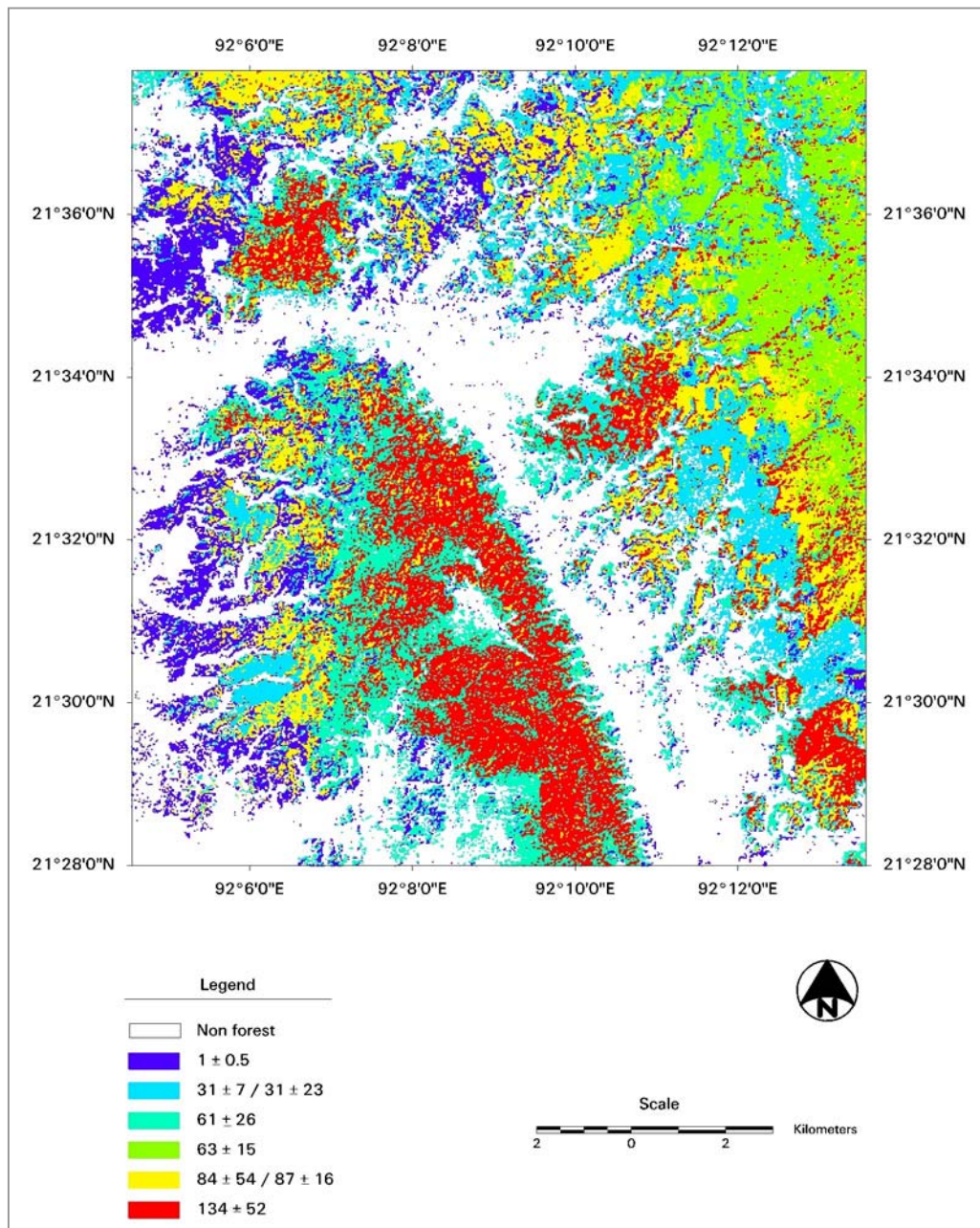
Figure 5.7 Carbon map of southern Chittagong 2001 using stratification

The distribution of carbon is closely associated with the vegetation type. The distribution of vegetation type usually follows certain factors for example, local topography and soil formation, management history etc. The highest amount of carbon in the above map is concentrated at the central and southern part and in some scattered patches of the other parts of the study area. The non-forest area, which is assumed to hold zero carbon content, divides the forest region into two separate blocks. The settlement and agricultural lands are usually located in the non-forest area.

The threat of any disturbance and consequently release of carbon is usually generated from the settlements.

5.3.2   Using regression technique

Plotting the variables in scattergram is often useful to understand the trend of relationship before modelling. Scattergrams showing the carbon content and individual band information are presented in figure 5.8.
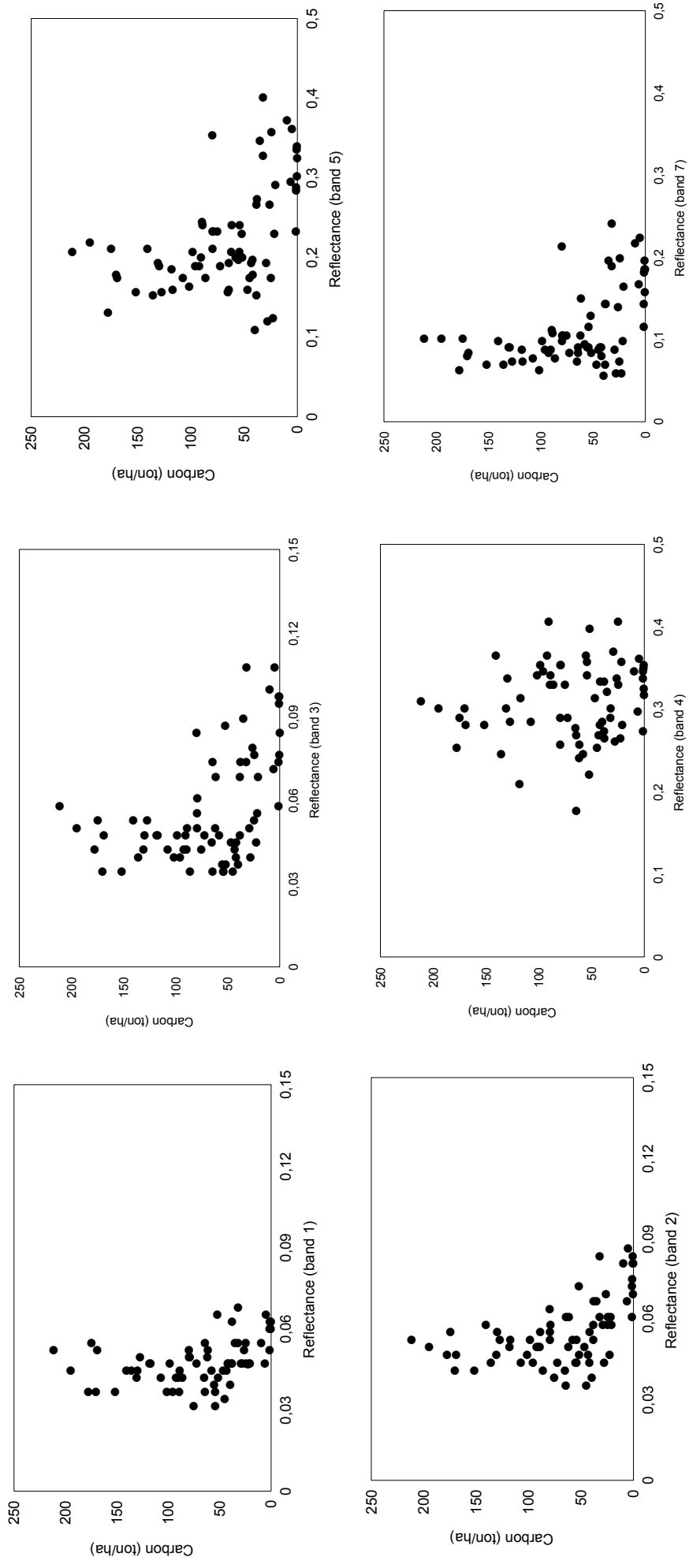
Figure 5.8 Scattergram of carbon content and Landsat ETM+ spectral bands reflectance

Most of the scatterplots show a negative trend between information on carbon content and spectral reflectance. The relationship differs with channels. Most of the bands (i.e. band 2, 3, 5 and 7) show a curvilinear relation. The other two bands show different patterns; band 1 shows a sharp negative trend and band 4 shows almost no relationship.

5.3.2.1   <u>Simple regression</u>

Simple regression examines the linear relationship between two variables. In real world situation many of the relationships are non-linear. In such situations transformation is required using simple algebra to fit the variables if non-linear regression software is unavailable. This study examined linear as well as a number of non-linear transformations to find an optimal model for predicting information on carbon from spectral reflectance. Coefficient of determination (r^2) is an important indicator of comparing the candidate models. Therefore, the current study used this criterion for pre-selecting the regression equations. The r^2 values calculated from different equations are presented in table 5.8.

Table 5.8 Coefficient of determination (r^2) between individual band spectral reflectance and carbon content for non-linear relationship

Equation type	Band 1	Band 2	Band 3	Band 4	Band 5	Band 7
Linear	0,167	0,264	0,241	0,025	0,226	0,242
Logarithmic	0,152	0,236	0,220	0,023	0,193	0,224
Inverse	0,134	0,198	0,186	0,019	0,141	0,180
Quadratic	0,184	0,286	0,245	0,029	0,236	0,243
Cubic	0,182	0,281	0,284	0,029	0,330	0,309
Compound	0,337	0,473	0,380	0,036	0,313	0,332
Power	0,305	0,421	0,356	0,037	0,280	0,321
S	0,266	0,356	0,312	0,037	0,218	0,271
Growth	0,337	0,473	0,380	0,036	0,313	0,332
Exponential	0,337	0,473	0,380	0,036	0,313	0,332
Logistic	0,337	0,473	0,380	0,036	0,313	0,332

The above result ($r^2 < 0.26$) is un-satisfactory to predict carbon using linear regression. The poorest result was obtained by using ETM+ band 4. The r^2 value was highest when band 2 was used. Transformations of variables mostly improved the relationship. Some cases (i.e. growth, exponential or logistic) the improvement was significant. Band 2 still provides the highest coefficient of determination ($r^2 = 0.47$, $r = 0.69$) after transformation.

Additionally a number of different spectral transformations were tested. Six different vegetation indices, six components of tasselled cap transformation and first three components of PCA were examined and the results are presented in table 5.9-5.11.

Table 5.9 Coefficient of determination (r^2) between vegetation indices and carbon content for non-linear relationship

Equation type	NDVI	RVI	SAVI	DVI	TVI	PVI
Linear	0,138	0,099	0,029	0,002	0,171	0,031
Logarithmic	0,135	0,127	0,029	0,003	0,173	0,031
Inverse	0,127	0,137	0,026	0,003	0,175	0,019
Quadratic	0,138	0,181	0,031	0,005	0,220	0,040
Cubic	0,139*	0,184	0,076	0,011	0,221*	0,082
Compound	0,201	0,190	0,046	0,005	0,229	0,052
Power	0,185	0,205	0,035	0,002	0,231	0,034
S	0,162	0,190	0,023	0,000	0,233	0,010
Growth	0,201	0,190	0,046	0,005	0,229	0,052
Exponential	0,201	0,190	0,046	0,005	0,229	0,052
Logistic	0,201	0,190	0,046	0,005	0,229	0,052

*Tolerance limits reached; some dependent variables were not entered

From the above result transformed vegetation index (TVI) generates the best result. Most of the cases transformation provides better results than the simple regression. S type of equation using TVI shows the highest r^2 value.

Table 5.10 Coefficient of determination (r^2) between tasseled cap transformation and carbon content for non-linear relationship

Equation type	Brightness	Greenness	Wetness	Component 4	Component 5	Component 6
Linear	0,210	0,053	0,221	0,035	0,035	0,059
Logarithmic	0,192	0,057	*	*	*	*
Inverse	0,172	0,038	0,113	0,034	0,024	0,005
Quadratic	0,250	0,077	0,226	0,093	0,041	0,086
Cubic	0,247	0,120	0,337	0,100	0,046	0,103
Compound	0,314	0,086	0,296	0,063	0,057	0,119
Power	0,285	0,061	*	*	*	*
S	0,254	0,024	0,185	0,009	0,044	0,016
Growth	0,314	0,086	0,296	0,063	0,057	0,119
Exponential	0,314	0,086	0,296	0,063	0,057	0,119
Logistic	0,314	0,086	0,296	0,063	0,057	0,119

* Independent variable has non-positive value

The brightness and wetness components of tasselled cap generate the highest correlation. Almost no relation was observed between the other components and carbon information. In general, transformations improve the value of r^2. The correlation coefficient was highest in the brightness component using growth, exponential and logistic equations and the value was 0.560 ($r^2 = 0.314$). The results are still not good enough for a satisfactory prediction using tasselled cap transformation.

Table 5.11 Coefficient of determination (r^2) between principal component and carbon content for non-linear relationship (DN values)

Equation type	Principal component 1	Principal component 2	Principal component 3
Linear	0,259	0,003	0,003
Logarithmic	0,252	0,003	**
Inverse	0,236	0,003	0,005
Quadratic	0,259	0,003	0,052
Cubic	0,259*	0,004	0,052*
Compound	0,326	0,001	0,001
Power	0,322	0,002	**
S	0,305	0,004	0,002
Growth	0,326	0,001	0,001
Exponential	0,326	0,001	0,001
Logistic	0,326	0,001	0,001

* Tolerance limits reached; some independent variables were not entered.

** Independent variable has non-positive values.

A relative better relation was observed in the first principal component. The last two components (component 2 and 3) show almost no correlation. The result improved when the first principal component was transformed. The compound, growth, exponential and logistic transformations showed the highest correlation (r = 0.571 / r^2 = 0.326). The result is yet not satisfactory enough to make a good prediction from the principal components.

It was expected that the various forms of spectral transformations would provide better correlation than the individual bands. But, the result was opposite. Therefore, in further analysis (i.e. multiple regression, regression with dummy variables) only individual bands were tested.

5.3.2.2   Multiple regression

Multiple regression equations were calculated using all different bands. All the variables were entered at the initial stage of analysis. The variables having less association with the carbon information were later removed step by step using backward elimination criteria. At the last stage the strongest predictor variable will remain in the model. The predictor variables and r^2 are presented in table 5.12.

Table 5.12 Coefficient of determination (r^2) between all bands spectral reflectance and carbon content by backward elimination

Model no	Variables used	Variables removed	Coefficient of determination (r^2)	Adjusted r^2
1	Bands 1,2, 3, 4, 5, 7		0,295	0,228
2	Bands 2, 3, 4, 5, 7	Band 1	0,295	0,240
3	Band 2, 4, 5, 7	Band 3	0,295	0,248
4	Bands 2, 4, 7	Band 5	0,284	0,252
5	Band 2, 7	Band 4	0,278	0,256
6	Band 2	Band 7	0,264	0,253

From the above result, band 2 is the strongest predictor of carbon content. The value of r^2 slightly increases with the addition of band 7 and band 4. However, further incorporation of bands did not improve the relationship. The above result is still poor and hence cannot be effectively used for prediction.

5.3.2.3   Additional information from image texture

Image texture was calculated using Landsat ETM+ pan data, as it has higher spatial resolution than the multi-spectral bands. A variety of window size, for example 3x3, 5x5, and 7x7 were tested. Finally, a 3x3 size was selected as it provides the best result. This information was later incorporated as additional variable in the multiple regression together with the individual band information. The relationships are presented in table 5.13

Table 5.13 Coefficient of determination (r^2) between image texture, all bands spectral reflectance and carbon content by backward elimination

Model no	Variables used	Variables removed	Coefficient of determination (r^2)	Adjusted r^2
1	Band 1, 2, 3, 4, 5, 7, Mean, Variance, Second moment, Homogeneity, Contrast, Dissimilarity, Entropy		0,476	0,354
2	Band 1, 3, 4, 5, 7, Mean, Variance, Second moment, Homogeneity, Contrast, Dissimilarity, Entropy	Band 2	0,475	0,365
3	Band 1, 3, 5, 7, Mean, Variance, Second moment, Homogeneity, Contrast, Dissimilarity, Entropy	Band 4	0,474	0,374
4	Band 1, 3, 5, 7, Mean, Variance, Second moment, Homogeneity, Contrast, Dissimilarity	Entropy	0,472	0,382
5	Band 1, 3, 5, 7, Mean, Variance, Homogeneity, Contrast, Dissimilarity	Second moment	0,467	0,388
6	Band 1, 3, 7, Mean, Variance, Homogeneity, Contrast, Dissimilarity	Band 5	0,452	0,380
7	Band 1, 7, Mean, Variance, Homogeneity, Contrast, Dissimilarity	Band 3	0,439	0,375

Incorporation of image texture in multiple regression has improved the relationship. The above table represents some surprising results. For example, band 2 that was the strongest predictor of carbon (table 5.12) was removed at the very early stage of analysis. If we consider the model 7, it has two bands (band 1, 7) and five components of image texture information and the r^2 value is 0.439 (r = 0.663). The relationship is still not very good but better than the previous results. The goal of the current study is to develop one operational tool for monitoring terrestrial carbon budgets in the tropics and therefore it should be kept in mind that most of the tropical forests are distributed in the developing countries, which often have limited availability of resources. For the calculation of image texture additional software, i. e. ENVI is required. The general module of ERDAS Imagine, the other widely used software for image processing does not provide this facility. Simultaneously, the improvement of the relationship was not quite satisfactory and hence second order texture information was not used in further analysis.

5.3.2.4   Additional information from dummy variables

From the scatter plot (figure 5.8) and raw data (Appendix VIII) it was noticed that the relationship between spectral response and carbon information might be slightly different for different types of vegetation. Therefore, it was decided to apply the dummy variables. Each vegetation class was considered as a source of different sets of dummy variables. The results are presented in table 5.14.

Table 5.14 Coefficient of determination (r^2) between all bands spectral reflectance and carbon content by backward elimination

Model no	Variables used	Variables removed	Coefficient of determination (r^2)	Adjusted r^2
1	Bands 1,2, 3, 4, 5, 7, Z_1, Z_2, Z_3, Z_4, Z_5, Z_6, Z_7		0,611	0,521
2	Bands 1, 2, 4, 5, 7, Z_1, Z_2, Z_3, Z_4, Z_5, Z_6, Z_7	Band 3	0,611	0,530
3	Band 2, 4, 5, 7, Z_1, Z_2, Z_3, Z_4, Z_5, Z_6, Z_7	Band 1	0,611	0,538
4	Bands 2, 4, 7, Z_1, Z_2, Z_3, Z_4, Z_5, Z_6, Z_7	Band 5	0,610	0,544
5	Band 2, 7, Z_1, Z_2, Z_3, Z_4, Z_5, Z_6, Z_7	Band 4	0,610	0,551
6	Band 2, Z_1, Z_2, Z_3, Z_4, Z_5, Z_6, Z_7	Band 7	0,608	0,557
7	Band 2, Z_1, Z_2, Z_3, Z_4, Z_5, Z_6	Z_7	0,605	0,560
8	Band 2, Z_1, Z_2, Z_3, Z_4, Z_6	Z_5	0,600	0,562
9	Band 2, Z_2, Z_3, Z_4, Z_6	Z_1	0,591	0,559

The above result is very impressive. The use of dummy variable has significantly improved the relationship. If we consider the model 9, it has five independent variables including information from one band, band 2. The rests are dummy variables that basically add a constant in the regression equation. The value of the coefficient of determination is 0.591 (r = 0.769), which is satisfactory.

From the previous result, the study discovered that the mathematical transformations of bands improve the relationship. For example, the coefficient of determination is 0.264 (r^2= 0.514) for predicting carbon using band 2 in simple regression; however, it is 0.473 (r^2 = 0.688) when used in

non-linear form (i.e. growth, exponential and logistic) (Table 5.8). All the three models are basically similar. They use an exponential relationship between the independent and dependent variables but their intercepts and/or coefficients are different. The current study has decided to use any of these equations (i.e. exponential) together with dummy variables to explore the improvement of relationship. The result is presented in table 5.15.

Table 5.15 Coefficient of determination (r^2) between all bands spectral reflectance and logarithm (base e) carbon content (exponential relationship)

Model no	Variables used	Variables removed	Coefficient of determination (r^2)	Adjusted r^2
1	Bands 1,2, 3, 4, 5, 7, Z1, Z2, Z3, Z4, Z5, Z6, Z7		0,890	0,865
2	Bands 1, 2, 3, 5, 7, Z1, Z2, Z3, Z4, Z5, Z6, Z7	Band 4	0,890	0,867
3	Band 1, 2, 3, 5, 7, Z1, Z2, Z3, Z4, Z5, Z6	Z7	0,890	0,869
4	Bands 2, 3, 5, 7, Z1, Z2, Z3, Z4, Z5, Z6	Band1	0,890	0,871
5	Band 2, 3, 7, Z1, Z2, Z3, Z4, Z5, Z6	Band 5	0,889	0,872
6	Band 2, 7, Z1, Z2, Z3, Z4, Z5, Z6	Band 3	0,887	0,873
7	Band 2, Z1, Z2, Z3, Z4, Z5, Z6	Band 7	0,887	0,874
8	Band 2, Z1, Z2, Z4, Z5, Z6	Z3	0,885	0,874
9	Band 2, Z2, Z4, Z5, Z6	Z1	0,881	0,872

The above result represents a significant improvement of the correlation. If model 7 is selected it has seven independent variables, one band and six dummy variables. The coefficient of determination is 0.887 (r = 0.942), which is quite impressive. Though incorporation of additional variables (model 1-6) slightly improves the relationship the current study recommends the utilization of model 7 as it has the lowest number of real independent variable. The details of the selected regression equation are presented in table 5.16.

Table 5.16 Coefficients of the selected regression model

Variable	Unstandardized Coefficients		Standardized Coefficients	t	
	B	Standard Error	Beta	Value	Significance
Constant	6,190	0,446		13,878	0,000
Band 2	-36,534	7,856	-0,297	-4,650	0,000
Z_1	-0,462	0,307	-0,085	-1,506	0,137
Z_2	-0,582	0,280	-0,149	-2,079	0,042
Z_3	-0,226	0,235	-0,072	-0,959	0,341
Z_4	0,945	0,288	0,309	3,280	0,002
Z_5	3,098	0,292	0,958	10,594	0,000
Z_6	-3,750	0,295	-1,037	-12,705	0,000

Form the above table it is noticed that the level of significance for each independent variable is quite high (except Z_3 and Z_1). The residual of the selected regression equation is presented in figure 5.9.

(a)

(b)
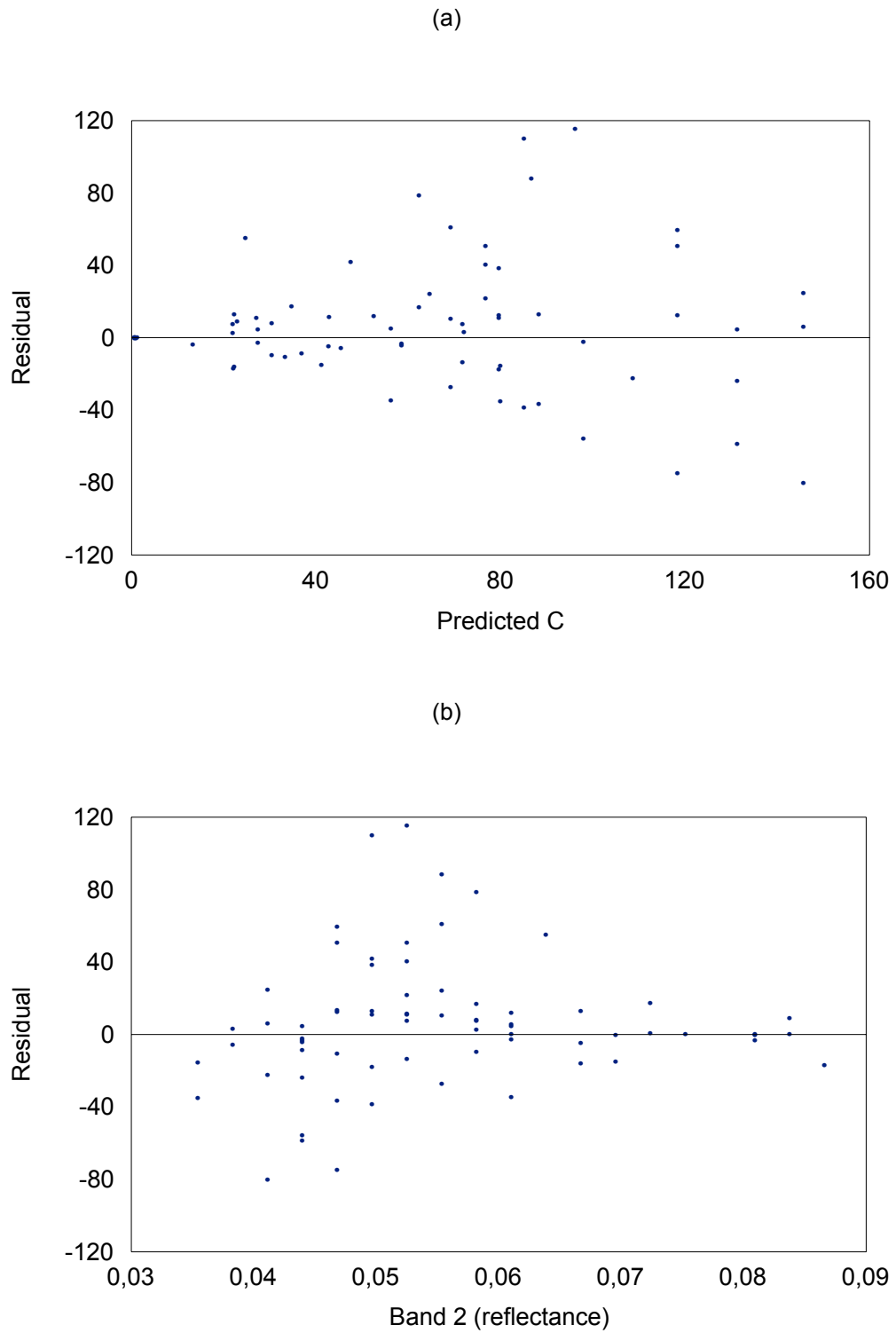
Figure 5.9 Residual analysis of the selected regression equation: (a) residual versus predicted carbon (b) residual versus band 2 reflectance

Residual plot (figure 5.9a) of the selected regression equation shows heterogeneous variance, which is the result of 'funnel effect'. This means that if the predicted carbon gets larger, the deviation of the residual from zero becomes greater. Therefore, it should be kept in mind that the error variance in the predicted model is not constant, but increases as the measured response increases. The plot of band 2 versus residual (Figure 5.9b) indicates that the model can make relative good prediction when band 2 has a very low (< 0.04) or high reflectance (> 0.06). Any prediction in between this spectral range (0.02 - 0.04) might incur a relative large amount of error. The reason for such behaviour is possibly originated from the coverage condition of vegetation canopy. The relation of carbon and the reflectance from band 2 is negative. So, when the canopy coverage is low the model will make a good prediction. On the other hand, when canopy is completely closed, the prediction capacity using optical data becomes poor, because it cannot extract the information from the understorey vegetation.

The estimate of carbon pool using the selected regression model is presented in table 5.17.

Table 5.17 Estimation of carbon pool of 2001 in southern Chittagong using regression

Carbon class	Area (ha)	Carbon (Total)
0-50	6 918	125 941
>50-100	8 980	632 757
>100-150	3 540	440 389
>150-200	701	119 100
>200-250	68	15 291
>250-300	8	2 263
>300-350	4	1 261
Non-forest	11 035	0
Total	31 255	1 337 000

The carbon map using regression is presented in figure 5.10.
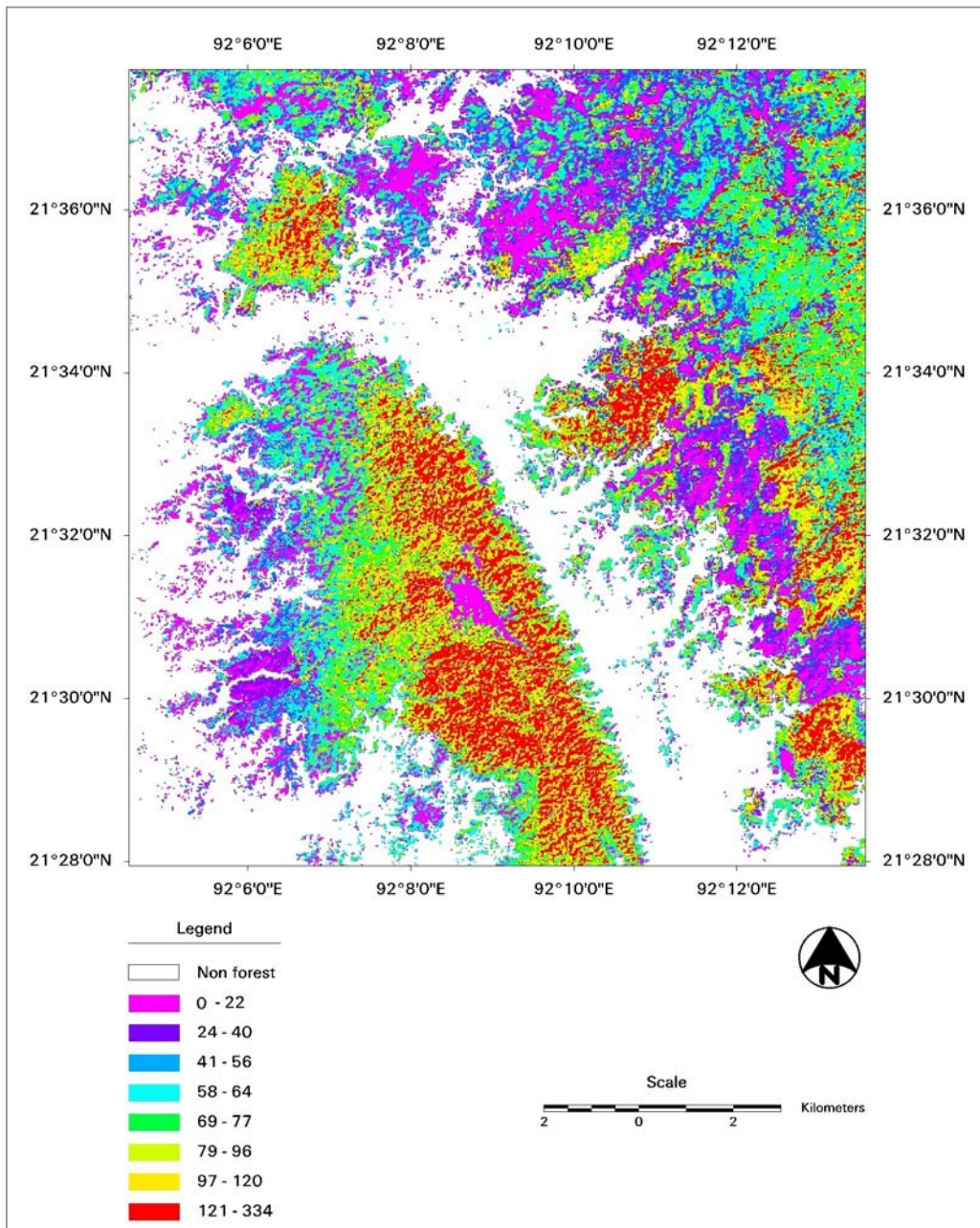
Figure 5.10 Carbon map of southern Chittagong 2001 using regression

5.3.3   *Using knn method*

The current study calculated the amount of carbon for recent time using *knn* method. The result is presented in table 5.18.

Table 5.18 Estimation of carbon content of the study area for 2001 using *knn* method

Carbon class	Area (ha)	Carbon (Ton)
0-50	7 892	153 063
>50-100	6 432	466 744
>100-150	2 730	338 145
>150-200	2 874	508 097
>200-250	291	61 647
Non forest	11 035	0
Total	31 255	1 527 696

The carbon map using *knn* method is presented in figure 5.11.
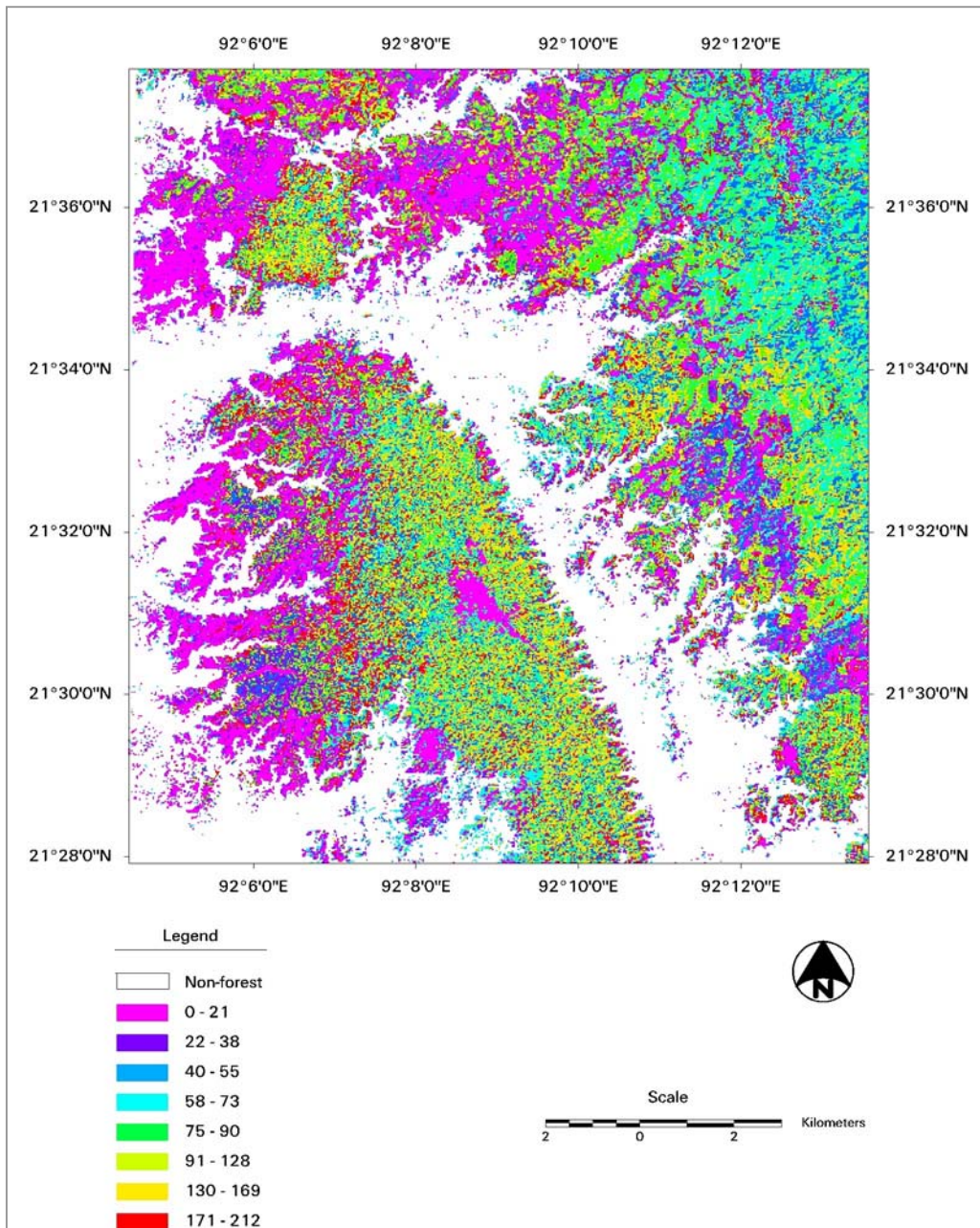
Figure 5.11 *Knn* estimate of carbon (ton/ha) 2001 in the study area

5.4   Comparing Three Methods

The accuracy of the three methods was tested from independent validation plots and the result is presented in Appendix IX. The table enlisted the actual and classified forest, observed and predicted carbon content and absolute bias generated from the each plot. Among the thirty validation sample plots nine were misclassified. From the bias test it can also be noted that the greater amount of errors were generated from the misclassified plots. This means that if the accuracy of the classification improves the forest attributes can be more precisely extracted from

the remote sensing data. Therefore, it is necessary to invent new sensors, which allow the separation of vegetation more accurately. Better algorithms for classification should also be explored.

Statistics of the accuracy test is presented in table 5.19. Stratification provides the minimum amount of RMSE and absolute bias. The standard error of bias was lowest when regression method was used. *Knn* generates the largest amount of error both in the three estimates.

Table 5.19 Statistics of validation test using three methods

Parameters	Stratification	Regression	*Knn*
RMSE	47,13	48,10	58,70
Mean bias	31,76	33,98	38,99
Standard error of bias	6,47	6,32	8,15

The result of the validation test is presented in a 1:1 graph (Figure 5.12). The plots located near the diagonal line predict more accurate results than the plots, which are dispersed from the line. Those plots located below the diagonal line are underestimated, whereas the plots located above the line are overestimated. The patterns of the distribution of plots calculated by stratification and regression are similar in nature, but are slightly different when *knn* method is used. Some of the plots in that figure are located at the similar location generated from the prediction of either stratification or regression but are different from *knn*. It is interesting to note that the accuracy is higher for certain plots using stratification or regression but lower when *knn* method is used. The result is opposite for some other plots. Therefore, it can be concluded that the accuracy of the result can be improved if we can successfully combine two or more methods.
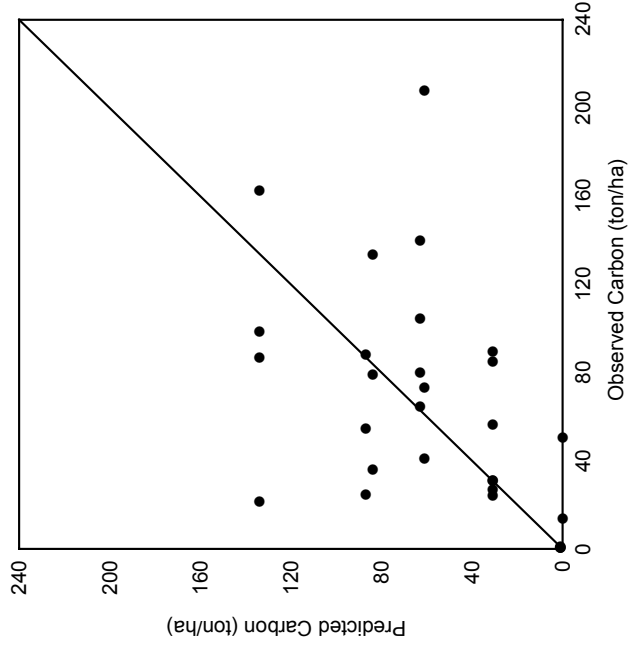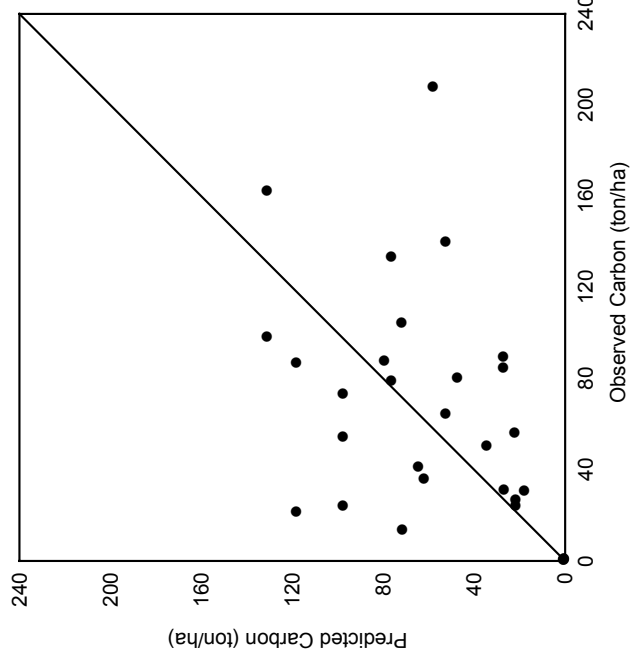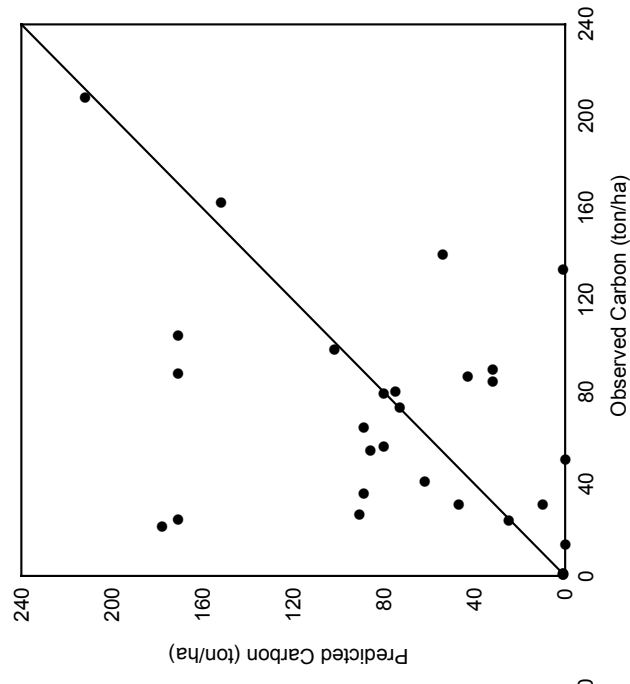
Figure 5.12 Validation test for estimating carbon from validation sample plots using three different methods

5.5 Assessment of Carbon in Historical Image

The carbon in the historical image was estimated by cross-calibration and regression technique. In this method 380 sample points were selected randomly from the recent and historical image to find out the cross-calibration coefficient. Points were only selected from the unchanged vegetation classes. Scatterplots show a definitive trend of the sample points towards the origin except band 7 (Figure 5.13). Calculation was done by simple regression technique that passes through the origin. Table 5.20 enumerated the coefficient and the precision of cross-calibration.

Table 5.20 Estimate of cross-calibration equation for TM 1992 to ETM+ 2001

Band	Coefficient b	*r*-square	Adjusted *r*-square
1	0,924	0,986	0,986
2	0,868	0,983	0,983
3	0,736	0,979	0,979
4	0,840	0,985	0,984
5	0,837	0,982	0,982
7	0,256	0,741	0,741

After cross-calibration the same regression equation was used to estimate the carbon in the historical image. The results of the estimation are presented in table 5.21 and figure 5.14.
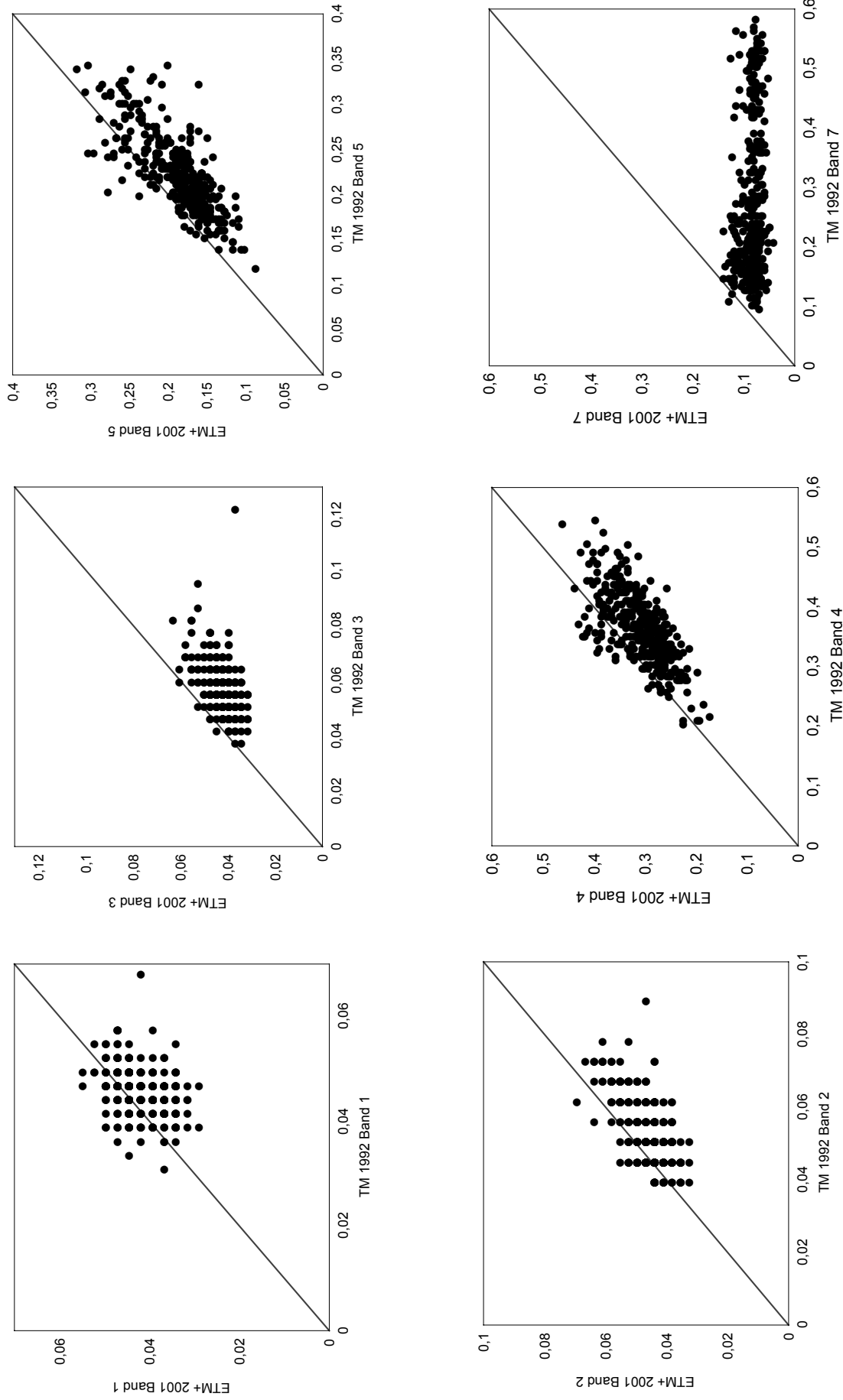
Figure 5.13 Scattergram of the selected plots of Landsat TM 1992 and ETM+ 2001 for radiometric normalization
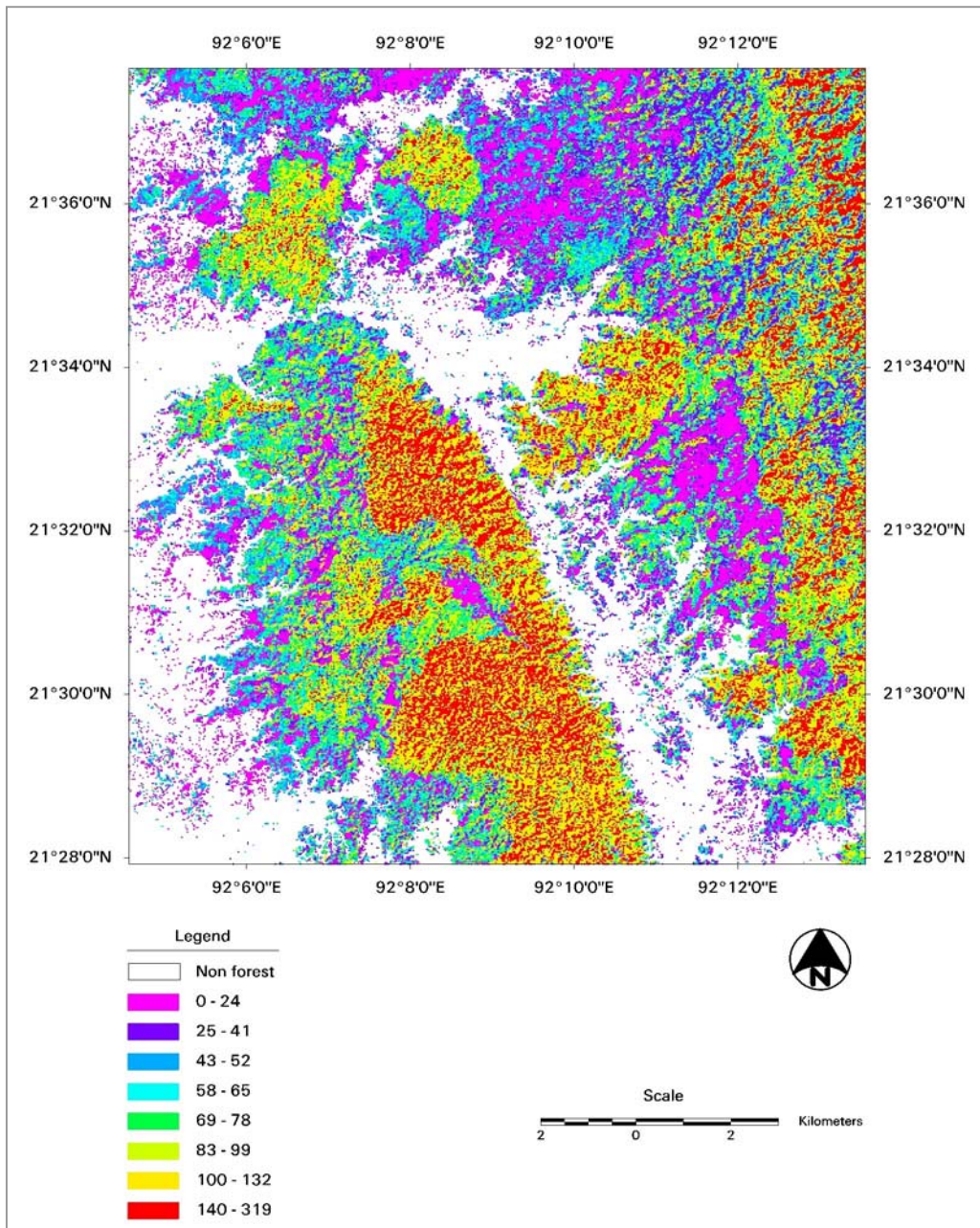
Figure 5.14 Carbon map of southern Chittagong 1992 using regression

Table 5.21 Estimation of carbon pool of 1992 using regression

Carbon class	Total area	Total carbon
0-50	6 806	180 121
>50-100	8 665	623 179
>100-150	6 389	911 478
>150-200	93	20 833
>200-250	5	1 444
>250-300	1	201
Non forest	9 295	0
Total	31 255	1 737 256

5.6   Estimation of Carbon Release

5.6.1   Assessment of deforestation by change matrix

Vegetation change matrix was calculated to find out the dynamics of vegetation change during the study period (Table 5.22). The end column of the vegetation change matrix represents the total area of origin, whereas the bottom row represents the total area of destination for forest cover change assessment. The diagonal (shaded) cell represents the stable classes. Upper right portion of the stable areas represents deforestation or degradation, whereas the lower left represents amelioration or increase of woody biomass. Each cell of the table shows the class of origin and class of destination. This helps the reader to identify the dimension of forest cover changes.

It is noticed that the primary and secondary forests are subject to a severe loss during the study period; loss of primary and secondary forest is about 35% and 56% respectively. The destruction of teak (scattered trees are also misclassified to this category) and indigenous plantation was not very severe. They have lost only about 15% and 17% respectively. Acacia has been recently introduced in the study area and was not available in 1992 image. Rubber plantation is extended dramatically

(about 56%). The bamboo areas have also slightly been increased, which is about 5%. The shrub vegetation has been tremendously extended and it is about 80%. Non-forest area has also been increased (about 19%).

Table 5.22 Forest cover change matrix of southern Chittagong 1992-2001 (area in ha)

Landsat 136/045 Year: 1992	Year: 2001	Natural forest vegetation			Plantation			Non-forest vegetation			Total 1992
		Primary forest	Secondary forest	Indigenous spp.	Teak	Acacia	Rubber	Bamboo	Shrubs	Non-vegetated	
Natural vegetation	Primary forest	2 687	273	248	1 344	53	346	613	132	371	6 067
	Secondary forest	444	340	240	271	16	281	513	119	125	2 349
	Indigenous spp.	200	136	958	325	160	262	62	525	372	3 000
Plantation	Teak	339	41	150	1 100	7	595	240	259	1 779	4 510
	Acacia	0	0	0	0	0	0	0	0	0	0
	Rubber	45	27	225	163	21	471	57	395	521	1 925
Non-forest vegetation	Bamboo	148	179	198	176	2	457	1 045	110	119	2 434
	Shrubs	17	26	346	55	28	218	22	649	314	1 675
Non-vegetated	Non-vegetated	70	12	189	312	54	376	14	834	7 434	9 295
	Total 2001	3 950	1 034	2 554	3 746	341	3 006	2 566	3 023	11 035	31 255

Forest cover maps of southern Chittagong in the recent and historical time are presented in figure 5.15-5.16.
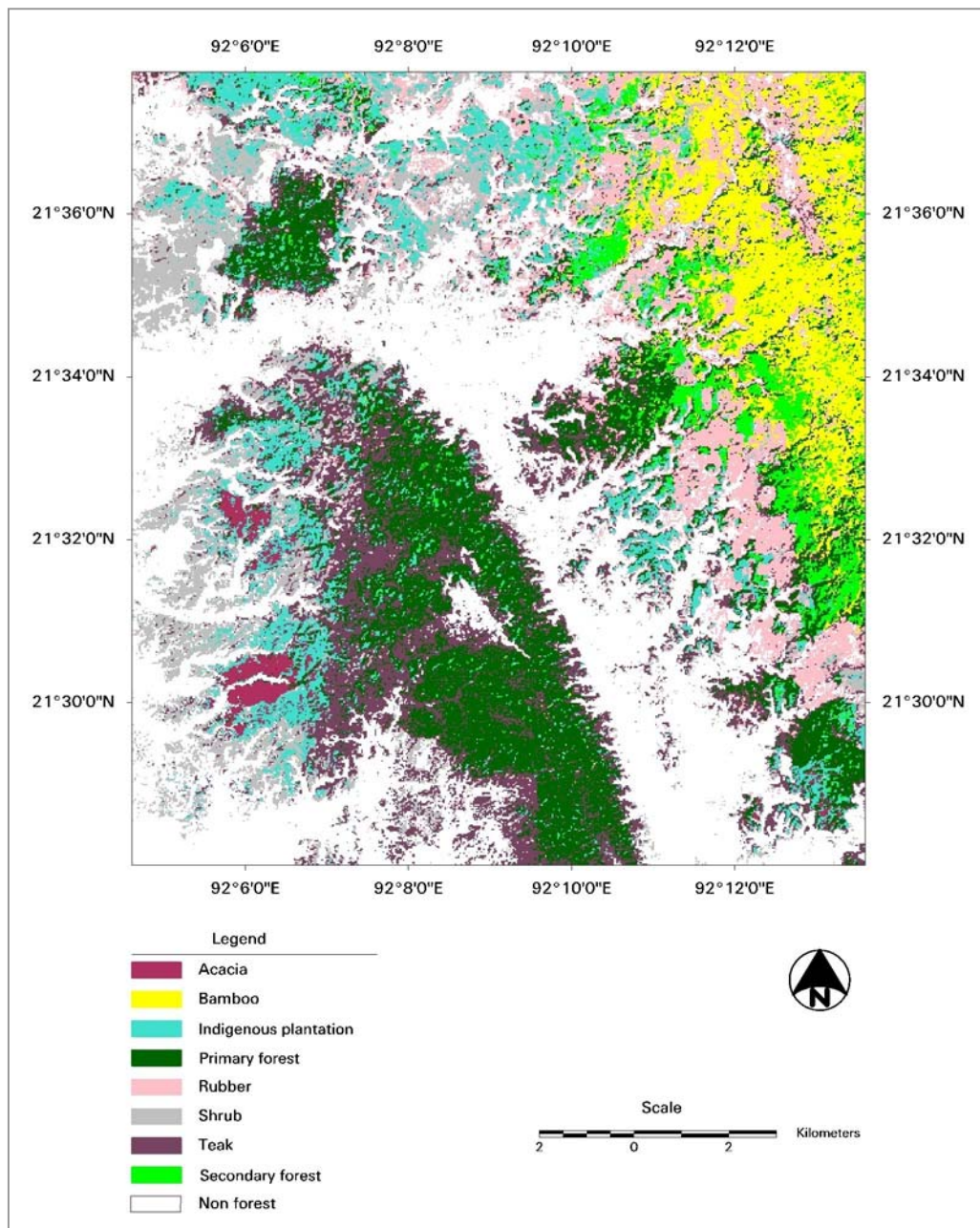
Figure 5.15. Forest cover map of southern Chittagong 2001

The above map shows the distribution of forest areas in the study region. The development of forest usually follows local topography, soil formation, management and landuse history etc. The major forest area is distributed scatteredly, some part is concentrated in the middle of south. Bamboos are mainly distributed in the north-eastern region. The non-forest area has separated the vegetated region into two separate blocks.
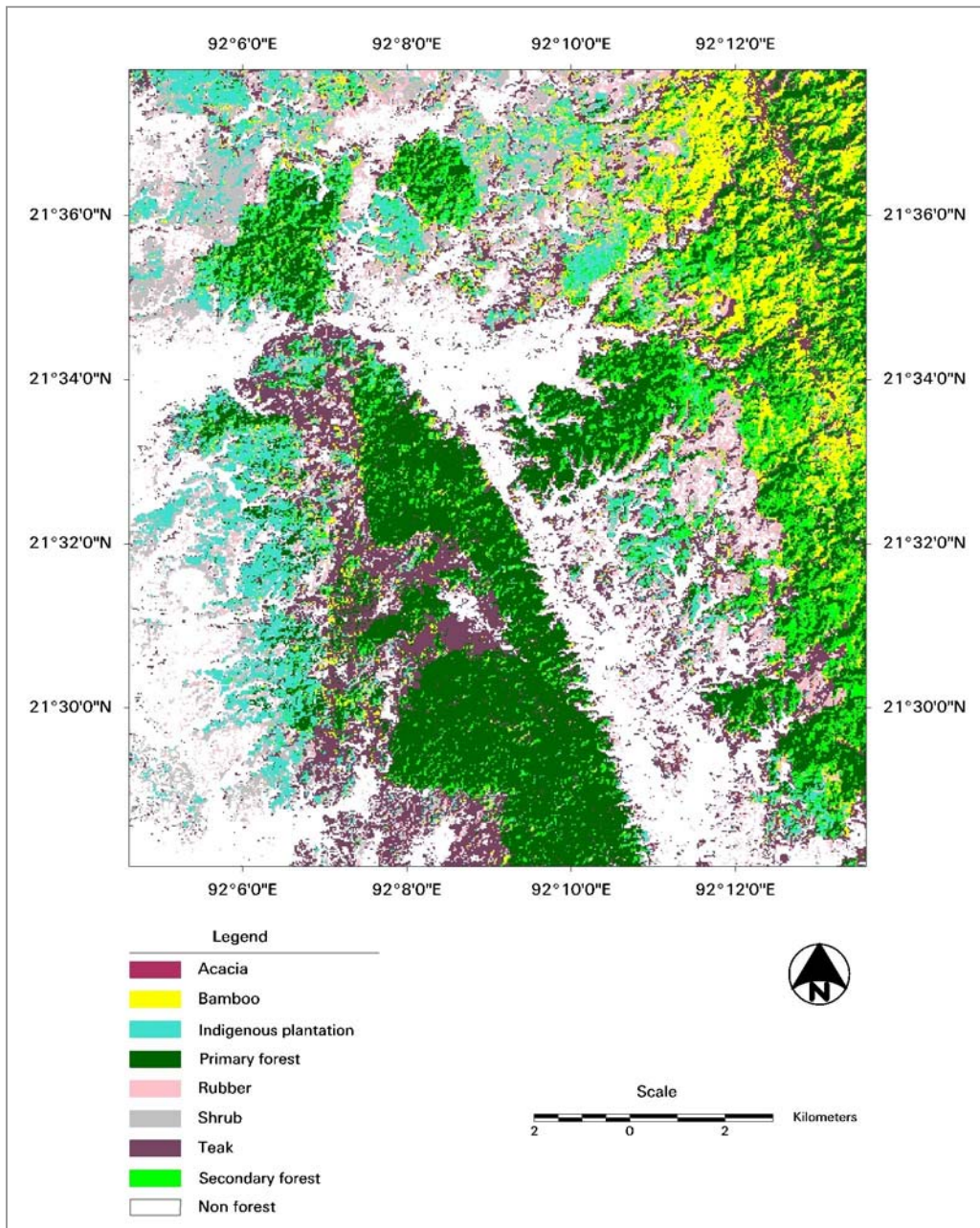
Figure 5.16 Forest cover map of southern Chittagong 1992

The vegetation change can be detected if the recent and historical maps are superimposed. The deforestation hotspots are distributed scatteredly. The drastic deforestation is noticed in the mid of north (local forest jurisdiction: Purnagram beat) where mature primary forest has been removed completely by plantation, shrub and non-forest. East part of that block, primary forest (Rajghat beat) has also been reduced in a certain extent and converted mostly to non-forest area. The mature primary forest in the south-eastern part (Gilatali beat) has also been partly replaced by plantation and non-forest. The successful development of Acacia plantation has also been noticed in the southwest (Kalirchara, Dhalirchara and Meherghona beat). Rubber plantation has been

151

raised successfully in the eastern part of the study area by private enterprises replacing mostly the primary and secondary forests.

5.6.2   Carbon dynamics in the study area

Table 5.23 represents the change of carbon budgets in the study area during the period under investigation. From the result it can be concluded that the major amount of carbon was released due to the conversion of primary forests. It should also be noted that

Carbon 2001 = Carbon 1992 + sequestration - release

Table 5.23 Estimates of carbon dynamics in southern Chittagong 1992-2001

Forest type	1992			2001			Change in mean carbon (ton/ha)	Change in total carbon (ton)
	Area (ha)	Carbon (ton/ha)	Total carbon (ton)	Area (ha)	Carbon (ton/ha)	Total carbon (ton)		
Primary forest	6 067	143,60	871 224	3 950	133,18	526 077	-10,42	-345 147
Secondary forest	2 349	86,37	202 883	1 034	101,40	104 849	15.03	-98 034
Plantation of ind.spp.	3 000	61,96	185 867	2 554	61,77	157 766	-0.19	-28 101
Teak	4 510	69,99	315 646	3 746	73,69	276 050	3,70	-39 596
Acacia	0			341	25,27	8 617	25,27	8 617
Rubber	1 925	23,24	44 739	3 006	31,14	93 594	7,90	48 855
Bamboo	2 434	47,36	115 270	2 566	65,25	167 434	17.89	52 164
Shrubs	1 675	0,97	1 627	3 023	0,86	2 614	-0.11	978
Non-forest	9 295			11 035				
Total	31 255	55,58	1 737 256	31 255	42,78	1 337 000	-12,80	-400 256

The positive value in the last two columns indicate sequestration and the negative value indicates release

The above result represents the distribution and the amount of carbon hold by different forest types both in the recent and historical time. The last two columns represent the change of carbon budget.

The changes in average carbon content indicate whether carbon was sequestrated or released by a particular class. This is an indication of amelioration or degradation of woody biomass. However, the change in total carbon hold by each class is not only the result of amelioration or degradation but also the result of conversion of forest cover from one to the other class.

Above table shows that around ten ton per ha carbon was released due to the degradation of primary forest during the study period. Most of the other classes show forest growth and carbon sequestration. The highest amount of carbon is sequestrated by acacia and it is about 25 ton per ha in nine years, i.e. 2,78 ton per ha per annum. The growth performance of bamboo and secondary forest was satisfactory and the amount of carbon sequestrated by these two classes was 18 and 15 ton per ha respectively. The class of indigenous plantation and shrub shows a negligible amount of carbon release.

The highest amount of total carbon was released from the degradation and conversion of mature primary forest. Secondary forests, teak and indigenous plantations have showed some amount of carbon release. On the other hand bamboo showed the highest amount of carbon sequestration. The class rubber has also sequestrated a considerable amount of carbon. Shrubs show a slight increase of total carbon, which is not the result of the growth of vegetation but the conversion of other classes into this cover type.

The above results show information on carbon sequestration or release by each class due to amelioration or degradation. This was only possible by using regression or even *knn* method. But stratification technique would not provide any information because the method assumes a fixed mean value for a particular class for both in the recent and historical time.

Carbon release and sequestration maps of southern Chittagong are presented in figure 5.17 and 5.18 respectively.

153
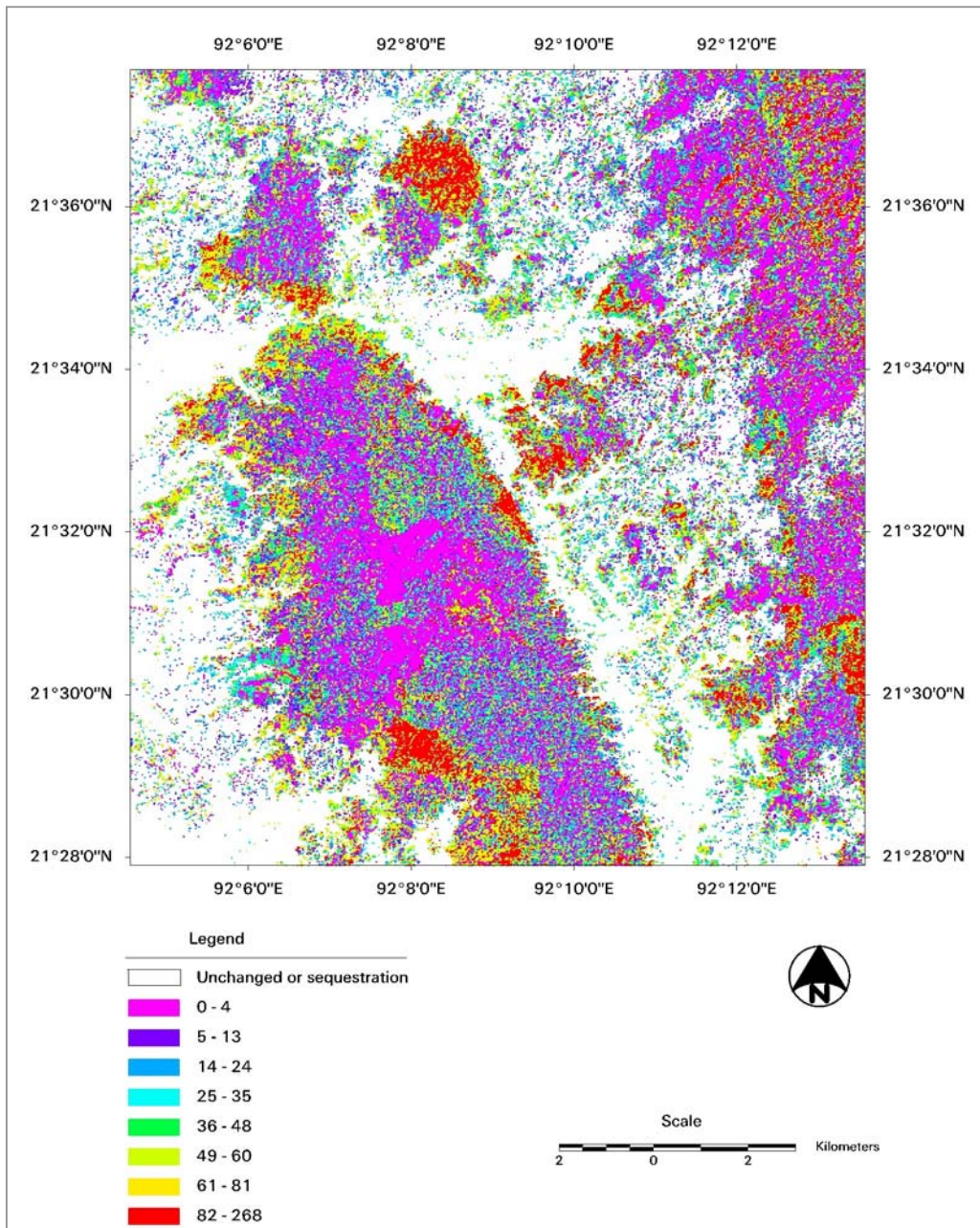
Figure 5.17 Carbon release map of southern Chittagong 1992-2001 using regression
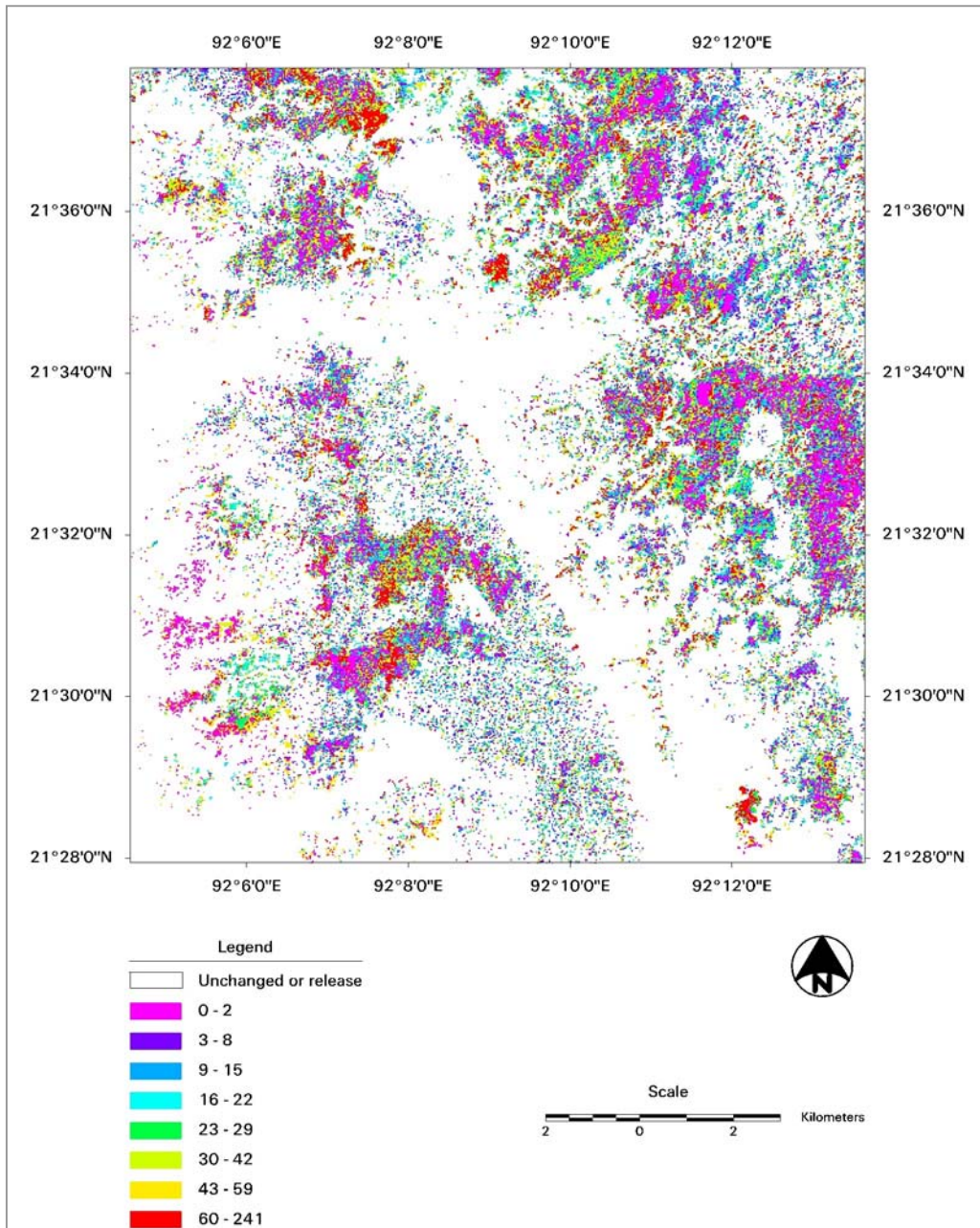
Figure 5.18 Carbon sequestration map of southern Chittagong using regression

5.7 Accuracy Assessment of Classification

The current study assessed the accuracy of classification from training set pixels. The matrix of the accuracy of classification for the recent image is presented in table 5.24.

Table 5.24 Error matrix of classification for Landsat ETM+ data 2001 from training set pixels

Classified data	Training set data	Natural forest vegetation			Plantation			Non-forest vegetation		Non-vegetated			Total (classified)
		Primary forest	Secondary forest	Indigenous spp.	Teak	Acacia	Rubber	Bamboo	Shrubs	Soil	Settlements	Water	
Natural vegetation	Primary forest	2636	36	65	284	3	2	3	0	0	0	0	3029
	Secondary forest	139	546	278	0	16	1	16	0	0	0	0	996
	Indigenous spp.	78	62	1505	9	40	7	0	6	0	0	0	1707
Plantation	Teak	254	3	4	1357	1	17	0	0	155	7	0	1798
	Acacia	9	0	86	2	633	0	0	0	0	0	0	730
	Rubber	18	3	8	23	0	1234	8	1	231	1	0	1527
Non-forest vegetation	Bamboo	2	10	1	0	0	7	722	0	0	0	0	742
	Shrubs	1	0	26	25	0	9	1	978	73	12	0	1125
Non-vegetated	Soil	2	0	0	125	0	169	1	59	3489	200	10	4055
	Settlements	5	0	5	15	2	0	0	7	83	2351	48	2516
	Water	1	0	0	5	0	0	0	0	4	69	1581	1660
Total (training pixel)		3145	660	1978	1845	695	1446	751	1051	4035	2640	1639	19885

In the above table the training set pixels those are accurately classified are located along the major diagonal of the error matrix (running from upper left to lower right-shaded cells). All the rest diagonal elements of the matrix represent errors of omission or commission. Omission errors correspond to non-diagonal column elements (e.g. 254 that should have been classified as primary forests were omitted from that category). Commission errors are represented by non-diagonal row elements (e.g. 125 teak plus 169 Rubber were improperly included in the soil category). The above matrix is summarised and presented in table 5.25.

Table 5.25 Summary of error matrix for classification of Landsat ETM+ data 2001 from training set pixels

Forest / Land cover type	Producer's accuracy		User's accuracy	
Primary forest	2636 / 3145	84%	2636 / 3029	87%
Secondary forest	546 / 660	83%	546 / 996	55%
Plantation of indigenous species	1505 / 1978	76%	1505 / 1707	88%
Teak	1357 / 1845	74%	1337 / 1798	74%
Acacia	633 / 695	91%	633 / 730	87%
Rubber	1234 / 1446	85%	1234 / 1527	81%
Bamboo	722 / 751	96%	722 / 742	97%
Shrubs	978 / 1051	93%	978 / 1125	87%
Soil	3489 / 4035	86%	3489 / 4055	86%
Settlements	2351 / 2640	89%	2351 / 2516	93%
Water	1581 / 1639	96%	1581 / 1660	95%
Overall accuracy = (2636 + 546 + 1505 + 1357 + 633 + 1234 + 722 + 978 + 3489 + 2351 + 1581) / 19885 = 86%				

The matrix of the accuracy of classification for the historical image is presented in table 5.26.

Table 5.26 Error matrix of classification for Landsat TM data 1992 from training set pixels

Classified data		Training set data											Total (classified)
		Natural forest vegetation		Plantation			Non-forest vegetation		Non-vegetated				
		Primary forest	Secondary forest	Indigenous spp.	Teak	Rubber	Bamboo	Shrubs	Soil	Settlements	Water		
Natural vegetation	Primary forest	2563	101	124	115	94	36	0	101	0	0		3134
	Secondary forest	442	377	163	27	185	101	0	16	0	0		1311
	Indigenous spp.	101	110	1164	64	35	11	35	414	1	0		1935
Plantation	Teak	19	8	75	1435	110	9	17	511	85	4		2273
	Rubber	2	9	94	45	522	1	120	259	10	1		1063
Non-forest vegetation	Bamboo	16	50	55	45	40	593	2	15	0	0		816
	Shrubs	0	2	225	26	129	0	511	288	26	0		1207
Non-vegetated	Soil	0	0	41	58	314	0	305	1523	341	23		2605
	Settlements	2	3	37	25	17	0	61	351	2068	118		2682
	Water	0	0	0	5	0	0	0	557	109	1493		2164
Total (training pixel)		3145	660	1978	1845	1446	751	1051	4035	2640	1639		19190

The above result can be summarised in table 5.27.

Table 5.27 Summary of error matrix for classification of Landsat TM data 1992 from training set pixels

Forest / Land cover type	Producer's accuracy		User's accuracy	
Primary forest	2563 / 3145	81%	2563 / 3134	82%
Secondary forest	377 / 660	57%	377 / 1311	29%
Plantation of indigenous spp.	1164 / 1978	59%	1164 / 1935	60%
Teak	1435 /1845	78%	1435 / 2273	63%
Acacia				
Rubber	522 / 1446	36%	522 / 1063	49%
Bamboo	593 / 751	79%	593 / 816	73%
Shrubs	511 / 1051	49%	511 / 1207	42%
Soil	1523 / 4035	38%	1523 / 2605	58%
Settlements	2068 / 2640	78%	2068 / 2682	77%
Water	1493 / 1639	91%	1493 / 2164	69%
Overall accuracy = (2563 + 377 + 1164 + 1435 + 522 + 593 + 511 + 1523 + 2068 + 1493) / 19190 = 64%				

The accuracy of classification was better for the recent image than the historical one. The reason might be that the forest type was verified from the field on recent years and the identification of pixel-class of the historical image was only done from this experience.

The error generated from the location uncertainty was tried to minimize by the geo-statistical approach discussed earlier. This approach can minimize bias and consequently improve correlation. However, it was not possible to verify the result using a differential GPS. Therefore, the analysis obtained from the geo-statistical approach was not finally included for presentation.

6   Discussion

6.1   Extracting Forest Biomass and Carbon Information from Satellite Data

The current study compares three methods; stratification, regression and *knn* for extracting forest biomass information and carbon content from satellite data. The study finally recommends a method, which is a regression technique, however it uses some information from the results of stratification in the form of dummy variables.

The study found an inverse relationship of spectral reflectance and above-ground standing biomass information except ETM+/TM band 4 where almost no relationship was noticed. The similar phenomena were noticed by many of the previous studies (Ardö 1992, Gjertsen 1996, Spanner *et al.* 1990, Horler and Ahren 1986, Roy and Ravan 1996). The inverse relationship between the biomass and spectral reflectance would be the result of increased canopy shadowing within larger stands and the decreased understorey brightness (soil brightness) due to increased density of biomass (Spanner *et al.* 1990). This result is agreed with the Alchrona (1988), who stated that there is an inverse relationship between amount of shadow and reflectance in all wavebands. Results from the study by Horler and Ahren (1986) specified this nature of behaviour for particular spectral regions, for example, band 5 or 7 of Landsat TM and stated that shadowing is a factor at least as important as leaf moisture content in influencing the spectral reflectance of forests in the shortwave infrared spectral region. Thus the higher spectral reflectance of the sample points with less biomass can be explained partially by smaller amount of shadow, which will result in a higher contribution to the spectral radiance from the background soil.

This study reported that the spectral reflectance of vegetation canopy ranges approximately from 3-10% in the visible range, 20-40% in the near infrared and 5-40% in the short-wave infrared region. These values are much lower than the reflectance of an ideal vegetation reflectance curve (figure 6.1). The reduced reflectance might be the result of the presence of shadow in vegetation canopies. This phenomenon has already been discussed in section 2.1.3.
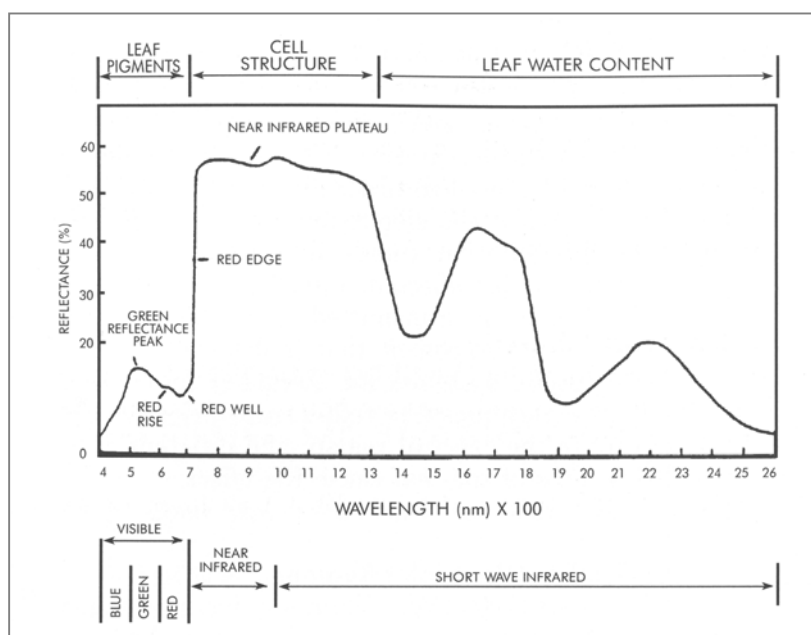
Figure 6.1 Spectral reflectance curve for a green leaf and dominant factors controlling leaf reflectance in the visible and near-infrared spectral regions (Bracher 1991)

The study found that the relationship between forest biomass content and spectral response from satellite data is poor in simple regression analysis and cannot be effectively used for prediction purpose. The value of the coefficient of determination, which expresses the proportion of variation in the response data that is explained by the model, is below 0.26. This result is quite consistent with many of the previous studies not only on tropical forests but also on temperate and boreal forests. The study by Steininger (2000) reported the above-ground dry biomass has a very poor correlation with Landsat TM bands in the tropical secondary forest for the study site in Bolivia (r^2 value was 0.03, 0.16, 0.00 and 0.03) however moderate in the site of Brazil (r^2 value was 0.05, 0.21, 0.49 and 0.37 for TM bands 3, 4, 5 and 7). Trotter *et al.* (1997) reported r^2 value of 0.17 for predicting volume of coniferous plantation in New Zealand using either band 3 or 4 of Landsat TM data. Häme *et al.* (1996) calculated r^2 values of 0.15-0.23 for estimating volume of coniferous forest using the visible red channel (band 3) of Landsat TM in southern Finland. Gjertsen (1996) reported the values of r^2 0.38, 0.28, 0.50 for SPOT XS1, XS2, XS3 and 0.29, 0.35 and 0.35 for TM band 3, 4 and 5 to predict coniferous stem volume for a selected test site of boreal needle-leaved, evergreen forest of Norway using simple linear regression.

The results of simple linear regression and the r^2 value found in the current study are not quite similar with some of the other studies. For example, Roy and Ravan (1996) found a good correlation for predicting forest biomass from all Landsat TM bands (r^2 0.59 to 0.76, for two dates, all types of ecosystem) except band 4 (r^2 value 0.18 to 0.49) in mixed deciduous and scrub forest

of Madav National Park, India using DN values as independent variables in simple linear regression. However, the study used only 22 sample plots, which is rather optimistic for a general conclusion. Their study also reported that the correlation degrades significantly when atmospherically corrected radiance values were used instead of digital numbers (r^2 values 0.25 to 0.43 for all bands except band 4, where 0.09 to 0.20), which is quite surprising. The study by Lu *et al.* (2002) found a surprising result for predicting forest biomass of the two study sites in Amazon forests. They reported that Landsat TM bands 5 and 4 were the best single band predictor of biomass and the r^2 values were 0.39 and 0.70 respectively. However, the current study found the r^2 value for band 4 is quite low ($r^2 = 0.03$) compared with the other bands.

The study found that the value of the coefficient of determination for predicting biomass and carbon information slightly improves when multiple regression is used with more than a single band. The improvement is steady in case of the addition of a second variable; however, any other subsequent addition does not show further improvement in a significant amount. The value of r^2 was 0.26 using one variable (band 2), after addition of the second variable (band 7) it improved to 0.28 and to 0.30, if all the bands were used in regression. This phenomenon was also reported by some of the previous studies (i.e. Häme *et al.* 1996, Thenkabail *et al.* 2004 etc.).

Many of the earlier studies found the similar value of r^2 for predicting biomass and volume from satellite data using multiple regression. Foody *et al.* (2003) reported that the values of r^2 were 0.30, 0.32 and 0.25 to predict tropical forest biomass in the selected test sites of Thailand, Brazil and Malaysia using all Landsat TM bands. Thenkabail *et al.* (2004) reported that the values of r^2 were 0.16 and 0.13 for predicting dry weight biomass in African rainforest of the Congo basin, southern Cameroon, using IKONOS and ETM+ data respectively for all vegetation types studied. Trotter *et al.* (1997) found that the r^2 value was 0.24 for relating all Landsat TM bands and volume of coniferous plantation in NewZeland. The study by Hyyppä *et al.* (2000) got r^2 values of 0.44 and 0.31 for predicting stem volume of boreal forest in southern Finland using Spot XS and Landsat TM bands respectively.

The result of regression in the logarithmic or exponential transformation shows some improvement instead of using in linear form. The current study found the values of r^2 were 0.34, 0.47, 0.38, 0.04, 0.31, 0.33 for predicting biomass and carbon content using Landsat ETM+ bands 1-5 & 7 in exponential form, which means that there is some improvement in the relationship. Some other studies also reported similar results. For example, Ardö (1992) found a relationship of 0.55, 0.61, 0.50, 0.23, 0.62 and 0.55 between forest volume and natural logarithm (ln) of Landsat TM bands radiance (1-5 & 7) for test sites of boreal forest in southern Sweden.

The information content of spectral windows in satellite bands is not the same and hence they show different degree of utility. Moreover, the usefulness of different bands for extracting forest biomass and carbon information varies with the method applied (Table 6.1). Band 5 has the utility

order 7 in regression; however, it has the highest order in stratification for extracting biomass and carbon information. In some cases the spectral channels have similar order of utility both in regression and stratification. The utility of TVI and NDVI is ordered in the position nine and ten for both in regression and stratification. It should be noted that the ordered list of the ten components is the same for both regression and stratification but their chronology is different.

Table 6.1 Utility of various remote sensing components for extracting biomass information using regression and stratification

Ordered list in regression	Component	R^{2}*	Information content (some parts adapted from Tucker 1978)	$\bar{V}$	Ordered list in stratification
1	Band 2	0,473	Slightly sensitive to chlorophyll plus green region characteristics	279,06	2
2	Band 3	0,38	Sensitive to chlorophyll	295,44	6
3	Band 1	0,337	Sensitive to chlorophyll and carotinoid concentrations	281,00	3
4	Band 7	0,332	Sensitive to water in plant leaves	284,12	4
5	Principal component 1	0,326	Combined information from all bands maximizing variance in a new spectral axis	294,14	5
6	Brightness	0,314	Soil brightness indicator, relation to the biomass content has not been described yet	305,58	8
7	Band 5	0,313	Sensitive to water in plant leaves	276,40	1
8	Wetness	0,296	Contrasts middle-infrared reflectance with visible and near-infrared reflectance, represents a degree of moisture sensitivity	303,06	7
9	TVI	0,229	Stretched Blue to the total of the visible reflectance	305,83	9
10	NDVI	0,201	Stretched NIR to red reflectance	350,21	10

*r^2 value in exponential equation

The current study found that the visible bands (band 2, 3 and 1) have the highest information content on forest biomass, when the regression method is used. They are followed by band 7. Similar results were obtained by the study of Franklin (1986). The study reported that the value of r^2 was higher for visible bands (0.22, 0.28, 0.29 for TM band 1, 2 and 3), however, lower for near

infrared (0.04, band 4) and mid infrared bands (0.03, band 7) in logarithmic transformation for predicting basal area of conifer, hardwood and mixed evergreen forest of California. However, this phenomenon was not supported by some of the other studies. Ardö (1992) found a highest correlation with band 5 (r^2 = 0.62), though band 2 (r^2 = 0.61) was quite close to it. The study by Steininger (2000) reported the aboveground dry biomass has a moderate correlation with Landsat TM band 5 in an exponential relationship for the tropical secondary forest of the study site in Brazil (r^2 value was 0.51).

The reason for improving the value of r^2 in transformation is due to the asymptotic nature of the relationship between spectral reflectance and biomass content. This could be the result of saturation effect. The figure 5.9(a) shows that low biomass values lie near to the zero residual line but point towards high biomass values were scattered away from that line. The above result agreed with Franklin (1986) who suggested that when the vegetation cover approaches 100%, the basal area (i.e. wood volume or wood biomass) continues to increase as the stand grows older, but the remotely sensed signal is not affected by this increase because it is most sensitive to the degree of crown closure.

NDVI is sometimes widely used for a lot of the vegetation studies, but has the lowest performance for predicting forest biomass and carbon information among the listed components in table 6.1. The r^2 values found in the current study were 0.14 in simple and 0.20 in exponential relationship. Many of the other studies have also reported similar results. A study of Häme *et al.* (1996) found the value of r^2 is 0.02 for predicting coniferous stem volume in southern Finland using NDVI. This indicates, that almost no relationship exists between these variables. Franklin (1996) reported that the relationship with ratio vegetation index (NIR/red channel of TM) was 0.15 in logarithm for predicting basal area in the test site of California. Trotter *et al.* (1997) reported that the r^2 value was better for the individual band data alone than for NDVI when relating Landsat TM bands and volume of coniferous plantation in New Zealand.

The application of dummy variables in regression has significantly improved the relationship. The dummy variables have been set from the result of optimal stratification. The value of r^2 was 0.89, which is quite excellent for a satisfactory prediction. Though dummy variables are sometimes applied in other sciences, however, it has not been applied earlier in remote sensing for extracting forest biomass and carbon information. Therefore no results from any other similar studies are available yet. This is a new finding for the science community.

6.2   Carbon Pool and Flux

The above-ground carbon pool in a tropical forest ecosystem varies with many factors, for example, with the types and stocking of forest, site quality, disturbing patterns etc. Local level studies can produce accurate results. However, uncertainties increase when it focusing on regional

and global level, unless a sound sampling system is applied to get the information from all the representative forest and stocking conditions. The current study estimated that mean aboveground carbon stored in the mature tropical wet evergreen and semi-evergreen forest of the study area was 133 ton/ha. The result is quite close to the estimate reported by Dixon *et al.* (1994). The study reported that tropical forest in Asia has a vegetation carbon density of 132-174 ton/ha. Brown and Lugo (1984) reported the biomass density for tropical undisturbed closed, logged and unproductive forests in Bangladesh were 176, 120 and 110 ton/ha (88, 60 and 55 ton/ha of carbon) respectively. Brown *et al.* (1993) reported that the mean carbon was 232 ton/ha in biomass as the potential aboveground mean carbon in 1980, whereas 87 ton/ha was the recoded as actual in the forests of Bangladesh. Brown (1997) mentioned that the above-ground biomass was 210, 150, 190 and 85 ton/ha (105, 75, 95 and 42,5 ton/ha carbon) for closed-large crowns, closed-small crowns, disturbed closed and disturbed open forest respectively for Bangladesh.

Primary forest biomass estimates varied from 290 to 495 t/ha in Rodontia (145 to 248 t/ha C), western Brazilian Amazon (Alves *et al.* 1997). Dixon *et al.* (1994) reported that smaller regions of Malaysia and Indonesia might contain up to 250 ton/ha of carbon. The study by Murdiyarso and Warsin (1995) reported that aboveground carbon was 300-325 ton/ha for primary humid evergreen forest of Sumatra, Indonesia.

Secondary forest holds much more lower amount of carbon. This study estimated that secondary forest has 100 ton/ha of carbon (75% of the primary forest). Secondary forest of Rodontia, Brazil, contains about 40-60% of biomass of the primary forest biomass (58 to 149 t/ha of C) after 18 years of abandonment (Alves *et al.* 1997). The clearing history of the secondary forest of the current study area is unknown. The area was allotted for felling in different coupes; the practice was stopped officially during late 1980s to stop further degradation of forest in the country.

Plantation has a relative lower carbon content than the primary and secondary forests. However, the amount of carbon sequestration by a plantation forest depends upon the species planted and its growth rate, site quality, cultural and tending operation, disturbance etc. Indigenous and teak plantations in the study area were estimated to have 60-75 ton/ha carbon. Rubber has about 30 ton/ha of carbon. Short rotation acacia has a relative lower amount of carbon (25 ton/ha).

Scrub vegetation has less than 1 ton/ha of carbon. This ecological zone is very close to the habitation. Most of the forest in the study area belongs to the Government property. The control system to protect forest for this region has broken down. The area seems to be under the process of repeated disturbance by human interference, which hinders the process of succession to form secondary forest.

About 4 00 250 ton of carbon was released during 1992-2001 (nine years) from our investigated test site. It means that about 44 473 ton/year (1 ton = 10^6 gram) was released from 31 255 ha

(about 313 sq. km) of the study area. Dixon *et al.* (1994) reported that the annual C flux from tropical Asian forest is –0.50 to –0.90 Pg/year (I Pg = 10^{15} gram, Appendix IV). The ratio of the C flux of the study area to that figure of continental scale is quite small (0.9 x 10^{-4} to 0.5 x 10^{-4}).

The test site has released around 13 ton/ha of carbon in 9 years, i.e. 1,4 ton/ha/year. Harmon *et al.* (1996) reported that during harvest approximately 50% of the living biomass is converted to additional woody debris that decay on site. Of the carbon removed from the site and distributed to the forest products sector, approximately 40% quickly returns to the atmosphere due to losses during primary and secondary manufacturing as well as to incineration and decomposition of short-lived forest products. They stated that the remaining forest products decompose slowly, at a rate of approximately 2% per year. This means that about 2 00 130 ton i.e. 0.71 ton/ha carbon (2.61 ton carbon di oxide, Appendix IV) was released to the atmosphere from our test site or is going to be released soon during the harvesting process. Another 80 050 ton of carbon (2 93 790 ton of carbon-di-oxide) has already been released or is going to be released shortly during the secondary manufacturing.

However, all the carbon removed from the ecosystem does not come back to the atmosphere immediately. The fate of carbon depends upon the end-use of forest products. Table 6.2 reports the durability of the forest products coming from the living pool and locked for the time period in dead pool. However, after the lifecycle the carbon might come to the atmosphere.

Table 6.2 Different lifespan of various commodities (locked carbon) (Eaggers 2002)

Category	Lifespan (years)	Included commodities
Short lifespan paper-products	1	Newsprint, shares of packing papers, paperboard, and printing and writing paper
Medium-short lifespan paper-products	4	Rest of packing paper, paperboard, and printing and writing paper
Short lifespan timber	1	Fuelwood, wooden packing materials and structural support materials
Medium-long lifespan timber	16	Part of swan timber and wood-based panels
Long lifespan timber	50	Rest of swan timber and wood-based panel

However, the estimate of the amount of carbon released to the atmosphere in the current study might varies in some extend, because results of a study in the U.S. regarding the fate of removed

biomass and durability of forest products were used. But those estimates vary with locality and type of wood. Such studies on local level are still quite absent.

7 Conclusion

7.1 Important Research Findings

The results of the current study provide partly new, partly specifically adapted methods to extract forest biomass/carbon information from satellite data. Usually the relationship between forest variables and spectral reflectance of satellite image using regression is very poor. The current study has explored an important finding regarding the use of dummy variables in the regression equation. Dummy variables obtained from the optimal stratification can significantly improve the correlation (section 5.3.2).

The study has successfully applied the image based COST calculation method developed by Chavez and compared the findings for a tropical region located near the seashore (section 5.1). The study has also generated the interpretation key and spectral library for the identification of tropical forests of southern Chittagong, which are currently not available (section 5.2).

Finally the study calculated the amount of carbon released from the selected area of southern Chittagong due to forest cover change (section 5.6). However, the global carbon budget would not be influenced by the change of carbon pool in a small test area, however, the global budget would be influenced by the change of regional / local budgets if it occurs in many places. Therefore, the result of the study is applicable to other forested region to estimate the carbon pool and investigate any change in that pool to understand the global carbon dynamics.

7.2 Limitation of the Study

7.2.1 Remote sensing data

The current study faced several limitations. One of the main constraints of the study is related to the limitations of information, which can be extracted from the optical satellite images. Low-cost optical data usually provide the spectral information in passive range. The information could be sufficient for detecting forest and forest types, but does not contain the information related to the canopy height, which is an important variable for estimating forest volume / biomass and eventually the carbon content. In the recent days the availability of laser scanning or even active remote sensing data could help to extract those information more precisely.

The other problem is the limited spatial resolution of data sets. Currently Landsat imagery provides a spatial resolution of 30-60 meter for the multispectral image of visible to thermal wavelengths. However, the use of very high-resolution data with a few meters of spatial resolution i.e. IKONOS or QuickBird could mitigate the problem. The current study did not use all those data sets, as they

are very costly. Any findings of research using those data sets cannot be applied in a large scale by developing countries, where most of the tropical forests are located due to financial constraints.

Satellite sensors acquire radiance values at-satellite level, which are later converted to DNs through the use of gain and offset values for distribution. Because of sensor degradation over time, gain and offset values are subject to periodic adjustments over the life of a system and are different for sensors even of the same type (e.g., Landsat 4 TM and Landsat 5 TM) (Musick 1986, Suits *et al.* 1988, Gallo and Eidenshink 1988). A specific radiance or reflectance level will not be expressed as a constant DN value over time or between sensors (Hill and Sturm 1991). Relationships between DN values and biophysical factors are therefore time and sensor specific (Graetz 1990). To minimize this problem, remotely sensed data for this study were converted to radiance values prior to statistical analysis. However, there might be still some errors as periodic adjustments of sensors are not continuously done and are rather available at certain time intervals.

7.2.2   Topography

Errors might also be incurred due to the topographic factors. The study area consists of slightly hilly terrain. The reflectance from the sun-facing slopes and opposite ones is not the same. The problem could be solved by topographic normalization using a digital elevation model (DEM). But currently no DEM is available with an acceptable resolution for the study area. The data of SRTM mission by NASA for that region is still not available. Results by Walsh (1987) and Cohen and Speis (1992) have demonstrated the topographic influence on monitoring forest stands.

7.2.3   Location uncertainty

The errors due to the location uncertainty can arise from two sources: (1) satellite data, which are geometrically corrected using topographic maps, (2) locating field sample plots by a portable GPS. The topographic maps covering the study area have been prepared during the colonial period and might contain errors, which should be adjusted by GPS. The current study used a portable GPS, which gathers information of position with 15m RMS. In contrast, differential GPS, which shows accuracy up to centimetre level, was not available during field sampling. Therefore, this study assumed that the biomass and carbon information for the measured plot matched with the particular pixel reflectance of the satellite image (30m size), which might not always be true. The field measurement value rather might contain information from the neighbouring pixels.

7.2.4   Mixed pixel and classification

The study generated a carbon map using regression with dummy variables. Though regression is a process of predicting variables in a continuous form, however, the use of dummy variables make it

discrete for a number of vegetation classes. In reality all the pixels do not belong to a particular class, but contain a mixture of two or more classes. Therefore, the accuracy of this study depends upon the accuracy of classification for certain classes, which have distinct dummy variables.

7.2.5 Sampling error

A certain degree of bias might be generated due to the constraints of ideal application of sampling technique. The study aimed to use stratified random sampling, but, in practice the exact principle of the technique might be absent in some extent due to the difficulties and restrictions of accessibility. Therefore, a considerable number of field sample plots were located near the route network. Similar problems were also noticed by Köhl *et al.* (1995). As the accessible areas are more vulnerable by disturbance, the remote places should have better stocking under the assumption that there is constant site productivity. This fact might affect the current study because the estimate using the stratification method generates the lowest amount of carbon content compared to the estimates obtained by the other two methods. The other problem might be related to the local field officials. They usually have a tendency to locate the field samples on the best stocking in their jurisdiction.

7.2.6 Measurement error

Two variables, tree height and diameter at breast height (*dbh*) were measured during field sampling and were later converted to biomass and carbon content. *Dbh* can be accurately measured by diameter tape. In contrast, heights of selected trees inside a plot were measured to get a better efficiency. Most of the height measuring instruments use the trigonometric principle, which needs a clear identification of treetops. But inside a dense tropical forest demarcation of treetops is often difficult due to the presence of heavy biomass and oval shapes of tree crown in some cases. Some errors might be added due to lack of proper identification of treetop. The heights of the remaining trees were estimated from the nearby measured height. This practice might have incurred some errors as well.

7.2.7 Estimation error

The accurate measurement of biomass and carbon content of forest requires destructive sampling, which is an expensive and time-consuming process. In some cases it is virtually impossible due to the prohibition of felling. Therefore, the study is highly depending on the allometric relationships between tree *dbh* and height with volume/biomass. The accuracy of this study relies to the accuracy of those relationships. Moreover, the respective equations were not available for all those species found in the tropical forest, because of its high biodiversity. Many of the species are not commercially important and consequently no relationship for those species has yet been

developed. Hence, the current study used an equation for the mixed species. Using that equation may have incurred a certain degree of errors.

Most of the available allometric equations were applicable to estimate volume, which was later converted to the biomass content using the wood density for a particular species. Wood density varies with the portion of wood, either sapwood or heartwood from stem or branches, or even the geographical position. However, the wood density was not available for all the species. In that case, a constant close to the average density of other species was used, which could have incurred a considerable error.

7.2.8 Lack of below-ground carbon information

Another limitation of the current study is related to the fact that it is only concerning the aboveground biomass. Below-ground processes have not been considered. There is currently no consensus about whether tropical deforestation results in a significant reduction of soil carbon stocks (IPCC/OECD 1994), although some evidence suggests that clearing and burning of forests may reduce soil carbon by various means, such as oxidizing carbon near the soil surface (Cerri *et al.* 1991, Kauffman *et al.* 1995) or causing decomposition of deep or shallow roots from the original forest (Nepstad *et al.* 1994). If deforestation or fragmentation leads to substantial losses of below-ground carbon, then our estimation would have to be modified accordingly.

7.3 Recommendation and Future Outlooks

The study has developed a method, which allows for the extraction of forest biomass and carbon information in a precise way. The method requires low-cost satellite imagery and some field sampling, which is indeed not that expensive to be conducted in a developing country. The technique can be successfully applied for periodic monitoring of forest condition and for updating biomass and carbon accounting. Thus it can be used as an operational tool for many of the tropical countries. However, there would be a generalization problem due to the coefficients and constants of the regression equation. This means that the values calculated for the study area cannot be used to predict forest biomass and carbon stock information for different regions or forest types, because the relationships between the forest biomass and their spectral reflectance depend upon the canopy cover, canopy optical properties, presence of shadows, understorey reflectance and topographic conditions, if no topographic normalization is applied. Though there are some relations of those factors with biomass, it is not strong enough for a successful prediction. Therefore, it is necessary to calculate those coefficients and constants in regression for particular regions and forest types. Such generalization problems have also been discussed by Foody *et al.* (2003), Woodcock *et al.* (2001) and others.

The study concludes with the following recommendations:

1. Use of dummy variables in regression provides better results for extracting forest biomass and carbon information over the methods of *knn* and traditional regression. Those dummy variables can be obtained from the result of stratification. Stratification generates a slightly better result in some cases. However, the method does not generate continuous information on pixel level, it rather provides discrete and constant information for the whole class, which is not appropriate in reality. On the other hand *knn* needs a huge number of field sample plots. Additionally details of statistics for prediction still are not available. However, it should also be kept in mind that the current study has only applied one form of k ($k = 1$).

2. Mature primary forest of the study area contains the highest amount of carbon (130-140 ton/ha) in unit of area for the study region. Any other forest types (except young secondary forest) do not contain more than 55% of the carbon storage which primary forest holds. Therefore, conversion of such forest will have a great impact on carbon release in a short period of time. During the last decade primary forest of the study area showed average degradation and carbon release of 1.2 ton/ha/year due to removal of timber from the forests. Therefore, the study recommends halting further degradation of mature primary forest by means of better protection and by better motivation of the local people.

3. The possibility of carbon sequestration by mature forest is limited because of the presence of mature and over-mature trees at a large extend, which exhibit a very slight or stagnant growth. On the other hand young secondary forests and young plantations have a high potential of carbon sequestration in near future, because the trees exhibit a high growth rate in their early stage of life. During the last decade the net sequestration by plantation in the study area was negligible perhaps due to the removal of timber by human activity. But young secondary forest in the study area has sequestrated carbon around 1.7 ton/ha/year because of their growth and because the area was not affected by human interference, as it is located in a remote place. Therefore, the conversion of mature forest to plantation for carbon sequestration is not recommended, not only due to the man-made pressure on forest and plantation but also for biodiversity and other ecological reasons.

4. Mature primary and young secondary tropical forests are easily distinguishable on Landsat ETM+ imagery. Bamboos, when dominant in the upper canopy, can also be separated. However, the presence of bamboo in a mixed form with other trees and as understorey is rather difficult to detect. Scrubby vegetation is also distinguishable on imagery. Some plantations can also be separated. Rubber (i.e. leafless stage) and acacia plantations can be easily detected. Plantations with indigenous forest can also be distinguished. However, in some cases they exhibit the similar reflectance as young secondary forests, especially

when the weeding operation is not regularly applied in the early stage of the plantation and the planted trees are intermixed with understorey natural vegetation. Teak can be separated from other plantations, but it is hard to distinguish it from scattered trees and degraded mature forests, as all these three categories show the similar reflectance.

5. Atmospheric correction and conversion of digital number to surface reflectance is necessary for multi-temporal studies, because the digital count is scene specific while the reflectance value is general. However, such a correction is sometimes not sufficient and an additional normalization between multi-date images is often required. This might be essential due to sensor degradation or even if multi-sensor imagery is used, as the spectral window for different bands in multi-sensor imagery is often similar but not the same.

The study has discovered an improved relationship in the regression equation and consequently it is expected that the method could be widely used for monitoring tropical forest biomass and carbon storage in near future. However, the applicability of the method is not only limited to tropical vegetation. It can also be applied to temperate and boreal forest conditions. However, the applicability of the method for such forests is rather simple. Because those forests are homogenous and have less variability than the tropical forest due to presence of a limited number of flora in the upper canopy often forming a canopy of homogenous height. In contrast, tropical forests are often diverged due to the presence of a large number of species. The change in the temperate and boreal forests is also limited. Carbon sequestration due to forest growth is much more slower in these forests than in the tropics. Forest destruction is rather extended and homogenous and is followed by the prescription of management plans in those forests. On the other hand trees in tropics have a high rate of growth. Small-scale clearings and removal of selected trees are very common there, which is rather difficult to monitor from satellite platform. The change in tropical forests often occurs in localized pattern, which are quite variable from place to place and are often not followed by the prescription of the management plans, even if those plans would exist.

Further studies can be carried out in order to incorporate height information and to improve the relationship. In that regard, the incorporation of laser-scanning data could improve the equation significantly. Most of the optical sensors heavily depend on the presence of green biomass on the top canopy. However, a major amount of above-ground carbon stored in a mature forest ecosystem is not sequestrated in the green biomass but in the tree trunks and branches. A main difficulty noticed by the current study was the lack of being able to acquire this information by most of the remote sensing optical sensor. Therefore, the specific task of remote sensing scientist would be to develop such types of sensors, which could also collect that information. Additional studies should also be carried out to extract forest biomass and carbon information from the microwave data, which has some penetration ability in combination with the optical image. Studies are also needed to make better prediction of forest attributes from remote sensing data using different

methods in combination. Finally, the study also missed the availability of appropriate allometric relations for a number of species growing in the study region. The task of local forest researchers is to carry out further investigations in this regard. Local studies for estimating the flow of carbon from forest to the atmosphere is quite absent. Further studies should be carried out in this regard.

8   References

Abelson, H. 1990. Uncertainties about global warming. *Science* **247** (4950) 1529.

Altman, N. S. 1992. An introduction to kernel and nearest-neighbour nonparametric regression. *American Statistician* **46:** 175-185

Alves, D.S., J.V. Soares, S. Amaral, E.M.K. Mello, S.A.S. Almeida, O. Fernandes da Silva, and A.M. Silveria, 1997: Biomass of primary and secondary vegetation in Rondonia, western Brazilian Amazon. *Global Change Biology* **3:** 451–462.

Andreadis, I., Glavas, E. and Tsalides, P. 1995. Image enhancement using color information. *International Journal of Remote Sensing* **16(12)**: 2285-2289.

Annon 1997. *ERDAS Imagine tour guides.* ERDAS Inc, Atlanta. 454p.

Anon. 1999. *The remote sensing data book.* G. Rees (*ed.*). Cambridge University Press, Cambridge. 262 p.

Anon 2002. Remote Sensing Data Sources for Estimating Forest Structure. http://www.forestera.nau.edu/VegModel_update.htm Internet edition (accessed March 2004)

Anthony, D. A. 1986. Die Grenzen und Möglichkeiten der visuellen Photointerpretation und computergestützter Luftbildauswertung zur Ansprache der mitteleuropäischen Baumarten. *PhD Thesis,* University of Freiburg.

Apps, M. J. and Kurz, W. A. 1991. *World Resour. Rev.* **3** 333

Ardö, J. 1992. Volume quantification of coniferous forest compartments using spectral radiance recorded by Landsat Thematic Mapper. *International Journal of Remote Sensing* **13(9):** 1779-1786.

Atmawidjaja, R. 1972. Stand volume determination using aerial photographs and the double sampling technique. *PhD thesis.* College of Forestry, Syracuse University. 114p.

Avery, T. E. and Berlin, G. L. 1992. *Fundamentals of Remote Sensing and Airphoto Interpretation* (5th edition). Macmillan, 472p.

Avery, T. E. and Burkhart, H. E. 1994. *Forest measurements.* (fourth edition). McGraw-Hill. 408 p.

Baten, S. A. 1969. Revised working plan for the forests of the Chittagong Division for the period from 1968-69 to 1977-78. Forest Department, Government of East Pakistan, Dhaka.

Birdsey, R. A. 1992. Carbon storage and accumulation in the United States Forest Ecosystems. Rep. WO-59, Department of Agriculture Forest Service, Washington DC.

Birdsey, R. A., Plantiga, A. J., Heath, L. S. 1993. *Forest Ecology and Management* **58:** 33

Botkin, D. B. and Keller, E. A. 1998. *Environmental Science: Earth as a living planet.* (2nd ed.). John Wiley & Sons. 649 p.

Bracher, G. A. 1991. Detection of nutrient stress in Douglas-fir seedlings using spectroradiometer data. *PhD thesis.* University of British Columbia, Vancouver. 236 p.

Brown, K. 1996. The Utility of Remote Sensing Technology in Monitoring Carbon Sequestration Agroforestry Projects. Arlington, VA: Winrock International Institute for Agricultural Development.

Brown, S. 1997. Estimating Biomass and Biomass Change of Tropical Forests: a Primer. *FAO Forestry Paper* 134, Rome, Italy.

Brown, S. 1999. Guidelines for Inventorying and Monitoring Carbon Offsets in Forestry-Based Projects. *World Bank Working Paper.* Washington, DC: World Bank Group.

Brown, S., Gillespie, J. R. and Lugo, A. E.. 1991. *Canadian Journal of Forest Research* **21:** 111.

Brown, S., Iverson, L. R. and Lugo, A. E. 1989. *Forest Science* **35** 881.

Brown, S., L. R. Iverson, A. Prasad, and D. Liu, 1993. Geographic distribution of carbon in biomass and soils of tropical Asian forests. *Geocarto International* **8(4):** 45-59

Carper, W. J., Lillesand, T. M. and Kiefer, R. W. 1990. The use of intensity-hue-saturation transformations for merging SPOT panchromatic and multispectral image data. *Photogrammetric Engineering & Remote Sensing* **56(4):** 459-467.

Carr, J. R. and Miranda, F. P. 1998. The semivariogram in comparison to the co-occurrence matrix for classification of image texture. *IEEE Transactions on Geoscience and Remote Sensing* **36(6):** 1945-1952.

Castel, T., Beaudoin, A., Stach, N., and Stussi, N., 2001. Sensitivity of space-borne SAR data to forest parameters over sloping terrain. Theory and experiment, *International Journal of Remote Sensing* **22(12):** 2351-2376.

Cerri, C. C., Volkor, B., Andreux, F., 1991. Nature and behavior of organic matter in soils under natural forest, and after deforestation, burning and cultivation, near Manaus. *Forest Ecology and Management* **38:** 247-257.

Champion, H. G., Seth, S. K. and Kattak, G. M. 1965. *Forest types of Pakistan.* Pakistan Forest Institute, Peshawar. 238 p.

Chaudhury, M. U. 1969. Working plan of Cox's Bazar Forest Division for the period from 1968-69 to 1977-78. Forest Department, Government of East Pakistan, Dhaka.

Chavez, P. S. Jr. 1975. Atmospheric, solar and MTF corrections for ERST digital imagery. *In.* Proceedings of the American Society of Photogrammetry, Fall Technical Meeting, Phoenix, AZ, p69.

Chavez, P. S. 1986. Digital merging of Landsat TM and digitized NHAP data for 1:24,000 scale image mapping. *Photogrammetric Engineering & Remote Sensing* **56(2):** 175-180.

Chavez, P. S. 1988. An improved dark-object subtraction technique for atmospheric scattering correction of multispectral data. *Remote Sensing of Environment* **214:**459-479.

Chavez, P. S. 1989. Radiometric calibration of Landsat Thematic Mapper multispectral images. *Photogrammetric Engineering & Remote Sensing* **55:** 1289-1294.

Chavez, P.S., Jr., 1996, Image-based atmospheric corrections—revisited and revised. *Photogrammetric Engineering and Remote Sensing* **62(9):**1025-1036.

Chavez, P. S. and Bowell, J. A. 1988. Comparison of the spectral information content of Landsat Thematic Mapper and SPOT for three different sites in the Phoenix, Arizona region. *Photogrammetric Engineering & Remote Sensing* **54(12):** 1699-1708.

Chavez, P. S. Jr., and Mackinnon, D. J. 1994. Automatic detection of vegetation changes in the southwestern United States using remotely sensing images. *Photogrammetric Engineering & Remote Sensing* **60(5):** 571-583

Chavez, P. S., Sides, S. C. and Anderson, J. A. 1991. Comparison of three different methods to merge multiresolution and multispectral data: Landsat TM and SPOT panchromatic. *Photogrammetric Engineering & Remote Sensing* **57(3):** 295-303.

Chen, Z., Elvidge, C. D., and Groeneveld, D. P. 1999. Vegetation change detection using high spectral resolution vegetation indices. Pp 181-190. *In.* Lunetta, R. S. and Elvidge, C. D. (eds). Remote Sensing Change Detection: Environmental monitoring methods and applications. Taylor & Francis, London.

Chiao, K. 1996. Comparisons of three remotely sensed data on forest crown closure and tree stem volume estimations. *International Archives of Photogrammetry and Remote Sensing* **XXXI(B7):** 123-130

Ciesla, W M. Wilson, E. T., Eav, B. B., and Ward, J. D. 1986. *Identification of Red Spruce and Frazier Fir on Large Scale CIR Aerial Photographs.* Fort Collins, Colorado: USDA Forest Service, Forest Pest Management/Methods Application Group. Report 87-1.

Cochran, W. G. 1977. *Sampling techniques* (3rd ed.). John Wiley & Sons, New York. 428 p.

Cohen, W. B. and Spies, T. A. 1992. Estimating structural attributes of Douglas Fir / Western Helmlock forest stands from Landsat and SPOT imagery. *Remote Sensing of Environment* **41:**1-17

Colwell, J. E. 1974. Vegetation canopy reflectance. *Remote Sensing of Environment* **3:** 175-183.

Congalton, R. G. and Green, K. 1999. *Assessing the Accuracy of Remotely sensed Data: Principles and practices.* Lewis Publishers, New York. 137 p.

Coppin, P. R. and Baues, M. E. 1994. Processing of multitemporal Landsat TM imagery to optimize extraction of forest cover change features. *IEE Transactions on Geoscience and Remote Sensing* **32(4):**918-927

Cover, T., and Hart, P. 1967. Nearest neighbor pattern classification. *IEEE Transactions on Information Theory* **13:** 21-27.

Curcio, J. A. 1961. Evaluation of atmospheric aerosol particle size distribution from scattering measurement in the visible and infrared. *J. Opt. Soc. Am.* **51:** 548-551.

Crist, E. P. and Cicone, R. C. 1984. A physically-based transformation of Thematic Mapper data- the TM Tasseled Cap. *IEEE Transactions on Geoscience and Remote Sensing* **22:** 256-263.

Crist, E. P., R. Laurin, and R. C. Cicone. 1986. Vegetation and soils information contained in transformed Thematic Mapper data. *In.* Proceedings of IGARSS' 86 Symposium, Pp1465-1470. Ref. ESA SP-254. Paris: European Space Agency.

Curran, P. J. and Milton, E. J. 1983. The relationship between the chlorophyll concentration , LAI and reflectance of s simple vegetation canopy. *International Journal of Remote Sensing* **4:** 247-255.

Das, D. K. 1990. Forest types of Bangladesh. Plant Taxonomy Series, *Bulletin 6.* Bangladesh Forest Research Institute, Chittagong.

Dees, M. J. Duvenhorst, C. P. Gross and B. Koch. 2000. Combining remote sensing data sources and terrestrial sample-based inventory data for the use in forest management inventories. Proceedings ISPRS, vol XXXIII, Amsterdam.

Dixon R.K. and J. Wisniewski (1995) *Water, Air and Soil Pollution* **85:** 101-110.

Dixon, R. K., Brown, S., Houghton, R. A., Solomon, A. M., Trexler, M. C. and Wisniewski, J. 1994. Carbon pools and flux of global forest ecosystems. *Science* **263:** 185-190

Draper, N. R. and Smith, H. 1998. *Applied regression analysis* (3rd edition). Wiley. 706 p.

Eaggers, T. 2002. The impacts of manufacturing and utilization of wood products on the European Carbon budget. European Forest Institute Internal Report 9, Joensuu, Finland.

Eastman, J. R. and Fulk, M. 1993. Long sequence time series evaluation using standardized principal components. *Photogrammetric Engineering & Remote sensing* **59(6):** 991-996

Efron, B. & Tibshirani, R. J. 1993. *An introduction to the bootstrap.* Chapman & Hall. 436 p.

Ekstrand, S. 1994. Assessment of forest damage with Landsat TM: Correction for varying forest stand characteristics. *Remote Sensing of Environment* **47:** 291-302.

Elvidge, C.D., Yuan, D., Weerackoon, R.D., and Lunetta, R.S., (1995), Relative Radiometric Normalization of Landsat Multispectral Scanner (MSS) Data Using an Automatic Scattergram Controlled Regression. *Photogrammetric Engineering and Remote Sensing* **61:**1255-1260.

FAO 1997. Estimating biomass and biomass change of tropical forests: A primer. *FAO Forestry Paper 134.* Food and Agriculture Organization of the United Nations, Rome.

FAO. 1999. State of the World's Forests. FAO, Rome.

FAO. 2000. Tropical deforestation literature: Geographical and Historical Patterns in the Availability of Information and the Analysis of Causes. Forest Resources Assessment Programme. Working paper 27, Rome

FAO. 2001. State of the World's forests 2001. Rome

Fazakas, Z. and Nilsson, M. 1996. Volume and forest cover estimation over southern Sweden using AVHRR data calibrated with TM data. *International Journal of Remote Sensing* **17(2)** 1701- 1709

Foody, G. M., Palubinska, G., Lucas, R. M., Curran, P. J., and Honzak, M. 1996. Identifying terrestrial carbon sinks: classification of successional stages in regenerating tropical forest from Landsat TM data. *Remote Sensing of Environment* **55:** 205-216

Foody, G. M:, Body, D. S. and Curran, P. J. 1996. Relations between tropical forest biophysical properties and data acquired in AVHRR channels 1-5. *International Journal of Remote Sensing* **17(7):** 1341-1355

Foody, G. M., Boyd, D. S. and Cutler, M. E. J. 2003. Predictive relations of tropical forest biomass from Landsat TM data and their transferability between regions. *Remote Sensing of Environment* **85:** 463-474

Franco-Lopez, H., Ek, A. R. and Bauer, M. E. 2001. Estimating and mapping of forest stand density, volume, and cover type using the k-nearest neighbors method. *Remote Sensing of Environment* **77:** 251-274

Franklin, J. 1986. Thematic mapper analysis of coniferous forest structure and composition. *International Journal of Remote Sensing* **7(10):** 1287-1301

Fransson, J. and H. Israelsson, 1999: Estimation of stem volume in boreal forests using ERS-1 C- and JERS-1 L-band SAR data. *International Journal of Remote Sensing of Environment* **20 (1):** 123-137

Fraser, R. S., Bahethi, O. P., and Al-Abbas, A. H. 1977. The effect of the atmosphere on the classification of satellite observation to identify surface features. *Remote Sensing of Environment* **6:** 229-249

Freese, F. 1962. Elementary forest sampling. U.S. Department of Agriculture Handbook 232, Government Printing Office, Washington, D. C. 91 p.

Gallo, K. P. and Eidenshink, J. C. 1988. Differences in visible and near-IR responses and derived vegetation indices for the NOAA-10 AVHRRs: A case study. *Photogrammetric Engineering & Remote Sensing* **54(4):** 485-490

Gates, D. M. 1970. Physical and Physiological properties of plants. Pp 224-252 in Remote Sensing with Special Reference to Agriculture and Forestry, Washington, DC. National Academy of Sciences.

Gates, D. M., Keegan, H. J., Schleter, J. C. and Weidner, V. R. 1965. Spectral properties of plants. *Applied Optics* **4:** 11-20.

Gausman, H. W. 1974. Leaf reflectance of near-infrared. *Photogrammetric Engineering & Remote Sensing* **40:** 183-191.

Gausman, H. W. 1977. Reflectance of leaf components. *Remote Sensing of Environment* **6:** 1-9

Gausman, H. W., Allen, W. A., and Cardenas, R. 1969. Reflectance of cotton leaves and their signature. *Remote Sensing of Environment* **1:**19-22

Gjertsen, A. K. 1996. Two-phase sampling for forest inventory based on satellite imagery. Parlow, E. *(ed.).* Proceedings of the 15th EARSeL Symposium, Basel, Switzerland, 4-6 September 1995. pp 63-71.

Glass, P. A., Londo, H. A., Evans, D. L., Parker, R. C. Belli, K. L., Matney, T. G., Schultz, E. B. and Roller, N. 2001. Enhancing Inventory Efficacy in Southern Forests by Stratification of Landsat Data. Third International Conference on Geospatial Information in Agriculture and Forestry, 5-7 November 2001. Denver, Colorado, USA.

Goel, N. S. 1988. Models of vegetation canopy reflectance and their use in estimation of biophysical parameters from reflectance data. *Remote Sensing Reviews* **4:** 1-221

Gong, P., Y. Sheng and G.S. Biging. 2002. 3D Model-Based Tree Measurement from High Resolution Aerial Imagery. *Photogrammetric Engineering & Remote Sensing* **68(11):** 1203-1212

Gonima, L. 1993. Simple algorithm for the atmospheric correction of reflectance images. *International Journal of Remote Sensing* **14(6):** 1179-1187.

Gonzalez, R. C. and Woods, R. E. 1992. *Digital image processing.* Reading. MA: Addison-Wesley, 1992.

Graetz, R. D. 1990. Remote sensing of terrestrial ecosystem structure: An ecologist's view. *In.* Hobbs and H. A. Mooney (eds.). *Remote Sensing of Biosphere Functioning [R].* Ecological Studies 79. Springer-Verlag, New York.

Grundman, O. 1984. Zur Aufstellung Von Interpretation-schusseln für du Schadeinstufung Von Fichte und Tanne in Infrarot-Farbbildern. Allgemein Forst Zeits 39 (43/44): 1093-1094.

Haan, J.F., Hovenier, J. W., Kokke, J. M. M., and Stokkom, H. T. C. 1991. Removal of atmospheric influences on satellite-borne imagery: a radiative transfer approach. *Remote Sensing of Environment* **37:**1-21.

Haapanen, R. and Ek, A. R. 2001. Software and instructions for *knn* applications in forest resources: Description and estimation. *Staff paper series 152.* Department of Forest Resources, University of Minnesota. 19p.

Hall, F. G., Strebel, D. E., Nickerson, J. E. and Goetz, S. J. 1991. Radiometric rectification: Toward a common radiometric response among multidate, multisensor images. *Remote Sensing of Environment* **35:** 11-27.

Häme, T., Salli, A., Andersson, K. and Lohi, A. 1996. Forest biomass estimation in northern Europe using NOAA AVHRR data. ESA Earth Observation Quarterly No. 52, *ESA Newsletters* (http://esapub.esrin.esa.it/eoq/eoq52/hame52.htm).

Haralick, R. M. 1979. Statistical and structural approaches to texture. Pp 45-60. *In.* Proceeding 4th International Joint Conference on Pattern Recognition.

Haralick, R. M., Shanmugam, K., and Dinstein, I. 1973. Textural features for image classification*. IEEE Transactions on Systems, Man, and Cybernetics.* **SMC-3 (6):** 610-621

Harding, R. A. and Scott, R. B. 1978. Forest Inventory with Landsat (phase II): Washington Forest Productivity Study. *Technical Report.* Department of Natural Resources, Washington. 221p.

Harmon, M. E., Ferrell, W. K. and Franklin, J. F. 1990. *Science* **247** 699

Harmon, M. E., Harmon, J. M., Ferrel, W. K., Brooks, D. 1996. Modeling carbon stores in Oregon and Washington forest products: 1900-1992. *Climate Change* **33:** 521-550

Hayden, R. , Dalke, G. W., Henkel, J. and Bare, J. E. 1982. Application of the IHS color transform to the processing of multisensor data and image enhancement. Pp 599-616. Proceedings, International Symposium on Remote Sensing of Arid and semi-Arid Lands, Cairo, Egypt,

Hershey, R. R. and Befort, W. A. 1993. Airphoto Guide to New England Forest Cover Types: a Stereo Selection Key in CIR. Randor, Pennsylvania: USDA Forest Service: General Technical Report.

Heute, A. R. 1988. A soil-adjusted vegetation index (SAVI). *Remote Sensing of Environment* **25:** 295-309

Heyman, O., 2000, Automatic extraction of natural object form 1-m remote sensing images, http://www.cobblestoneconcepts.com/ucgis2summer/heyman/heyman.htm.

Hildebrandt, G. 1996. Fernerkundung und Luftbildmessung für Forstwirtschaft, Vegetationskartierung und Landschaftsökologie. Wichmann, Heidelberg. 676p.

Hill, J. and Sturm, B. 1991. Radiometric correction of multitemporal Thematic Mapper data for use in agricultural land-cover classification and vegetation monitoring. *International Journal of Remote Sensing* **12(7):** 1471-1491

Holm, R. G., Jackson, R. D., Yuan, B., Moran, M. S. Slater, P. N., and Bigger, S. F. 1989. Surface reflectance factor retrieval from Thematic Mapper data*. Remote Sensing of Environment* **27:**47-57

Horler, D. N. H. and Ahern, F. J. 1986. Forestry information content of Thematic Mapper data. *International Journal of Remote Sensing* **7(3):** 405-428

Horler, D. N. H., Dockray, M. and Barber, J. 1983.The red edge of plant leaf reflectance. *International Journal of Remote Sensing* **4:** 273-288

Houghton, R. A. 1996. Land-use change and terrestrial carbon: the temporal record. Pp 117-134 *In.* M. J. Apps and D. T. Price (eds). Forest ecosystems, forest management and global carbon cycle. NATO ASI Series, vol 140. Springer, Berlin Heidelberg New York,.

Houghton, R. A., and J. L. Hackler. 2001. Carbon Flux to the Atmosphere from Land-Use Changes: 1850 to 1990. ORNL/CDIAC-131, NDP-050/R1. Carbon Dioxide Information Analysis Center, U.S. Department of Energy, Oak Ridge National Laboratory, Oak Ridge, Tennessee, U.S.A.

Houghton, R.A., and J.L. Hackler. 2002. Carbon Flux to the Atmosphere from Land-Use Changes. *In.* Trends: A Compendium of Data on Global Change. Carbon Dioxide Information Analysis Center, Oak Ridge National Laboratory, U.S. Department of Energy, Oak Ridge, Tenn., U.S.A.

Howard, J. A. 1959.The classification of woodland in western Tanganyika by type mapping from aerial photographs. *Empire forestry Review* **38:** 348-364

Huang, C., Yang L., Wylie, B., and Homer, C., 2001, A strategy for estimation canopy density using landsat 7 ETM+ and high resolution over large areas, Procesing of the Third International Conference on Geospatial Information in Agriculture and Forestry, Denver, Niv. 5-7, 2001.

Hudak, A. T., Lefsky, M. A., Cohen, W. B., and Berterreche, M., 2002, Integration of lidar and landsat ETM+ data for estimating and mapping forest canopy height *Remote Sensing of Environment* **82:** 397-416

Huguenin, R. L., Karaska, M. A., Blaricom, D. V. and jensen, J. R. 1997. Subpixel classification of bald cypress and trupelo gum trees in Thematic Mapper imagery: *Photogrammetric Engineering & Remote Sensing* **63(6):** 717-725

Hyyppa, J., Engdahl., M., Koskinen, ., Inkinen, M., Hyyppa, H., and Hallikainen, M., 1996, Feasibility of ERS-1/2 Interferometry for forest inventory. ERS SAR Interferometry Workshop 1996. Remote Sensing Laboratories, University of Zurich. 30 Sep - 2 Oct, 1996. http://www.geo.unizh.ch/rsl/fringe96/papers/hyyppae-et-al/

Hyyppä, J., Hyyppä, H., Inkinen, M., Engdahl, M., Linko, S. and Zhu, Y. 2000. Accuracy comparison of various remote sensing data sources in the retrieval of forest stand attributes. *Forest Ecology and Management* **128**: 109-120

IPCC 1992. Climate change: The supplementary report to the IPCC Scientific Assessment. WMO/UNEP. *In.* Houghton, J. T., Callander, B. A. and Varney, S. K. (Eds.). Cambridge University Press. 200 p.

IPCC 2000. Land Use, Land-Use Change, and Forestry. Special Report of the Intergovernmental Panel on Climate Change. *In.* Robert T. Watson, Ian R. Noble, Bert Bolin, N. H. Ravindranath, David J. Verardo and David J. Dokken (Eds.) Cambridge University Press, p 375.

IPCC/OCED. 1994. Intergovernmental Panel on Climate Change (IPCC)/ Organization for Economic Cooperation and Development (OECD) Joint Programme. Greenhouse Gas Inventory. OECD. Paris, France, 3 volumes.

Irish, R. 2004. Landsat 7 science data users handbook: Greenbelt, Maryland, Goddard Space Flight Center. electronic version, http://ltpwww.gsfc.nasa.gov/IAS/handbook/handbook_toc.html (accessed July 2004)

Jacquez, G. M. and Waller, L. A. 2000. The effect of uncertain locations on disease cluster statistics. Pp 55-64. *In.* H. T. Mowrer and R. G. Congalton *(eds)* Quantifying spatial uncertainty in natural resources: Theory and applications for GIS and remote sensing. Ann Arbor, Michigan.

Jakubauskas, M. E. 1996. Thematic Mapper characterisation of Lodgepole pine seral stages in Yellowstone National Park, USA. *Remote Sensing of Environment* **56:**118-132

Jakubauskas, M. E. and Price, K. P. 1997. Empirical relationships between structural and spectral factors of Yellowstone Lodgepole pine forests. *Photogrammetric Engineering & Remote Sensing* **63(12):** 1375-1381

Jarvis, P. G., James, G. B. and Landsberg, J. J. 1976. Coniferous forests. Pp 171-240. *In.* J. L. Monteith (ed.) Vegetation and the Atmosphere, vol 2. New York: Academic Press.

Jensen, J. R. 1996. Introductory digital image processing: A remote sensing perspective, Prentice Hall, New Jersey, 316 p.

Johnson, E. W. 2000. *Forest sampling desk reference.* CRC Press. 985 p.

Jordan, C. F. 1969. Derivation of leaf area index from quality of light on the forest floor. *Ecology* **50:** 663-666.

Katila, M. and Tomppo, E. 2001. Selecting estimation parameters for the Finnish multi-source National Forest Inventory. *Remote Sensing of Environment* **76:** 16-32

Kauffman, J. B., Cummings, D. L., Ward, D. E., Babbitt, R., 1995. Fire in the Brazilian Amazon. 1. Biomass, nutrient pools, and losses in slashed primary forests. *Oecologia* **104:** 397-408.

Kauth, R. J. and Thomas, G. S. 1976. The Tasseled Cap- A graphic Description of Spectral-Temporal Development of Agricultural Crops as seen by Landsat. *Proceedings:* 2nd International Symposium on Machine Processing of Remotely Sensed Data. Purdue University, West Lafayette.

Kawata, Y., Ohatani, A., Kuasaka, T., and Ueno, S. 1990. Classification accuracy for the MOS-1 MESSER data before and after the atmospheric correction. *IEEE Transaction on Geoscience and Remote Sensing* **28:**755-760

Keller, J. M., Gray, M. R., and Givens, J. E. Jr. 1985. A fuzzy k-nearest neighbor algorithm. *IEEE Transaction on Systems, Man and Cybernetics* **15:** 580-585

Kellogg, W. W. 1989. Economic and political implications of climate change. Presented at the conference on technology-based confidence building: Energy and Environment. University of California, Los Alamos National Laboratory. July 9-14, 1989.

Khan, S. A. 1979. Revised working plan for the forests of Chittagong Division (for the years 1978-79 to 1987-88). Volume 1. Forest Department, Government of Bangladesh, Dhaka.

Knipling, E. B. 1970. Physical and physiological basis for the reflectance of visible and near infrared radiation from vegetation. *Remote Sensing of environment* **1**: 115-159

Köhl, M. 1994. Statistisches Design für das zweite Schweizerische Landesforstinventar: Ein Folgeinventurkonzept unter Verwendung von Luftbildern und terrestrischen Aufnahmen. Mitteilungen der Eidg. Forschungsanstalt für Wald, Schnee und Landschaft, Band 69, 141 S.

Köhl, M. and Kushwaha, S. P. S. 1994. A four-phase sampling method for assessing standing volume using Landsat TM data, aerial photography and field assessment. *Commonwealth Forestry Review* **73(1):** 35-42

Köhl. M., Scott, C. T. and Zingg, A. 1995. Evaluation of permanent sample surveys for growth and yield studies: a Swiss example. *Forest Ecology and Management* **71:** 187-194

Körner, C. 1989. The nutritional status of plants from high altitudes. A worldwide comparison. *Oecologia* **81:** 379-391

Koutsias, N., Karteris, M. and Chuvieco, E. 2000. The use of intensity-hue-saturation transformation of Landsat-5 Thematic Mapper data for burned land mapping. *Photogrammetic Engineering & Remote Sensing* **66(7)**: 829-839.

Krinov, E. L. 1947. Spectral Reflectance Properties of Natural Formations. Technical Translation TT-439. National Research Council of Canada, Ottawa.

Kumar, R. and Silva, L. F. 1973. Light ray crossing through leaf section. *Applied Optics* **12:** 2950-2954

Kurz, W.A., M.J. Apps, T.M. Webb, and P.J. McNamee. 1992. The Carbon Budget of the Canadian Forest Sector: Phase I. Forestry Canada, Northwest Region, Northern Forestry Centre, Edmonton, Alberta. Information Report NOR-X-326.

Kurz, W. A. and Apps, M. J. 1993. *Water, Air and Soil Pollution* **70:** 163.

Lee, K. 1990. Characterization of forest stands using spaceborne radar and optical remote sensing data. *PhD Thesis.* Department of Forest and Wood Sciences. Colorado State University. Fort Collins, Colorado. 206p.

Leyk, S., Köhl, M. and Poncét, F. 2002. Application of Future TerraSAR Data for Improvement of Forest Resource Assessments, ForestSAT Symposium, Heriot Watt University, Edinburgh,5 -9 August, 2002. http://www.forestry.gov.uk/pdf/leyk.pdf/$FILE/leyk.pdf

Liang. S., Fallah-Adl, H., Kalluri, S., Jaja, J., Kaufman, Y. J., and Townshend, J. R. G. 1997. An operational atmopsheric correction algorithm for Landsat Thematic Mapper imagery over the land. *Journal of Geophysical Research* **102(17):**173-186

Liao, J., Gao, H., and Shao, Y., 1999, The potential of multiparameters SAR data in forest application of China, in, http://www.gisdevelopment.net/aars/acrs/1999/ps6/ps61285.shtml

Lillesand, T. M. and Kiefer, R. W. 2000. *Remote sensing and image interpretation.* (4th edition). John Wiley & Sons, New York.

Linton, O., & Härdle, W. 1998. Nonparametric regression. *In.* S. Kotz, C. B. Read & D. L. Banks (eds). Encyclopedia of Statistical Sciences. Update vol. 2 Nerw York: Wiley. pp 470-485

Lu, D., Mausel, P., Brondizio, E. and Moram, E. 2002. Above-ground Biomass Estimation of successional and mature forests using TM images in the Amazon basin. Symposium on Geospatial Teory, Processing and Applicaation, Ottawa 2002.

Lund, H. G. 1997. Forestry. *In* Philipson W. R. (Chief editor). Manual of Photographic Interpretation. 2nd edition. American Society of Photogrammetry and Remote Sensing. 399-440 pp.

Lunetta, R. S. 1999. Applications, project formulation and analytical approach. Pp 1-19. *In.* Lunetta, R. S. and Elvidge, C. D. (eds). Remote sensing change detection: Environmental monitoring methods and application. Taylor & Francis.

MacDicken, K.G. 1997. A Guide to Monitoring Carbon Storage in Forestry and Agroforestry Projects. Winrock International Forest Carbon Monitoring Program. Arlington, Virginia: Winrock International Institute for Agricultural Development.

Maracci, G. and Aifadopoulou, D. 1990. Multi-temporal remote sensing study of spectral signatures of crops in the Thessaloniki test site. *International Journal of Remote Sensing* **11(9):** 1609-1615.

Markham, B. L. and Baker, J. L. 1983. Spectral characteristics of the Landsat-4 MSS sensors. *Photogrammetric Engineering and Remote Sensing* **49(6):** 811-833

Markham, B.L., and J.L. Barker, 1986, Landsat MSS and TM post-calibration dynamic ranges, exoatmospheric reflectances and at-satellite temperatures. EOSAT Technical Notes, August 1986.

Matthews, R., G.J. Nabuurs, V. Alexeyev, R.A. Birdsey, A. Fischlin, J.P. MacLaren, G. Marland, and D. Price, 1996: WG3 Summary: Evaluating the role of forest management and forest products in the carbon cycle. *In.* M.J. Apps, and D.T. Price (eds.). Forest ecosystems, forest management and the global carbon cycle. NATO Advanced Science Institute Series, NATO-ASI Vol I 40, Berlin, Heidelberg, Proceedings of a workshop held in September 1994 in Banff, Canada, pp. 293-301.

Matti, K. and Tomppo, E. 2001. Selecting estimation parameters for the Finnish multiresource National Forest Inventory. *Remote Sensing of Environment* **76:** 16-32.

McGraw, J. B., Warner, T. A., Key, T. L., and Lamar, W. R., 1998, High spatial resolution remote sensing of forest trees, http://cas.bellarmine.edu/tietjen/Ecology/high_spatial_remote_s.htm.

McRoberts, R. E., Nelson, M. D., Wendt, D.G. 2002. Stratified estimation of forest area using satellite imagery, inventory data, and the k-Nearest Neighbors technique. *Remote Sensing of Environment* **82** 457-468

Miller Jr., G. T. 1999. *Environmental science.* (7th edition). Wadsworth Publishing Company. 566 p.

Moeur, M. Crookston, N. L. & Stage, A. R. 1995. Most similar neighbor analysis : a tool to support ecosystem management. *In.* J. E. Thomson (ed.). Analysis in support of ecosystem management. Analysis workshop III. pp 31-44. Washington, DC. USDA Forest Service Ecosystem Management Analysis Center.

Moore, P. D., Chaloner, W. G., and Stott, P. 1996. *Global environmental change.* Blackwell Science, Oxford 244 p.

Moran, M. S., Jackson, R. D., Slater, P. N. and Teillet, P. M. 1992. Evaluation of simplified procedures for retrieval of land surface reflectance factors from satellite sensor output. *Remote Sensing of Environment* **41:** 169-184

Moss, M. E. and Lins, H. F. 1989. Water resources in the twenty-first century: a study of the implications of climate uncertainty. U.S. Geological Survey Circular 1030. Washington, D. C.: U.S. Department of the Interior.

Mouer, M. 1988. Nearest neighbor inference for correlated multivariate attributes. *In.* A. R. Ek., S. R. Shifley and T. E. Burk (eds.) Forest Growth Modelling and Predicttion. Proceedings of the IUFRO Conference. Vol 2. Pp 716-723. St. Paul, MN: Society of American Foresters (SAF publication 87.12).

Mouer, M. and Stage, A. R. 1995. Most similar neighbor- an improved sampling inference procedure for natural resource planning. *Forest Science* **41 (2):** 337-359

Muinonen, E. & Tokola, T. 1990. An application of remote sensing for communal forest inventory. *In.* The usability of remote sensing for forest inventory and planning. Proceedings from SNS/IUFRO workshop 35-42. Umea°, Sweden: Remote Sensing Laboratory, Swedish University of Agricultural Sciences (Report 4).

Murtha, P. A. 1997. Vegetation. In. W. R. Philipson (ed.) *Manual of Photographic Interpretation.* American Society for Photogrammetry and Remote Sensing (2nd edition). 689p.

Murtha, P. A., Johnson, A. H., and Strang, R. M. 1980. Photo interpretation of fire damage to trees in a Ponderosa Pine /Bunchgrass Community. Pp 351- 359. *In.* Proceedings: 6th Canadian Symposium on Remote Sensing, Ottawa. Canadian Remote Sensing Society.

Musa, M. K., Hussin, Y. A. and Weir, M. 2000. Remotely sensed multi-data fusion for sustainable forest management: A case study from northern Selangor, Malaysia. Pp 232-240. *In.* Niedzwiecki, T. Z. and Brach, M. (eds.). Proceedings of the conference on Remote Sensing and Forest Monitoring, June 1-3, Rogow, Poland.

Musick, H. B. 1986. Temporal change of Landsat MSS albedo estimates in arid rangeland. *Remote Sensing of Environment* **20:**107-120

Myers, V. I., Heilman, M. D., Lyon, R. J. P., Namken, L. N., Simonett, D., Thomas, J. R., Wiegand, C. L. and Wooley, J. T. 1970. Soil, water and plant relations. Pp 253-297. *In.* Remote Sensing with Special Reference to Agriculture and Forestry, Washington DC, National Academy of Sciences.

Nelder, J. A. and Mead, R. 1965. A simplex method for function minimization. *Computer Journal* **7:** 391-398.

Nelson, R. F., Kimes, D. S., Salas, W. A. and Routhier, M. 2000. Secondary forest age and tropical forest biomass estimation using Landsat Thematic Mapper Imagery. *Bioscience* **20(5):** 419-431

Nepstad, D. C., Carvalho, C. R., Davidson, E. A., Jipp, P. H., Lefebre, P. A., Negreirs, P., Silva, E. D., Stone, T. A., Trumbore, S. E., Vieira, S. 1994. The role of deep roots in hydrological cycles of Amazonian forest and pastures. *Nature* **372:** 666-669

Nilsson, M. 1997. Estimation of forest variables using satellite image data and airborne lidar. *PhD dissertation.* Swedish University of Agricultural Sciences, Umea°, Sweden.

Nilsson, S. and W. Schopfhauser, 1995: The carbon-sequestration potential of a global afforestation program. *Climatic Change* **30:** 267-293.

Olson, J. S., J. A. Watts, and L. J. Allison. 1983. Carbon in Live Vegetation of Major World Ecosystems (ORNL-5862). Oak Ridge National Laboratory, Oak Ridge, Tennessee.

Olson, J. S., J. A. Watts, and L. J. Allison, 1985. Major World Ecosystem Complexes Ranked by Carbon in Live Vegetation (NDP-017). Carbon Dioxide Information Center, Oak Ridge National Laboratory, Oak Ridge, Tennessee.

Peterson, D. L., Spanner, M. A., Running, S. W., Teuber, K. B. 1987. Relationsips of thematic mapper simulator data to leaf area index of temperature coniferous forests. *Remote Sensing of Environment* **22 :** 323-341.

Philip, M. S. 1998. *Measuring trees and forests* (reprint). CABI Publishing, Oxon. 310 p.

Pidwirny, M. 2004. *Fundamentals of physical geography.* Department of Geography, Okanagan University College, British Columbia. http://www.physicalgeography.net/fundamentals/contents.html. (accessed 15 June, 2004)

Post, W. M., Peng, T., Emanuel, W. R., King, A. W., Dale, V. H. and De Angelis, D. L. 1990. The global carbon cycle. *American Scientist* **78:** 310-326.

Potter, J. F. 1974. Haze and sun angel effects on automatic classification of satellite data-simulation and correction. Proc. Soc. Photo-Opt. Instrum. Eng. 51:73-83

Pouliot, D., A., King, D. J., Bell, F. W., and Pitt, D. G. 2002. Automated tree detection and delineation in high-resolution digital camera imagery of coniferous forest regeneration. *Remote Sensing of Environment.* **82:** 322-334

Prentice, I. C. et al. 2001. Chapter 3 : The Carbon Cycle and Atmospheric CO2 *In.* JT, Yihui, D. (Eds). The Intergovernmental Panel on Climate Change (IPCC) Third Assessment Report. Houghton. Cambridge University Press, Cambridge.

Press, W. H., Teukolsky, S. A., Vetterling, W. T. and Flannery, B. P. 1994. *Numerical recipes in C. The art of scientific computing.* New York: Cambridge University Press. 994 p.

Puhe, J. and Ulrich, B. 2001: *Global climate change and human impacts on forest ecosystems*. Ecological Studies 143, Springer, Berlin

Richards, J. A., and Jia, X. 1999. Interpretation of hyperspectral image data. Pp 313-337. Remote sensing digital image analysis : an introduction. Springer, Berlin ; New York.

Richards, K. R. and Andersson, K. P. 2004. What is in the Sink? Technological Support for National Inventories of Forest Carbon (draft) http://www.spea.indiana.edu/Richards/Research/WhatisintheSink-Draft13.pdf Internet edition (accessed June 2004).

Richardson, A. J., Everitt, J. H., and Gausman, H. W. 1983. Radiometric estimation of biomass and nitrogen contents of Alicia Grass. *Remote Sensing of Environment* **13:** 179-184.

Rodhe, H. 1990. A comparison of the contribution of various gases to the greenhouse effect. *Science* **248** 1218.

Rouse, J. W. Jr., Hass, R. H., Schell, J. A., and Deering, D. W. 1973. Monitoring vegetation systems in the great plains with ERST. Pp 309-317. *In* Proceedings: ERST-1 Symposium, 3rd National Aeronautical and Space Administration NASA SP 351.

Rowan, L. C., Wetlaufer, P. H., Goetz, A. F. H., Billingsley, F. C. and Stewart, J. H. 1974. Discrimination of rock types and detection of hydrothermally altered areas in south-central Nevada by the use of computer-enhanced ERST images, US Geological Survey Professional Paper 883. 35p.

Rowe, R., Sharma, N. and Browder, J. 1992; Deforestation: Problems, Causes and Concerns. *In.* Sharma, N. P. (ed.). Managing the World's Forests: Looking for Balance Between Conservation and Development. Kendall/Hunt Publishing. Iowa. pp.33-45

Roy, P. S. and Ravan, S. A. 1996. Biomass estimation using satellite remote sensing data- An investigation on possible approaches for natural forest. *Journal of Bioscience* **22(4):** 535-561.

Sabol, D. E., Gillespie, A. R., Adams, J. B., Smith, M. O., and Tucker, C. J. 2002. Structural stage in Pacific Northwest forests estimated using simple mixing models of multispectral images. *Remote Sensing of Environment* **80:**1-16

Sader, S. A., Waide, R. B., Lawrence, T. W. and Joyce, A. T. 1989. Tropical forest biomass and successional age Class relationships to a vegetation index derived from Landsat TM data. *Remote Sensing of Environment* **28:** 143-156

Salvador, R. and Pons, X. 1998. On the reliability of Landsat TM for estimating forest variables by regression techniques: A methodological analysis. *IEEE Transaction on Geoscience and Remote Sensing* **36(6):** 1888-1897

Santoro, M., Askne, J., Smith, G., and Frasson, E. S., 2002, Stem volume retrieval in boreal forest from ERS-1/2 interferometry. *Remote Sensing of Environment* **81:** 19-35.

Schlesinger, W. H. 1984. The world carbon pool in soil organic matter: a source of atmospheric CO2. *In.* Woodwell G. M. (ed) The role of terrestrial vegetation in the global carbon cycle: measurement by remote sensing. Scientific Committee on Problems of the Environment Report 23. Wiley, New York, pp 111-124.

Schott, J. R. 1997. *Remote sensing: The image chain approach.* Oxford University Press, 394p.

Schott, J. Salvaggio, C. and Volchok, W. 1988. Radiometric scene normalization using pseudoinvariant features. *Remote Sensing of Environment* **26:**1-16

Sheng, Y., Gong, P., and Biging, G. S., 2001, Model-based conifer-crown surface reconstruction from high-resolution aerial images. *Photogrammetric Engineering & Remote Sensing* **68(8)** 957-965.

Shiver, B. D., Borders, B. E. 1996. *Sampling techniques for forest resource inventory.* Wiley.

Short, N. 1982. Principles of computer processing of Landsat data. Appendix A. Pp. 421-453. *In.* The Landsat Tutorial Workbook. Publication 1078. Washington: National Aeronautics and Space Administration.

Siegal, B.S., Gillespie, A. R. and Skley, J. E. 1980. *Remote Sensing in Geology.* Wiley, New York. 120p.

Sing, A. 1989. Digital change detection techniques using remotely-sensed data. *International Journal of Remote Sensing* **10:** 989-1003

Singh, A. and Harrison, A. 1985. Standardized principal components. *International Journal of Remote Sensing* **6:** 883-896

Slater, P. N., Doyle, F. J., Fritz, N. L. and welch, R. 1983. Photographic systems for remote sensing. Pp 231-291. *In.* Estes, J.E., E.J. Hajic, and L.R. Tinney (eds.), Manual of Remote Sensing (2nd edition). Vol 1. American Society of Photgrammetry. Falls Church, VA.

Smith, J. A., Liu, T. L. and Ranson, K. J. 1980. The Lambertian assumption and Landsat data. *Photogrammetric Engineering Remote Sensing* **46:** 1183-1189.

Song, C., Woodcock, C. E., Seto, K. C., Lenney, M. P. and Macomber, S. A. 2001. Classification and change detection using Landsat TM data: When and how to correct atmospheric effects?. *Remote Sensing of Environment* **75:**230-244

Spanner, M. A., Pierce, L. L., Peterson, D. L. and Running, S. W. 1990. Remote sensing of temperate coniferous forest leaf area index: the influence of canopy closure, understorey vegetation and background reflectance. *International Journal of remote Sensing* **11(1):** 95-111

Steininger, M. K. 2000. Satellite estimation of tropical secondary forest above-ground biomass: data from Brazil and Bolivia. *International Journal of Remote Sensing* **21 (6&7):** 1139-1157

Suits, G., Malila, W. and Weller, T. 1988. The prospects of detecting spectral shifts due to satellite sensor aging. *Remote Sensing of Environment* **26:** 17-29

Thenkabail, P. S., Enclona, E. A., Ashton, M. S., Legg, C. and Dieu, M. J. D. 2004. Hyperion, Ikonos, Ali and ETM+ sensors in the study of African rainforests. *Remote Sensing of Environment* **90:** 23-43.

Thomson, A. G. 1992. A multi-temporal comparison of two similar Landsat Thematic Mapper images of upland North Wales, UK. *International Journal of Remote Sensing* **13(5):** 947-955.

Titus, J. G., Leatherman, S. P., Everts, C. H., Moffatt, and Nichol Engineers, Kriebel, D. L. and Dean, R. G. 1985. Potential impacts of sea level rise on the beach at Ocean City, Maryland. Washington, D. C. US Environmental Protection Agency, Office of Policy planning and Evaluation.

Tokola, T., Pikänen, J., Partinen, S. and Muinonen, E. 1996. Point accuracy of a non-parametric method in estimation of forest characteristics with different satellite materials. *International Journal of Remote Sensing* **17(12):** 2333-2351.

Tomar, M. S. 1968. Manual of Photo-interpretation in Tropical Forests – Southern Zone (Kerala and Madras). Government of India. Pre-Investment Survey of Forest Resources UNSF/GOU/FAO Project IND/100/9, Unpublished report, 35p.

Tomar, M. S. 1970. Manual of Photo-Interpretation for Tropical Deciduous Forests of Bastar Region. Government of India. Pre-Investment Survey of Forest Resources unpublished report, 102p.

Tomppo, E. 1991. Satellite image-based national forest inventory of Finland. *International Archives of Photogrammetry and Remote Sensing* **28(7.1):** 419-424

Tomppo, E. 1993. Multi-source national forest inventory of Finland. Pp 53-61. *In.* A. Nyyssönen, S. Poso, J. Rautala (eds.). Proceedings of II-vessalo Symposium on National Forest Inventories *Research Papers 444.* The Finnish Forest Research Institute.

Tomppo, E., 1996: Multi-source national forest inventory of Finland. In: *New Thrusts in Forest Inventory.* [Paivinen, R., J. Vanclay, and S. Miina (eds.)]. European Forest Institute, Joensuu, Finland, pp. 27–41.

Tomppo, E. 1997a. Application of remote sensing in Finnish national forest inventory. Pp 375-388. *In.* Application of remote sensing in European forest monitoring. International Workshop Proceedings. Vienna, Austria.

Tomppo, E. 1997b. Recent status and further development of the Finnish multi-source forest inventory. *In.* Managing the resources of the World's forests. Lectures given at the Marcus Wallenberg Prize Symposium. Pp 53-69. The Marcus Wallenberg Foundation Symposia Proceedings, p 11. Falun, Sweden: The Marcus Wallenberg Foundation.

Tomppo, E., Nilsson, M., Rosengren, M., Aalto, P. and Kennedy, P. 2002. Simultaneous use of Landsat TM and IRS-1C WIFS data in estimating large area tree stem volume and aboveground biomass. *Remote Sensing of Environment* **82:** 156-171.

Trotter, C. M., Dymond, J. R. and Goulding, C. J. 1997. Estimation of timber volume in a coniferous plantation forest using Landsat TM. *International Journal of Remote Sensing* **18(10):** 2209-2223

Tucker, C. J. 1978. A comparison of satellite sensor bands for vegetation monitoring. *Photogrammetric Engineering and Remote Sensing* **44(11):** 1369-1380

Tucker, C. J. 1979. Red and Photographic infrared linear combinations for monitoring vegetation. *Remote Sensing of Environment* **10:** 23-32

Turner, D. P., Koerper, G. J., Harmon, M. E. and Lee, J. J. 1995. A carbon budget for forests of the conterminous united state. *Ecological Applications* **5:** 421-436.

Vermote, E. F., tanre`, D., Deuze, J. L., Herman, M. and Morcrette, J. J. 1997. Second simulation of the satellite signal in the solar spectrum 6S, *6s User's Guide Version 2,* NASA Goddard Space Flight Center, Code 923, Greenbelt, MD.

Vincent, R. K. 1973. Spectral ratio imaging methods for geological remote sensing from aircraft and satellites. Pp 377-397. *In.* Proceedings of the American Society of Photogrammetry, Management and Utilization of Remote Sensing Data Conference, Sioux Falls, SD.

Vitousek, P.M. 1991. Can planted forests counteract increasing atmospheric carbon dioxide? *Journal of Environmental Quality* **20:** 348-354.

Walsh, S. J. 1987. Variability of Landsat spectral responses of forests in relation to stand and site characteristics. *International Journal of Remote Sensing* **8(9):** 1289-1299

Whittaker, R. H. and G. E. Likens. 1973. Carbon in the biota. *In.* Woodwell, G. M. and E. V. Pecan (eds). Carbon and the biosphere. US Atomic Energy Commission Symposium Series 30. National Technical Information Service, Springfield, pp 281-302.

Woodcock, C. E., Macomber, S. A., Pax-Lenney, M. and Cohen, W. B. 2001. Monitoring large areas for forest change using Landsat: Generalization across space, time and Landsat sensors. *Remote Sensing of Environment* **78:** 194-202

Wooley, J. T. 1971. Reflectance and transmittance of light by leaves. *Plant Physiology* **47:** 656-662.

Zahir-Ud-Din, A. S. M. 1954. Aerial Survey of Chittagong Hill Tracts Forests. *Pakistan Journal of Forestry* **4:** 237-240.

Zeide, B. 1980. Plot size optimization. *Forest Science* **26:** 251-257.

Appendices

List of Appendices

APPENDIX I

A - I.   Calculation of atmospheric correction

A. Calculation for historical image (Landsat TM 1992)

Table 1: Conversion of minimum DN value to at-satellite minimum spectral radiance

Band	QCAL	LMAX1	LMIN1	QCALMAX	L1.min
1	55	15.21	-0.15	255	3.162941
2	22	29.68	-0.28	255	2.304784
3	22	20.43	-0.12	255	1.652941
4	12	20.62	-0.15	255	0.827412
5	5	2.719	-0.037	255	0.017039
7	3	1.438	-0.015	255	0.002094

Table 2: Computation of the radiance of a dark object (assumed reflectance as 1%)

Band	ESUN1	q (solar zenith angle)	d (Earth-Sun distance)	pi	L1.1%
1	195.70	53.48	0.986188	3.141593	0.637103
2	182.90	53.48	0.986188	3.141593	0.595432
3	155.70	53.48	0.986188	3.141593	0.506883
4	104.70	53.48	0.986188	3.141593	0.340852
5	21.93	53.48	0.986188	3.141593	0.071393
7	7.45	53.48	0.986188	3.141593	0.02426

Table 3: Computation of haze correction

Band	L1.haze
1	2.525838
2	1.709352
3	1.146059
4	0.486560
5	-0.054350
7	-0.022170

B. Calculation for recent image (Landsat ETM+ 2001)

Table 1: Conversion of minimum DN value to at-satellite minimum spectral radiance

Band	QCAL	LMAX1	LMIN1	QCALMAX	L1.min
1	58	191.6	-6.2	255	38.789804
2	40	196.5	-6.4	255	25.427451
3	31	152.9	-5.0	255	14.195686
4	22	157.4	-5.1	255	8.919608
5	11	31.06	-1.0	255	0.382980
7	10	10.8	-0.35	255	0.087255
8	22	243.1	-4.7	255	16.678824

Table 2: Computation of the radiance of a dark object (assumed reflectance as 1%)

Band	ESUN1	q (solar zenith angle)	D (Earth-Sun distance)	pi	L1.1%
1	1969.00	47.007903	0.986305	3.141593	6.356494
2	1840.00	47.007903	0.986305	3.141593	5.940045
3	1551.00	47.007903	0.986305	3.141593	5.007070
4	1044.00	47.007903	0.986305	3.141593	3.370330
5	225.70	47.007903	0.986305	3.141593	0.728624
7	82.07	47.007903	0.986305	3.141593	0.264945
8	1368.00	47.007903	0.986305	3.141593	4.416294

Table 3: Computation of haze correction

Band	L1.haze
1	32.4333103
2	19.4874062
3	9.18861588
4	5.54927806
5	-0.3456436
7	-0.1776905
8	12.2625293

APPENDIX II

A - II.   Projection parameters used for geometric correction

Map Information

Site : Landsat ETM+/TM 136-045

Geographical Extent

                    Latitude   Longitude

Upper Left   92 04 35 E   21 38 17 N

Upper Right   92 13 45 E   21 38 09 N

Lower Left   92 04 24 E   21 27 42 N

Lower Right   92 13 36 E   21 27 33 N

Map Series Used

Source: Topographic maps,

                          Survey General of Bangladesh

Scale   1:50,000

Date   Variable

Projection Type   Lambert Conformal Conic

Spheroid   Everest

Datum   Indian (Bangladesh)

False easting: 2743185.699 meters

False northing: 914395.233 meters

Longitude of central meridian: 90:00:00 E

Latitude of 1st standard parallel: 23:09:00 N

Latitude of 2nd standard parallel: 28:48: 00 N

Latitude of origin of projection: 26:00:00 N

APPENDIX III

A - III.   Accuracy of GPS and geodetic points

Geodetic point no	Location	Geographic position	
		Actual	**Measured**
FM-0209	Cox's Bazar	21°26'25.8"	21°26'25.9"
		91°58'10.4"	91°58'10.5"
FM-0283	Badarkhali	21°43'05.2"	21°43'05.6"
		91°57'22.4"	91°57'22.7"
FM-0426	Satkania	22°04'50.6"	22°04'50.8"
		92°01'44.4"	92°01'44.5"
FM-0428	Keranirhat	22°05'39.9"	22°05'40.4"
		92°04'55.9"	92°04'56.2"
FM-0590	Ramu	21°24'57.9"	21°24'58.2"
		92°06'39.90"	90°06'40.1 "

Figure A-II. Geodetic pillar and acquiring geographic position by a handheld GPS

Appendix IV

A - IV.   Conversion units for estimating carbon

Table 1. Conversion units for estimating carbon content (IPCC 200)

1 tonne (t)	1000 kilogram (kg)	106 gram (g)	1 Megagram (Mg)
1 Megatonne (Mt)	1,000,000 t	1012 g	1Teragram (Tg)
1 Gigatonne (Gt)	1,000,000,000 t	1015 g	1 Petagram (Pg)
1 hectare (ha)	10,000 square metre (m^2)		
1 square kilometee (km^2)	100 hectare (ha)		
1 tonne per hectare (t ha^{-1})	100 gram per square metre (g m^{-2})		
1 tonne carbon	3.67 tonne carbon dioxide (t CO^2)		
1 tonne carbon dioxide	0.273 tonne carbon (t C)		
1 tonne	0.984 imperial ton	1.10 US ton	2,204 pound
1 hectare (ha)	2.471 acre		
1 square kilometre (km^2)	0.386 square mile		
1 tonne per hectare (t ha^{-1})	892 pound per acre		

APPENDIX V

A - V.   Allometric relations to estimate volume of standing trees from measured dbh and height

Table 1. Allometric relationship for different species in the plantations of Bangladesh

Species	Allometric relations (total volume overbark)	References
Dipterocarpus turbinatus	$V = 0.000390878 + 0.00064549776D^2 + 0.0001478277DH + 0.00002407D^2H$	(Choudhury and Davidson 1984)
Syzigium grande	$V = 0.00019297\ D^2 + 0.000029437 + 0.0002489\ DH + 0.0000243726\ D^2H$	(Choudhury and Davidson 1984)
Tecktona grandis	$Ln(V) = 1.62116\ \ln(D) + 1.6483\ \ln(H) - 9.48076$	Latif *et al.* 1986
Acacia auriculiformis	$Ln(V) = -9,125 + 1,918*Ln(D) + 0,67988*Ln(H)$	Latif *et al.* 1995
Acacia mangium	$Ln(V) = -9,1426 + 1,7612*Ln(D) + 0,83335*Ln(H)$	Latif *et al.* 1993

D is dhb in cm

H is total height in m and

V is total volume overbark in m^3

Table 2. Allometric relationship for different species in natural forests of Bangladesh (Latif *et al.* 1986)

Species	Allometric relation	
	total volume overbark	**Branchwood volume factor**
Aphanamixis polystachya	Ln (V) = 1.9328 ln (D) + 0.6992 ln (H) – 8.9863	F = 0.07395 (1.0 – e –0.18846 D) 4054.6
Artocarpus chaplasha	Ln (V) = 2.13197 ln (D) + 0.294608 ln (H) – 8.66393	F^1 = 1 / (9.179182 + 1546.113e-0.0965741 D)
Bombax ceiba	Ln (V) = 1.9419 ln (D) + 0.5276 ln (H) – 9.1013	
Dipterocarpus gracilis	Ln (V) = 1.8660 ln (D) + 0.9648 ln (H) – 9.4406	
Dipterocarpus costatus	Ln (V) = 1.76514 ln (D) + 1.00107 ln (H) – 9.1692675	F = 0.0005324126 D – 0.0000034916D2 – 0.01252606
Dipterocarpus turbinatus	Ln (V) = 1.64852 ln (D) + 1.13061 ln (H) – 9.187185	F = 0.000190656 D + 0.000004132 D^2 – 0.005090909
Duabanga grandiflora	V = 0.0004129 D^2 + 0.001298 H + 0.0000247 D^2H – 0.5127	F = 1/(5.2419 + 416737.9e-0.2012D)
Mangifera sylvatica	Ln (V) = 2.0808 ln (D) + 0.6926 ln (H) – 8.9048	F^2 = 0.2134 – 0.008965 D + 0.00009556 D^2
Schima wallichi	V = 0.05978 – 0.00003151 D^2 + 0.01648 H + 0.00002781D^2H	F = 0.09787 – 3.0658 e – 0.1131D
Swintonia	Ln (V) = 1.81484 ln (D) + 0.827986 ln (H)	F = 0.2927091 (1- e -0.0287884 D)

[1] Conversion factor (F) of Branchwood volume is computed by multiplying total volume overbark by the factor and then to be added to the total volume to get total volume including branches
[2] Since this is a quadric, extrapolation much beyond the range of the data would be unwise

floribunda	– 8.862135955	12.07019
Syzygium grande	$V = 0.08566 + 0.0002378\ D^2 + 0.011944\ H + 0.000023649\ D^2H$	$F^3 = 0.004358\ D - 0.000032\ D^2 - 0.09923815$
Terminalia bellerica	$Ln\ (V) = 1.7826\ ln\ (D) + 0.6257\ ln\ (H) - 8.3245$	$F = 0.00002085\ D^{-2.4536}$
Tetrameles nudiflora	$Ln\ (V) = 1.85222\ ln\ (D) + 0.687905\ ln\ (H) - 8.492536$	$F = 0.0000124585\ D3.444204^4$
Mixed species group	$Ln\ (V) = 1.59316\ ln\ (D) + 0.940025\ ln\ (H) - 8.3367$	$F = D\ /\ (17.6668D - 0.1012375\ D^2 - 241.9453)$

D is dhb in cm

H is total height in m and

V is total volume overbark in m^3

---

[3] If F is negative set F = 0
[4] up to a diameter of 100 cm then use constant F = 0.166

APPENDIX VI

A - VI.   Some common species of the study area and their densities

(http://www.worldagroforestrycentre.org/sea/products/afdbases/wd/index.htm and FAO 1997)

Species Name	Density			Moisture content (%)	Notes	Reference
	Low	Medium	High			
Acacia auriculiformis	-	404	-	-	Thailand	Prosea Database, PROSEA
Acacia mangium	530	610	660	15	-	Oey Djoen Seng (1951) in Soewarsono, PH (1990)
Actinodaphne sp	430	-	815	15	-	Prosea 5(3) p:45
Adina cordifolia	-	580	-	-	-	FAO 1997
Alstonia scholaris	270	300	490	15	-	Martawijaya *et al.* 1992
Anisoptera scaphula	510	-	815	15	-	Prosea 5(1) p:102
Antidesma ghaesembilla	580	660	740	15	-	Oey Djoen Seng (1951) in Soewarsono, PH (1990)
Aphanamixis polystachya	600	690	750	15	-	Oey Djoen Seng (1951) in Soewarsono, PH (1990)
Artocarpus chaplasha	-	241	-	-	-	Prosea 2 p:81
Artocarpus sp.	420	640-875	945	15	-	Prosea 5(2) p:60
Beilschmiedia sp	430	470-680	815	15	-	Prosea 5(2) p:78
Bombax ceiba	120	300	470	15	-	Anon 1981

Bursera serrata	-	590	-	-	-	FAO 1997
Callicarpa sp.	340	410	480	15	-	Oey Djoen Seng (1951) in Soewarsono, PH (1990)
Calophyllum sp	-	680	-	15	average	Prosea 5(1) p:115
Carallia sp.	640	-	1050	15	-	Prosea 5(3) p:135
Cassia fistula	760	920	1050	15	-	Oey Djoen Seng (1951) in Soewarsono, PH (1990)
Ceriops decandra	-	960	-	15	-	Oey Djoen Seng (1951) in Soewarsono, PH (1990)
Cinnamomum sp.	350	370	860	15	-	Prosea 5(2) p:131
Cordia dichotoma	390	480	620	15	-	Oey Djoen Seng (1951) in Soewarsono, PH (1990)
Dillenia pentagyna	560	690	820	15	-	Prosea 5(2) p:182; Oey Djoen Seng (1951) in Soewarsono, PH (1990)
Diospyros sp.	-	1030	-	15	-	Oey Djoen Seng (1951) in Soewarsono, PH (1990)
Diospyros toposia	-	870	-	15	sapwood	Oey Djoen Seng (1951) in Soewarsono, PH (1990)
Dipterocarppus gracilis	580	730	1000	15	-	Martawijaya *et al.* 1992
Dipterocarpus turbinatus	750	-	850	-	Vietnam	Nguyen Ngoc Chinh *et al.* 1996.
Eugenia sp.	450	520-925	1100	15	-	Prosea 5(2) p:442
Ficus benghalensisi	-	480	-	15	sapwood	Oey Djoen Seng (1951) in Soewarsono, PH

					(1990)
Ficus sp.	190	-	740	15	-	Prosea 5(3) p:233
Firmiana sp.	355	-	400	15	-	Prosea 5(3) p:239
Garcinia sp.	-	910	-	-	-	Memed, R., Paribotro, S. and Kliwon S. 1981
Glochidion sp.	440	-	890	15	-	Prosea 5(3) p:258
Gmelina arborea	400	-	560	-	-	Agroforestry tree Database, ICRAF
Hevea brasiliensis	550	610	700	15	-	Oey Djoen Seng (1951) in Soewarsono, PH (1990)
Hopea odorata	620	-	930	15	-	Prosea 5(1) p:251
Kandelia candel	540	580	640	15	-	Oey Djoen Seng (1951) in Soewarsono, PH (1990)
Lagerstroemia speciosa	580	690	810	15	-	Martawijaya *et al.* 1992
Lannea coromandelica	-	430	-	15	-	Oey Djoen Seng (1951) in Soewarsono, PH (1990)
Macaranga denticulata	-	410	-	15	-	Oey Djoen Seng (1951) in Soewarsono, PH (1990)
Mangifera indica	630	670	730	15	-	Oey Djoen Seng (1951) in Soewarsono, PH (1990)
Mangifera sp.	410	450	800	15	-	Prosea 5(2) p:324
Meliosma pinnata	340	400	430	15	sapwood	Oey Djoen Seng (1951) in Soewarsono, PH (1990)
Michelia champaca	510	560	620	15	-	Oey Djoen Seng (1951) in Soewarsono, PH

						(1990)
Microcos sp.	290	-	840	15	-	Prosea 5(3) p:379
Mitragyna parvifolia	-	641	-	12	average density	Forestry Compendium, CAB International
Myristica sp.	-	540	-	-	-	The Wood Exchange (http://www.thewoodexchange.info)
Phyllanthus emblica	730	840	940	15	-	Oey Djoen Seng (1951) in Soewarsono, PH (1990)
Pterocarpus dalbergioides	-	775	-	12	Andaman Islands	Prosea 5(1) p:379
Pterocarpus spp.	-	440	-	-	basic density in Brazil	Fearnside, P.M. 1997
Pterospermum sp.	300	-	780	15	-	Prosea 5(3) p:480
Quercus sp	520	815	1100	15	-	Prosea 5(2) p:410
Quercus velutina	-	650	-	-	-	Woods of the World (http://www.forestworld.com)
Randia sp.	-	910	-	15	-	Oey Djoen Seng (1951) in Soewarsono, PH (1990)
Salix tetrasperma	420	420	430	15	-	Oey Djoen Seng (1951) in Soewarsono, PH (1990)
Sapium baccatum	310	350	420	15	-	Anon 1981
Schima wallichii	700	-	800	-	Vietnam	Nguyen Ngoc Chinh *et al.* 1996
Spondias sp.	245	320	480	15	-	Prosea 5(3) p:532
Sterculia sp	120	250-600	760	15	-	Prosea 5(2) p:424

Swintonia floribunda	610	770	880	15	-	Oey Djoen Seng (1951) in Soewarsono, PH (1990)
Syzygium claviflorum	720	-	880	15	-	Prosea 5(2) p:451
Syzygium cumini	730	800	870	15	-	Oey Djoen Seng (1951) in Soewarsono, PH (1990)
Syzygium species	-	690	-	-	-	FAO 1997
Tectona grandis	590	700	820	15	-	Oey Djoen Seng (1951) in Soewarsono, PH (1990)
Terminalia chebula	-	880	-	12	-	Prosea 5(2) p:483
Tetrameles nudiflora	250	320	420	15	-	Prosea 5(3) p:554; Oey Djoen Seng (1951) in Soewarsono, PH (1990)
Toona ciliata	-	530	-	14	Malaysia, Thailand	PROSEA Timber Tree,CD ROM series
Vitex glabrata	720	740	780	15	-	Prosea 5(2) p:508; Oey Djoen Seng (1951) in Soewarsono, PH (1990)
Vitex sp	340	520-940	1010	15	-	Prosea 5(2) p:502
Xanthophyllum flavescens	-	805	-	12	The Philippines	PROSEA Timber Tree,CD ROM series
Ziziphus sp.	1020	1080	1140	15	-	Oey Djoen Seng (1951) in Soewarsono, PH (1990)

Note: If the Moisture content is undefined, it should be assumed as 15%

APPENDIX VII

A - VII.   List of species found in the study area

Scientific Name	Local name	Family
Acacia auriculiformis Griseb.	Akashmoni	Leguminosae
Acacia mangium Willd.	Mangium	Leguminosae
Actinodaphne sp / Dehaasia kurzi (Thunb).	Madanmasta	Rubiaceae
Adina cordifolia Hook.	Mala	Rubiaceae
Adina cordifolia Hook.	Sandang	Rubiaceae
Aegialitis rotundifolia Roxb.	Nunia	Plumbagiceae
Alstonia scholaris (L.) R. Br.	Chatian	Apocynaceae
Amaranthus tricolor L.	Denga	Amarantheaceae
Anisoptera scaphula Roxb.	Boilum	Dipterocarpaceae
Antidesma ghaesembilla Gaertn.	Elena	Euphorbiaceae
Aphanamixis polystachya (Wall.) R. N. Park.	Royna	Meliaceae
Aphanamixis polystachya Wall. R. N. Park.	Pitraj	Meliaceae
Areca catechu L.	Gua	Palmae
Artocarpus chaplasha Roxb.	Chapalish / Chhram	Moraceae
Artocarpus lakoocha Roxb.	Barta	Moraceae
Beilschmiedia pseudomicrocarpa	Chongri	Lauraceae

Bursera serrata Wall.	Gutguttya	Burseraceae
Callicarpa arborea Roxb.	Bormala	Verbenaceae
Calophyllum polyanthum Wall.	Kamdev, Pouia	Guttiferae
Carallia lucida Roxb.	Kiabong	Rhizophoraceae
Cassia fistula L.	Bandarlathi	Leguminosae
Cassia fistula L.	Sonalu	Leguminosae
Ceriops decandra Griff. Ding Hou	Guttya	Rhizophoraceae
Cinnamomum iners Reinw.	Tejbohu	Lauraceae
Cordia dichotoma Fors f.	Bohari	Boraginaceae
Curcuma longa L.	Haldi	Zingiberaceae
Derris trifoliata Lour.	Kalilata	Leguminosae
Dillenia pentagyna Roxb.	Hargeza / Akushi	Dilleniaceae
Diospyros peregrina L.	Gab	Ebena
Diospyros toposia Ham.	Gabgula	Ebenaceae
Diospyros toposia Ham.	Katgula	Ebenaceae
Dipterocarpus gracilis Bl.	Sil garjan	Dipterocarpaceae
Dipterocarpus turbinatus Gaertn.	Garjan	Dipterocarpaceae
Elaeocarpus robustus Roxb.	Jalpai	Elaeocarpaceae
Engelhardita spicata Lesch. Ex. Bl.	Dad	Juglandaceae

Ficus benghalensis L.	Bat	Moraceae
Ficus hispida L f.	Dumur	Moraceae
Firmiana colorata R. Br.	Ujal	Sterculaceae
Garcinia cowa Roxb.	Kao	Guttiferae
Gardenia coronaria Ham.	Kanyari	Rubiaceae
Glochidion lanceolarium Dalz.	Kechua	Euphorbiaceae
Glochidion multiloculare Muell.-Arg.	Paniaturi	Euphorbiaceae
Glycosmis pentaphylla (Retz.) A. DC.	Rang gash	Rutaceae
Hevea brasiliensis	Rubber	Euphorbiaceae
Holigarna longifolia Roxb.	Barola	Anacardiaceae
Hopea odorata Roxb.	Telsur	Dipterocarpaceae
Kandelia candel L. Druce	Gora	Rhizophoraceae
Lagerstroemia speciosa (L.) Pers.	Jarul	Lythraceae
Lannea coromandelica (Houtt.) Merill.	Bhadi	Anacardiaceae
Macaranga denticulata Muell.-Arg.	Bura	Euphorbiaceae
Maesa indica Wall.	Ramjani	Myrsinaceae
Mangifera indica	Am (Mango)	Anacardiaceae
Mangifera sylvatica Roxb.	Uriam	Anacardiaceae

Marinda angustifolia Roxb.	Pandogi	Rubiaceae
Meliosma pinnata Maxim.	Adaliya	Sabiaceae
Michelia champaca L.	Champafool,	Magnoliaceae
Microcos paniculata L.	Assar	Tiliaceae
Mitragyna parvifolia (Roxb.) Korth.	Dakrum	Rubiaceae
Myristica linifolia	Am-barola	Anacardiaceae
Paspalum scrobiculatum Boj.	Goaicha	Graminae
Phyllanthus emblica L.	Amloki	Euphorbiaceae
Pithecellobium clypearia Benth.	Kuramara	Leguminosae
Pterocarpus chelonioides (L. f.) DC.	Dharmara	Bignoniaceae
Pterocarpus dalbergioides	Padauk	Leguminosae
Pterospermum acerifolium Willd.	Moos	Sterculaceae
Quercus acuminata Roxb.	Kalibatna	Fagaceae
Quercus spicata Sm.	Batana	Fagaceae
Quercus velutina Lindl.	Sil batana	Fagaceae
Randia dumetorum Lamk.	Mankata	Rubiaceae
Salix tetrasporma	Panijoma	Salicaceae
Sapium baccatum Roxb.	Kala boil / Champata	Euphorbiaceae
Schima wallichii	Chilauni	Theaceae

Spondias pinnata (L. f.) Kurz	Amrah	Anacardiaceae
Swintonia floribunda Griff.	Civit/Amchandul	Anacardiaceae
Syzygium claviflorum (Roxb,) Wall.	Nali jam	Myrtaceae
Syzygium cumini	Putijam	Myrtaceae
Syzygium grande (Wt.) Wall.	Dhakijam	Myrtaceae
Syzygium grandis (Wt.) Wall.	Jam	Myrtaceae
Syzygium syzygiodes Merr.	Khorijam	Myrtaceae
Syzygium wallichi Wall.	Dholijam	Myrtaceae
Tectona grandis L. f.	Teak	Verbenaceae
Tephrosia purpurea (L.) Pres.	Lohamohori	Leguminosae
Terminalia chebula Retz	Haritaki	Combretaceae
Tetrameles nudiflora R. Br.	Chundul	Datiscaceae
Toona ciliata J. Roem.	Toon	Meliaceae
Trewia polycarpa Benth.	Latim	Euphorbiaceae
Vitex glabrata Heyne	Goda / Harina	Vitaceae
Xanthophyllum flavescens Roxb.	Hansak	Polygalaceae

N.B. Some of the local names were not found in the literature and therefore included in the mixed species group

APPENDIX VIII

A - VIII.   Raw data collected by field survey

SI no.	Str. no	Plot no	Vegetation type	Latitude (N)	Longitude (E)	Owner	Range	Beat	Carbon (Ton/ha)
1	1	1	*Acacia auriculiformis*	21°30'09,9"	92°05'53,2"	BFD	Meherghona	Dhalirchara	22,87
2	1	2	*Acacia auriculiformis*	21°30'09,0"	92°06'09,4"	BFD	Meherghona	Dhalirchara	24,93
3	1	3	*Acacia auriculiformis*	21°30'09,5"	92°06'20,4"	BFD	Meherghona	Dhalirchara	38,32
4	1	4	*Acacia auriculiformis*	21°30'10,8"	92°06'34,2"	BFD	Meherghona	Dhalirchara	28,14
5	1	1	*Acacia mangium*	21°35'19,3"	92°09'12,3"	BFD	Idgarh	Idgarh	40,03
6	1	2	*Acacia mangium*	21°29'46,7"	92°06'06"	BFD	Joarianala	Head quarter	29,40
7	2	1	Bamboo	21°34'40,3"	92°12'03,9"	USF	Ali Khjang*		89,54
8	2	2	Bamboo	21°34'28,0"	92°12'04,3"	USF	Ali Khjang		54,40
9	2	3	Bamboo	21°34'22,3"	92°11'58,4"	USF	Ali Khjang		55,42
10	2	4	Bamboo	21°34'18,2"	92°11'52,3"	USF	Ali Khjang		45,06
11	2	5	Bamboo	21°35'15,3"	92°12'37,4"	USF	Ali Khjang		75,44
12	2	6	Bamboo	21°35'03,8"	92°12'32,6"	USF	Ali Khjang		64,59
13	2	7	Bamboo	21°34'43,4"	92°12'23,6"	USF	Ali Khjang		54,44
14	3	1	Dhakijam	21°35'33,7"	92°09'52,8"	BFD	Idgarh	Idgarh	61,65
15	3	2	Dhakijam	21°28'01,0"	92°13'19,2"	BFD	Baghkhali	Gilatali	127,59
16	3	3	Dhakijam	21°28'46,2"	92°13'02,2"	BFD	Baghkhali	Gilatali	46,80

17	3	4	Dhakijam	21°28'43,5"	92°13'15,2"	BFD	Baghkhali	Gilatali	117,35
18	3	5	Dhakijam	21°33'52,1"	92°06'04,9"	BFD	Bhomoriaghona	Head quarter	26,20
19	3	1	Garjan	21°35'03,7"	92°09'35,3"	BFD	Idgarh	Idgarh	195,15
20	3	2	Garjan	21°36'15,5"	92°05'24,2"	BFD	Fulchari	Fulchari	41,98
21	3	3	Garjan	21°36'17,9"	92°05'35,6"	BFD	Fulchari	Fulchari	79,57
22	3	4	Garjan	21°37'26,6"	92°05'54,2"	BFD	Fulchari	Khutakhali	79,26
23	3	5	Garjan	21°37'25,0"	92°06'02,1"	BFD	Fulchari	Khutakhali	130,01
24	3	6	Garjan	21°37'30,5"	92°05'59,0"	BFD	Fulchari	Khutakhali	140,97
25	3	7	Garjan	21°37'44,9"	92°06'08,6"	BFD	Fulchari	Khutakhali	98,70
26	3	8	Garjan	21°29'48,6"	92°06'14"	BFD	Joarianala	Head quarter	21,77
27	3	1	Telsur	21°29'48"	92°06'28,1"	BFD	Joarianala	Head quarter	5,24
28	4	1	Primary forest	21°33'28,1"	92°05'48,8"	BFD	Bhomoriaghona	Head quarter	211,72
29	4	2	Primary forest	21°33'29,1"	92°05'42,9"	BFD	Bhomoriaghona	Head quarter	169,30
30	4	3	Primary forest	21°33'17,4"	92°05'32,8"	BFD	Bhomoriaghona	Head quarter	174,98
31	4	4	Primary forest	21°30'11,3"	92°09'38,2"	BFD	Idgarh	Baishari	136,00
32	4	5	Primary forest	21°30'15,7"	92°09'40,2"	BFD	Idgarh	Baishari	177,93
33	4	6	Primary forest	21°30'48,8"	92°09'49,3"	BFD	Idgarh	Baishari	72,62
34	4	7	Primary forest	21°33'10,5"	92°10'07,3"	BFD	Idgarh	Idgarh	43,41

35	4	8	Primary forest	21°33'23,6"	92°10'54,2"	BFD	Idgarh	Idgarh	107,60
36	4	9	Primary forest	21°33'29,5"	92°10'49,2"	BFD	Idgarh	Idgarh	170,52
37	4	10	Primary forest	21°35'18,3"	92°06'11,9"	BFD	Fulchari	Rajkhat	131,01
38	4	11	Primary forest	21°35'26,4"	92°06'35,8"	BFD	Fulchari	Rajkhat	151,98
39	4	12	Primary forest	21°29'33,3"	92°12'59,4"	BFD	Baghkhali	Gilatali	65,38
40	5	1	Rubber	21°34'04,3"	92°11'23,8"	Private	Manjur** Choudhury		9,85
41	5	2	Rubber	21°34'02,2"	92°11'25,7"	Private	Manjur Choudhury		35,35
42	5	3	Rubber	21°33'41,5"	92°11'40,6"	Private	Manjur Choudhury		38,36
43	5	4	Rubber	21°33'38,1"	92°11'39,5"	Private	Manjur Choudhury		6,27
44	5	5	Rubber	21°33'25,5"	92°11'52,5"	Private	Masud Parvez**		24,56
45	5	6	Rubber	21°33'12,4"	92°12'03,6"	Private	Masud Parvez		20,99
46	5	7	Rubber	21°33'16,5"	92°11'52,3"	Private	Masud Parvez		32,26
47	5	8	Rubber	21°33'12,2"	92°11'37,3"	Private	Masud Parvez		79,93
48	6	1	Shrub	21°35'04,7"	92°04'46,2"	BFD	Fulchari	Napithkhali	0,20
49	6	2	Shrub	21°35'12,5"	92°04'47,8"	BFD	Fulchari	Napithkhali	0,64
50	6	3	Shrub	21°35'24,5"	92°04'56,7"	BFD	Fulchari	Napithkhali	0,54
51	6	4	Shrub	21°35'23,0"	92°05'08,7"	BFD	Fulchari	Napithkhali	1,36
52	6	5	Shrub	21°34'58,5"	92°05'23,6"	BFD	Fulchari	Napithkhali	1,37
53	6	6	Shrub	21°35'17,2"	92°05'15,8"	BFD	Fulchari	Napithkhali	1,19

54	6	7	Shrub	21°35'08,0"	92°04'59,7"	BFD	Fulchari	Napithkhali	0,81
55	7	1	Teak	21°31'22,2"	92°08'59,8"	BFD	Joarianala	Bengdeba	58,18
56	7	2	Teak	21°31'10,8"	92°08'57,8"	BFD	Joarianala	Bengdeba	118,33
57	7	3	Teak	21°28'14,0"	92°13'33,5"	BFD	Baghkhali	Gilatali	79,55
58	7	1	Teak coppice	21°34'04,2"	92°06'20,6"	BFD	Bhomoriaghona	Head quarter	32,13
59	7	2	Teak coppice	21°29'18,1"	92°07'21,2"	BFD	Joarianala	Head quarter	64,57
60	7	3	Teak coppice	21°29'09,8"	92°07'24,4"	BFD	Joarianala	Head quarter	52,36
61	7	4	Teak coppice	21°29'32,8"	92°07'24,4"	BFD	Joarianala	Head quarter	37,96
62	7	5	Teak coppice	21°31'37,1"	92°08'01,0"	BFD	Joarianala	Bengdeba	42,14
63	7	6	Teak coppice	21°31'48,7"	92°08'30,6"	BFD	Joarianala	Bengdeba	62,02
64	8	1	Secondary forest	21°33'35,2"	92°11'38,4"	USF	Ali Khjang		101,54
65	8	2	Secondary forest	21°33'53,7"	92°11'34,3"	USF	Ali Khjang		51,89
66	8	3	Secondary forest	21°33'47,9"	92°11'31,1"	USF	Ali Khjang		86,47
67	8	4	Secondary forest	21°33'18,2"	92°12'05,3"	USF	Ali Khjang		88,97
68	8	5	Secondary forest	21°33'20,9"	92°12'04,5"	USF	Ali Khjang		92,43
69	8	6	Secondary	21°33'23,5"	92°12'04,5"	USF	Ali Khjang		95,98

			forest						
70	8	7	Secondary forest	21°33'25"	92°12'05,7"	USF	Ali Khjang		90,58

BFD: Bangladesh Forest Department

USH: Unclassified Stated Forest controlled by District Commissioner

*: Name of the mouza

**: Name of the owner

APPENDIX IX

A-IX Comparing the accuracy of three different methods for predicting carbon

Sl. no	Plot no.	Forest type	Classified	Measured C (Ton/ha)	Predicted C (Ton/ha)			Absolute bias (ton/ha)		
					Stratification	Regression	Knn	Stratification	Regression	Knn
1	1	Acacia	Acacia	26,87	31,00	21,93	91,00	4,80	2,53	0,80
2	2	Acacia	Acacia	24,24	31,00	21,93	25,00	49,55	56,87	132,55
3	3	Acacia	Acacia	31,14	31,00	26,99	47,00	147,12	149,86	3,88
4*	4	Acacia	Mature forest	21,58	134,00	118,31	178,00	35,54	32,80	3,54
5	1	Bamboo	Bamboo	140,11	63,00	52,73	54,00	28,72	31,46	10,72
6	2	Bamboo	Bamboo	104,36	63,00	72,01	171,00	0,10	0,30	0,10
7	3	Bamboo	Bamboo	80,29	63,00	47,53	75,00	0,01	0,41	0,01
8	1	Ind. Plantation	Ind. Plantation	79,20	84,00	76,68	80,00	0,27	0,14	0,27
9	2	Ind. Plantation	Teak	208,12	61,00	58,26	212,00	0,45	0,35	0,45
10	3	Ind. Plantation	Ind. Plantation	133,55	84,00	76,68	1,00	47,20	31,50	43,80
11*	4	Ind. Plantation	Young forest	24,51	87,00	97,92	171,00	12,34	24,58	0,34
12	5	Ind. Plantation	Young forest	88,04	87,00	79,55	171,00	58,64	62,28	57,64
13	1	Mature forest	Mature forest	98,46	134,00	131,25	102,00	25,53	34,30	23,47
14	2	Mature forest	Mature forest	162,72	134,00	131,25	152,00	53,80	57,43	52,80
15	3	Mature forest	Mature forest	86,80	134,00	118,31	43,00	0,00	12,94	21,00
16	4	Mature forest	Teak	73,34	61,00	97,92	73,00	62,49	73,41	146,49
17	1	Rubber	Rubber	89,64	31,00	27,36	32,00	1,04	8,48	82,96
18	2	Rubber	Rubber	56,53	31,00	22,23	80,00	4,13	4,94	64,13
19	3	Rubber	Rubber	84,80	31,00	27,36	32,00	6,76	2,31	0,76
20	4	Rubber	Rubber	31,00	31,00	18,06	10,00	0,14	4,15	15,86
21	1	Shrub	Shrub	0,90	1,00	0,60	1,00	112,42	96,73	156,42
22	2	Shrub	Shrub	1,01	1,00	0,60	1,00	50,44	15,78	50,44
23	3	Shrub	Shrub	0,73	1,00	0,60	1,00	19,81	23,44	20,81
24	4	Shrub	Shrub	0,55	1,00	0,90	1,00	13,58	58,13	13,58
25	1	Teak	Non-forest	50,44	0,00	34,66	0,00	77,11	87,37	86,11
26	2	Teak	Teak	41,19	61,00	64,64	62,00	41,36	32,35	66,64
27	3	Teak	Non-forest	13,58	0,00	71,71	0,00	17,29	32,76	5,29
28	1	Young forest	Young forest	54,39	87,00	97,92	86,00	32,61	43,52	31,61
29	2	Young forest	Bamboo	64,64	63,00	52,73	89,00	1,64	11,91	24,36
30	3	Young forest	Ind. Plantation	35,99	84,00	62,30	89,00	48,01	26,31	53,01

* Major source of errors for bias calculation